INSTITUTO POLITÉCNICO NACIONAL

ESCUELA SUPERIOR DE INGENIERÍA QUÍMICA E INDUSTRIAS EXTRACTIVAS

SECCIÓN DE ESTUDIOS DE POSGRADO E INVESTIGACIÓN

"BIOLOGICAL HYALURONIC ACID – BASED AND CHONDROITIN SULFATE – BASED HYBRID HYDROGELS WITH GREAT POTENTIAL FOR CARTILAGE SUBSTITUTION AND REGENERATION"

T E S I S

PARA OBTENER EL GRADO DE:

DOCTOR EN CIENCIAS EN METALURGIA Y MATERIALES

P R E S E N T A

M. en C. DANIELA ANAHÍ SÁNCHEZ TÉLLEZ

DIRECTORES DE TESIS

DRA. LUCÍA TÉLLEZ JURADO ESIQIE-IPN

DR. LUIS MARÍA RODRÍGUEZ LORENZO ICTP-CSIC

CIUDAD DE MÉXICO   ENERO 2019

INSTITUTO POLITÉCNICO NACIONAL
SECRETARÍA DE INVESTIGACIÓN Y POSGRADO

ACTA DE REVISIÓN DE TESIS

En la Ciudad de ___México___ siendo las ___12:00___ horas del día ___17___ del mes de ___diciembre___ del ___2018___ se reunieron los miembros de la Comisión Revisora de la Tesis, designada por el Colegio de Profesores de Estudios de Posgrado e Investigación de ___ESIQIE___ para examinar la tesis titulada:

"Biological hyaluronic acid-based and chondroitin sulfate-based hybrid hydrogels with great potential for cartilage substitution and regeneration"

Presentada por el alumno:

SÁNCHEZ	TÉLLEZ	DANIELA ANAHÍ
Apellido paterno	Apellido materno	Nombre(s)

Con registro: | A | 1 | 5 | 1 | 0 | 5 | 6 |
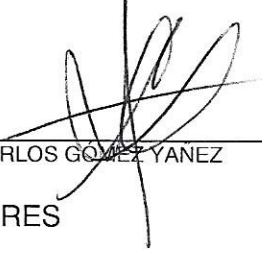
aspirante de:

DOCTORADO EN CIENCIAS EN METALURGIA Y MATERIALES

Después de intercambiar opiniones los miembros de la Comisión manifestaron **SU APROBACIÓN DE LA TESIS**, en virtud de que satisface los requisitos señalados por las disposiciones reglamentarias vigentes.

LA COMISIÓN REVISORA

Directores de tesis

DRA LUCÍA TÉLLEZ JURADO

DR. LUIS MARÍA RODRÍGUEZ LORENZO

DR. HÉCTOR JAVIER DORANTES ROSALES

DRA. ELSA MIRIAM ARCE ESTRADA

DR. JOSÉ ORTIZ LANDEROS

DR. CARLOS GÓMEZ YANEZ

ESCUELA SUPERIOR DE INGENIERIA QUIMICA E INDUSTRIAS EXTRACTIVAS
SECCIÓN DE ESTUDIOS DE POSGRADO E INVESTIGACIÓN

PRESIDENTE DEL COLEGIO DE PROFESORES

DRA. GUADALUPE SILVA OLIVER

INSTITUTO POLITÉCNICO NACIONAL
SECRETARÍA DE INVESTIGACIÓN Y POSGRADO

CARTA CESIÓN DE DERECHOS

En la Ciudad de México el día **17** del mes de **diciembre** del año **2018**, la que suscribe **Daniela Anahí Sánchez Téllez** alumn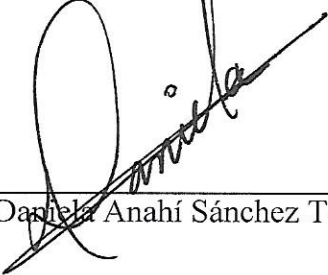a del **Programa de Doctorado en Ciencias en Metalurgia y Materiales**, con número de registro **A151056**, adscrito a la **Escuela Superior de Ingeniería Química e Industrias Extractivas**, manifiesto que soy el autor intelectual del presente trabajo de Tesis bajo la dirección de la **Dra. Lucía Téllez Jurado** y el **Dr. Luis María Rodríguez Lorenzo** y cedo los derechos del trabajo titulado: *"Biological hyaluronic acid – based and chondroitin sulfate – based hybrid hydrogels with great potential for cartilage substitution and regeneration"*, al Instituto Politécnico Nacional para su difusión, con fines académicos y de investigación.

Los usuarios de la información no deben reproducir el contenido textual, gráficas o datos del trabajo sin el permiso expreso del autor y/o directores del trabajo. Este puede ser obtenido escribiendo a las siguientes direcciones **danielatellez06@gmail.com** y **ltellezj@ipn.mx**. Si el permiso se otorga, el usuario deberá dar el agradecimiento correspondiente y citar la fuente del mismo.

_____
Daniela Anahí Sánchez Téllez

AGRADECIMIENTOS

Al *Instituto Politécnico Nacional (IPN)* por ser mi escuela, mi centro de enseñanza y donde iniciaron mis estudios de investigación.

A la *Escuela Superior de Ingeniería Química e Industrias Extractivas (ESIQIE)* por ser mi case de estudios y donde mis primeros pasos como ingeniera química e investigadora comenzaron.

Al *Instituto de Ciencia y Tecnología de Polímeros del Consejo Superior de Investigaciones Científicas (ICTP-CSIC)* con sede en Madrid, España en donde realice dos años de mi proyecto de investigación doctoral.

Al Colegio Guadalupe por darme las bases de una excelente educación académica, moral y humana.

Con mucha admiración, respeto y amor a mi asesora, la *Dra. Lucía Téllez Jurado*, quien siempre me ha orientado y ha sido un gran ejemplo a seguir de superación personal y profesional. Gracias por coordinar parte de este trabajo.

Al *Dr. Luis María Rodríguez Lorenzo* por su aporte académico y por el apoyo personal y profesional durante mi estancia de investigación en el ICTP-CSIC. Gracias por coordinar parte de este trabajo.

A los sinodales, la *Dra. Elsa Miriam Arce Estrada*, el *Dr. Carlos Gómez Yáñez*, el *Dr. José Ortiz Landeros* y el *Dr. Héctor Javier Dorantes Rosales* por sus valiosos comentarios llenos de experiencia que guían mi camino como investigadora.

Al *Grupo de Biomateriales* del ICTP-CSIC por acogerme en su grupo de investigación y en su laboratorio.

Al *Consejo Nacional de Ciencia y Tecnología (CONACYT)* por brindarme su apoyo financiero de manutención mediante la beca nacional de doctorado y la beca mixta de movilidad internacional.

Al *programa Enhancing Mobility between Latin America, Caribbean and the European Union in Health and Environment (EHME-CSIC 2015)* por brindarme su apoyo financiero de manutención.

A la Beca de Estímulo Institucional de Formación de Investigadores (BEIFI) por otorgarme su apoyo financiero durante el doctorado.

DEDICATORIA

A *Dios* por iluminar mi camino y por ser mi confidente y mi fuerza en todo momento.

Dedico especialmente esta tesis con gran amor a mis papás, *Guadalupe* y *Arturo*, porque gracias a ustedes, a su buena educación y su entrega total hoy soy una mujer profesionista, plena y llena de virtudes. Gracias por ser mis consejeros y grandes ejemplos a seguir. Gracias por ser maravillosas personas, por estar llenos de amor, paciencia, sabiduría, trabajo… y por enseñarme a ser un mejor ser humano cada día. Sin ustedes no sería quien soy. Este trabajo es de ustedes. Los amo.

A mi hermano *Arturo* por enseñarme a ser una guerrera y a jamás rendirme ante situaciones adversas. Te quiero.

A mi Hannah preciosa por recordarme todos los días la inocencia y la belleza infinita que aún puede existir en el mundo. Te quiero princesa.

A mi tía Lucía, que además de ser mi asesora es una de las personas que más quiero. Gracias por ser un gran ejemplo a seguir y por influir positivamente en mi vida profesional y personal.

A mis abuelitos.

A mis tías y tíos por apoyarnos a mí y a mi familia en los tiempos complicados. Especialmente a mi tío José Luís Téllez Jurado que me cuida desde el cielo.

A mis primas y primos, especialmente a mi primita Stephanie Cisneros Téllez por su apoyo profesional y por ser como una hermana para mí. Te quiero.

A mi Vito, mi corazón, por cuidarme y apoyarme en todo momento, en todo lugar y de todas las maneras posibles. Te amo.

Dedico y agradezco este trabajo a todas y aquellas personas que han sido unos ángeles por acompañarme durante estos años de estudio.

"El mayor enemigo del conocimiento no es la ignorancia es la ilusión de conocimiento"

Stephen Hawking

INDEX

LIST OF FIGURES

LIST OF TABLES

En el presente trabajo se estudian y desarrollan geles biológicos tridimensionales que puedan imitar la matriz extracelular del cartílago, cumpliendo la función de andamios tisulares en la sustitución y regeneración del cartílago dañado. Los hidrogeles son atractivos en la ingeniería de tejidos ya que son estructuralmente similares a la matriz extracelular de muchos tejidos vivos, además que pueden ser elaborados bajo condiciones moderadas. En el caso de tejido cartilaginoso articular, la base para su alta resistencia a la compresión es su red tridimensional de fibras poliméricas rellenas de fluido tisular, por lo que el desarrollo de geles hidratados a base de compuestos poliméricos naturales que mejor asemejen el ambiente químico y físico de la matriz extra celular del cartílago articular, y que además ayude a la proliferación y diferenciación celular de los condrocitos, hace de los geles biológicos grandes candidatos en la reparación del cartílago.

A lo largo de la vida, el cartílago sufre un remodelado interno continuo conforme las células reemplazan las moléculas de la matriz perdidas al paso del tiempo. El recambio normal de la matriz depende de la capacidad de los condrocitos de detectar los cambios en la composición matricial, por lo que a medida que el organismo envejece, la composición de la matriz se modifica y los condrocitos pierden su capacidad de responder a estos estímulos, acelerándose su degradación. Aunado a lo anterior, el cartílago articular adulto exhibe muy poca capacidad intrínseca para repararse debido a la falta de vasos sanguíneos, por lo que pequeñas lesiones conllevan a daños progresivos en la región y a una degeneración en las articulaciones, causando dolor y pérdida de movimiento.

La estructura y propiedades mecánicas del cartílago están directamente relacionadas con la composición y arquitectura de su matriz extra celular, la cual está compuesta de fibrillas de colágeno y macromoléculas de proteoglicanos unidas de tal manera que resisten la deformación. Mientras que la flexibilidad de las fibrillas de colágeno le permite a la matriz resistir la fuerza de tensión, proveyéndole cierta rigidez, en la compresión, los proteoglicanos mantienen la orientación de las fibrillas y la estabilidad de la estructura dentro de la matriz. Sabiendo que el agrecano es un componente dominante en la matriz extracelular del cartílago, compuesto por ácido hialurónico y proteoglicanos, los cuales son conjugados covalentes de los glicosaminoglicanos (GAG), como el sulfato de condroitina (SC) y el sulfato de queratina, sintetizar un hidrogel con una estructura y constituyentes similares al cartílago natural podría soportar mejor la regeneración de éste. De acuerdo a la literatura, se sabe que mientras el ácido hialurónico (AH) puede promover la integración del tejido recién formado, el sulfato de condroitina (SC) puede promover la segregación celular de colágeno de tipo II y de glicoproteínas; por lo que el objetivo en este trabajo será preparar geles porosos inyectables a base de ácido hialurónico (HA) y sulfato de condroitina (SC) modificados con 3-aminopropiltrietoxisilano para disminuir su hidrofilicidad natural, reforzándolos con fibras de colágeno sintetizadas por electrohilado y sembrados con células mesenquimales que reproduzcan las propiedades del cartílago nativo.

In this work, the development of three-dimensional biological hybrid hydrogels that may mimic the articular cartilage Extra Cellular Matrix (ECM) and fulfill the function of scaffolds in the replacement and regeneration of damaged cartilage tissue are studied. Hydrogels are attractive in Tissue Engineering due to their similar structure with that of ECM in living tissue, their synthesis can be made under moderate conditions and their addition to the body can be done though minimum invasion. In the case of articular cartilage, its high compressive strength is due to its three-dimensional network made up of polymeric nanofibers and filled up with fluid tissue, so the development of hydrated polymeric-based gels that best resemble the chemical and physical environment of ECM in the articular cartilage, and which can help cell proliferation and differentiation, makes biological gels great candidates for cartilage repair.

Throughout lifetime, the cartilage undergoes continuous internal remodeling as cells replace the lost of matrix molecules over time. Normal and continuous turnover of the matrix depends of the ability of chondrocytes to detect changes in the matrix composition, so as the body ages, the matrix composition is modified and chondrocytes lose their ability to respond to these stimuli, and in consequence, accelerating cartilages degradation process. In addition, the adult articular cartilage exhibits very little intrinsic ability to repair itself due to the lack of blood vessels, so small lesions lead to progressive damage and therefore a degeneration in the joints, causing pain and loss of motion.

The structure and mechanical properties of cartilage are directly related to the composition and architecture of the ECM, which is composed by collagen fibrils linked in that way to macromolecules of proteoglycans that the matrix can resist deformation. While collagen fibrils flexibility enables the matrix to resist tension forces, providing a certain degree of rigidity, the proteoglycans help to keep fibrils orientation and the structure stability within the matrix during compression forces. Knowing that aggrecan, composed by hyaluronic acid and proteoglycans, which are covalent conjugates of glycosaminoglycans (GAG) such as chondroitin sulfate and keratin sulfate, is a key component in the ECM, synthesizing a hydrogel with similar components and structure to that of natural cartilage, may better withstand the cartilage regeneration.

According to literature, since hyaluronic acid can promote the integration of newly formed tissue, and chondroitin sulfate may promote the release of collagen type II and glycoproteins by cells; the aim of this work is to prepare injectable porous gels based on hyaluronic acid and chondroitin sulfate, modified with 3-aminopropyltriethoxysilane to reduce natural hydrophilicity. Moreover, to improve biocompatibility and mechanical properties, the gels are reinforced with collagen fibers synthesized by electrospinning and seeded with mesenchymal cells. These strategies will help to mimic the natural cartilage properties.

INTRODUCTION

Cartilage suffers a continuous internal remodeling as chondrocytes replace matrix molecules over time. Remodeling depends on chondrocytes capacity of detecting changes in the matrix composition. As the body ages, the matrix composition is modified and chondrocytes lose their capability of detecting those changes, enhancing an accelerated degradation in cartilage tissue. Since adult cartilage exhibits little intrinsic ability of healing itself due to lack of blood vessels, any focal lesion leads to progressive damage and degradation of joints, causing in patients severe pain and loss of motion [1].

Cartilage is a tough and flexible form of connective tissue. Its extracellular matrix (ECM) contains high concentrations of glycosaminoglycans (GAGs) and proteoglycans that interact with collagen and elastic fibers. The firm consistency of cartilage ECM allows tissue to bear mechanical stresses without permanent distortion. The dry weight of hyaline cartilage is 40% collagen embedded in a firm and hydrated gel of proteoglycans and structural glycoproteins. Most of collagen in hyaline cartilage is type II, although small amounts of other collagen types are also present. Aggrecan (250 kD), with approximately 150 glycosaminoglycan (GAG) side chains of chondroitin sulfate and keratin sulfate, is the most abundant proteoglycan in hyaline cartilage. Hundreds of these proteoglycans are bound noncovalently by link proteins to long polymer chains of hyaluronic acid. Later, these proteoglycan complexes bind to the surface of collagen type II fibrils. Finally, water bound to GAGs in the proteoglycans constituting up the 60%-80% of weight of the fresh hyaline cartilage. Therefore, a full understanding of ECM is the clue to develop strategies to repair and regenerate living cartilage tissue.

Currently, there are no clinical satisfactory solutions for cartilage tissue regeneration [2-4]. The most widely used clinical procedure to heal cartilage injury involves penetrating the wound to the subchondral bone, allowing the access of blood flow and new biological material [5-8]. However, such clinical treatments often result in the formation of fibrocartilaginous tissue (**Figure 1**), which is weaker than the original one, failing to integrate properly with surrounding tissue, and degrading over a period between 6 to 12 months [9-13].
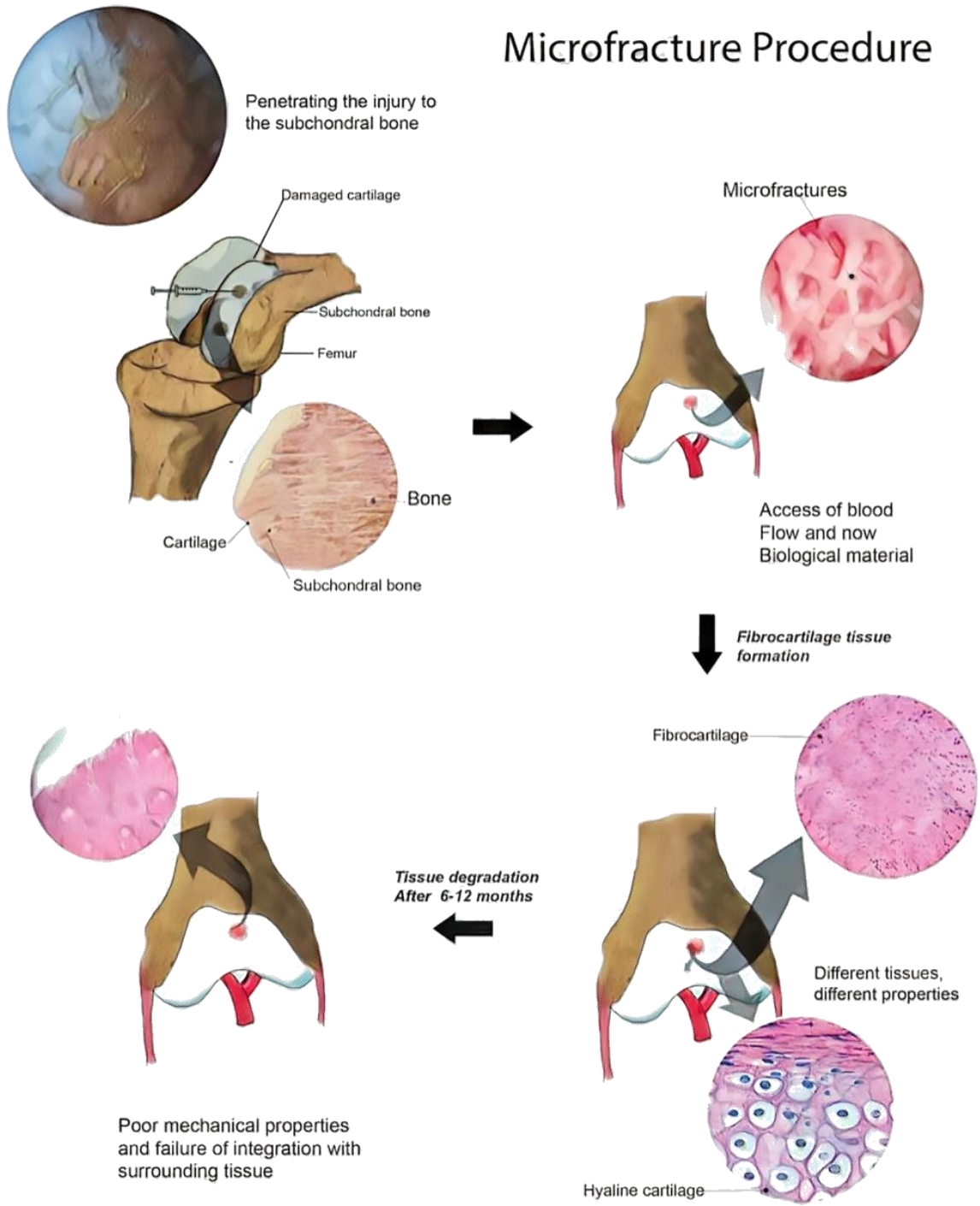
Figure 1. Common clinical procedure used to heal cartilage injury [14].

During the last few years, material scientists and tissue engineers have tried to help clinicians by confronting the challenge of manufacturing porous 3D scaffolds which resemble the chemical composition and architecture (**Figure 2**) of the extracellular matrix (ECM) of cartilage [15-21]. Most of the studies are directed to determine how chemical composition and architecture influence cellular phenotype, differentiation, integration and extracellular matrix secretion during *in vitro* [22-27] and *in vivo* [28-34] assays.
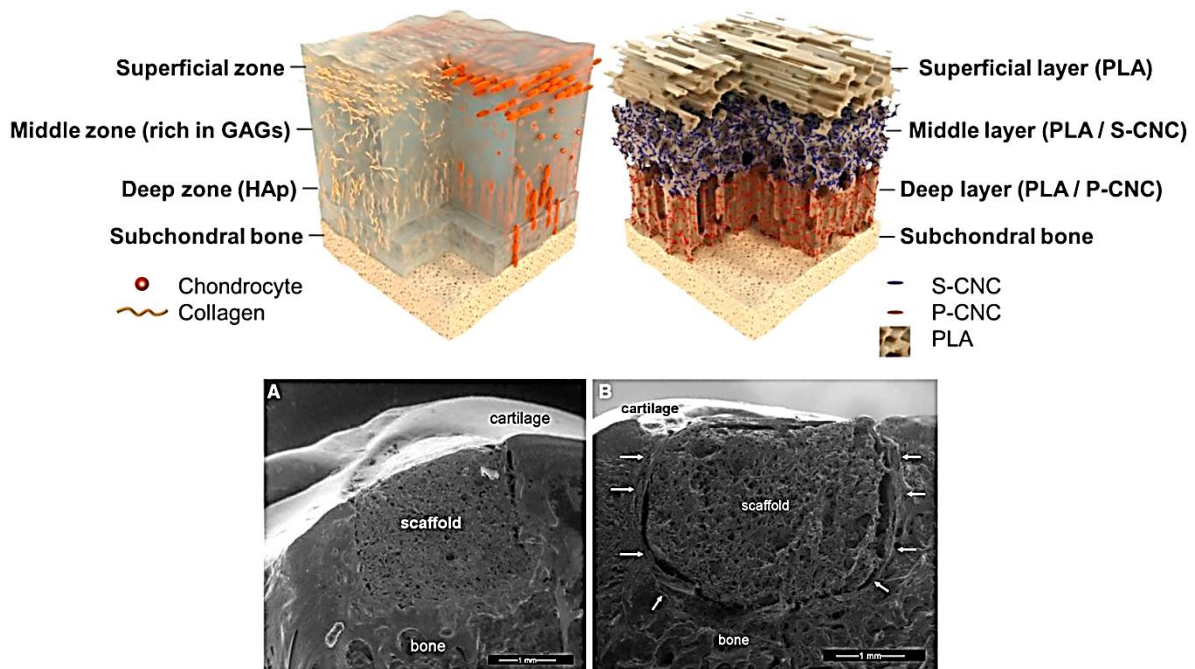
Figure 2. Top. How artificial scaffolds try to mimic the anisotropic characteristic in cartilage tissue [35, 36]. Reprinted with permission of [35] Sandra Camarero-Espinosa *et al. Biomaterials*, 74: 42-52. **Bottom.** Matrix regeneration within a macroporous non-degradable implant for osteochondral defects is not enhanced with partial enzymatic digestion of the surrounding tissue. (**A**) Environmental scanning electron microscopy of a longitudinal slice taken through the cartilage-bone-implant. The specimen was retrieved at the 1 month post-operative time point. Good integration between the implant and the surrounding bone and articular cartilage was observed. (**B**) Environmental scanning electron microscopy image of a longitudinal slice taken through the cartilage-bone-implant construct at 3 months. Fibrous encapsulation of the implant is highlighted by arrows. Reprinted with permission of [36] Aaron J. Krich *et al. J. Mater. Sci. Mater*, Med., 24: 2429-2437.

Several natural and synthetic polymers are being used to create novel materials, as collected in **Table 1**, in attempts to produce scaffolds for tissue engineering and regenerative medicine having clinical application [37].

Table 1. Scaffolds in clinical and preclinical use for cartilage regeneration.

Application	Material	Problem-Result	Ref.
Nose (dorsal augmentation material in rhinoplasty)	Tissue-engineered chondrocyte PCS (Porcine Cartilage-derived Substance) scaffold construct.	Preliminary animal study: Excellent biocompatibility, neocartilage formation starts. However, it was not confirmed that the constructs contributed to the formation of neocartilage.	[38]
Knee (subchondral bone)	Osteochondral biomimetic nanostructured scaffold Maioregen®	Better results in healing complex lesions in comparison with the implantation of a purely chondral scaffold.	[39]
	Cell-free biphasic scaffold: collagen-hydroxyapatite osteochondral scaffold	Statistically significant improvement in clinical scores. At 5 years, between 60.9% and 78.3% of the cases showed complete filling of the cartilage, complete integration of the graft, intact repaired tissue surface and homogeneous repaired tissue.	[40]
	Nanostructured biomimetic three-phasic collagen-hydroxiapatite construct	The implantations to treat chondral and osteochondral knee defects were effective in terms of clinical outcome, although MRI detected abnormal findings.	[41]
Knee (chondral defects)	Autologous ovine MNC Cell-seeded and cell-free DL-poly-lactide–*co*–glycolide (PLGA) scaffolds	The engineered tissue had not local or systemic adverse effects. However, only a poor integration of the tissue engineering product into adjacent tissue was reached and the formed ECM was not mature enough for long-lasting weight-loading resistance.	[42]
	Type I collagen-hydroxyapatite (Maioregen®) nanostructural biomimetic osteochondral scaffold	The use of the Maioregen® scaffold is a good procedure for the treatment of large osteochondral defects; however, the lesion site seems to influence the results. Patient affected in the medial femoral condyle showed better results.	[43]
	DeNovo (RevaFlex) engineered tissue graft	Preliminary evidence suggests that DeNovo ET implant is capable of spontaneous matrix formation with no immune response, improving function and recreating hyaline-like cartilage.	[44]
Knee (femoral condyles)	Biphasic cylindrical osteochondral composite construct of DL-poly-lactide–*co*–glycolide (PLGA). Its lower body is impregnated with β-tricalcium phosphate (TCP)	The regenerated osteochondral tissue was evaluated as a tissue of acceptable quality. Regenerated cartilage was defined as being hyaline when the ground substance was homogeneous without fibrous texture.	[45]
Tibial plateau (osteochondral scaffold)	Osteochondral biomimetic collagen-hydroxiapatite scaffold (Maioregen®, Fin-ceramica, Faenza, Italy)	MRI abnormalities. Clinical outcome with stable results up to a mid-term follow-up.	[46]
Microfractured defect (for filling microfractures)	BioCartilageTM, product containing dehydrated, micronized allogeneic cartilage, implanted with the addition of platelet rich plasma	No human clinical outcomes data available. Data regarding results are limited to expert opinion.	[47]
	Chondroitin sulfate adhesive-Poly(ethylene glycol) diacrylate (PEGDA) hydrogel system combined with standard microfracture surgery	Significant increase in tissue fillers with defects in a short-term follow-up.	[48]
Knee (for donor site filling)	Artificial TruFit cylinders made of fully synthetic material called PolyGraft®-Material: 50% copolymer (PDLG), composed of 85% poly(D,L-lactide) and 15% glycolide; 40% calcium sulfphae, 10% PGA fibers	No clinical improvement could be found. The regeneration of the filled defects took more than 2 years, even though TruFit Plugs are supposed to stimulate cartilage and bone cell migration from the surrounding tissue to the synthetic cylinders.	[49]
	Porous poly(ethylene oxide)terephthalate/butylene terephthalate) (PEOT/PBT) implants	Treated defects did not cause postoperative bleeding. Well integration. Surface stiffness was minimally improved compared to controls. Considerable biodegradation after 9 months. Congruent fibrocartilaginous surface repair with interspersed fibrous tissue formation in implanted sites. Donor site: fibrocartilaginous surface repair.	[50]
Shoulder	Engineered hyaluronic acid membrane, Hyalograft®	Using the hyaluronic membrane had no effect on the final outcome. No difference was observed between the fibrocartilage tissue formed after implementing microfractures and the fibrocartilage tissue grown on the hyaluronic acid membrane scaffold.	[51]

However, the complexity of the physical structure and properties of cartilage, including mechanical [52-56], anisotropic [57-59], nonlinear [60-62], inhomogeneous [63-65] and viscoelastic properties [66-68], are thought to be directly related to the failing of most of the attempts made to fabricate artificial substitutes for cartilage [69-73]. As a consequence, there are not yet biomaterials for cartilage regeneration in clinical use with satisfactory results. Scaffolds based on tissue-engineered constructs, osteochondral biomimetic scaffolds, cell-free biphasic or three-phasic scaffolds, autologous scaffolds, engineered-tissue grafts, porous implants have not demonstrated to be a satisfactory solution in clinical application. Therefore, it seems evident that there is a need to design more suitable scaffolds and to develop new types of materials which can be used for cartilage regeneration.

In the case of articular cartilage repair, the required materials must provide successful mechanical properties, biological delivery, fixation of the device in situ and stability to the joint. Besides, the assays done to these materials need to be based on the intended biological effect and potential risks which have to be evaluated, such as toxicity, dedifferentiation, immunogenicity and contamination. Some preclinical trials with little animal models, such as rats and white New Zealand rabbits, are necessary to predict how biomaterials may behave during clinical assays. Moreover, some preliminary studies can be done in cadaveric human bodies; however extensive trials with large animal preclinical models are mandatory to obtain market approval. Therefore, just a few of the novel materials or tissue protocols are allowed to have clinical application or even to be commercialized. When trying to compare different studies of novel materials once they are introduced into clinical practice, there are other problems: (1) lack of homogeneity due to the different studied population; (2) short- and mid-follow-ups; (3) use of different evaluation systems; (4) new scaffold-based strategies for cartilage regeneration, either cell seeded or cell-free biomaterials; (5) procedures which differ in scaffold fixation methods, surgical approaches and postoperative rehabilitation phases. Therefore, there is the need among scientists, clinicians, industry and regulatory experts to improve communication and collaboration in order to overcome all the barriers in tissue engineering and to establish a defined road map to reach clinical application.

In the present work, a 3D biological hybrid hydrogel is designed in order to mimic the extracellular matrix of hyaline cartilage. This biomaterial should obey the following functions: i) to reproduce the function of damaged cartilage, ii) to optimize the interface material-tissue, and iii) to prepare minimum invasive systems to the body.

GENERAL AIM

To develop biological 3D hybrid hydrogels capable of mimicking the natural cartilage extracellular matrix by using polysaccharides as hyaluronic acid (HA) and chondroitin sulfate (CS) modified by 3-aminopropyl triethoxysilane (APTES) and crosslinked with a PDMS-modified SiO_2 organic-inorganic structure in order to decrease their natural hydrophilicity. Polysaccharide-based PMDS-modified SiO_2 organic-inorganic hybrid hydrogels will be evaluated to study their physical, chemical, rheological and biological properties in order to establish their capability to work as biomaterials for cartilage substitution and regeneration.

SPECIFIC AIMS

1. To chemically modify and hybridize hyaluronic acid (HA) and chondroitin sulfate (CS) for the preparation of non-toxic hybrid hydrogels in order to provide them slow degradation kinetics, through the amidation of carboxylic groups in HA and CS with the amine groups of APTES molecules.
2. To crosslink hyaluronic acid (HA) and chondroitin sulfate (CS) by a three dimensional PDMS-modified SiO₂ organic-inorganic matrix through the hydrolysis-condensation reactions (*sol-gel* method) among the inorganic modifier (APTES), the silica alkoxide (TEOS) and the silicone (PDMS).
3. To study gelling degree by varying polysaccharide concentration, pH of synthesis and temperature of synthesis.
4. To study the effect of drying process in the polysaccharide-based hybrid hydrogels swelling and degradative properties.
5. To study biological properties, cytotoxicity and cell proliferation, by culture of fibroblast and mother cells into the polysaccharide-based hybrid hydrogels.

BACKGROUND AND STATE OF THE ART

1.1 ARTICULAR CARTILAGE: COMPOSITION AND STRUCTURE

Cartilage is a tough and resilient type of connective tissue that provides cushioned and low-friction surfaces for joints. Cartilage is made of chondrocytes embedded in extensive extracellular matrix (ECM). Chondrocytes synthesize and keep regulated ECM components. These cells are located in matrix cavities, called *lacunae*. Collagen, hyaluronic acid, proteoglycans and several glycoproteins are the principal macromolecules existing in all types of cartilage. There are three types of cartilage tissue: hyaline cartilage, elastic cartilage and fibrocartilage.

Physical properties of cartilage tissue depend on electrostatic bonds between flexible collagen-and-elastin fibers and the GAGs linked to densely packed proteoglycans, notably aggrecan. Its semi-rigid consistency is attributed to water bound to the negatively charged sulfated GAG chains extending from the proteoglycan core proteins. The high content of bound water allows cartilage to serve as a shock absorber.

Hyaline cartilage, also called articular cartilage, is the most common form of cartilage tissue in the body. The ECM of hyaline cartilage is homogenous and glassy, rich in fibrils of collagen type II and aggrecan complexes with bound water. Hyaline cartilage is a viscoelastic semitransparent thin film (2-5 mm of thickness) located on the articular surfaces of movable joints, on the walls of larger respiratory passages (nose, larynx, trachea, bronchi), on the ventral ends of ribs and on the epiphyseal plates of long bones [74, 75].

Cartilage tissue is avascular, meaning that it lacks blood vessels, lymphatics, and nerves. It receives nutrients by diffusion from capillaries in adjacent connective tissue, the perichondrium. Cartilage is formed by: 1) an aqueous suspension of proteins, metabolites and several inorganic ions such as calcium, sodium and chlorine, making up 60% to 80% of its total weight; 2) chondrocytes, 2% of its total weight, which are necessary for production, maintenance and continuous remodeling of surrounding matrix; and 3) extracellular matrix (ECM) composed by collagen fibrils (most of the collagen in hyaline cartilage is type II),

proteins and proteoglycans formed primarily by hyaluronan, chondroitin sulfate and keratin sulfate. ECM composes between 40% to 60% of the dry weight and more than 95% of the total volume in cartilage tissue [75].

Fundamental substance of hyaline cartilage contains two classes of glycosaminoglycans: chondroitin sulfate and keratin sulfate. Both sulfates bind to a central protein to form a proteoglycan monomer. The most important proteoglycan monomer in hyaline cartilage is aggrecan (250 kDa). Each molecule contains about 100 chains of chondroitin sulfate and up to 60 molecules of keratin sulfate. Due to sulfate groups, the aggrecan molecules possess a large negative charge with affinity for water molecules. Each linear molecule of hyluronan is associated to a large number of aggregan molecules (more than 300). Link proteins bind noncovalently the protein core of proteoglycans to the linear hyaluronic acid molecules. Chondroitin sulfate side chains of the proteoglycan bind electrostatically to the collagen fibrils, forming a cross-linked matrix, as shown in **Figure 3**. Physical properties of these matrix components produce a highly hydrated, pliable material with great strength. Approximately 75% of the wet weight of hyaline cartilage is water.

In summary, proteoglycans are highly hydrophilic. This property allows water to enter through osmosis process into extracellular matrix; but hydration and swelling capacity are limited by collagen fibrils.
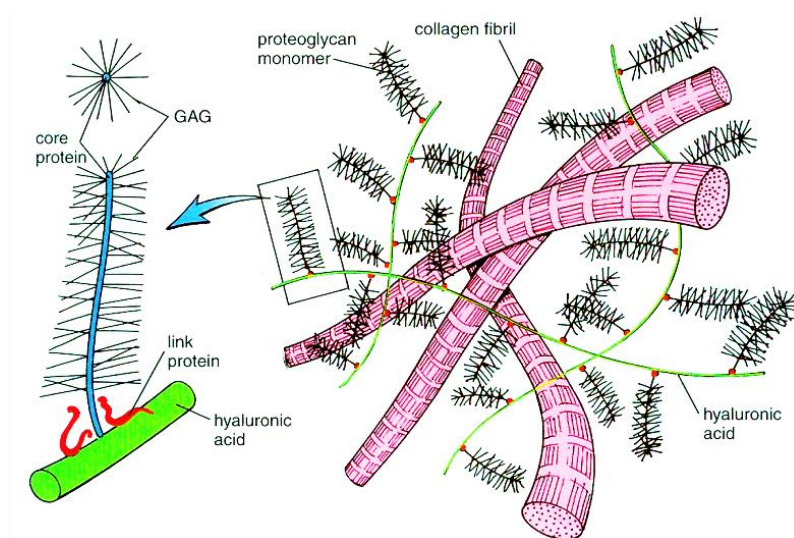
Figure 3. Schematic representation of the most abundant molecules in cartilage matrix showing the interaction between type II collagen fibrils and proteoglycans linked to hyaluronic acid.

1.1.1 ARTICULAR CARTILAGE: DEFECTS AND TREATMENTS

Since the entire structure of cartilage tissue lacks blood or lymphatic vessels, cell infiltration into a normal inflammatory process after injury does not occur; therefore the injured tissue heals poorly or even may not, leading to chronic-degenerative osteoarthritis disease. Osteoarthritis is a chronic condition that commonly occurs during aging and involves gradual loss and changes in the physical properties of hyaline cartilage tissue lining in joints. The articular cartilage tissue fragments released by wear-and-tear forces trigger secretion of matrix metalloproteinases and other factors from macrophages in adjacent tissues, intensifying damage, pain and inflammation within the joint. Joints that are weight-bearing (knees, hips) or heavily used (wrist, fingers) are most likely to cartilage degeneration.

Focal defects in cartilage tissue may be chondral or osteochondral. Chondral lesions do not affect the subchondral bone. They occur inside the cartilage and do not heal spontaneously. In osteochondral lesions, chondroprogenitor mesenchymal cells can invade the lesion by penetrating it through the vascularized subchondral bone and then forming new cartilage-like tissue. Spontaneous partial repair may occur as fibrous tissue is formed, but its functional properties are not the same as natural hyaline cartilage [1].

Medical experience has observed that there is no treatment that promotes complete recovery of cartilage tissue. Despite this, there are several medical treatments that have been used over time to replace damaged cartilage. One of these treatments is to replace cartilage with either small scaffolds from some cartilage tissue that bears lower load on the joints (autografts) or with complete allografts. However, these techniques have serious disadvantages: 1) the small amount of cartilage available in the body for transplantation (mainly from the patella, the femoral condyle or the proximal fibula); 2) the very possible damages caused in the donor site; and 3) the lack of resistance of the grafts to the forces imparted on the joint surface.

The most widely used clinical procedure to heal cartilage involves penetrating the wound to the subchondral bone, by abrasion or perforation, allowing the access of blood flow and new biological material. Unfortunately, depending on the patient, the formed microfracture can stimulate the formation of either non-cartilaginous tissue, fibrocartilaginous tissue or hyaline-type cartilage tissue, whose mechanical properties and duration are different from native tissue [1].

1.2 HYDROGELS IN CARTILAGE REGENERATION

Hydrogels are emergent candidates for applications in cartilage regeneration. Hydrogels are three-dimensional hydrophilic polymer networks made up of water-soluble polymers, crosslinked by either covalent or physical methods [76] (**Figure 4**) to form a water-insoluble hydrogel [77, 78].
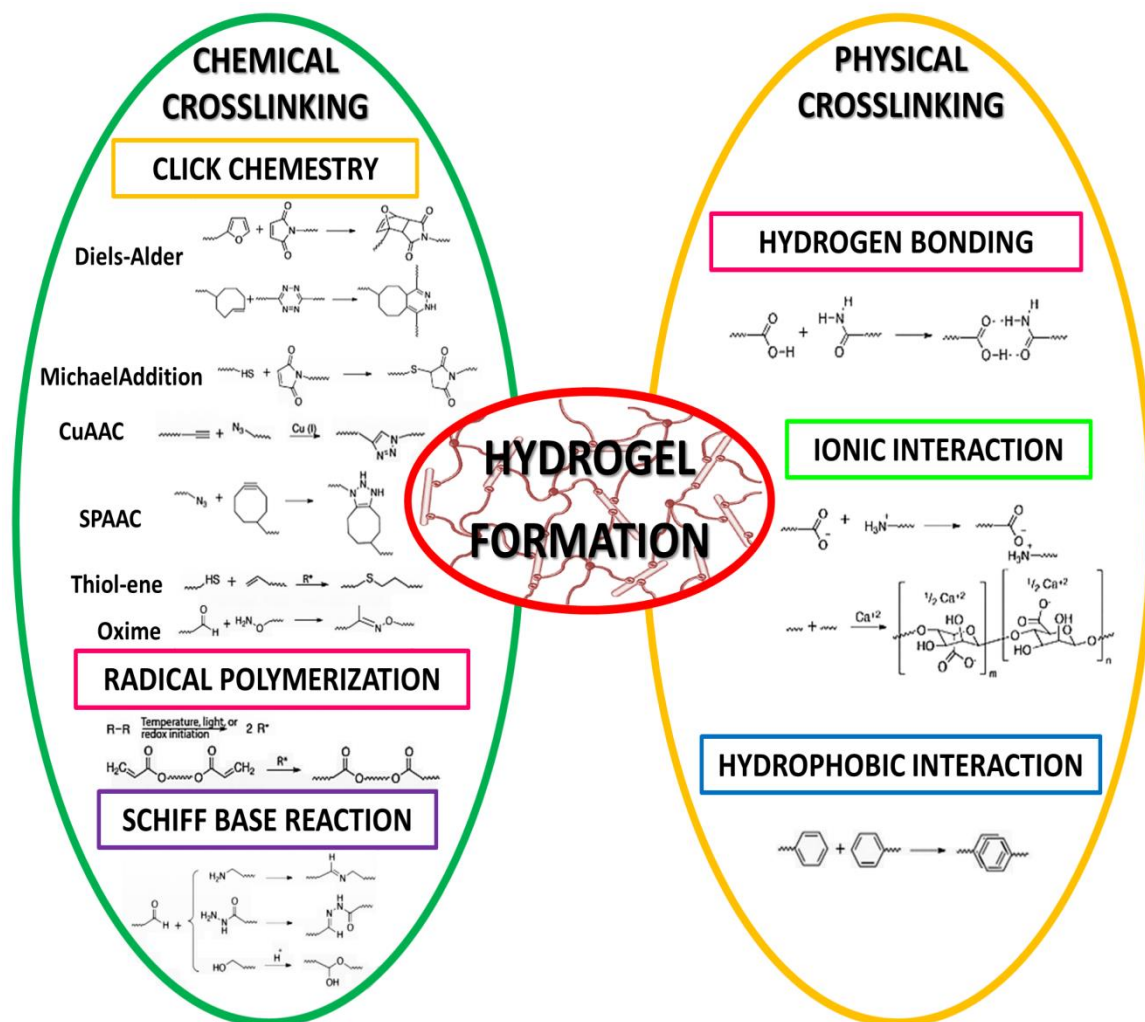
Figure 4. Chemical and physical crosslinking methods used to form hydrogels [14].

Hydrogels can be composed of natural polysaccharides [79-81], proteins [82-86] or synthetic polymers [87-89]. Hydrogels are able to swell and retain great portions of water, from 20% to 99% by weight, when placed in aqueous solutions [90-92]. Hydrogels, tested as matrices to build up scaffolds, provide highly desirable 3D environments for cell growth, holding a great promise for the regeneration of cartilaginous tissue as *in vitro* and *in vivo* studies showed [93-98]. Several studies use cells to catalyze tissue formation while being distributed in 3D hydrogel matrices. Cell matrix adhesion to hydrogel is an important interaction which regulates stem cell survival, self-renewal, and differentiation. Using 3D culture systems (hydrogels) may provide an appropriate niche, scaffolding and environmental bioactive signals for cells. Depending on their physical structure and chemical composition, hydrogels can preserve a compositional and mechanical similarity with the native extracellular matrix of cartilage [99-102]. These properties are necessary for controlling cell response, differentiation and functional tissue regeneration [103-110].

One important reason for the choice of hydrogels in cartilage applications is the possibility of making them injectable which offers advantages over solid scaffolds such as the possibility of using a non-invasive approach. Injectable hydrogels can fill any shape defect and they may provide a homogeneous cell distribution within any defect size or shape prior to gelation [1, 111-114]. Over recent years, a variety of naturally [115-122] and synthetically [123-125] derived materials such as silk [126, 127], resilin [128], chitosan [129], chondroitin sulfate [130], hyaluronic acid [131-134], gelatin [135], agarose [136], alginate [137] poly(vinyl alcohol) (PVA) [99, 138], poly(acrylic acid) [139], acrylamide [140] and many others have been used to form injectable hydrogels for cartilage repair.

Collagen II and glycosaminoglycans (GAGs) are cartilage-specific extracellular matrix components; they play a crucial role in regulating the expression of chondrocytic phenotype and in supporting chondrogenesis. They have been used for *in vitro* and *in vivo* assays [141]; many attempts have been made with different GAGs precursors of hydrogels to provide an appropriate biochemical and biomechanical environment for cells [142-149]. Unfortunately, hydrogels derived from GAGs degrade really fast, thus different chemical modifications have to be introduced. Several crosslinking degrees are necessary in attempt to modulate their degradation kinetics. However, their biological response is also modified [150-154]. In general, the studies found on literature can be divided into two main types: (1) cell-free hydrogel scaffolds; and (2) cell-seeded hydrogel scaffolds.

1.2.1 CELL – FREE HYDROGEL SCAFFOLDS

Investigations based on cell-free hydrogel scaffolds focus on their physico-chemical characterization and mechanical properties [155]. These studies allow a full understanding of physical and chemical interactions within materials and how these interactions may affect biological and mechanical properties of scaffolds.

Poly(ethylene glycol) (PEG) and derived hydrogels are ones of the most widely used synthetic polymer for tissue engineering. The modulus for bovine articular cartilage, measured in compression mode, is 950 KPa, which is close to the value of the fully hydrated polyethylene glycol diacrylate (PEG-DA) hydrogel [91]. Polyvinyl alcohol is another synthetic polymer widely used to form hydrogels due to their excellent biocompatibility, high permeability to fluids (showing an equilibrium water content of 32% $\pm$ 5) and low friction coefficients (μ) in the range of 0.02 to 0.05 against smooth and wet substances. Some studies on PVA-based scaffolds aim to demonstrate that under tribological loading, friction and wear characteristics compatible to natural articular cartilage can be achieved [156]. As low friction coefficients are required for engineered cartilage, polyvinyl alcohol (PVA)/polyvinylpyrrolidone (PVP) hydrogels were synthesized with different polymerization degrees: 1700, 2400 and 2600 for the PVA; and different polymer concentrations: 10% *w/w*, 15% *w/w* and 20% *w/w* of PVA/PVP. It was found that the inner structures of hydrogels tend to be denser when polymer concentration and polymerization degree of PVA increase. While the friction coefficient increases (from 0.037 to 0.044) with an increment in the polymerization degree of PVA (average increase rate is approximate 3%), the friction coefficient decreases (from 0.033 to 0.03 for a 2.5 N load; from 0.049 to 0.045 for a 7.5 N load) with an increment in the polymer concentration (from 10% to 20%) in the low load region and under liquid lubrication. Thus, there is the need to keep friction coefficients stable under lubricated conditions [157].

Another study using PVA-based hydrogels, crosslinked with trimetaphosphate (STMP), revealed that fully hydrated hydrogels were covalently crosslinked systems when mechanically tested, with a rheological behavior (the *G'* changed from 0.01 MPa (0.01 Hz) to 0.02 MPa (15 Hz)) similar to that of tibia cartilage (*G'* = 0.03 for tissue surface and *G'* = 0.11 for overall tissue) [90]. As previously said, it is an important challenge to develop scaffolds which possess mechanical properties mimicking those of cartilage tissue, since cartilage is a complex nonlinear, viscoelastic and anisotropic extracellular matrix structure. T. Chen *et al.* [158]

reported that hydrodynamic conditions, simulating the motion-induced flow fields between the articular surfaces within the synovial joint, induce the formation of a distinct superficial layer on tissue engineered cartilage hydrogels. These hydrodynamic conditions enhance, on the superficial layers, the production of cartilage matrix proteoglycan, type II collagen and a highly aligned fibrillary matrix which resembles the alignment pattern in native tissue surface zone.

Since many materials do not exhibit a low friction coefficient or withstand several loading cycles, some of them are infiltrated with an interpenetrating network hydrogel to form functional scaffolds which provide load-bearing and tribological properties, similar to native cartilage ones. For example: (1) a porous three-dimensionally woven poly(ε-caprolactone) fiber scaffold was infused with a "tough-gel" made of alginate and polyacrylamide [87]; (2) a boundary lubricant functionalized PVA-based hydrogel was developed to be used as a synthetic replacement for focal defects in articular cartilage [159]. Other techniques to develop hydrogels with high mechanical strength are: by using a double network or two-step polymerization [92, 160]; or by functionalizing hydrogels with different organic or inorganic molecules [161].

1.2.2 CELL – SEEDED HYDROGEL SCAFFOLDS

Cell-based hydrogel scaffold therapy is one of the main strategies being investigated in cartilage regeneration. Several scaffolds and materials are being evaluated. These studies focus on whether or not the hydrogels provide an appropriate biochemical and biomechanical environment for long-lasting hyaline-type cartilage regeneration. Decellularized extracellular matrices from natural tissues like dermis or adipose are being studied as functional biologic scaffolds (**Figure 5**). It is possible to ensure the bioactivity of a substrate when scaffolds are seeded with a specific cell type, either chondrocytes or stem cells, and if these cells are able to proliferate regardless of "natural" conditions. As an example, G. Giavaresi, *et al.* [162] evaluated *in vitro* the biological influence of a decellularized human dermal extracellular matrix on human chondrocytes (NHAC-kn) and mesenchymal stromal cells (hMSC). The study showed that at 24 h after seeding, cells adhered consistently to dermal membranes (NHAC-kn = 93% and hMSC = 98%); at 7 days, cell viability index was 98% for both cell cultures seeded on dermal membranes; and after 14 days of culture, the indexes increased significantly for

both cell cultures ($p < 0.0005$; NHAC-kn = 136% and hMSC = 263%). Furthermore, a bio-hybrid composite scaffold, composed by combining a decellularized Wharton's jelly extracellular matrix with the polyvinyl alcohol (PVA)-based hydrogel, demonstrated its ability in promoting chondrocyte adhesion and scaffold colonization [163]. Other studies are examining extracellular matrices developed from porcine articular cartilage [164]. Although these substrates worked as proper scaffolds for the growth of cells, their therapeutic and functional efficiency in cartilage regeneration still need to be proved. Other cell therapies include implanting chondrogenic lines differentiated from mesenchymal stem cells (MSC) into different polysaccharides or synthetic hydrogels. Collagen hydrogels have proved to provide an appropriate 3D environment for MSC chondrogenesis, isolated from Wharton's jelly of human umbilical cord, and to be cytocompatible matrices with great potential for cartilage engineering [165].
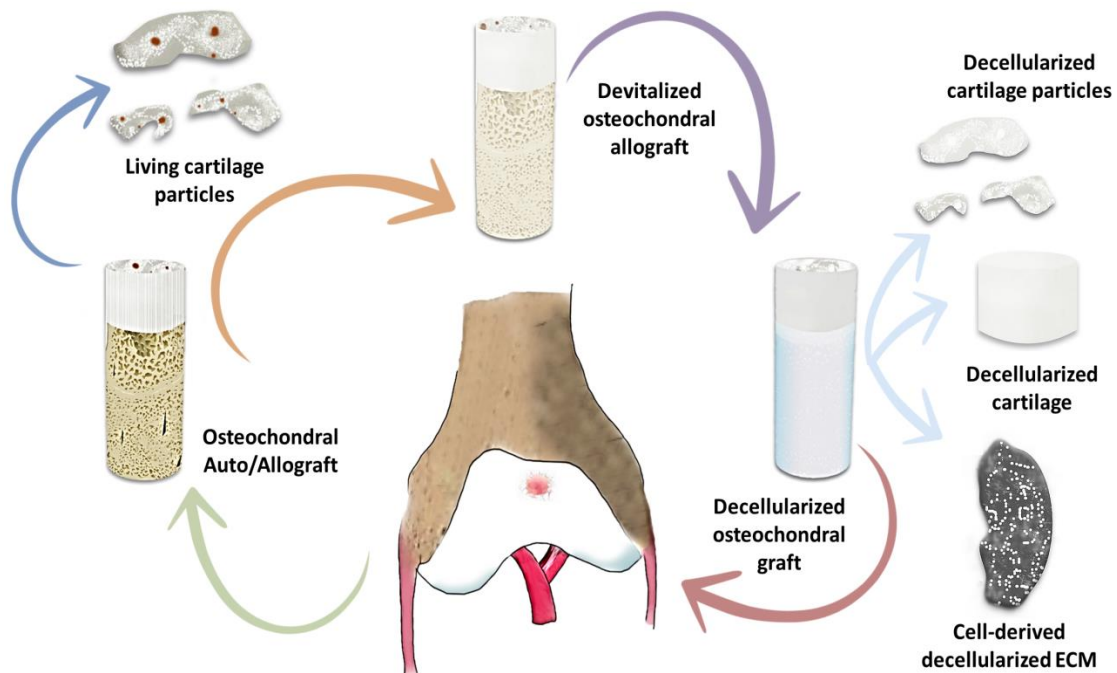
Figure 5. Matrix-based scaffold approaches for cartilage regeneration [14].

One of the problems being reported when using cell therapies is the dedifferentiation of chondrocytes when cultured in two-dimensional cultures, making them less functional for cartilage repair. L. Wu *et al.* [166] hypothesized that functional exclusion of dedifferentiated chondrocytes can be achieved by detecting domains formation of collagen molecules deposited by chondrogenic cells into 3D environments. They reported a method which allows separation of functionally active chondrogenic cells, which produce high levels of collagen II, from functionally inferior dedifferentiated cells, which produce collagen X.

To avoid dedifferentiation of cells once they are forming constructs, J. Lam *et al.* [167] investigated the ability of cell-laden bilayer hydrogels, by encapsulating chondrogenically and osteogenically pre-differentiated mesenchymal stem cells, by varying the period of chondrogenic pre-differentiation prior to implantation. Therefore, cell phenotype could be optimized in order to achieve ideal tissue repair. Furthermore, since regeneration of human articular cartilage is limited, various cellular sources have been studied, including adult and juvenile chondrocytes.

Some studies have compared the formation of cartilage tissue, produced by juvenile, adult and osteoarthritic chondrocytes, inside 3D biomimetic hydrogels composed of poly(ethylene glycol) and chondroitin sulfate. It was found that after the cultured time, juvenile chondrocytes showed a greater upregulation of chondrogenic gene expression than adult chondrocytes, while OA chondrocytes showed a downregulation [105]. Another strategy being studied is the evaluation of therapeutic effects of intra-articular injections of hydrogels containing drugs used to treat osteoarthritis symptoms [168].

Some other studies are meant to analyze how the structure and fabrication methods of the scaffolds influence cells behavior. Due to their intimate contact with chondrocytes, scaffolds are important components of cell niche. Investigations into micro-architecture of scaffolds have revealed that mean pore size is cell-type specific and influences cellular shape, differentiation and extracellular matrix secretion (**Figure 6**). Studies in collagen-hyaluronic acid scaffolds, fabricated with different mean pore size, showed that scaffolds with the largest mean pore size (300 μm) stimulated significantly a higher cell proliferation, chondrogenic gene expression and cartilage-like matrix deposition [169].

When using synthetic materials to produce hydrogels, it is necessary to determine their *in vitro* pore size and mechanical stiffness after being rehydrated, in order to predict

their *in vivo* behavior. J.H. Hui *et al.* [170] found that freeze-dried oligo[poly(ethylene glycol)fumarate] (OPF) hydrogels with a pore size ranged from 20 to 433 μm in diameter and a mechanical stiffness of 1 MPa when rehydrated, enhance the formation of hyaline-fibrocartilaginous mixed tissue. However, these hydrogels, implanted alone into cartilage defects, are insufficient to generate a homogenously hyaline cartilage repair tissue.

H. Kwon *et al.* [171] demonstrated that scaffolds, with different pore size and fabrication methods, influence the microenvironment of chondrocytes and their response to proinflammatory substances. Having high levels of proinflammatory cytokines can cause cartilage destruction and instability of the engineered cartilage tissue. These authors found that silk scaffolds with larger pore sizes support higher levels of cartilage matrix and leach more efficiently proinflammatory cytokines into the medium, influencing cartilage gene expression.
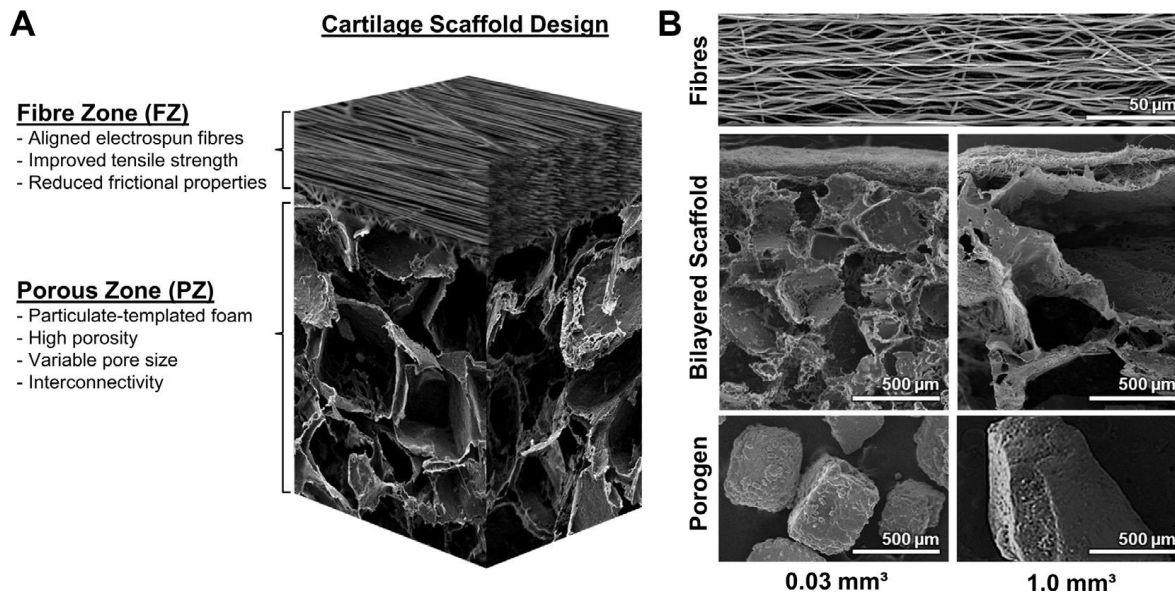
Figure 6. Bilayered cartilage scaffold (**A**) schematized by a diagram illustrating the electrospun fiber zone (FZ) deposited on a particulate-templated foam (PZ). The combination of the two distinct zones is designed to yield an anisotropic scaffold with a smooth articular surface and a more porous region for ECM deposition. (**B**) Electron microscopy images (top) of the aligned fiber zone that is shared between both scaffold varieties, (middle) the complete bilayered scaffolds with 0.3 mm³ (left) and 1.0 mm³ (right) pores, and (bottom) the sodium chloride porogens used to produce their respective scaffolds. Reprinted with permission from [172] J.A.M. Steele et al. Combinational scaffold morphologies for zonal articular cartilage engineering. *Acta Biomaterialia*. 10: 2065–2075.

Furthermore, each zone of cartilage tissue varies in regard to biochemical content, morphology and biomechanical function. Deeper cartilage zones present higher stiffness, higher proteoglycan concentration but lower cellular density and same collagen concentration along cartilage tissue.

In a general structural perspective, cartilage can be simplified into two main regions: (1) the superficial zone which exhibits a high tensile strength and low friction coefficient to keep a smooth articulation; (2) a dense ECM region rich in proteoglycan molecules which give the tissue adequate compressive mechanical properties by producing a high osmotic pressure within the tissue. Therefore, when fabricating a bilayer or three-layer scaffold, pore size and fabrication method of each layer influence the microenvironment of chondrocytes.

As shown by J.A.M. Steele *et al.* [172], tissue engineering scaffolds can be designed to vary in morphology and function, offering a template: (1) to mimic the structural organization and functional interface of cartilage superficial zone; (2) to increase the extracellular matrix production; (3) to enhance the anisotropic mechanical properties. These authors fabricated a multi-zone cartilage scaffold by electrostatic deposition of polymer microfibers onto particulate-templated scaffolds with 0.03 mm^3 and 1.0 mm^3 porogens. They demonstrated that bilayered scaffolds can closely mimic some of the structural characteristics of native cartilage due to: (1) the addition of aligned fiber membranes enhances the mechanical and surface properties of scaffolds; (2) zonal analysis of scaffolds showed region-specific variations in chondrocyte number, sulfated GAG-rich extracellular matrix and chondrocytic gene expression; (3) smaller porogens (0.03 mm^3) yield higher GAGs accumulation and aggrecan gene expression.

There are other studies focused on calcified cartilage zone, which provides mechanical integration between articular cartilage and subchondral bone. W.D. Lee *et al.* [173] developed tissue-engineered osteochondral-like constructs with bone marrow stromal cells (BMSC), as single cell source. Cartilage tissue and a porous bone substitute substrate were formed with an interfacial zone of calcified cartilage. The authors found that the presence of calcified cartilage increased the shear load that the construct may withstand at the interface. However, preclinical studies are needed to determine if these osteochondral-like constructs could repair joint defects *in vivo*.

It is important to understand the multi-scale biomechanical behavior of cartilage tissue, in order to realize the connection among joint kinematics, tissue-level mechanics, cell mechanics and mechanotransduction, matrix mechanics and the nanoscale mechanics of matrix macromolecules. Therefore, understanding mechanical behavior at each scale helps to correlate cell biology, matrix biochemistry and tissue structure/function of cartilage (**Figure 7**).
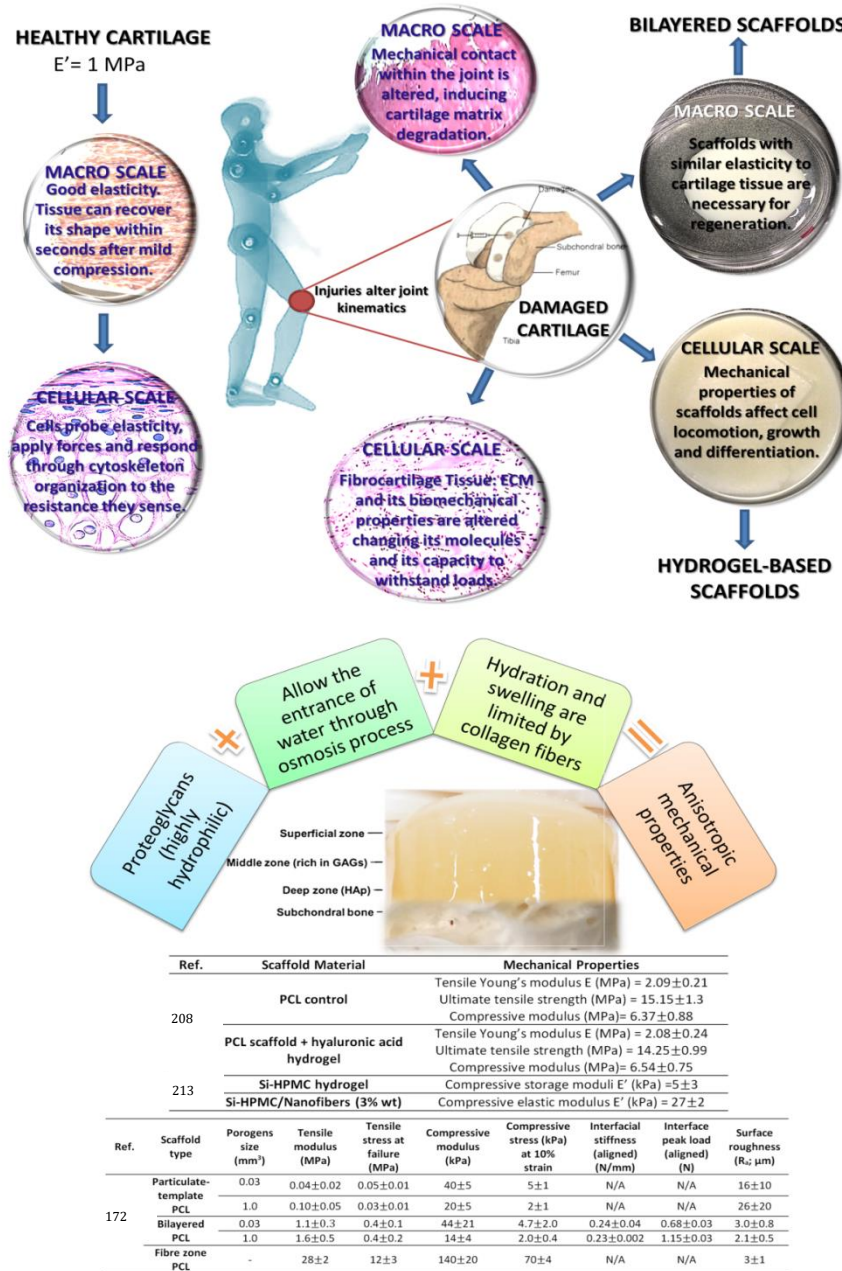
Figure 7. Correlation among the multi-scale biomechanical behavior of cartilage tissue [14].

Evaluating cell-free and cell-based hydrogels reviewed above, only a few of these biomaterials have been used in clinical applications [47, 48, 78, 174-177] because of four main unsolved problems in tissue engineering: (1) toxicity of some crosslinking agents [178]; (2) lack of mechanical integrity [159, 179-185]; (3) poor control of gelation kinetics [186, 187]; (4) unsuitable degradation kinetics [188-192].

Since some of the reactions used to synthesize hydrogels are limited due to their complexity, the use of cytotoxic reagents, instability of some functional groups, possible side reactions and low coupling efficiency, there is the need to explore and exploit simple and highly efficient methods which may be applicable to a great variety of biodegradable polymeric precursors.

1.3 POLYSACCHARIDE HYDROGELS VERSUS SYNTHETIC HYDROGELS

The degradation rate and mechanical properties of manufactured hydrogels must be compatible with the growth of new tissue [112]. As mentioned before, hydrogels can be made of either natural or synthetic polymers, each of them with advantages and disadvantages, or even a combination of both, whether or not a reduction of disadvantages from the individual components can be obtained. When using natural precursors, good biocompatibility and bioactivity are ensured in the hydrogel scaffolds. However, there will be a high degradation rate, in contact with body fluids or medium, and a limited mechanical behavior, since natural polymer components are extracted from tissues and subsequently reconstructed to form hydrogels [193, 194]. Nevertheless, the strength of these natural hydrogels can be increased by making the polymer matrix denser, using a chemical crosslinking or making chemical modifications. On the other hand, using synthetic precursors may provide appropriate physical and chemical properties for hydrogel scaffolds; however a good cell biological response and an adequate degradation rate may not occur [195, 196]. The strength of the synthetic hydrogels can be raised by changing the molecular weight of the starting polymers, increasing polymer concentration or even the degree of functionalization, using reactive groups during the crosslinking reaction.

1.3.1 MANUFACTURING TECHNIQUES AND THEIR INFLUENCE ON HYDROGEL PROPERTIES

Depending on the polymer precursors, hydrogels can be synthesized in different ways. In the first step a polymer is modified with a functional group; then the polymer is crosslinked, either physically or chemically, to form a three-dimensional structure. While chemical hydrogels are covalently crosslinked, physical hydrogels are not. Crosslinking can take place at the same time or after the copolymerization [197]. *In situ* crosslinked cytocompatible injectable hydrogels can be formed using: (1) non-toxic chemical crosslinkers, as in the Michael Addition Reaction, Click Chemistry, Schiff Base Reaction, and photo-crosslinking reactions; (2) enzymes for a biological crosslinking; (3) physical interactions, such as ionic and hydrophobic ones; (4) supramolecular chemistry utilizing self-assembly molecules [198].

The morphology and physico-chemical structure of hydrogels also depend on processing conditions applied during their formation, for example using electro spinning or cryogelation techniques. Hydrogel morphologies may range from fibrils, characteristic of protein-based hydrogels such as collagen and fibrin, to amorphous, characteristic of synthetic hydrogels such as PEG. When using the electrospinning technique, it is possible to obtain hydrogels with aligned fibrils morphologies. F. Mirahmadi *et al.* [199] added degummed chopped silk fibers and electrospun silk fibers to thermosensitive chitosan/glycerophosphate hydrogels, to reinforce scaffolds for hyaline cartilage regeneration. The results showed that mechanical properties of hydrogels were significantly enhanced; besides the composition of the scaffolds supported the chondrogenic phenotype. Nevertheless, when using cryogelation, because of ice crystals, a controlled porosity can be induced into hydrogels, helping them recovering their shape [200].

Another method to fabricate three-dimensional porous hybrid scaffolds for articular cartilage repair is combining freeze-dried [190, 201, 202] natural components with synthetic polymers, provide scaffolds with mechanical strength and an environment similar to natural ECM, to let chondrocytes proliferate. Lyophilization or freeze-drying technique produces highly porous structures with open pores throughout the scaffolds. The pores are introduced into the scaffolds, first by ice crystal formation, then by freeze-drying them. For this reason pore architecture reflects the ice crystal morphology [202]. Novel collagen/polylactide (PLA), chitosan/PLA, and collagen/chitosan/PLA hybrid scaffolds were fabricated by freeze-drying

technique [203]. It was observed that collagen binds water inside the scaffold structure and it helps cells to penetrate into the hybrid scaffolds.

To enhance anisotropic properties of cartilage scaffolds, aligned unidirectional pores can be formed depending on the real alignment of cells and the type of extracellular matrix that has to be repaired. Collagen-hybrid scaffolds, constructed by directional freezing, were studied. When varying freezing rates and suspension media, it is possible to obtain collagen-hybrid scaffolds with unidirectional pores, tunable pore sizes and pore morphologies [202]. The results demonstrated that directed horizontal ice dendrite formation and vertical ice crystal nucleation are responsible for aligned unidirectional ice crystal growth and, consequently, for aligned unidirectional pore structure of the collagen-hybrid scaffolds.

Since conventional fabrication techniques may not provide a precisely control of pore size, interconnectivity or pore geometry for scaffolds, solid freeform fabrication (SFF) techniques are now being used to produce 3D scaffolds with an organized interconnected pore structure which ensures good functionality and good mechanical strength, necessary to maintain new cartilage formation.

Bioprinting and plotting are being used as freeform fabrication techniques. These emerging techniques are used to fabricate viable 3D tissue constructs through a precise deposition of cells in hydrogels [204]. However, scaffolds, fabricated by these printing systems, often lack of flexibility and adequate mechanical properties [141, 205]. T. Xu *et al.* [206] described the construction of a hybrid inkjet printing/electrospinning system that can be used to fabricate viable cartilage engineered tissue. They fabricated a five-layer construct, 1 mm thick, made of electrospun polycaprolactone fibers alternated with inkjet printing of rabbit elastic chondrocytes suspended in a fibrin-collagen hydrogel. One week after printing, evidence showed more than 80% of cell viability, cell proliferation and formation of cartilage-like tissue in the five-layer construct, both *in vitro* and *in vivo* assays, and demonstrated an improvement of mechanical properties, in comparison with printed alginate or fibrin-collagen hydrogels.

Novel techniques of tissue scaffold fabrication, as ultrafast pulse DLW lithography, are attractive due to their 3D structuring capability, spatial resolution, scaling flexibility and diversity of working materials.

1.3.2 DEGRADATION KINETICS, PHYSICAL PROPERTIES (APPLICABILITY) AND BIOLOGICAL EFFECTS

Hydrogels degradation kinetics should be compatible with new tissue formation kinetics, in order to ensure a good integration of the construct. If hydrogels degrade very fast, it will trigger occurrence of defects in the formed tissue, such as cysts. On the other hand, if a very slow degradation occurs, hydrogels will inhibit the formation of new biological material and their integration with the surrounding tissue.

Degradation of hydrogels can take place by either hydrolytic or enzymatic mechanisms. The hydrolytic degradation happens when hydrogel is kept in contact with fluids by breaking the polymer chains or the crosslinked network. This type of degradation mechanism can be controlled by limiting the amount of degradable precursor, used to synthesize hydrogels. The enzymatic degradation is caused by cells when they begin to invade the hydrogel or when encapsulated cells within the hydrogel start to proliferate or migrate throughout it.

Many natural origin proteins have sites of cleavage in the protease, allowing hydrogels to degrade during the replacement of the ECM. This type of degradation may also depend on the degree and the type of chemical crosslinking in the hydrogels used as scaffolds [200].

1.3.3 SPECIFICITIES OF POLYSACCHARIDE – BASED HYDROGELS

When trying to manufacture biomimetic scaffolds for cartilage tissue regeneration, naturally-derived hydrogels are widely used, due to their macromolecular properties and because the employed biopolymers are part of the natural tissue that needs to be healed. Most of the studied naturally-derived hydrogels are based on biopolymers such as collagen, gelatin, chitosan, hyaluronic acid, chondroitin sulfate, agarose, alginate and fibrin [112, 207].

1.3.4 BIOLOGICAL RESPONSE OF POLYSACCHARIDE-BASED HYDROGELS

Since hyaluronic acid is a fundamental component of natural cartilage matrix, some studies have shown its importance and its good qualities as an excellent naturally derived polymer.

Injections of hyaluronan into osteoarthritic joints have proved to restore viscoelasticity, augment joint fluid flow, normalize endogenous hyaluronan synthesis, and provide joint function [112, 115]. Some other studies [197] have demonstrated that hyaluronic acid is favorable for cell response, by maintaining chondrogenic phenotype and increasing collagen type II production and angiogenesis during *in vivo* assays.

Another example of an excellent natural polymer is chitosan. Chitosan can easily form polyelectrolyte complexes with hyaluronan and chondroitin sulfate [115, 208]. X.Hu *et al.* [197] tried to mimic the natural cartilage extracellular matrix by synthesizing a biological hydrogel made of hyaluronic acid, chondroitin sulfate modified with 11-azido-3,6,9-tri-oxaundeca-1-amin and gelatin modified with propiolic acid, via click chemistry. Even though the molecular modifications made to the biopolymers let biological hydrogels have good response (making chondrocytes adhere and proliferate on them during *in vitro* assays), degradation process was too fast. They showed a loss of 45% w in 4 weeks, and a release of 20% w of gelatin and 10% w of chondroitin sulfate during the first two weeks, leading to macroscopic shrinkage of hydrogels.

Furthermore, when combining both naturally-derived and synthetically-derived polymers, adequate degradation kinetics and biological response can be achieved. H. Park *et al.* [132] created, by photocrosslinking, injectable hydrogels consisting of methacrylated glycol chitosan (MeGC) and hyaluronic acid. The photopolymerized hydrogels were cytocompatible. The incorporation of hyaluronic acid increased cell proliferation while encapsulated chondrocytes improved the cartilaginous extracellular matrix production.

Following the same guideline, based on fabricating a hybrid scaffold containing both biological and synthetic components, B. R. Mintz *et al.* [208] studied a hybrid scaffold, made of a hyaluronic acid-based hydrogel combined with a porous poly(ε-caprolactone) material. They tried to understand better the interface and the potential for integration between tissue engineered cartilage scaffolds and surrounding native tissue. They noticed that precursors provide a microenvironment which supports chondrocyte infiltration and proliferation, while maintaining seeded phenotype and structural integrity over a 6-week culture period.

1.4 FUTURE TRENDS: FROM COMBINATION OF MATERIALS TO HYBRID HYDROGELS

Identified problems hindering the application of hydrogels in cartilage regeneration, as described along this paper, include: mechanical properties [209] and mechanical instability [208, 210]; dedifferentiation of chondrocytes [166]; toxicity of some of the used crosslinking agents [178]; poor control of gelation kinetics [186, 187]; unsuitable degradation kinetics [188-192]. **Figure 8** illustrates the combining requirements needed to create materials with biomimetic features.
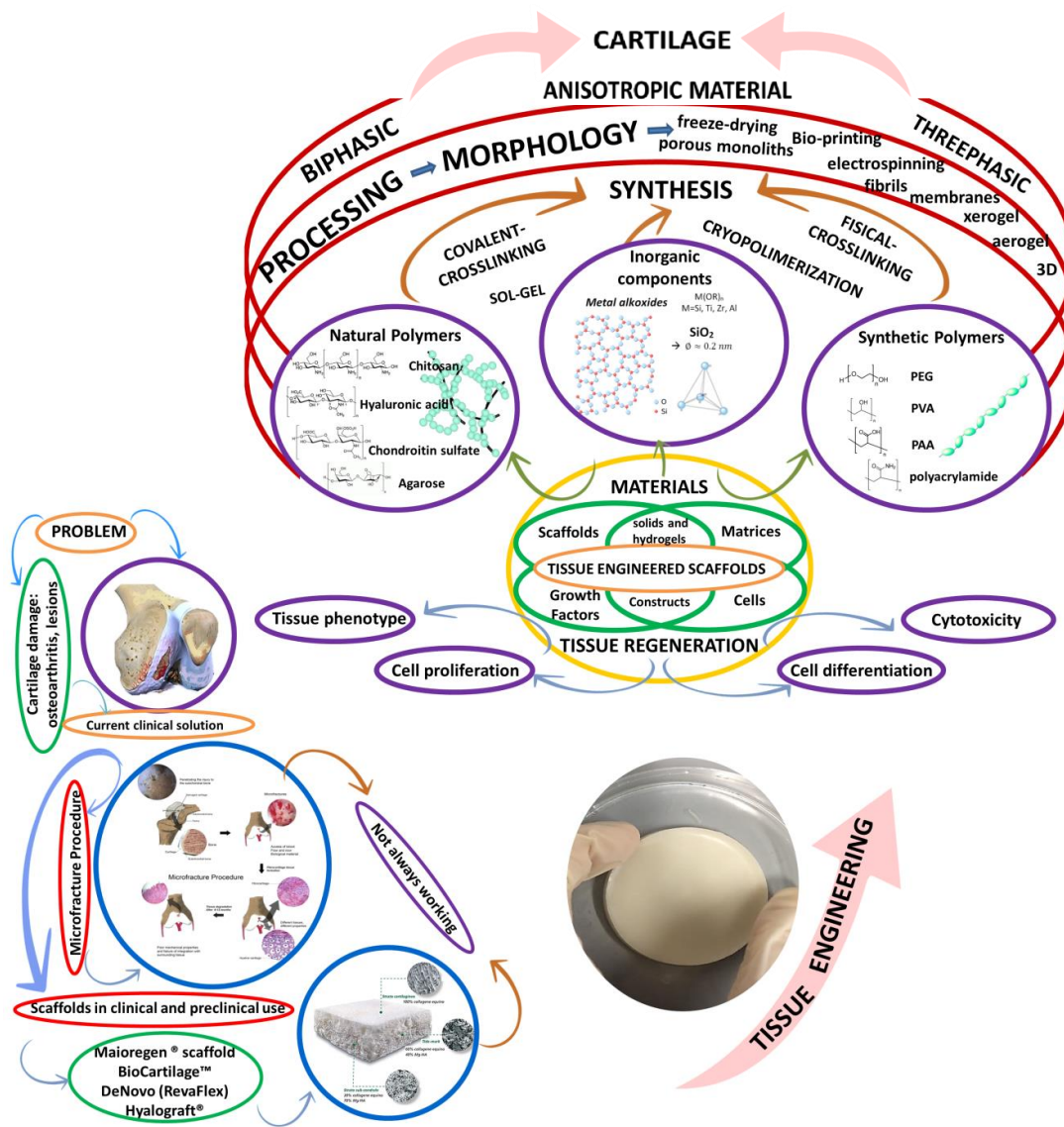
Figure 8. Correlation between current cell-based scaffolds used for cartilage regeneration [14].

Mechanical instability inhibits the integration of hydrogels with the surrounding native cartilage tissue when they are implanted [208, 210]. In order to synthesize mechanically stable hydrogels and improve their mechanical properties, several options have been proposed. One of the most promising options relays on the principle that materials combination must show the ability to support matrix formation [209], as demonstrated by K.W.M Boere *et al.* [84]. In this research, it was determined that, when grafting two materials covalently (a 3-D-fabricated poly(hidroxymethylglycolide–*co*–ε–caprolactone)/poly(ε-caprolactone) thermoplastic polymer scaffold, functionalized with methacrylate groups and covalently linked to a chondrocyte-laden gelatin methacrylamide hydrogel), the binding strength between the materials improved significantly, resulting in the enhanced mechanical integrity of the reinforced hydrogel. Embedded chondrocytes in hydrogel scaffolds also showed significant cartilage-specific matrix deposition, both *in vitro* and *in vivo* assays.

Another promising option to enhance mechanical stability is by regenerating cartilage and bone tissue simultaneously using a two-phased scaffold, since ceramic-to-bone interface has a better and faster integration compared to hydrogel-to-cartilage interface [84]. Additionally it has been observed that bone integration is much faster than cartilage integration, occurring during 2 and 24 weeks after transplantation, respectively.

It is possible to have a stable fixation of a cartilage scaffold by exploring a fixation technique with the subchondral bone [205]. One way to accomplish this stable fixation is fabricating an osteochondral scaffold which facilitates fixation and integration with the surrounding cartilage tissue, accelerating the repair of defected articular cartilage when implanted. The general idea is that bone scaffolds act as anchors, providing mechanical stability for cartilage tissue regeneration, besides, the join between the bone component and the cartilage component should be strong enough to prevent dislocation or delamination on *in vivo* environment. In order to follow the theory mentioned above, Y.-J. Seol *et al.* [205] reinforced osteochondral scaffolds by developing combined scaffolds, made of hydrogel scaffolds anchoring to cartilage tissue and ceramic scaffolds anchoring to bone tissue. For *in vivo* assay, the combined scaffolds were press-fitted into osteochondral tissue defects, in rabbit knee joints. Hydrogel scaffolds and combined scaffolds were compared. After 12 weeks, *in vivo* experiments demonstrated that regeneration of osteochondral tissue, especially articular cartilage tissue regeneration, was better with combined scaffolds than with hydrogel

scaffolds. Hydrogel scaffolds could not keep their initial position, suggesting that ceramic scaffolds in combined scaffolds provided mechanical stability for hydrogel scaffolds.

Moreover, G. Camci-Unal *et al.* [201] realized that combined hydrogels can be biologically and physically tuned to yield within a range of different cell responses and, according to these responses, combined hydrogels may show potential therapeutic possibilities to treat either chondral or osteochondral lesions.

Following this trend, S.S. Yang *et al.* [141] developed a 3D plotting system to manufacture a biphasic graft which consists of cartilage and subchondral bone for application to osteochondral defects. A combined material (PLGH/alginate) was fabricated as supporting structure to induce a mature osteochondral graft. Cartilage-derived ECM or hydroxyapatite substances were blended with alginate and plotted together with human fetal cartilage-derived progenitor cells, either in the cartilage layer or in the subchondral bone one. The plotted biphasic osteochondral graft showed good integration between layers because no structural separation was observed, while there was dominant cartilage and bone tissue formation during differentiation assay. One of the limitations of using the osteochondral approach in combination with bone marrow derived MSCs is their terminal differentiation, as they seem to follow an endochondral ossification which can arrest differentiation at a stable cartilage hyaline-like phenotype during the chondrogenic process. For this reason, a chondrogenic stimulator, such as the recently described kartogenin which regulates Runx1 expression [211], has to be incorporated with a known inducer of chondrogenic differentiation and a suppressor of hypertrophy.

Another alternative to fulfill the inadequate mechanical strength of hydrogel is constructing a solid-supported thermogel, comprising hydrogel systems or demineralized bone matrix. H. Huang *et al.* [212] combined chitosan thermogel with demineralized bone matrix to produce solid-supported hydrogel scaffolds. This type of scaffolds provided sufficient strength for cartilage regeneration. They retained homogeneously more bone-derived mesenchymal stem cells (BMSCs) and they proved to have superior matrix production and chondrogenic differentiation in comparison with pure hydrogels and demineralized matrix by their own.

Using fibers of different natural materials to reinforce hydrogels is another way to offer mechanical strength to hybrid scaffolds [204, 210]. Mechanical characteristics can be improved or modified using different strategies: (1) varying the number of fiber layers in the laminate; (2) combining different kinds of fibers and nanofiber sheets; (3) modifying crosslinking degree of hydrogels and fibers; (4) changing fibers content and surface treatment; (5) shifting fiber orientation.

Fibers anisotropy is an excellent property to reach strong mechanical reinforcement at low charge levels. For example, N. Buchtová *et al.* [213] developed an injectable hydrogel based on a silanized cellulose derivative: hydroxypropyl methylcellulose interlinked with silica fibers. They proved that the compressive modulus of the hydrogel could be tunable, depending on the covalent bonding between biopolymer and silica fibers. In other approaches, the incorporation of bioactive species, such as cells, growth factors, peptides and proteins into the materials, is proposed to improve hydrogel scaffolds properties [77, 214].

It can be deduced, from the reviewed studies, that combination of components yield up reinforced mechanical properties. However, to overcome the other requirements mentioned above, something different has to be done from the already investigated methods to fabricate materials. In author's opinion, there is a barely explored alternative in material science: studying the potential of hybrid hydrogels based on natural polymers and inorganic components. Hybrids are considered to be materials formed by two components bonded at a molecular level. Commonly one of these components is organic and the other one is inorganic. The new hybrid materials (**Figure 9**) may show superior characteristics in comparison with the two component phases. This possibility may offer a great potential to design new materials with the complex properties required for cartilage regeneration.

Since degradation rate and mechanical properties can be fine-tuned through chemical and/or physical modifications on either naturally or synthetically derived scaffolds, an excellent opportunity is given to hybrids to emerge as a promising solution for cartilage regeneration. When fine-tuned, hybrids can acquire amorphous, semicrystalline, hydrogen-bonded or supramolecular physical structures [112, 209].
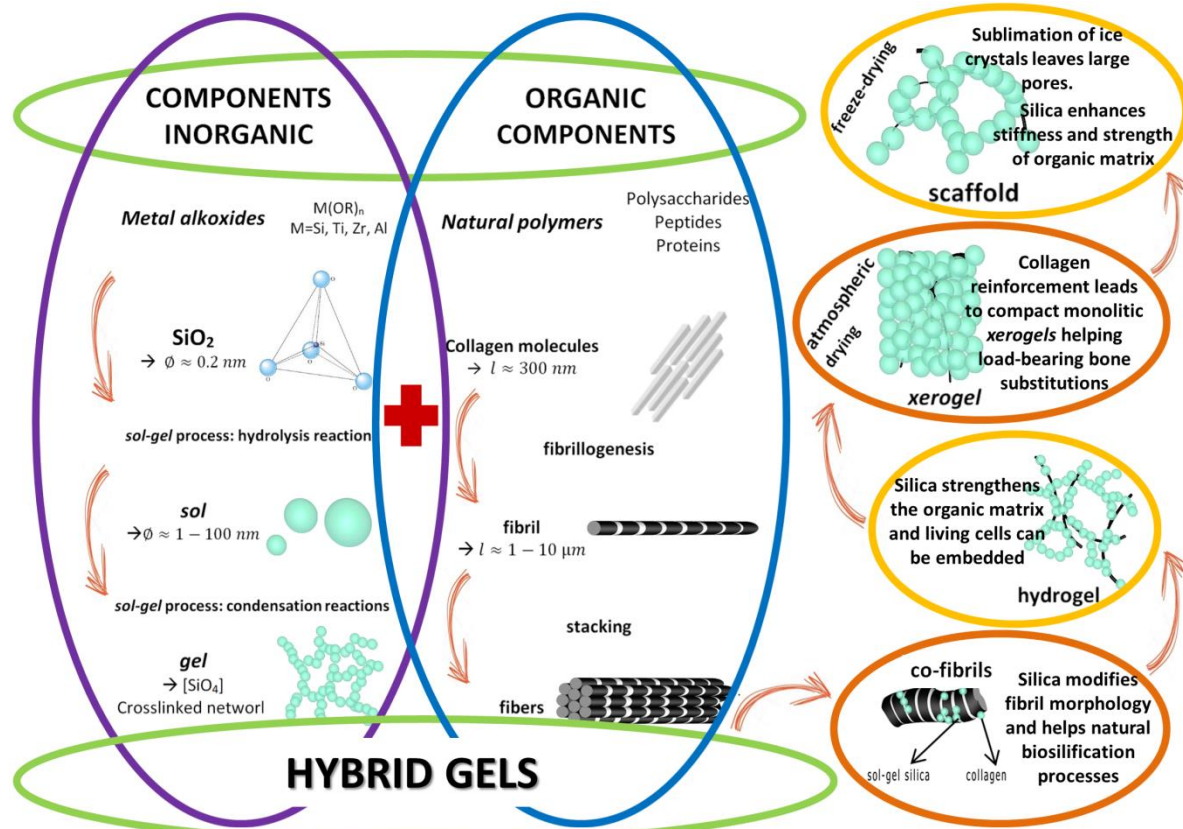
Figure 9. Advantages of hybrid *gels*. From soft mineralized hydrogels to hard compact *xerogels* [14].

Hydrogels made from purely organic precursors are being used as viable materials for cartilage repair due to their ability to retain grate portions of water, swollen, distend and exhibit large changes of dimensions (volume changes of several- to 10-fold are common) [215, 216]. These characteristics provide hydrogels with a low interfacial tension with water and other fluids, allowing them to reduce mechanical friction between tissues during implantation.

The hydrophilic characteristics of hydrogels are caused by the presence of special hydrophilic molecules ($-OH, -CONH, CONH_2$ and $-SO_3H$) found in the polymeric components. These molecules give hydrogels different absorption potential [215] and the ability to respond to a range of different stimuli, including temperature, pH, salt, specific (bio)chemical signals, and electric fields [216]. Nevertheless, hydrogels, based on a certain type of precursors, undergo uniform volumetric expansion and contraction, in response to several stimuli; therefore, the great added value of hybrid hydrogels is combining their precursors potential and restrictions. For example, to determine their degradation kinetics

and enhanced biological and mechanical properties, it is possible to use: stiffer components like silica-based materials, which restrict swelling in hydrogels in certain positions or directions; or natural polysaccharide-based polymers hybridized with inorganic materials (hydroxyapatite, SiO_2, or demineralized bone matrix), which restrict the number and type of hydrophilic molecules.

A further step may be the integration of nanotubes with different chemical composition into hybrid scaffolds which may provide them with bioactive and mechanical properties. This is the case of three-dimensional porous collagen sponges where single-walled carbon nanotubes are incorporated into [217]. The incorporation of single-walled carbon nanotubes improved cell proliferation and GAGs production in the *in vivo* microenvironment, because nanotubes were internalized by cells, with benefit for controlled and localized delivery of biological factors. Another study is the design of a biomimetic nanostructured composite cartilage scaffold, via biologically-inspired rosette nanotubes (RNTs) and biocompatible non-woven poly (L-lactic acid) (PLLA) [218]. It was concluded that, RNTs have a similar morphology with native collagen fibers when self-assembled in aqueous conditions, and besides they increase glycosaminoglycan, collagen and protein production; their nanotopography and surface chemistry enhance chondrogenic differentiation. Another study tested the biocompatibility of 3D artificial hexagonal-pore shaped hybrid organic-inorganic microstructured scaffolds in a rabbit model [219].

The association of silica and polysaccharides within composites or hybrids has demonstrated therapeutic benefits in a wide range of bio-inspired silica-collagen materials [220]. Although this kind of materials has been prepared over nearly 15 years, their application in cartilage regeneration treatments has not been exploited. The great value of hybrid materials (**Figures 7, 8**) is that it can be synthesized a large variety of structures and properties, from soft mineralized hydrogels to hard compact *xerogel,* depending on the soft (cartilage) or hard (osteochondral) tissue wanted to be repaired or regenerated.

Moreover, to fully comprehend these potential materials and to raise their value for the development of innovative biomedical devices for cartilage regeneration, it is important studying the interplay between the organic-inorganic precursors, which is to follow carefully the polymer self-assembly process and the inorganic condensation mechanisms. Therefore, biological, mechanical and degradation properties can be modulated, guaranteeing bioactivity, cytocompatibility, and an eventual biocompatibility.

MATERIALS AND METHODS

2.1 EXPERIMENTAL DEVELOPMENT

In this chapter, synthesis, modification and crosslinking of polysaccharide-based hybrid hydrogels are detailed. Techniques and equipment used for the characterization and determination of physical, chemical, mechanical, degradative and biological properties are described. The experimental development of synthesis and characterization of hybrid hydrogels is carried out as shown in **Figure 10**.
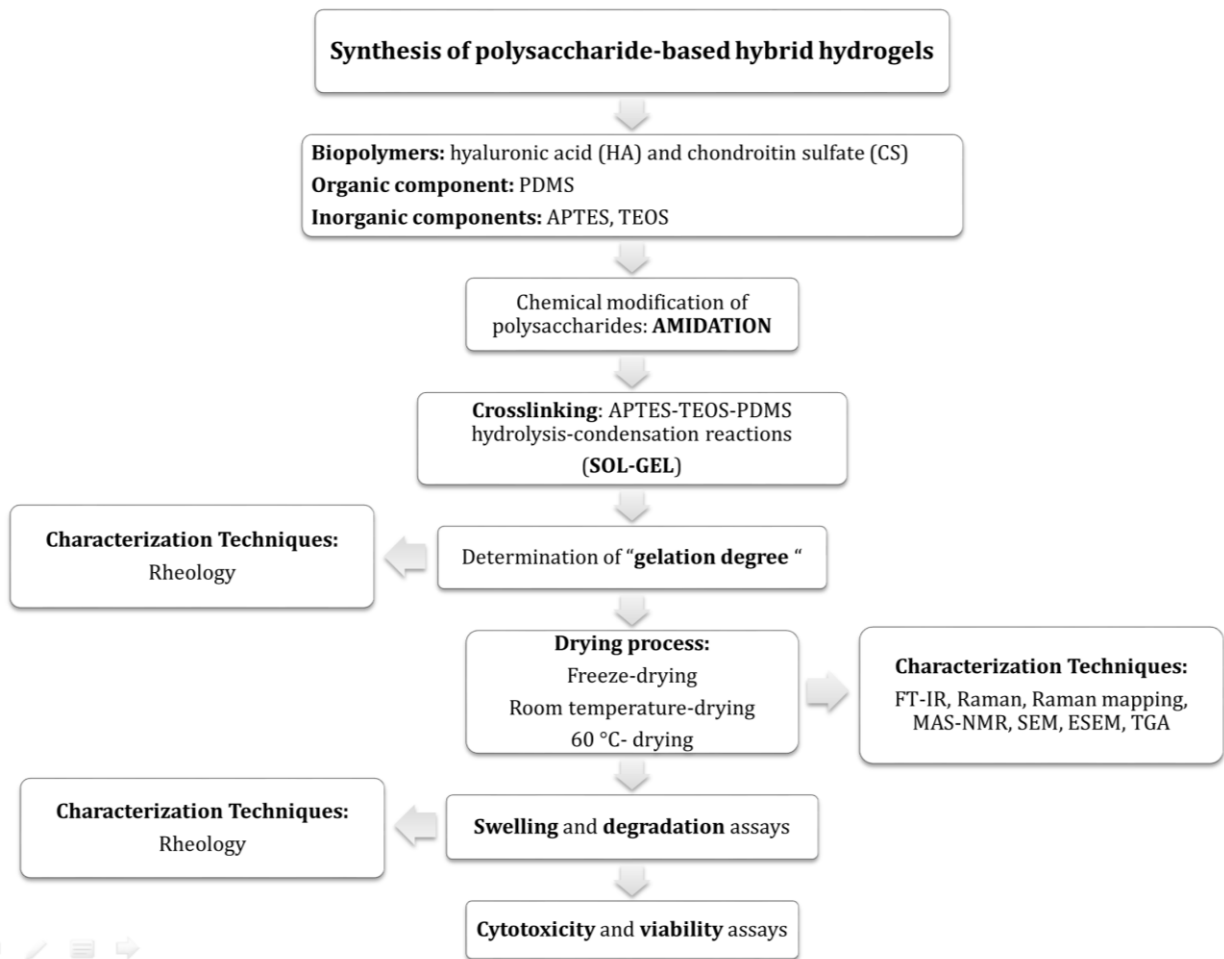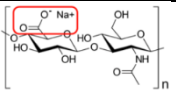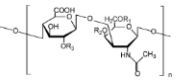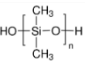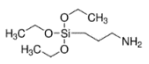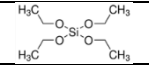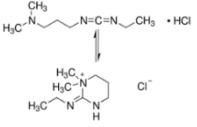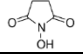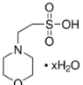
Figure 10. Experimental development to obtain polysaccharide-based hybrid hydrogels.

2.2 SYNTHESIS OF THE POLYSACCHARIDE – BASED HYBRID HYDROGELS

A synthesis process was developed to modulate degradation kinetics and to improve biological, mechanical and rheological properties of hyaluronic acid (HA) and chondroitin sulfate (CS). This process allows the hybridization and crosslinking of polysaccharides with the following organic-inorganic compounds: 1) polydimethylsiloxane (PDMS); 2) 3-aminopropyltriethoxysilane (APTES); 3) tetraethylorthosilicate (TEOS). The inorganic components restrict swelling and the number of hydrophilic molecules within polysaccharides, decreasing their degradation rate and increasing resistance to manipulation. The chemicals used to synthesize the polysaccharide-based hybrid hydrogels are shown in **Table 2**.

Table 2. Chemical reagents used during synthesis process.

Table 1. **Chemical reagents used during synthesys process.CHEMICAL NAME**	**SHORT NAME**	**STRUCTURE**	**MW** $\left(g/mol\right)$	**DENSITY** $\left(g/cm^3\right)$	**PURITY**	**TRADE MARK**
Hyaluronic acid sodium salt $(C_{14}H_{21}NNaO_{11})_n$	HA		403.316	--	--	BioIberica
Chondroitin Sulfate sodium salt $(C_{14}H_{22}NNaO_{16}S)_n$	CS		515.371	--	--	BioIberica
Polydimethylsiloxane hydroxyterminated $HO(SiC_2H_6O)_nH$	PDMS		550	0.95	100%	Sigma-Aldrich
3-aminopropyl Triethoxysilane $H_2N(CH_2)_3Si(OC_2H_5)_3$	APTES		221.37	0.946	$\geq$ 98%	Sigma-Aldrich
Tetraethylorthosilicate $Si(OC_2H_5)_4$	TEOS		208.33	0.933	98%	Sigma-Aldrich
N-(3-Dimethylaminopropyl)-N'ethylcarbodiimide hydrochloride $C_8H_{17}N_3 \cdot HCl$	EDC		191.70	--	$\geq$ 98%	Sigma-Aldrich
N-Hydroxysuccinimide $C_4H_5NO_3$	NHS		115.09	--	98%	Sigma-Aldrich
2-(N-Morpholino) ethanesulfonic acid hydrate $C_6H_{13}NO_4S \cdot xH_2O$	MES		195.24 (anhydrous basis)	--	$\geq$ 99.5%	Sigma-Aldrich

2.2.1 CHEMICAL MODIFICATION AND CROSSLINKING OF POLYSACCHARIDES

The hybridization process requires two stages:

a) *Chemical modification and hybridization* of hyaluronic acid sodium salt (HA), **Figure 11,** and chondroitin sulfate sodium salt (CS), **Figure 12,** by amidation of their carboxyl groups (R-COO$^-$Na) with the amine group (-NH$_2$) of 3-aminopropyltriethoxysilane (APTES). Amidation takes place when N-(3-Dimethylaminopropil)-N'ethylcarbodiimide hydrochloride (EDC) activates the carboxyl group for the coupling of the primary amine in APTES to form the amide bond (C=N). EDC is commonly used in combination with N-hydroxysuccinimide (NHS) which acts as a carboxylic acid activating agent. To keep an acid pH in the solution, necessary for the amidation reaction to happen, 2-(N-Morpholino)ethanesulfonic acid hydrate (MES) is used as buffer agent. MES presents minimal variations to salts, its pKa changes minimally with temperature and it is chemically and enzymatically stable.
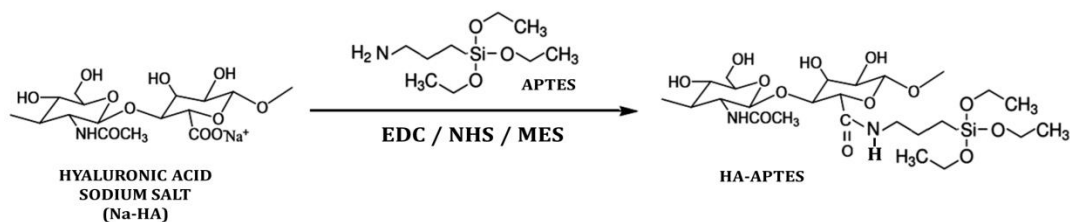
Figure 11. Chemical modification and hybridization of hyaluronic acid sodium salt.
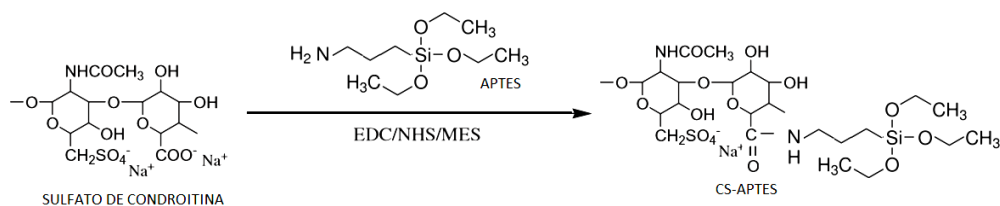
Figure 12. Chemical modification and hybridization of chondroitin sulfate sodium salt.

b) *Crosslinking* of hyaluronic acid sodium salt (HA), **Figure 13,** and chondroitin sulfate sodium salt (CS), **Figure 14,** by forming a hybrid hydrogel with a three dimensional PDMS-modified SiO$_2$ organic-inorganic matrix. *Sol-gel* method is used to form the 3D

hybrid matrix. In this method, the hydrolysis-condensation reactions occur among the inorganic modifier (APTES), the silica alkoxide (TEOS) and the silicon (PDMS).
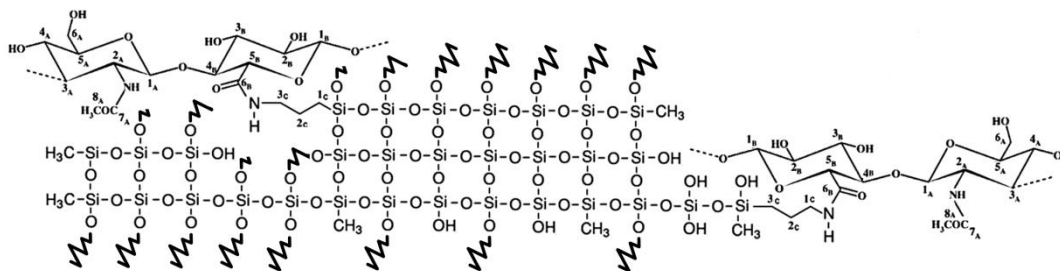
Figure 13. Crosslinking of hyaluronic acid by a PDMS-modified SiO_2 organic-inorganic matrix.
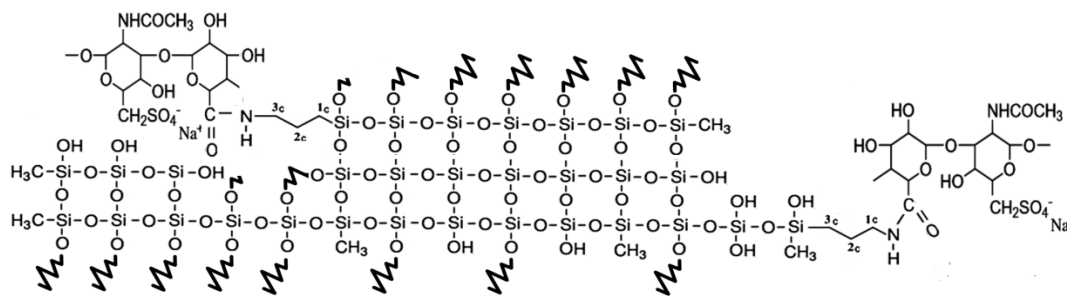
Figure 14. Crosslinking of chondroitin sulfate by a PDMS-modified SiO_2 organic-inorganic matrix.

2.2.2   PREPARATION OF POLYSACCHARIDE – BASED HYBRID SCAFFOLDS

Polysaccharide-based hybrid hydrogels are prepared in two steps: 1) chemical modification and hybridization *via* amidation and 2) crosslinking *via sol-gel* method, as shown in **Figure 15**. After optimization of the chemical modification reaction of polysaccharides, four concentrations of polysaccharide aqueous solutions are studied:

1) For hyaluronic acid solutions: $\left[67\,^{mg}/_{ml}\right]; \left[50\,^{mg}/_{ml}\right]; \left[33\,^{mg}/_{ml}\right]$

2) For chondroitin sulfate solutions: $\left[100\,^{mg}/_{ml}\right]$

The sample code of each hybrid hydrogel is assigned according to: 1) polysaccharide concentration solution; 2) pH in synthesis process; 3) type of drying process; for example: 1) **67HA − 6RT** hybrid hydrogel stands for $\left[67\,^{mg}/_{ml}\right]$ of **HA** synthesized at $pH = 6$ and dried at **room temperature**; 2) **33HA − 7T** hybrid hydrogel stands for $\left[33\,^{mg}/_{ml}\right]$ of **HA** synthesized at $pH = 7$ and dried at a **temperature** of 60 ℃.
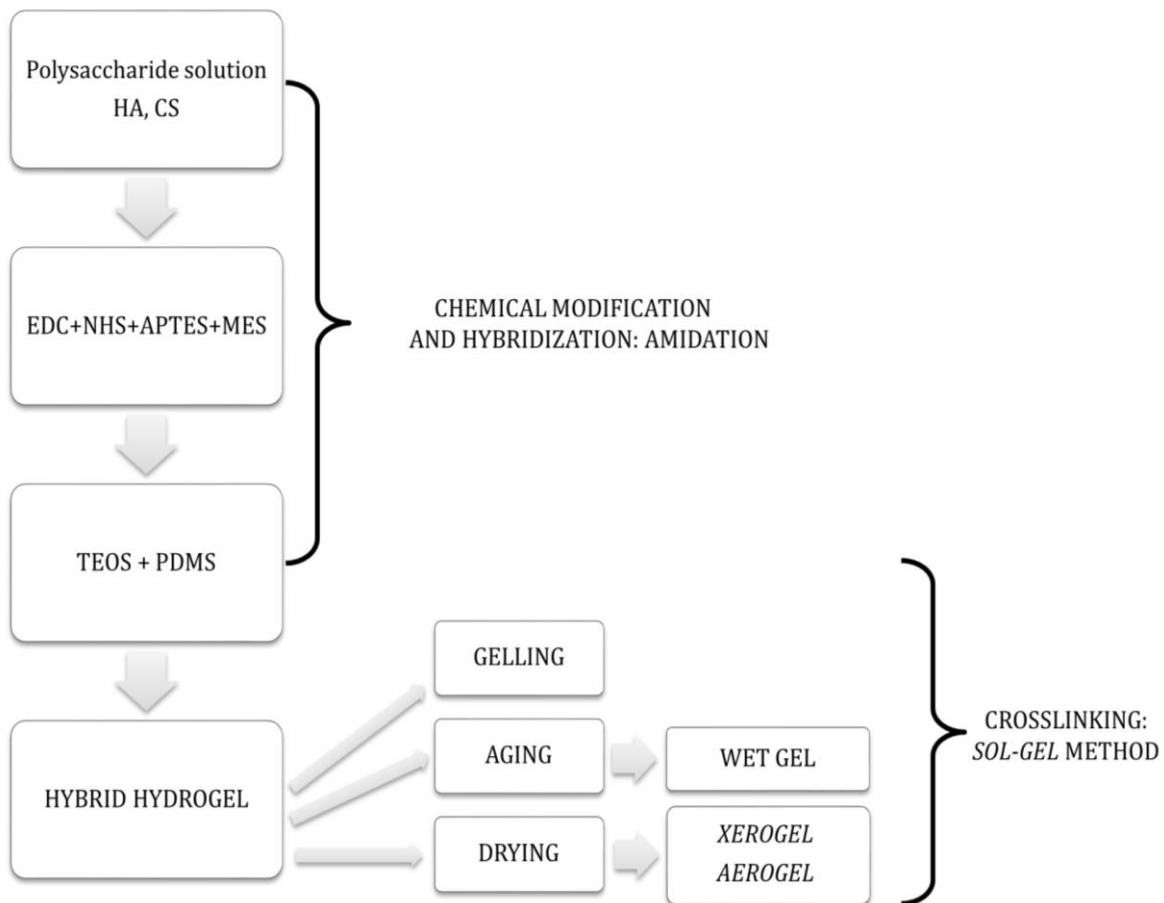
Figure 15. Synthesis procedure of polysaccharide-based hybrid hydrogels.

2.3 CHARACTERIZATION OF POLYSACCHARIDE – BASED HYBRID HYDROGELS

Several characterization techniques are used to evaluate and analyze the hybrid hydrogels: 1) Fourier Transform Infrared Spectroscopy; 2) Raman Spectroscopy; 3) Nuclear

Magnetic Resonance; 4) Scanning Electron Microscopy; 5) Environmental Scanning Electron Microscopy; 6) Thermogravimetric Analysis; 7) Rheology; 8) MTT assay;9) Alamar Blue Assay.

2.3.1 STRUCTURAL CHARACTERIZATION

Structural characterization techniques are used to monitor polysaccharide chemical modification and crosslinking reactions. These characterization techniques help to comprehend the chemical structure of the hybrid hydrogels by identifying functional groups and bond types.

2.3.1.1 FOURIER – TRANSFORM INFRARRED SPECTROSCOPY (FTIR)

FT-IR spectra were obtained at room temperature in a Perkin Elmer Spectrum Two spectrometer coupled with and Attenuated Total Reflection, Perkin Elmer (ATR-FTIR). Spectra are recorded in transmittance mode in the range from 400 to 600 cm^{-1} by 16 scans and with a resolution of 4 cm^{-1}. The samples (hydrogels in powders) did not need previous preparation for the measurements.

2.3.1.2 RAMAN SPECTROSCOPY AND RAMAN MAPPING

Raman spectra were carried out in a Renishaw InVia Reflex Raman system (Renishaw plc, Wotton-under-Edge, UK), consisting of a grating spectrometer with a Peltier-cooled charge-coupled device (CCD) detector, coupled to a confocal microscope. The Raman scattering was excited using a diode laser at a wavelength of 785 nm. The laser beam was focused on the sample with a 0.85 x 100 microscope objective. The laser power was 160 mW, the exposure time was three seconds and the number of accumulations for the Raman measurements was two. The spectra were processed using Renishaw WiRE 3.3 software.

For Raman mapping, samples were struck by a 785 nm laser for 5 hours in order to obtain Raman spectra. Samples were scanned using a 0.75 x 50 microscope objective. The spot size in each sample was 1.277 μm. The acquisition time was 1 second and 20 accumulations were performed per spot.

2.3.1.3 MAGIC ANGLE SPINNING – NUCLEAR MAGNETICRESONANCE

The solid-state MAS-NMR spectra were obtained with a Bruker Advance TM 200WB spectrometer equipped with a wide-mouth superconducting magnet (89 mm) operating at 9.4 Teslas with a frequency of 400 MHz. The purpose is to study $Q, D,$ and T structural units in the three-dimensional organic-inorganic networks of the polysaccharide-based hybrid hydrogels.

2.3.2 MORPHOLOGICAL CHARACTERIZATION

These techniques, SEM and ESEM, were used to observe and analyze: 1) the morphology of the designed polysaccharide-based hybrid hydrogels after drying processes; 2) their swelling process when being hydrated; 3) their adherence to PCL scaffolds; 4) the hydrolytic degradation process after being soaked into PBS during acellular degradation tests.

2.3.2.1 SCANNING ELECTRON MICROSCOPY (SEM)

The morphological characterization of the polysaccharide-based hybrid hydrogels was performed in a high resolution JEOL Scanning Electron Microscope, model JSM6701F. The voltage used to take images at several magnifications was 15 kV and the working distance was 8 mm to prevent samples from being degraded due to their organic-inorganic character. The analyzed samples were adhered to a copper sample holder using graphite adhesive tape. A layer of gold-palladium was deposited on the samples to make them conductive. The metal deposition was carried out with a Sputter coater Polaron SC7640 with a gold target at 40 mA for 90 seconds.

2.3.2.2 ENVIRONMENTAL SCANNING ELECTRON MICROSCOPY (ESEM)

The environmental morphological characterization of the polysaccharide-based hybrid hydrogels was carried out in a Philips XL 30 Scanning Electron Microscope. The chosen dried hybrid hydrogel was zooming at 150X magnification at a working voltage of 15 kV. An increasing water pressure, from 0.6 torr to 7.2 torr, was applied to the sample in intervals of 30 seconds between each increasing pressure.

2.3.3 THERMAL CHARACTERIZATION

Polysaccharide-based hybrid hydrogels were thermally characterized to identify temperatures at which thermal decomposition occurs. This technique gives necessary

information to stablish synthesis, drying and sterilization temperatures in order to avoid an early degradation of the biopolymers.

2.3.3.1 THERMOGRAVIMETRIC ANALYSIS

Thermogravimetric analysis of hybrid hydrogels was performed on dried samples in a TA instrument, model TGA Q5000 V20.13. Samples were heated from 25 °C to 800 °C at a heating rate of 10 $^{\circ}C/_{min}$10°C/min, keeping a constant air flow of 10 $^{ml}/_{min}$.

2.3.4 RHEOLOGICAL CHARACTERIZATION

Rheological measurements of polysaccharide-based hybrid hydrogels were carried out using stress-controlled oscillatory rheometer ARG2 TA Instruments using parallel plate geometry. *Sol* samples were measured using 40 mm diameter top plate aluminum (Al) geometry. *Gel* samples were measured using 25 mm diameter steel plate geometry. Dynamic time sweep analysis was carried out in *sol* samples at 1.6% strain, ≈0.25 N normal forces, a frequency of 0.75 Hz and at 37 °C and 40-45 °C from 0 to 5000 seconds in order to analyze *sol-gel* transition time. Dynamical oscillatory frequency sweeps were carried out in *gel* samples (aging and swollen hydrogels) to determine the viscoelastic properties of polysaccharide-based hybrid hydrogels, by obtaining storage (G') (elastic behavior) and loss (G") (viscous behavior) moduli at different aging and soaking times. These measurements were performed at 37 °C with constant strain (0.1866%), setting normal force at ≈0.25 N and the frequency from 0.1 to 10 Hz.

2.3.5 SWELLING DEGREE

Wet and dried polysaccharide-based hybrid hydrogel samples were soaked into flasks with 20 mL of phosphate buffer solution ($pH = 7.4$) at 37 ± 0.5 °C. Four replica of each sample were tested.

Swelling degree (%S) is defined as shown in **Equation 1**:

$$\%S = \frac{W_t - W_0}{W_0} * 100$$ **Equation 1**

Where, W_t is the weight of the swollen hybrid hydrogels at time t and W_0 is the initial weight of the hybrid hydrogels. The equilibrium hydration degree, W_e, is defined as the value at which swollen degree is constant during three different times.

2.3.6   HYDROLYTIC DEGRADATION

Hydrolytic degradation of hybrid hydrogels was tested by soaking the sample into 20 mL of phosphate buffer solution (PBS) ($pH = 7.4$) at 37 ± 0.5 °C. Four replica of each sample were tested. The samples were soaked at intervals of 1, 3, 7, 14, 21, 28, 35 and 42 days and weight after being dried at 37 °C. Hydrolytic degradation was also followed by changes in pH. Weight loss was calculated as defined in **Equation 2**:

$$\%Weight\ loss = 100 - \frac{W_2}{W_1} * 100 \qquad\qquad \textbf{Equation 2}$$

Where, W_2 is the weight of the dried hybrid hydrogels after being soaked at time t and W_1 is the initial weight of dried hybrid hydrogels.

2.3.7   *IN VITRO* ASSAYS, CYTOTOXICITY AND CELL PROLIFERATION

Cytotoxicity (MTT assay) was carried out using fibroblast and mother cells. Cells were cultured at 37 °C in a humidified atmosphere under standard conditions (95% air and 5% CO_2) by using a semi-complete medium [Dulbecco's Modified Eagle Medium, Sigma (DMEM)]. For 500 mL of medium, 200 mM L-glutamine and 50 mg/mL gentamicin were added. Specimens were sterilized by soaking them into an ethanol-water (70%-30%) solution for 3 minutes and then immersed into sterile PBS to remove excess of ethanol. To start the assays, specimens were soaked into 5 mL of fresh sterile medium (DMEM) for 1, 2, 3, 4, 7, 10 and 14 days at 37 °C with continuous stirring. Once the materials ended the immersion time, the "old medium or eluent" was removed and frozen. Cells were seeded in 96-well culture plates at a density of 15×10^4 cell/mL per well with 100 μL of "old medium" and incubated at 37 °C for 24 hours. The "old medium" was replaced by 100 μL/well of MTT reagent, (3-[4,5-dimethylthiazol-2-yl]-2,5-diphenyltetrazolium bromide)-sodiumsuccinate, dissolved in PBS and then incubated at 37 °C for 4 hours. The excess of MTT reagent was removed and 100

μL/well of dimethyl sulfoxide was added to dissolve formazan crystals, which are formed by the reduction of the MTT reagent which reacts with the mitochondrial dehydrogenase, only present in living cells. The amount of formazan crystals is taken as an indicator of cell viability. Analysis of UV-vis at 570 nm of absorbance was measured using variance (ANOVA) equipment. The results were performed with respect to TMX=100% (control sample) at a significant level of $p < 0.05$.

The Alamar Blue® assay is designed to quantitatively measure cell proliferation. Using the REDOX indicator *resazurin* (oxidized form) is possible to spectrophotometrically measure the cellular proliferation. Resazurin is a blue and non-fluorescent reagent; thus, mearing the changes in the fluorescence of the dyed cells within the intracellular environment, modifications in the number of metabolic active cells can be detected. Cell proliferation (Alamar Blue® assay) was carried out using fibroblast cells. Cells were cultured at 37 °C in a humidified atmosphere under standard conditions (95% air and 5% CO_2) by using a semi-complete medium [Dulbecco's Modified Eagle Medium, Sigma (DMEM)]. Specimens were sterilized by soaking them into an ethanol-water (70%-30%) solution for 3 minutes and then immersed into sterile PBS to remove excess of ethanol. To start the assays, specimens were soaked into 5 mL of fresh sterile medium (DMEM) for 1, 4, 7 and 14 days at 37 °C. Once the materials ended the immersion time, the "old medium or eluent" was removed and frozen. Cells were seeded in 96-well culture plates at a density of 15×10^4 cell/mL per well with 100 μL of "old medium" and incubated at 37 °C for 24 hours. 100 μL/well of Alamar Blue® reagent was added directly to cells in "old culture medium" and then incubated at 37 °C for 4 hours, protected from direct light. To stop the reaction of Alamar Blue® reagent, 50 μL of 3% SDS was added. Analysis of UV-vis at 570 nm of absorbance was measured using variance (ANOVA) equipment. The results were performed with respect to TMX=100% (control sample) at a significant level of $p < 0.05$.

ANALYSIS AND DISCUSSION

3.1 CHEMICAL MODIFICATION AND HYBRIDIZATION OF POLYSACCHARIDES: MODIFICATION AND CROSSLINKING *VIA* CARBOXYL GROUP

Carbodiimides are used as activator agents of carboxyl groups. EDC is a water-soluble carbodiimide used to modify and crosslink proteins. EDC reacts with carboxyl groups to form O-acylisourea. When a primary amine acting as a nucleophile reacts with the O-acylisourea *via* nucleophilic attack, an amide and a soluble urea derivative (by-product) are formed; as shown in **Figure 16**. The reaction mechanisim between a primary amine and a carboxylic acid using a carbodiimide starts with the protonation of nitrogen in the carbodiimide. The nucleophiliic attack in the carboxylate anion is favored thanks to the reduced electron density in the central carbon of the carbodiimide. However, if the O-acylisourea, an unstable intermediate in aqueous solutions, is found in the absence of nucleophiles or it does not react with the primary amine, this unstable intermediate suffers a hydrolysis, then the carboxyl groups are regenerated and the stable N-acylisourea is formed *via* cyclic electronic displacement [221].
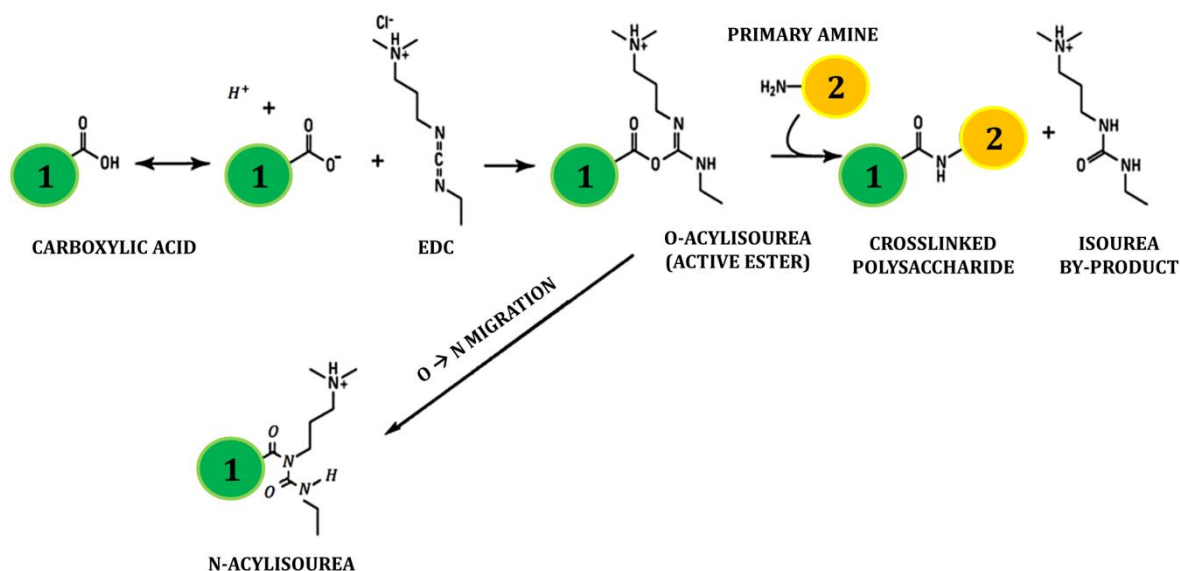
Figure 16. Reaction mechanism between (1) carboxylic acid and carbodiimide (EDC) with and without (2) amines. Molecules (1) and (2) can be peptides, proteins, polysaccharides or any molecule having a carboxyl and primary amino group.

To catalyze this type of chemical reactions, acidic conditions are needed. To achieve a better efficiency in the chemical modification of polysaccharides using EDC, the solution reaction must have pH values 4.5 - 6.5. Acidic conditions can be obtained using a buffer agent like MES or any buffer agents lacking of carboxylic acids and amines. Phosphate buffer solutions with neutral pH up to 7.2 can be used, although the reaction efficiency will be less. This disadvantage can be overcome by increasing the amount of EDC added to the reaction solution.

NHS is often used along with EDC in the coupling reactions to improve efficiency and create dry-stable intermediates (amino-reactants). EDC couples the carboxyl to NHS forming a NHS ester, which is considerably more stable than the O-acylisourea intermediate. The whole mechanism allow the primary amine to have an efficient conjugation at physiological pH, as shown in **Figure 17**.
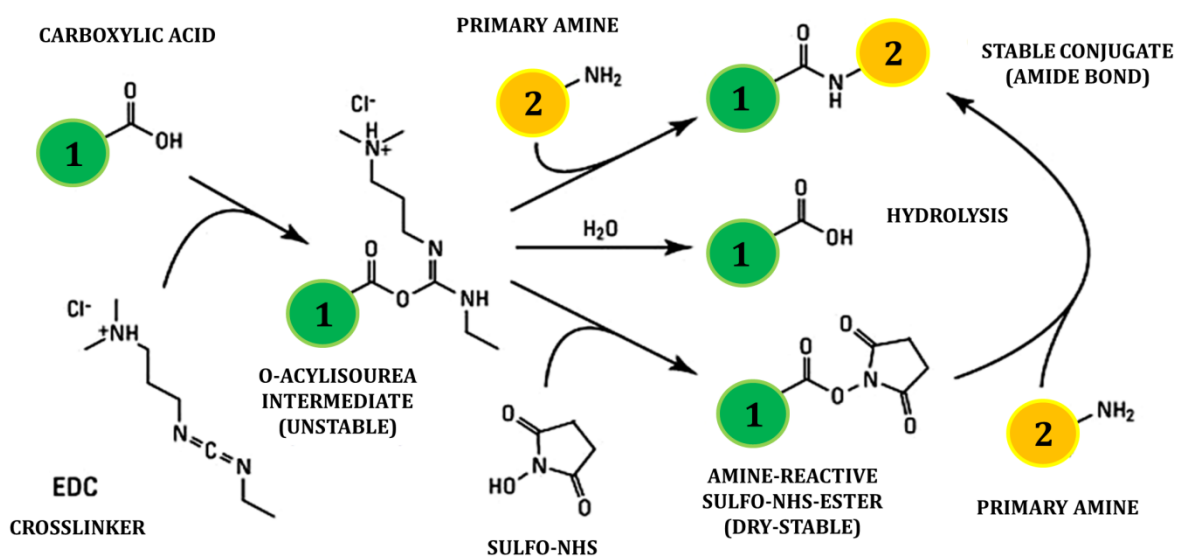
Figure 17. Reaction mechanism between (1) carboxylic acid and (2) the primary amine using NHS and carbodiimide (EDC). Molecules (1) and (2) can be peptides, proteins, polysaccharides or any molecule having a carboxyl and primary amino group.

3.1.1 AMIDATION OF HYALURONIC ACID SODIUM SALT, A CHEMICAL MODIFICATION *VIA* CARBOXYL GROUP

The amidation of hyaluronic acid salt is followed when an amine group ($-NH_2$) in APTES molecules couples to the carbonyl group (COO^-) in the hyaluronic acid sodium salt by using EDC and NHS as catalysts, as shown in **Figure 18**.
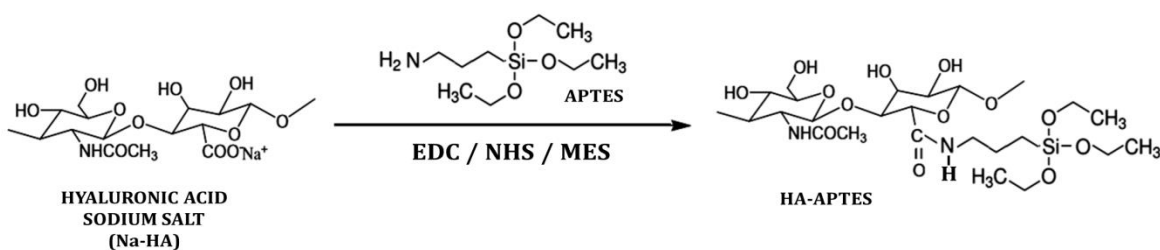
Figure 18. Amidation of hyaluronic sodium salt (Na-HA) with 3-aminopropyltriethoxysilane (APTES).

According to the reaction mechanism proposed in **Figure 17**, the amidation of hyaluronic acid sodium salt with APTES molecules occurs as follows (**Figure 19**):
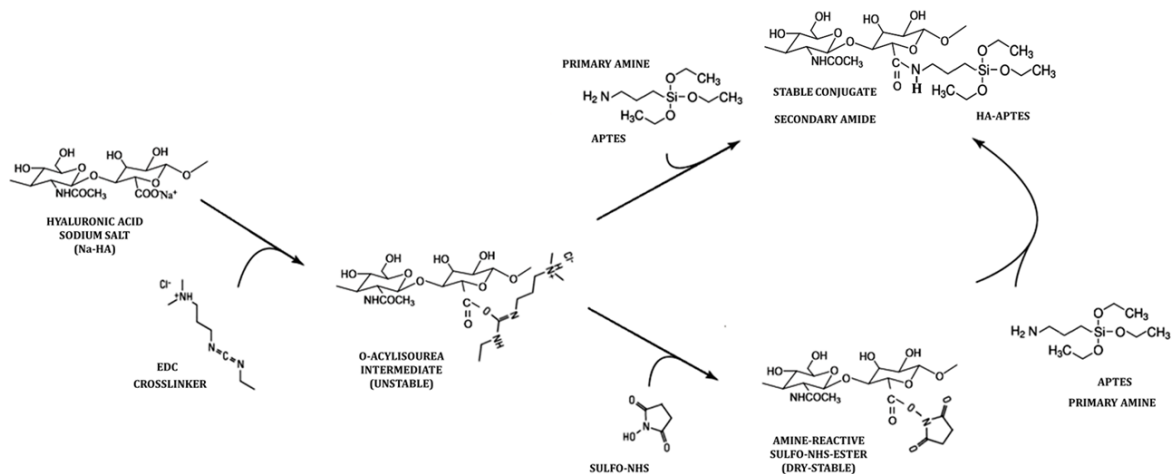
Figure 19. Reaction mechanism between hyaluronic acid sodium salt and APTES to using NHS and EDC.

3.1.2 AMIDATION OF CHONDROITIN SULFATE SODIUM SALT, A CHEMICAL MODIFICATION *VIA* CARBOXYL GROUP

The amidation of hyaluronic acid salt is followed when an amine group $(-NH_2)$ in APTES molecules couples to the carbonyl group (COO^-) in the hyaluronic acid sodium salt by using EDC and NHS as catalysts, as shown in **Figure 20**.
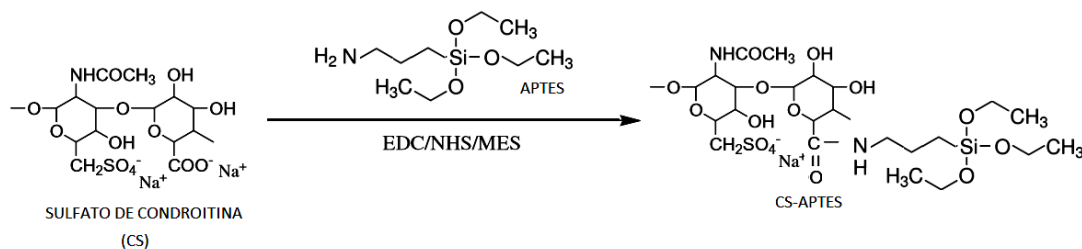
Figure 20. Amidation of chondroitin sulfate sodium salt (Na-CS) with 3-aminopropyl triethoxysilane (APTES).

According to the reaction mechanism proposed in **Figure 17**, the amidation of hyaluronic acid sodium salt with APTES molecules occurs as follows (**Figure 21**):
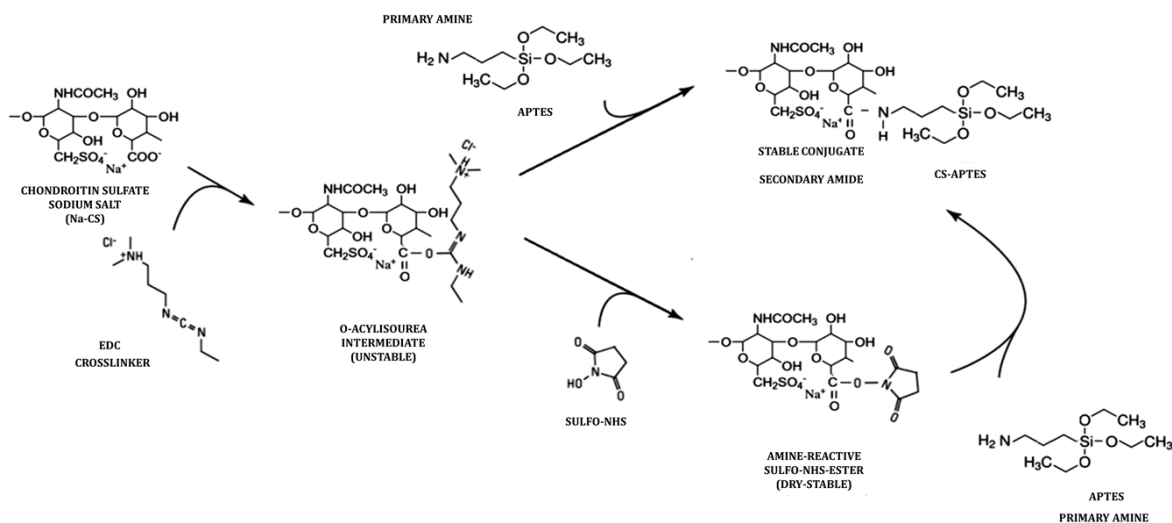
Figure 21. Reaction mechanism between chondroitin sulfate sodium salt and APTES using NHS and EDC.

3.1.3 CROSSLINKING OF POLYSACCHARIDES WITH A 3D PDMS-MODIFIED SiO₂ ORGANIC-INORGANIC MATRIX: A HYBRID HYDROGEL

Sol-gel method is used to form the 3D hybrid PDMS-modified SiO₂ organic-inorganic matrix to crosslink polysaccharides (hyaluronic acid sodium salt and chondroitin sulfate sodium salt). In this method, the hydrolysis-condensation reactions occur among the inorganic modifier (APTES), the silica alkoxide (TEOS) and the silicon (PDMS).

The modifier 3-aminopropyltriethoxysilane (APTES, $NH_2 - C_3H_7Si(OR)_3$, where R corresponds to ethyl groups $-C_2H_5$) and the silica alkoxide tetraethylorthosilicate (TEOS, $Si(OR)_4$, where R also corresponds to ethyl groups $-C_2H_5$) act as precursors and tracers of silica network. During the hydrolysis reaction, the ethoxy groups (OR) from APTES, **Figure 22**, and TEOS, **Figure 23**, are attacked by water molecules to be hydrolyzed and form silanol $(Si - OH)$ groups. Simultaneously, an ethanol molecule $(C_2H_5 - OH)$ is formed per each hydrolyzed radical.

$$H_2N \diagdown \diagup Si \begin{matrix} O-CH_2CH_3 \\ | \\ -O-CH_2CH_3 \\ | \\ O-CH_2CH_3 \end{matrix} + 3H_2O \leftrightarrow H_2N \diagdown \diagup Si \begin{matrix} OH \\ | \\ -OH \\ | \\ OH \end{matrix} + 3 CH_3CH_2 - OH$$
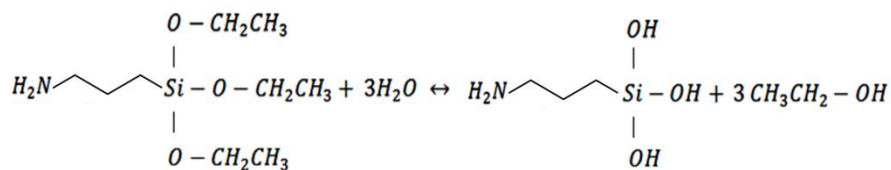
Figure 22. Hydrolysis reaction of 3-aminopropyltriethoxysilane (APTES).

$$CH_3CH_2 - O - Si \begin{matrix} O-CH_2CH_3 \\ | \\ -O-CH_2CH_3 \\ | \\ CH_3CH_2 - O \end{matrix} + 4H_2O \rightarrow OH - Si \begin{matrix} OH \\ | \\ -OH \\ | \\ OH \end{matrix} + 4CH_3CH_2 - OH$$
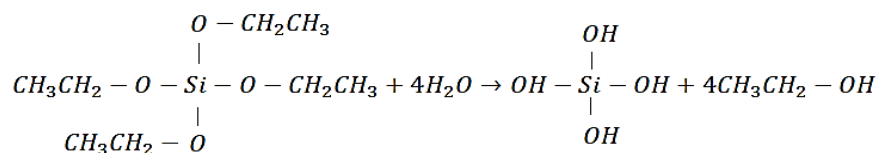
Figure 23. Hydrolysis reaction of tetraethylorthosilicate (TEOS).

Once the hydrolysis is carried out, silanol groups (Si-OH) are condensed, leading to the condensation/alcoholysis reactions. In these reactions, water molecules are eliminated to form a dense continuous inorganic SiO_2 matrix. Reaction rate of hydrolysis reactions is faster than reaction rate of condensation reactions.

Condensation reactions can occur either between an ethoxy radical ($Si - O - CH_2CH_3$) and a hydrolyzed radical ($Si - OH$) from APTES or TEOS, as shown in **Figure 24** and **Figure 25**, respectively, to form ethanol molecules; or between two hydrolyzed radicals from APTES molecules (**Figure 26**) and TEOS molecules (**Figure 27**) to form water molecules. The final APTES-TEOS condensed product is shown in **Figure 28**.
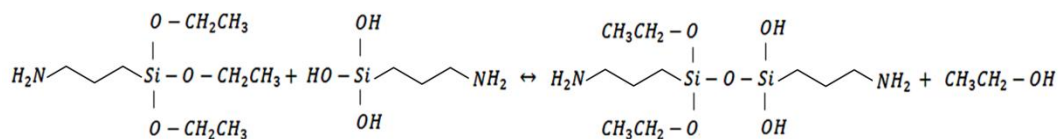
Figure 24. Condensation reactions in APTES molecules between ethoxy radical and hydrolyzed radical.
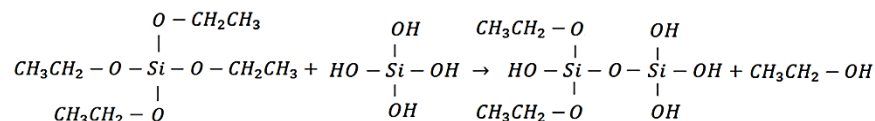
Figure 25. Condensation reactions in TEOS molecules between ethoxy radical and hydrolyzed radical.
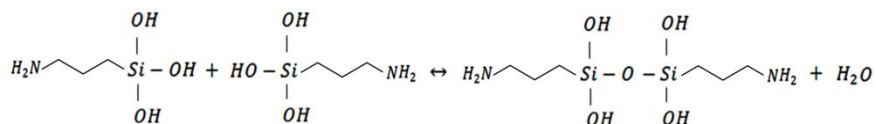
Figure 26. Condensation reactions in APTES molecules between hydrolyzed radicals.
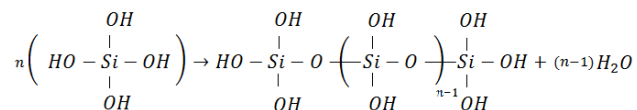
Figure 27. Condensation reactions in TEOS molecules between hydrolyzed radicals.
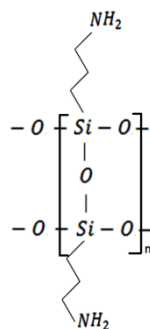
Figure 28. Condensation reactions between hydrolyzed radicals from APTES and TEOS to form SiO_2 network.

The organic modification within the SiO_2 network is carried out through the incorporation of poly(dimethylsiloxane) (PDMS), an organic modifier and network extender. Since PDMS structure is similar to silica structure by having a $Si - O - Si$ backbone and hydroxyl terminated groups $(-OH)$, PDMS can condense with APTES and TEOS hydrolyzed radicals $(Si - OH)$ (**Figure 29**), extending and giving the silica network its silicon properties.
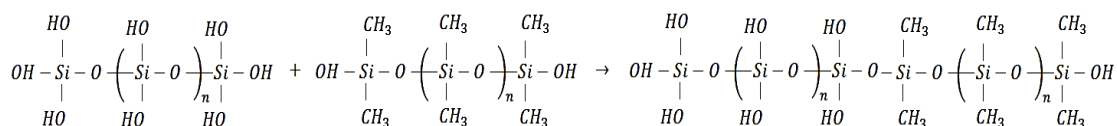
Figure 29. Polycondensation reactions between PDMS and hydrolyzed radicals from APTES and TEOS to form a PDMS-modified SiO_2 organic-inorganic network.

Thus, chemical crosslinking of hyaluronic acid sodium salt (HA) is carried out through the PDMS-modified SiO_2 organic-inorganic network, building up a hybrid hydrogel with a 3D matrix (**Figure 30**) containing HA chains randomly distributed and stabilized by Van der Waals interactions (hydrogen bonds, electrostatic interactions, hydrophobic forces, etc.).
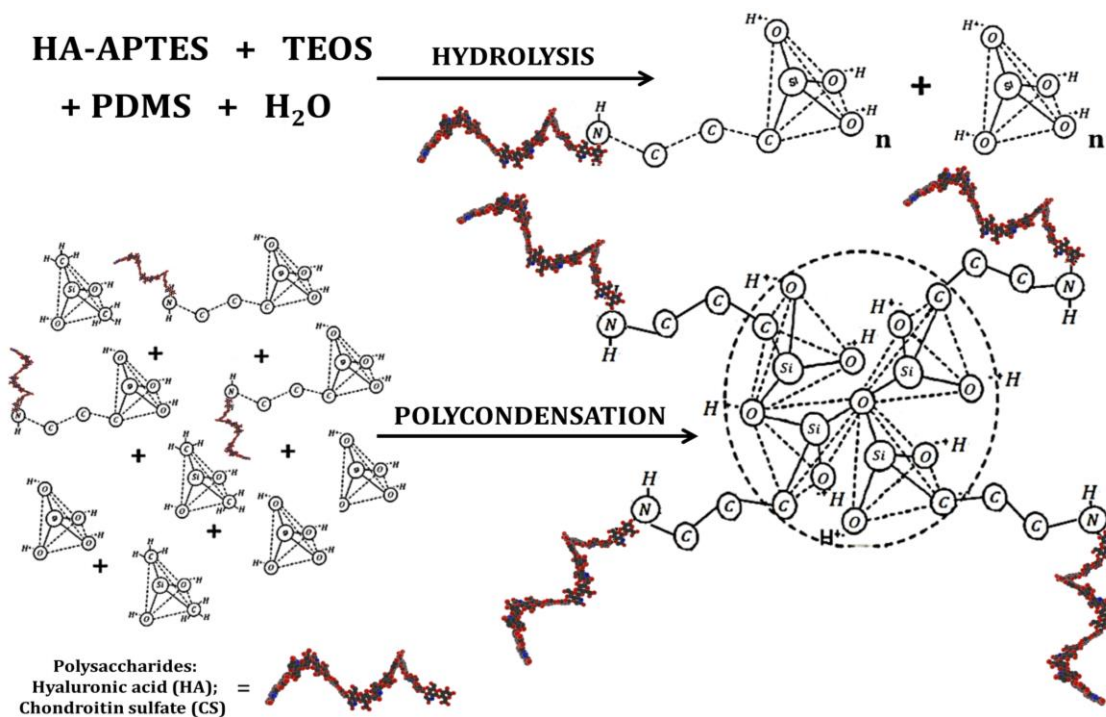
Figure 30. Chemical crosslinking of polysaccharides with a PDMS-modified SiO_2 organic-inorganic network forming hybrid hydrogels.

3.2 GELLING TIME IN POLYSACCHARIDE – BASED HYBRID HYDROGELS

Gelling time or *sol-gel* transition time in hybrid hydrogels was monitored during crosslinking reactions through their rheological properties. *Sol-gel* transition is considered to be the intersection point between storage (G') (elastic behavior) and loss (G'') (viscous behavior) moduli $(G' = G'')$ of polymeric fluids. When *sol-gel* process starts, it involves the conversion of monomers into a colloidal solution (*sol*) that acts as a precursor for an integrated network (*gel*) of organic-inorganic polymer crosslinked chains. In the *sol* state, the small solid particles suspended in a continuous liquid medium show a predominant viscous behavior; meaning that the loss modulus (G'') is greater than the storage modulus (G'). As *sol* evolves gradually towards the formation of the *gel* crosslinked network containing both, liquid and solid phases, the molecular weight of the *gel*-like material increases as well as its storage modulus (G'). When both moduli get the same value $(G' = G'')$ the *sol* has reached its gelling point.

The viscoelastic properties of hybrid hydrogels are evaluated through a dynamic mechanical analysis (stress-strain tests), which is divided in two steps:

1) Performing a *stress sweep step* at a fixed oscillation frequency, which can be set between 0.1 to 100 Hz (f=1 Hz, standard value) in order to determine the percentage of oscillation strain (%) at which the *sol* keeps a linear viscoelastic range (LVR), by fulfilling the Hooke Law, defined in **Equation 3** as:

$$\sigma = G * \gamma \qquad\qquad \textbf{Equation 3}$$

Where, σ is the applied stress; G is the relaxation modulus; and γ is the deformation of hybrid hydrogels.

2) Performing a *time sweep step* under two conditions established on the *stress sweep step*: 1) fixed oscillation frequency; 2) oscillation strain (%); in order to study the *sol-gel* transition time from $G'' > G'$ to $G' > G''$ in hybrid hydrogels. Time sweeps can be made at a certain temperature.

3.2.1 GELLING TIME IN HYALURONIC ACID – BASED PDMS-MODIFIED SiO_2 ORGANIC – INORGANIC HYBRID HYDROGELS

Gelling time of hybrid hydrogels allows establishing a direct relationship between *sol-gel* transition time and the hydrolysis-condensation reaction rate. Since the *sol-gel* method is a dynamic process, its reaction parameters influence the hydrogel crosslink-process. These parameters include: 1) type of precursors; 2) ratio between alkoxide and water; 3) temperature; 4) pH; 5) concentrations of reactants.

In the polysaccharide-based hybrid hydrogels, the starting HA aqueous solution shows a direct influence on the hydrolysis-condensation reaction rate and therefore on the *sol-gel* transition time because the stability and reactivity of the silicon alkoxide (TEOS, APTES) and silicone (PDMS) are influenced by a steric factor due to the bulky polysaccharide chains (HA), which slow down the hydrolysis reactions of TEOS, APTES and PDMS. Moreover, the hydrolysis-condensation reaction states that a water ratio $\left(R_w = {H_2O}/{alkoxide} \right)$ of 2 is needed to convert every alkoxide molecule to SiO_2. Therefore, when increasing water content into the reaction system, it inhibits the condensation reactions of APTES-TEOS-PDMS, which function as network formers; resulting into shorter and less crosslinked chains.

Silica (SiO_2) structure is made up tetrahedral silicate units in which the silicon atom is located in the middle of the tetrahedron and the oxygen atoms are placed in each vertex. The oxygen atoms, in turn, are joined by sharing their corners through bridges of oxygen, forming an uninterrupted three-dimensional network. When the SiO_2 structure is modified with a silicone, like PDMS, in high concentrations; PDMS not only will act as a modifier, but it will also function as network former. Since the PDMS-modified SiO_2 network will be formed through hydrolysis-condensation reactions, once it is attached to the hyaluronic acid biopolymer chain, the electron density of the different Si atoms (from APTES, TEOS, PDMS), the pH and the temperature in the *sol-gel* method will influence the crosslinking reaction rate. The electron density on Si atoms influences the reaction rate as follows:

$$Si - R > Si - OR > Si - OH > Si - O - Si$$
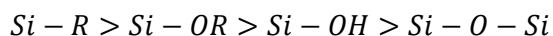
Since acid catalyzed reactions demand a high electron density, PDMS and TEOS along with an acid pH (pH=4.5-6.5), which was needed to increase the efficiency of the chemical modification of hyaluronic acid with APTES during amidation reaction, will catalyze the

hydrolysis reactions and enhance the formation of straight crosslinked chains of a PDMS-modified SiO_2 network.

Figure 31 shows the dynamic time sweep analysis carried out in *sol* samples at 1.6% strain, ≈0.25 N normal force, a frequency of 0.75 Hz and 37 °C and 40 °C from 0 to 5000 seconds in order to analyze their *sol-gel* transition time. It is observed that the hybrid hydrogels with higher concentration of hyaluronic acid ($67HA > 50HA > 33HA$), that is reaction systems with less amount of water, and with a higher reaction temperature lead to shorter gelling times. Since the hyaluronic acid polymer chains act as network former, faster crosslinking rates occur. At a macro scale, HA high concentration hybrid hydrogels are constituted by denser and stiffer organic (HA)- inorganic (PDMS-modified SiO₂) polymer networks chemically crosslinked.
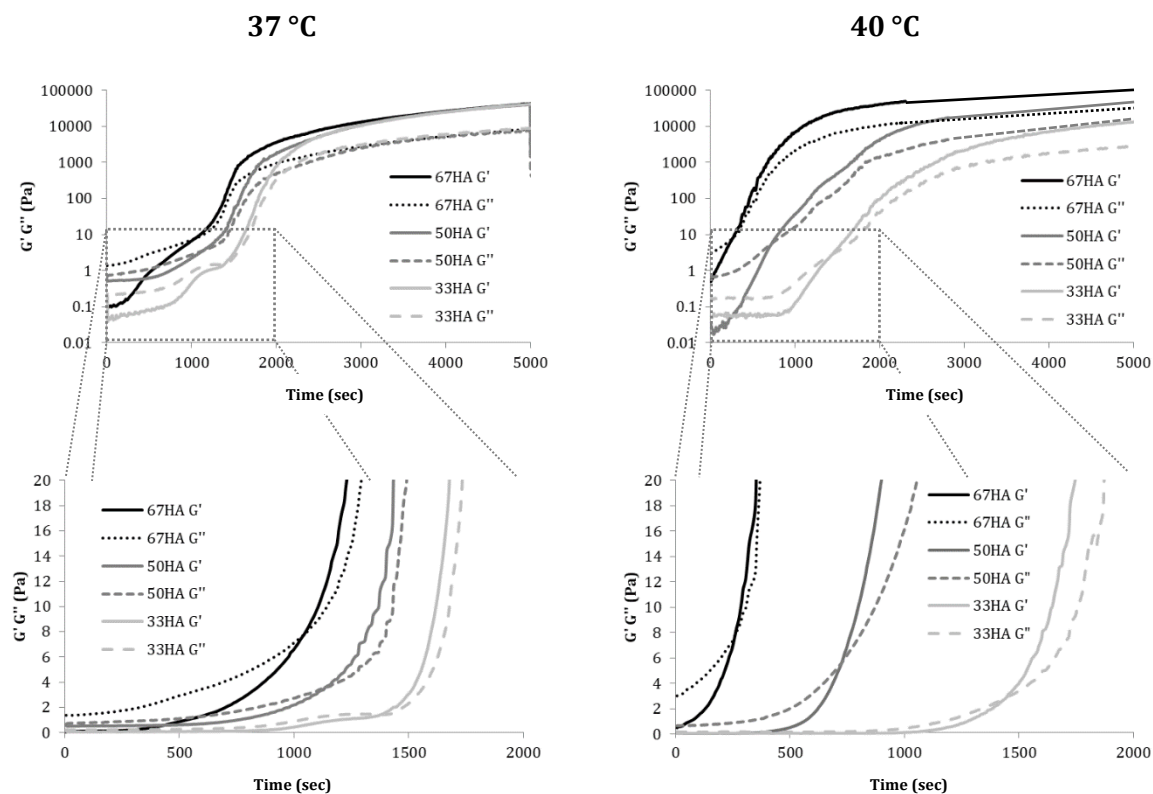
Figure 31. Analysis of *sol-gel* transition time by dynamic time sweep of hyaluronic acid-based hybrid hydrogels at 37 °C and 40 °C synthesized at 6 *pH*.

3.2.2 GELLING TIME IN CHONDROITIN SULFATE – BASED PDMS-MODIFIED SiO_2 ORGANIC-INORGANIC HYBRID HYDROGELS

Figure 32 shows the dynamic time sweep analysis carried out in *sol* samples at 1.6% strain, ≈0.25 N normal force, a frequency of 0.75 Hz and 37 °C, 40 °C and 50 °C from 0 to 5000 seconds in order to analyze their *sol-gel* transition time. It is observed that hybrid hydrogels shortens significantly their gelling times as reaction temperature increases ($50 \,°C > 45 \,°C > 37 \,°C$). Since temperature acts as catalyzer, faster crosslinking rates occur.
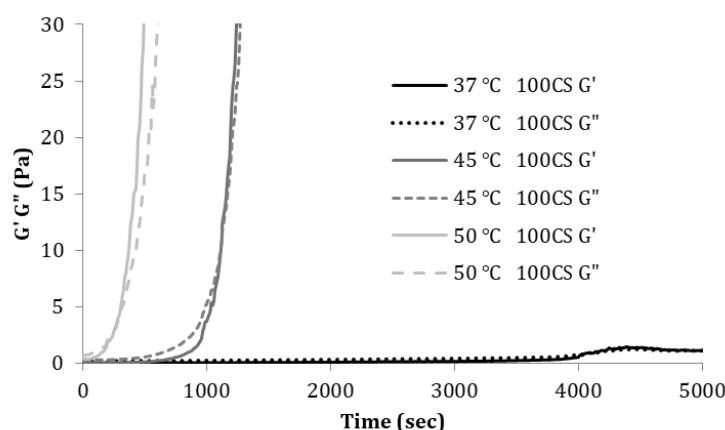
Figure 32. Analysis of *sol-gel* transition time by dynamic time sweep of chondroitin sulfate-based hybrid hydrogels at 37 °C, 45 °C and 50 °C synthesized at 6 *pH*.

3.3 AGING TIME IN POLYSACCHARIDE – BASED HYBRID HYDROGELS

Aging stage consists in keeping the *wet gel* inside a closed container for a period of time, immersed into the liquids it released. The released liquids are due to the continuous poly-condensation reactions, which take place between unreacted polymer chains and the surface of the *gel* already formed. Thus, the material shrinks while losing weight as it expels the liquids trapped within its matrix. The expelled liquids are water, byproducts (ethanol) and unreacted reagents. The polysaccharide-based hybrid hydrogels are aged for 10 days (syneresis process). Once the time ends, the containers are opened and the materials are dried in three different ways: 1) freeze-drying, 2) room temperature drying; 3) 60 °C temperature drying.

To analyze rheological properties of 50HA-*pH*6 and 50HA-*pH*7 hybrid hydrogels during aging process were evaluated by monitoring the storage modulus (G') and loss modulus (G") as a function of frequency through rheometry by dynamic oscillatory measurements with 25 mm diameter parallel plate geometry, revealing the evolution of hydrolysis-condensation reactions by densifying and hardening the crosslinking structure.

The materials were carefully placed into the lower plate after which the upper plate was lowered to a 2.5 mm gap. After that, dynamical oscillatory frequency sweeps for HA-based hybrid hydrogels were performed at 25 °C (room temperature) with constant strain (0.1866%) and the frequency was set from 0.1 to 10 Hz.

Storage modulus (G') and loss modulus (G'') of HA-based hybrid hydrogels exhibited similar linear rheological behaviors, (**Figure 33**) regardless of the *pH* of synthesis. G' and G" values remained almost constant as frequency increased. However, G' modulus of 50HA-*pH*6 hydrogels were stronger (~7000 Pa) than G' modulus of 50HA-*pH*7 hydrogels (~4000 Pa).

A   **B**
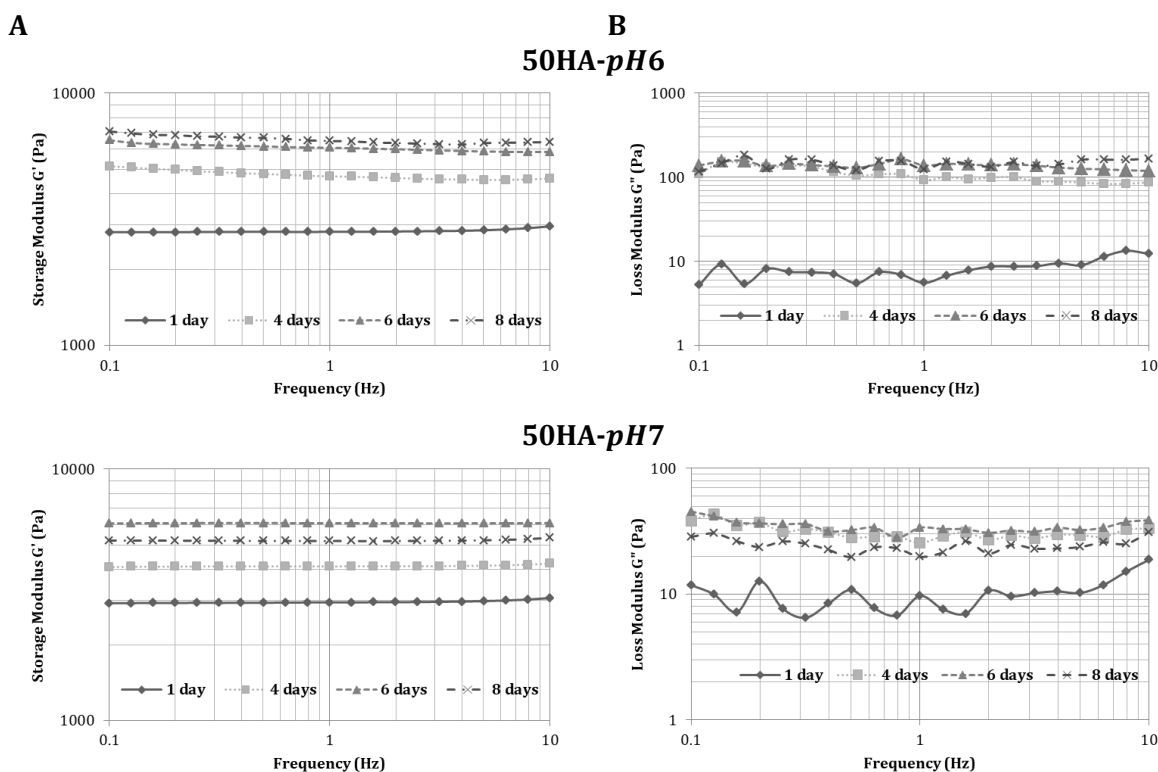
Figure 33. Dynamic oscillatory frequency sweep curves for 50HA-*pH*6 and 50HA-*pH*7 hybrid hydrogels. **(A)** Storage modulus and **(B)** loss modulus as a function of frequency (Hz) for aging time of 50HA-*pH*6 and 50HA-*pH*7 hybrid hydrogels.

This linear rheological behavior implied that the HA-based hydrogels have similar microstructure, bearing dynamic deformations; though, 50HA-*pH*6 hydrogels revealed to have a stronger densified crosslinked structure, which resulted from better *sol-gel* reaction efficiency, boosted by acidic conditions. It was observed that storage modulus (G') was far higher than loss modulus (G") in the range of the whole frequency sweep, which means that great proportion of energy was stored in the deformation of the hydrogel itself. The highly elastic nature of these HA-based hybrid hydrogels was thus indicated.

Fluctuations in loss moduli (G") of both 50HA-*pH*6 and 50HA- *pH*7 could be attributed to the mixture of liquids (water, ethanol and unreacted reagents) entrapped within its structure.

Physical appearance of hybrid hydrogels is shown in **Figure 34** once their aging time has finished. At higher concentration of HA (67HA-6W>50HA-6W >33HA-6W) the hybrid hydrogels showed a denser and rigid structure, decreasing their bouncing capability.
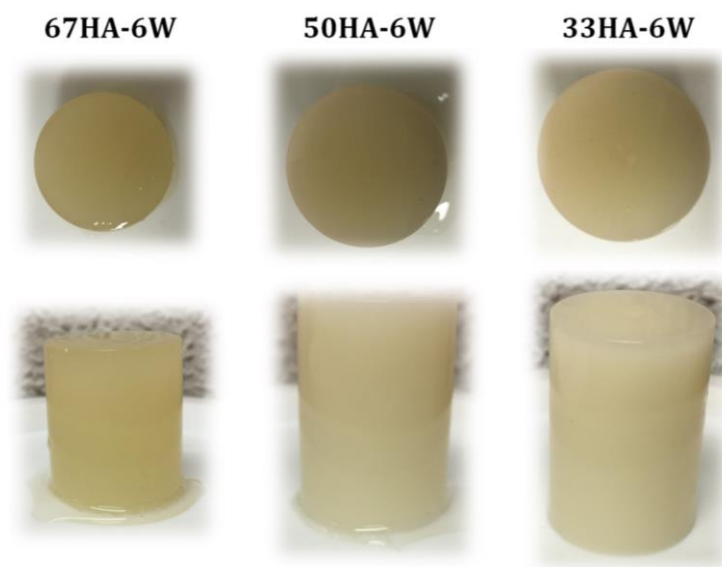
Figure 34. Physical appearance of hyaluronic acid-based hybrid hydrogels once aging time is finished.

3.4 DRYING OF POLYSACCHARIDE – BASED HYBRID HYDROGELS

The physical appearance of hybrid hydrogels depends on their composition and drying processes.

Freeze-drying: The *wet gels* are freeze at -20 °C for 24 hours and then freeze-dried for one week at -20 °C and 1 mBa. When the liquids trapped inside the *gels* are freeze, little ice crystals are formed. The size of the ice crystals will determine the number, type and size of the pores formed in the *aerogels*.

Room temperature drying: The *wet gels* are dried at room temperature ($\approx$25 °C) till all the liquids trapped inside their networks are eliminated. This can be notice when the xerogels reach a relative constant weight. During this time, polycondensation reactions continue to occur on the *gels* surface, enhancing the *xerogels* to have a dense structure.

60 °C temperature drying: The *wet gels* are dried at room temperature for 24 hours and then placed in an oven and dried at 60 °C for 24 hours. At this temperature all remaining liquids inside their networks are removed, converting the hybrid hydrogels into *xerogels*.

When synthesizing the hybrid hydrogels at different ($pH = 6; pH = 7$), their syneresis and aging processes change their physical appearance and structure. After 10 days of aging time, the hybrid hydrogels synthesized at $pH = 6$ presented a higher degree of initial shrinkage and showed more exuding liquids than the hybrid hydrogels synthesized at $pH = 7$, as shown in **Figure 35**. However, after being dried through the different drying processes, the hybrid hydrogels ($pH = 7$) showed a greater degree of shrinkage than hybrid hydrogels ($pH = 6$).

Since acid pH ($pH = 4.5 - 6.5$) catalyzes the hydrolysis reactions and enhances the formation of straight crosslinked chains of a PDMS-modified SiO_2 network, the hybrid hydrogels ($pH = 6$) had better reaction efficiency since hydrolysis-condensation reactions continue to occur during syneresis and aging processes. A higher crosslinking degree in the hybrids ($pH = 6$) can be assumed as a higher amount of condensation water is expelled during the aging process; resulting in the formation of denser hybrids.

After drying processes, the structure in hybrids continues to shrink. In room-temperature dried hydrogels, a maximum degree of shrinkage is reached, resulting in hybrids

with dense and rigid structures. In 60 °C-dried hydrogels, the maximum degree of shrinkage is stopped since the water remaining within their structure is evaporated constantly at 60 °C. These hybrid hydrogels also presented a rigid structure. In freeze-dried hydrogels, their maximum degree of shrinkage is stopped when they are freeze. Due to vacuum and freeze temperatures, the condensation water crystals are sublimated really fast, leaving visible pores inside the structure.

A.
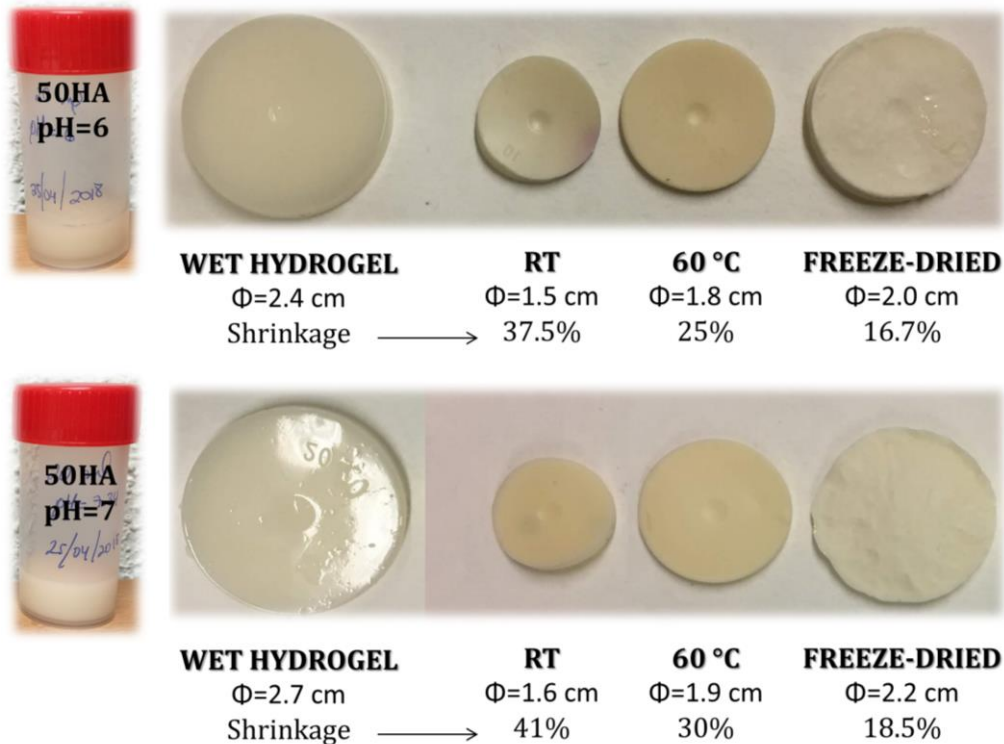
B.

Figure 35. Physical appearance of polysaccharide-based hybrid hydrogels before and after drying processes. **(A)** Physical appearance of HA-*pH*6 and HA-*pH*7 hybrid hydrogels. **(B)** Physical appearance of 100CS-*pH*7 hybrid hydrogels.

3.5 CHARACTERIZATION OF HYALURONIC ACID – BASED PDMS-MODIFIED SiO_2 ORGANIC-INORGANIC HYBRID HYDROGELS

HA-based hybrid hydrogels are characterized to determine their chemical, structural and morphological properties.

3.5.1 STRUCTURAL CHARACTERIZATION OF HA – BASED HYBRID HYDROGELS BY FOURIER – TRANSFORM INFRARED SPECTRSCOPY (FTIR)

The infrared spectra of HA-based hybrid hydrogels are shown in **Figure 36**. The band between 3100-3600 cm^{-1} corresponds to the symmetric stretching vibration of the hydroxyl group $-OH$ [222, 223]. It also may be attributed to the overlapping of the $O-H$ and $N-H$ stretching vibration of functional groups engaged in hydrogen bonds [223-225]. The band at 1740 cm^{-1} can be related to stretching vibration $(\vartheta_{C=O})$ of carboxyl $COOH$ group in hyaluronic acid [224, 225]. However, it may also be due to the self-condensation between the $-COO^-Na^+$ and $-OH$ groups in hyaluronic-based materials [226]. The absorption peak at 1650 cm^{-1} can be assigned to amide I groups, mainly stretching vibration $\vartheta_{C=O}$ of amide $C=O$ group accepting one or two hydrogen bonds [225]. At 1620 cm^{-1}, there is the band related to stretching vibrations $\vartheta_{C=O}$ of carboxyl COO^- group accepting zero or one hydrogen bond [225]. The band at 1560 cm^{-1} is assigned to the formation of the amide II bonding between the carboxyl COO^- group in HA and the amine group in APTES [226]. This band is mainly assigned to bending vibrations δ_{N-H} of amide $N-H$ group establishing one hydrogen bond [224, 225]. The spectral region between 1500 cm^{-1} and 1250 cm^{-1} shows several bands due to APTES [223]: 1) bending vibration $\delta(NH_2)$ at 1463 cm^{-1}, 2) asymmetric bending vibration $\delta_a(CH_3)$ at 1444 cm^{-1}, 3) bending vibration $\delta(Si-CH_3)$ of $Si-CH_3$ bonds at 1410 cm^{-1}, 4) bending vibration $\delta(CH_3)$ at 1380 cm^{-1}. Moreover, the band at 1405 cm^{-1} can be attributed to the stretching vibrations ϑ_{C-O^-} of carboxyl COO^- group accepting zero or one hydrogen bond [225]. The band located at 1259 cm^{-1} is related to the symmetric deformation of the CH_3 group in the $Si-(CH_3)_2$ bonds from PDMS [227, 228]. The band at 1220 cm^{-1} is assigned to the stretching vibration ϑ_{C-O} of carboxyl $COOH$ group in hyaluronic acid [225]. The intense band between 950 and 1200 cm^{-1} correspond to the $C-O$ stretching vibration ϑ_{C-OH} in alcohols. The shoulder at 1165 cm^{-1} is assigned to the antisymmetric stretching vibrations ϑ_{C-O-C} in glycosidic groups within saccharide structures [224, 225]. Moreover, the vibration

mode ϑ_{C-OH} of alcohol II and the vibration of the ring mode ϑ_{C-O-C} in hyaluronan molecules are assigned at 1080 cm^{-1} [225].

The PDMS-modified SiO$_2$ network formed during the hydrolysis-condensation reactions of APTES-TEOS-PDMS can also be seen in the FT-IR spectra. The most intense region appears between 1200 and 900 cm^{-1} [223, 228], including several vibrations: 1) at 1167 cm^{-1}, CH_3 rocking; 2) at 1105 cm^{-1}, the asymmetric stretching $\vartheta_{a\,Si-O-C}$ 3) at 1080 cm^{-1}, the symmetric stretching ϑ_{Si-O-C}; 4) at 1088 and 1034 cm^{-1}, the asymmetric stretching $\vartheta_{a\,Si-O}$ in $Si-O-Si$ bonds; 5) at 1053 cm^{-1}, the asymmetric stretching $\vartheta_{a\,C-O}$ of ethanol, byproduct in hydrolysis reactions. Near 1000 cm^{-1}, bands corresponding to $Si-O$ stretching vibration of silicate network appears [227]. Nevertheless, the stretching vibrations of silanol ($Si-OH$) groups observed at 975 cm^{-1} and siloxane bonding ($Si-O-Si$) observed at 1030 cm^{-1} overlap with the stretching vibration of hydroxyl groups of hyaluronan. The band at 895 cm^{-1} is attributed to asymmetric stretching $\vartheta_a(Si-O)$ in $Si-OH$ bonds from PDMS [228]. The band at 850 cm^{-1} corresponds to the presence of hybrid crosslinked SiO_2 (Q units) – PDMS (D units) structures; in other words, it is assigned to (TEOS) $Si-O-Si$ (PDMS) bonds. The band located at 793 cm^{-1} is assigned to $Si-X$ bonds, where $X=O,C$; $Si-O$ bonds correspond to the silicon tetrahedron $[SiO_4]$ and $Si-C$ bonds correspond to PDMS and APTES molecules [227, 228].

The FT-IR spectra of the 67HA, 50HA and 33HA hybrid hydrogels show four important bands, determining the successful formation of an organic-inorganic hybrid hydrogel: 1) the band at 1560 cm^{-1} attributed to the amide II, confirming the grafting between APTES and hyaluronic acid; 2) the bands at 975 and 895 cm^{-1} assigned to $Si-OH$ bonds, proving hydrolysis reactions; 3) the band at 850 cm^{-1} corresponding to (PDMS) $Si-O-Si$ (TEOS) bonds, showing the incorporation of PDMS within the 3D SiO_2 network; 4) the band at 790 cm^{-1} assigned to $[SiO_4]$ and $Si-C$ bonds, ensuring an inorganic crosslinking of hyaluronic acid.

The drying process influenced the final state of hybrid hydrogels. The FT-IR spectra of hybrid hydrogels dried at room temperature and 60 °C show bands in the region between 1300-900 cm^{-1} attributed byproducts (ethanol), unreacted intermediates (o-acylisoureas, amine-reactive-esters) and unreacted reagents. However, these bands are not present in freeze-dried hybrid hydrogels due to the supercritical conditions at which they were dried.

Freeze-dried HA-based hybrid hydrogels
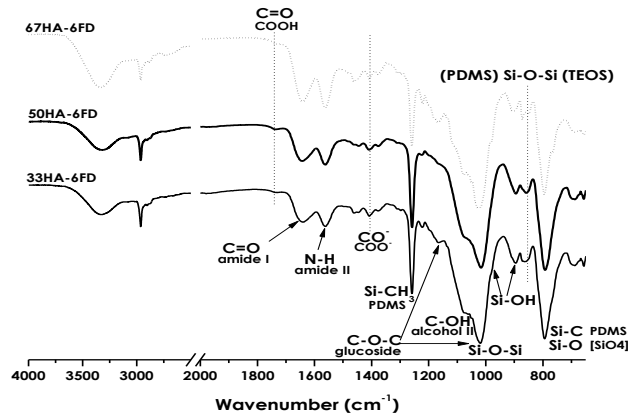
Room temperature-dried HA-based hybrid hydrogels
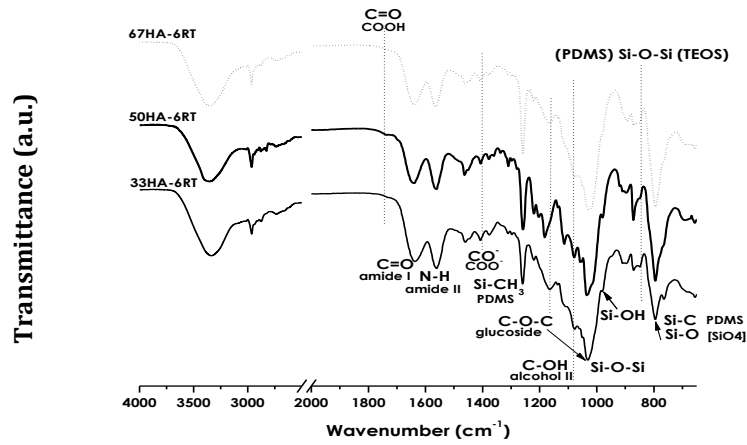
60° C dried HA-based hybrid hydrogels

Figure 36. FT-IR spectra of HA-based hybrid hydrogels synthesized at 6 *pH*.

Compering the three compositions along with their drying processes, the freeze-drying process shows to be the best method to obtain purified hydrogels; however the room temperature drying process shows the best formation of crosslinking hybrid network.

Table 3 presents a summary of the most representative absorption bands in FT-IR spectra, their position and the functional group to which they belong.

Table 3. Assignments of the main bands in FT-IR spectra of hybrid HA-based hydrogels.

Wavenumber (cm^{-1})	Assignment
3540	ϑ_{O-H} weakly hydrogen bonded $O - H$ group of alcohols [225]
3358	$\vartheta_{a\,N-H}\ldots$ hydrogen bonded $N - H$ groups from APTES [223]
3300	$\vartheta_{O-H}\ldots$ of alcohols (broad band)[225]
3295	$\vartheta_{N-H}\ldots$ hydrogen bondeded $N - H$ groups from APTES [223]
3275	$\vartheta_{N-H}\ldots$ hydrogen bondeded $N - H$ groups (broad band)[225]
3100	$\vartheta_{N-H}\ldots$ Fermi resonance [225]
2962	$\vartheta_{a\,C-H}$ in CH_3 from APTES [223], PDMS [228]
1740	$\vartheta_{C=O}$ of carboxyl $COOH$ group in hyaluronic acid [224, 225] Self condensation between $-COOH$ and $-OH$ in hyaluronic acid [226]
1648	Amide I, mainly $\vartheta_{C=O}\ldots$ of amide $C = O$ group accepting one or two hydogen bonds [225]
1620	$\vartheta_{C=O}$ of carboxyl COO^- group accepting zero or one hydrogen bond [225]
1560	Amide II, mainly δ_{N-H} of amide $N - H$ group establishing one hydrogen bond [224-226]
1463	$\delta(NH_2)$ from APTES [223]
1444	$\delta_a(CH_3)$ from APTES [223]
1410	$\delta_a(Si - CH_3)$ of $Si - CH_3$ bonds from APTES [223]
1405	ϑ_{C-O^-} of carboxyl COO^- group accepting zero or one hydrogen bond [225]
1380	$\delta_{C-H}\ldots-CH_3$ from APTES [223]
1259	δ_{CH_3} in $Si(CH_3)_2$ from PDMS [228]
1220	ϑ_{C-O} of carboxyl COO^- group in hyaluronic acid [225]
1167	CH_3 rocking from TEOS and APTES [223, 228]
1165	$\vartheta_{a\,C-O-C}$ glycoside [225]
1105	$\vartheta_{a\,Si-O-C}$ from TEOS and APTES [223, 228]
1080	ϑ_{C-OH} of alcohol II and ϑ_{C-O-C} ring mode ϑ_{Si-O-C} from TEOS [228]
1088, 1034	$\vartheta_{a\,Si-O}$ in $Si - O - Si$ bonds [228]
1053	$\vartheta_{a\,C-OH}$ of alcohol II [223]
975	$Si - OH$ in silica containing materials [227]
895	$\vartheta_{a\,Si-O}$ in $Si - OH$ from PDMS [228]
850	Crosslinked SiO_2 (Q units) – PDMS (D units) structures [227]
793	$Si - X$ bonds, where $X = O, C$ [227]

Note: ϑ, stretching vibrations; δ, bendign vibrations; $\nu_{C-OH\ldots}$, the $C - O$ stretching vibration of an alcohol establishing one hydrogen bond; ν_{C-OH}, the $C - O$ stretching vibration of an alcohol establishing no hydrogen bond.

3.5.2 STRUCTURAL CHARACTERIZATION OF HA – BASED HYBRID HYDROGELS BY RAMAN SPECTROSCOPY

The Raman spectra of the HA-based hybrid hydrogels are shown in **Figure 37**. The identified bands were assigned according to literature data [229-237]. Several Raman bands related to silica-based hybrid materials and hyaluronic acid hydrogels are observed in the HA-based hybrid hydrogels Raman spectra. A listing of the wavenumber positions and the assignments of the Raman bands is available on **Table 4**. From the Raman spectra it can be observed that the intensity of the bands depends on the hydrogel composition and drying process.

In the Raman spectra of HA-based hybrid hydrogels there are several Raman scattering due to different bond vibrations related to hyaluronic acid (HA) [236, 237]: 1) the band at 820 cm^{-1} is due to stretching vibrations of $C - O - C$ bonds from the hyaluronic acid repetitive units (D-glucuronic acid and N-acetyl-D-glucosamine, linked via alternating β-(1→4) and β-(1→3) glycosidic bonds); 2)the band at 1047 cm^{-1} is attributed to $C - C$ and $C - O$ stretching bonds; 3) the band at 1081 cm^{-1} is assigned to $C - OH$ bond; 4) the bond at 1122 cm^{-1} is assigned to $C - OH$ and $C - H$ bonds; 5) the band at 1205 cm^{-1} is attributed to CH_2 groups; 6) the band at 1370 cm^{-1} is assigned to $C - H$ bending bond; 7) the band at 1405 cm^{-1} is due to $C - N$ stretching bond and the deformation of $C - H$ bond.

The Raman bands due to the chemical modification of HA with APTES are the followings [229, 230]: 1) the band around 1415 cm^{-1} may be assigned to the bending vibration of CH_2 group bonded to the Si atom ($Si - CH_2$); 2) the bands at frequencies of 1015 cm^{-1} and 1308 cm^{-1} arise from the stretching vibration of skeletal stretch and CH_2, respectively; 3) the band at 850 cm^{-1} can be assigned to carbon chain vibration modes; 4) the band at 1060 cm^{-1} comes from the stretching vibration of $C - C$, which is near the Si atom in the carbon chain.

Several other bands due to PDMS-modified SiO_2 crosslinking appear in the Raman spectra: 1) the band at 1135 cm^{-1} is attributed to the $Si - O - Si$ bond-bending vibration [230]; 2) the bands around 1036 cm^{-1} and 945 cm^{-1} are assigned to $O - Si - O$ bonds [231]; 3) the band around 980 cm^{-1} is due to $Si - OH$ bonds [231]. Moreover, the following bands show the correct incorporation of PDMS into the SiO_2 network [232-235]: 1) the bands around 1415 cm^{-1} and 1265 cm^{-1} are assigned to the asymmetric and symmetric bending vibration of CH_3 group from PDMS, respectively; 2) the band at 865 cm^{-1} is attributed to the symmetric

rocking of CH_3 from PDMS; 3) the band at 790 cm^{-1} is due to $C - Si - C$ asymmetric stretching vibration and to the rocking vibration of CH_3 group from PDMS; 4) the band at 707 cm^{-1} is due to $C - Si - C$ symmetric stretching vibration ; 5) the band at 689 cm^{-1} is attributed to $Si - CH_3$ symmetric rocking ; 6) the band at 495 cm^{-1} is assigned to $O - Si - O$ bonds.

The 67HA, 50HA and 33HA hybrid hydrogels show slightly differences in their Raman spectra. The bands related to PDMS-modified SiO_2 organic-inorganic hybrid structure differ in intensity. Gelling time and drying process affect the HA-based PDMS-modified SiO_2 organic-inorganic hybrid structure during hydrolysis-condensation reactions as can be seen in the Raman spectra (**Figure 37**). The intensity of some important bands related to the crosslinking process and the incorporation of PDMS into the SiO_2 structure varies depending on the drying process. By keeping constant both composition and reaction parameters, the hydrolysis and condensation reactions were modified by the mobility of the remaining liquids, hence the hybrid structure of the hydrogels was modified by the rate in which the remaining liquids (water, ethanol, unreacted reagents) were removed.

Likewise, structural changes are caused by drying process, polycondensation rate can also yield them, being affected by the concentration of the starting HA solution and the initial amount of water in the hybrid system. Variation on micro and nanostructure can be found in TEOS-PDMS hybrid materials when modulating water-solvent ratios [233]. During *sol* sate, prior to gelation, the hydrolysis and condensation reactions occur at a certain rate; however, when gelling transition starts, the reaction rate decreases due to the reduction in the mobility of the components. Therefore, when allowing the hybrid hydrogels to age and then dried at a constant but slow rate, the hydrogel network will be reinforced through further polymerization, increasing and decreasing the intensity in Raman bands attributed to $Si - O - Si$ bonds and $Si - OH$ bonds, respectively.

The difference among the 67HA, 50HA and 33HA hybrid hydrogels spectra indicates that the materials are chemically crosslinked, having zones rich in SiO_2 and PDMS. However, by using Raman spectroscopy is not possible to establish if PDMS is either incorporated into the hybrid network or entrapped within the hybrid hydrogel.

Freeze-dried HA-based hybrid hydrogels
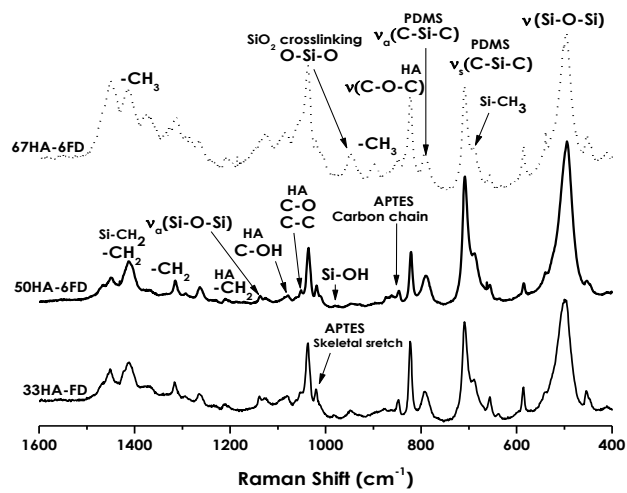
Room temperature HA-based hybrid hydrogels
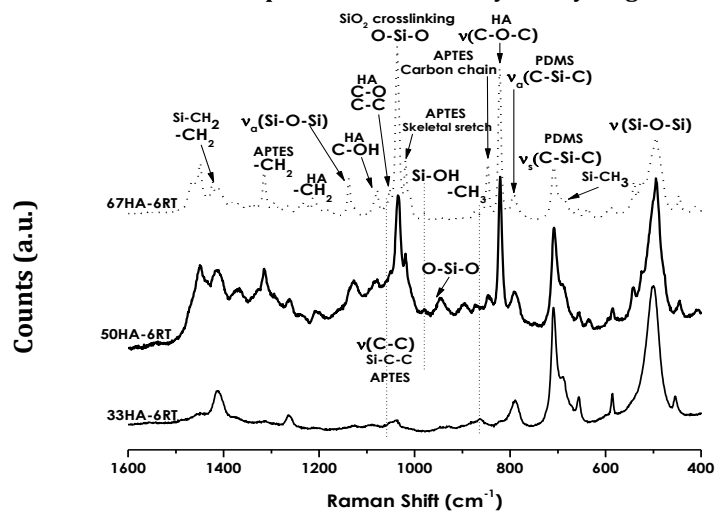
60° C dried HA-based hybrid hydrogels
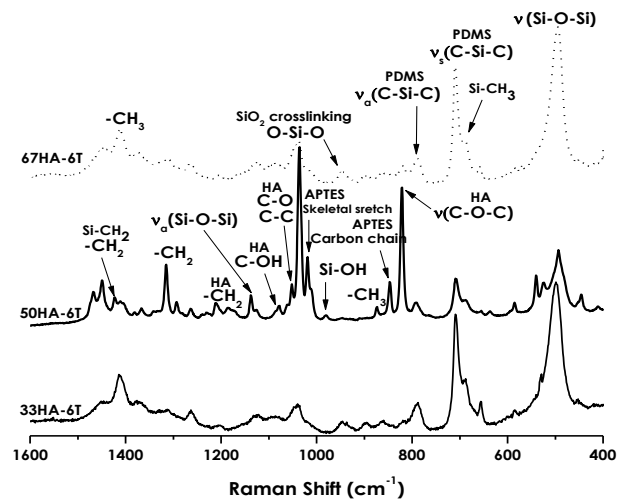
Figure 37. Raman spectra of HA-based hybrid hydrogels synthesized at 6 *pH*.

Letting the hybrid hydrogels to dry at room temperature gives them the opportunity to polycondense and densify their PDMS-modified SiO_2 network, but byproducts may continue to be trapped within the hydrogel structure. On the other hand, when the liquids are removed through supercritical conditions, by freeze-drying process, the polycondensation of PDMS-modified SiO_2 network is freeze, so it does not have the chance to get reinforced. Finally, when drying the hybrid hydrogels at 60 °C, the liquids are evaporated at a faster rate than when they are dried at room temperature. Temperature may be involved in the chemical kinetics of hydrolysis-condensation reaction. Most of the organic byproducts may be expelled from the PDMS-modified SiO_2 network, helping the hydrogels to densify their structure.

Table 4. Assignments of the main bands in Raman spectra of HA-based hybrid hydrogels.

Raman Shift (cm⁻¹)	Assignment
1415	CH_2 bending from $Si-\boldsymbol{CH_2}$ [229, 230] and CH_3 asym. bending from PDMS [232]
1405	$C-N$ stretching; deformation $C-H$ [236, 237]
1402	$\delta(Si-\boldsymbol{CH_2})$ [230]
1370	$C-H$ bending [236, 237]
1308	CH_2 stretching [229, 230]
1265	CH_3 sym. bending from PDMS [232]
1205	CH_2 groups [236, 237]
1135	$v_{as}(Si-O-Si)$ crosslinking [230]
1122	$C-OH$; $C-H$ [236, 237]
1081	$C-OH$ [236, 237]
1047	$C-C$; $C-O$ stretch [236, 237]
1036,945	$O-Si-O$ crosslinking [231]
1060	$C-C$ stretching from $v(Si-\boldsymbol{C}-\boldsymbol{C})$ [229, 230]
1015	Skeletal stretch [229, 230]
980	$Si-OH$ [231]
865	CH_3 sym. rocking from PDMS [232, 235]
850	Carbon chain[229, 230]
820	$v(C-O-C)$ of D-glucuronic acid and N-acetyl-D-glucosamine rings from HA
790	$v_a(C-Si-C)$ and CH_3 rocking from PDMS [233-235]
707	$v_s(C-Si-C)$ from PDMS [232-234]
689	$Si-\boldsymbol{CH_3}$ sym. rocking [232, 235]
495	$Si-O-Si$ sym. stretch [232, 235] and $\delta(O-Si-O)$ [233, 234]

3.5.3 STRUCTURAL CHARACTERIZATION OF HA-BASED HYBRID HYDROGELS BY ¹³C AND ²⁹Si MAGIC ANGLE SPINNING (MAS) – NUCLEAR MAGNETIC RESONANCE SPECTROSCOPY (NMR)

FT-IR and Raman spectroscopies were really useful techniques to understand some of the chemical characteristics of the designed hydrogels: 1) a possible HA-APTES grafting (chemical modification of HA molecules); 2) a possible chemical crosslinking of HA with an SiO_2 inorganic network; 3) a possible chemical incorporation of PDMS into the SiO_2 network, not only being entrapped within the hybrid hydrogel structure. Nevertheless, Nuclear Magnetic Resonance spectroscopy will confirm if the designed hydrogels can be labeled as organic-inorganic hybrid materials: hyaluronic acid chemical crosslinked by a PDMS-modified SiO_2 inorganic network.

According to literature data [238, 239], the hyaluronan molecule presents several types of carbons: 1) the methyl carbon (8A) resonance is at 24.7 ppm; 2) resonance due to carbon 2A ($C - NHCOC_3H$) bearing the $NHCOCH_3$ group is at 56.4 ppm; 3) resonance due to the methylene carbon 6A is at 62.8 ppm; 4) resonances at about 70 and 84 ppm, due to carbons 4A and 3A, respectively, appear as shoulders; 5) anomeric carbons 1A and 1B show a resonance at 103 ppm; 6) resonance due to carbon 7A is observed at 178 ppm; 8) the very intense resonance observed at about 76 ppm is due to all other methane carbons, 5A, 2B, 3B and 5B.

Moreover, the APTES molecule contains five types of carbons [240-243]: 1) two carbons attached to silicon through oxygen bonds ($Si - O - CH_2 - CH_3$), giving peaks at around 60 ppm and 17 ppm, corresponding to carbon C4 and carbon C5, respectively; and 2) three CH_2 carbons from the propyl group attached to the silicon ($Si - CH_2 - CH_2 - CH_2 - NH_2$), giving peaks at 43.5 ppm, 23 ppm and 13 ppm. The peak at 11 ppm corresponds to carbon C1 ($CH_2 - Si$) directly attached to silica. Peaks at 23 ppm and 43.5 ppm correspond to carbon C2 (CH_2) and carbon C3 ($CH_2 - NH_2$)of the propyl chain, respectively.

¹³C MAS NMR is not a quantitative technique thus the intensity and/or area of the resonances in a ¹³C MAS spectra cannot be considered for a quantitative evaluation [238]. However, ¹³C MAS NMR spectra of the HA-based hybrid hydrogels, shown in **Figure 38**, can prove the coupling of APTES (primary amine) with HA molecules to yield amide bonds.
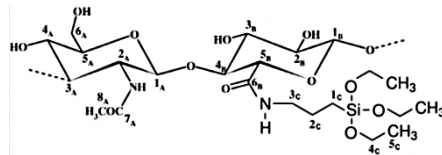
Freeze-dried HA-based hybrid hydrogels
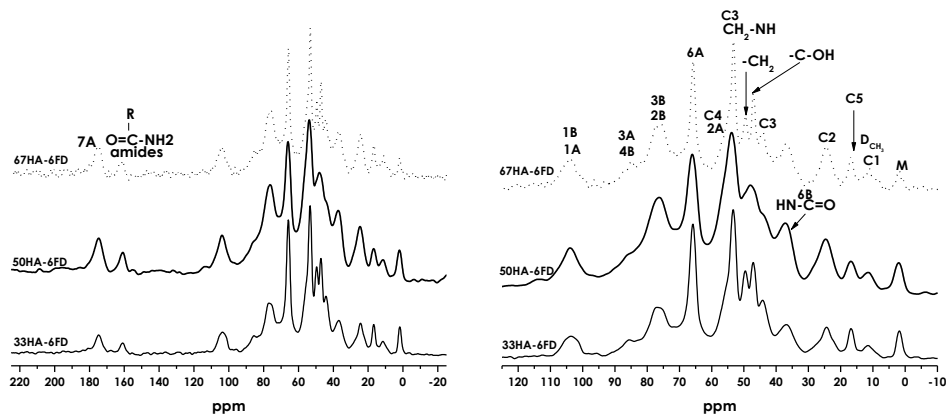
Room temperature dried HA-based hybrid hydrogels
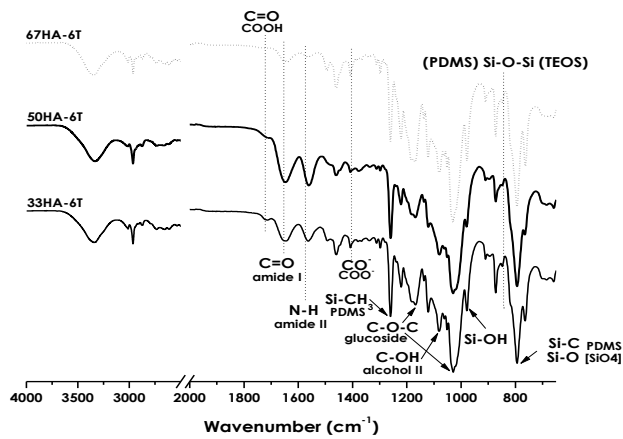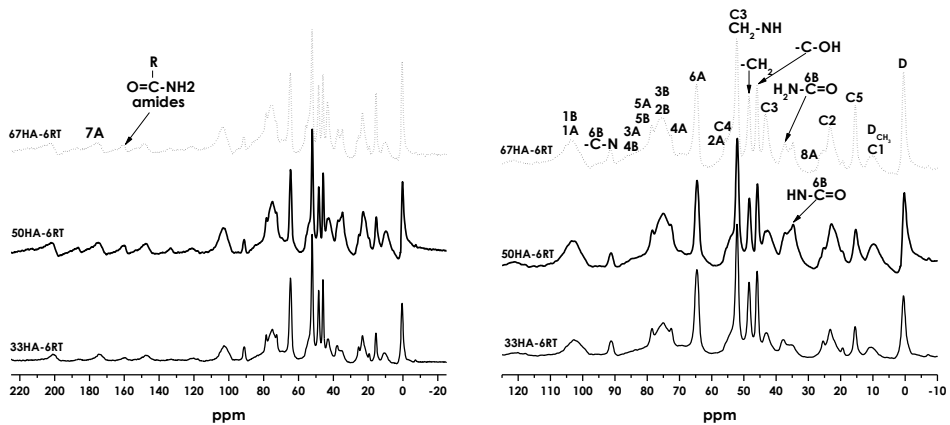

60° C dried HA-based hybrid hydrogels
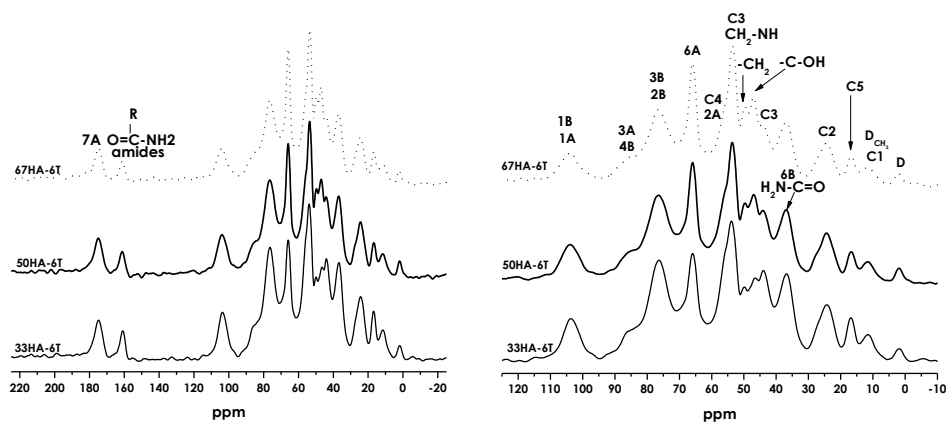
Figure 38. ^{13}C MAS NMR spectra of HA-based hybrid hydrogels synthesized at 6 *pH*.

66

The following resonance peaks confirm the amidation of HA with APTES: 1) resonance at 36 ppm [240, 244] is attributed to the carbon 6B from HA directly attached to the nitrogen atom of APTES molecules, resulting in the formation of an amide bond ($O = C - NH$); 2) resonance at 53 ppm [241] is assigned to carbon C3 ($CH_2 - NH$) bearing the grafting of hyaluronan molecules ($CH_2 - NH - HA$). However, the presence of the peak at 43.5 ppm, assigned to carbon C3 ($CH_2 - NH_2$), indicates that not all of the APTES molecules were attached to hyaluronan; 3) resonance at 160 ppm [244], attributed to amides, may also confirm HA-APTES coupling.

^{13}C MAS NMR spectra of hybrid hydrogels dried at room temperature present two resonances, one at 36 ppm and the other at 38 ppm, both attributed to (carbon 6B from HA) $-C - NH$ and $-C - NH_2$ bonds, respectively. Resonance at 36 ppm confirms HA-APTES coupling, as mentioned before. Resonance at 38 ppm [244] may be attributed to amine reactive intermediates resulting from reactions between EDC and NHS with HA. These intermediates may have not reacted with the primary amine (APTES), triggering their entrapment within the PDMS-modified SiO_2 network as the structure got densified when drying at room temperature. However, ^{13}C MAS NMR spectra of freeze-dried hybrid hydrogels and hybrid hydrogels dried at 60 °C do not present a sharp resonance at 38 ppm since the amine reactive intermediates may have been expelled from the PDMS-modified SiO_2 network through drying processes.

Resonance peak at 46 ppm attributed to $-C - OH$ can be due to self-condensation between the $-COO^- Na^+$ and $-OH$ groups in hyaluronic-based materials [226]. Moreover, the presence of resonances at 60 ppm and 17 ppm due to carbons C4 and C5 in APTES molecules and resonance at 48 ppm [244] due to $-CH_2$ in TEOS suggest that hydrolysis reactions may have not occur in all ethyl groups within the APTES and TEOS molecules to form silanol ($Si - OH$) groups. Finally, the chemical incorporation of PDMS into the SiO_2 network can be observed in the resonances peaks arising from the chain end M siloxane units at 1.8 ppm and the D siloxane units at 0.6 ppm [245].

Structural changes caused by hydrolytic-polycondensation reactions in HA-based hybrid hydrogels can be detected by ^{29}Si MAS NMR spectroscopy. The formation of monodentate, bidentate or polymeric Si species in the studied HA hybrid hydrogels can be observed in the ^{29}Si MAS NMR spectra shown in **Figure 39**.
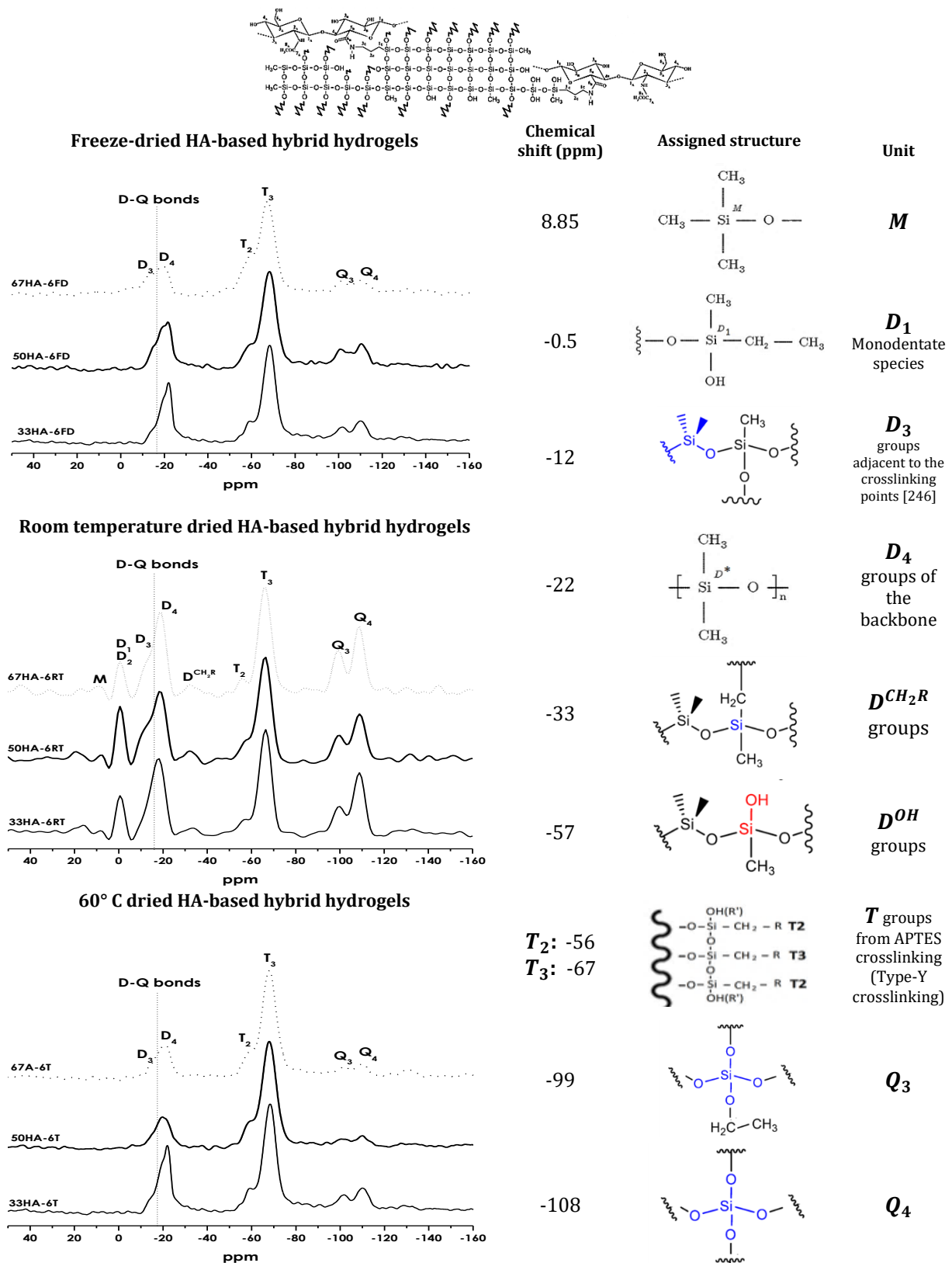
Figure 39. ^{29}Si MAS NMR spectra of HA-based hybrid hydrogels synthesized at $6\ pH$.

The ^{29}Si MAS NMR spectra of HA-based hybrid hydrogels show several Si resonances, proving the formation of a PDMS-modified SiO_2 organic-inorganic network crosslinking the hyaluronic acid. The hybrid hydrogels spectra show signals between -40 ppm and -80 ppm belonging to the grafted organic groups (HA-APTES) [247]. Specifically, these signals, $\boldsymbol{T}$ units, are attributed to trifunctional species (APTES) covalently bonded to organosilanes precursors (TEOS-PDMS) through hydrolysis-polycondensation reactions between one, two or three ethoxy groups from APTES and the $-OH$ groups from TEOS and PDMS.

Trifunctional species, $\boldsymbol{T}$ units ($CH_2CH_2CH_2NH_2 \cdot SiO_3$), are labeled as follows: 1) monodendate species, T_1 from -46 ppm to -50 ppm, are assigned to a) hydrolyzed aminopropylsilane, $CH_2CH_2CH_2NH_2-\boldsymbol{Si}(-OR/H)_3$ or b) aminopropylsilane silicon attached via one siloxane bond, $(-O-)_1\boldsymbol{Si}-CH_2CH_2CH_2NH_2$ and/or $CH_2CH_2CH_2NH_2-\boldsymbol{Si}(-OSi)(-OR/H)_2$. Note: the chemical shift at -46 ppm, corresponding to chemical shift of silicon in liquid (APTES) may indicate free silane molecules physically adsorbed on the hybrid hydrogels surface; 2) bidendate species, T_2 at -56 ppm, are assigned to aminopropylsilane silicon attached via two siloxane bonds, $(-O-)_2\boldsymbol{Si}-CH_2CH_2CH_2NH_2$ and/or $CH_2CH_2CH_2NH_2-\boldsymbol{Si}(-OSi)_2(-OR/H)$; and 3) crosslinked species, T_3 at -67 ppm, associated to aminopropylsilane silicon attached via three siloxane bonds, $(-O-)_3\boldsymbol{Si}-CH_2CH_2CH_2NH_2$, $T_3, T_m = RSi(OSi)_m(OR')_{3-m}, m \leq 3, R, R' = H$ or hydrocarbon chain). [241-243, 248].

Other chemical shifts may appear in the ^{29}Si MAS NMR spectra of HA-based hybrid hydrogels between -80 to -120 ppm, assigned to tetra-functional $\boldsymbol{Q}$ structural units (SiO_4). Signals of silanol ($Si-OH$) groups associated with vicinal or free silanols and siloxanes can appear: 1) Q_1 at -83 ppm is assigned to $\boldsymbol{Si}(OSi)_1(OH)_3$ structural units; 2) Q_2 at -92 ppm is assigned to $\boldsymbol{Si}(OSi)_2(OH)_2$ structural units.; 3) Q_3 at -101 ppm is assigned to $\boldsymbol{Si}(OSi)_3OH$ structural units; 4) Q_4 at -110 ppm is assigned to $\boldsymbol{Si}(OSi)_4$ structural units, ($Q_4, Q_n = Si(OSi)_n(OH)_{4-n}, n \leq 4$) [248, 249].

In the ^{29}Si MAS NMR spectra of HA-based hybrid hydrogels the Q_4 structural units represent interlinked SiO_4 tetrahedrons in the interior of the mesopore structure of hybrid hydrogels, while Q_3, Q_2 structural units, associated to silanol ($Si-OH$) groups, are located on the hydrogels surface. The chemical shifts referred to T_2 and T_3 indicate the formation of new siloxane linkages ($Si-O-Si$) of APTES silicon with surface silicon Q_3, Q_2 structural units from TEOS. The relative high intensity of T_3 chemical shift indicates that the incorporated aminopropyl groups are closely packed into the internal surface of HA-hybrid hydrogels,

suggesting that surface silanol $(Si - OH)$ groups, associated to Q_2 and Q_3 structural units in hybrid hydrogels are attached to aminopropylsilane (APTES) molecules *via* siloxane bonds [243]. Although T_2 signal has low intensity in ^{29}Si MAS NMR spectra, it implies different grafting degrees for different hybrid-organosilanes hydrogels composition [241]. The relative absence of chemical shifts between -46 and -50 ppm due to T_1 prompts that unreacted APTES molecules are not trapped within the *aerogels* and *xerogels* PDMS-modified SiO_2 structure [242].

Two distinct groups of silicon (Si) structural units coming from PDMS are observed; one type at the chain ending (M units) and the other type being characteristic of the silicon atoms within the chain (D units). These silicon units are labeled according to the standard shorthand nomenclature for siloxane polymers. The ^{29}Si MAS NMR spectra of hybrid hydrogels show two resonance peaks due to the incorporation of PDMS within the SiO_2 structure: 1) M siloxane units at a maximum of ~7 ppm due to ending PDMS chains; 2) D siloxane units within the silicon chain at a maximum of ~20 ppm [245].

Furthermore, in the ^{29}Si MAS NMR spectra of HA-based hybrid hydrogels show chemical shifts between -4 to -23 ppm, which are assigned to difunctional dimethylsiloxane $\boldsymbol{D}$ structural units $((CH_3)_2 \cdot SiO_2)$ [246, 248, 249]. According to the different composition and drying process in HA-based hybrid hydrogels, D species can vary: 1) monodendate species, D_1 and D_2 at -4 ppm and -7 ppm, respectively; 2) bidentate species, D_3 at -10 ppm; 3) crosslinked species, D_4 between -14 ppm to -23 ppm, which are described as D_A near -16 ppm; D_B near -19 ppm and D_C near -21 ppm. Some authors [227, 250] have assigned the chemical shift D_A between -15.5 ppm and -17.5 ppm to D units crosslinked to oxide-based structures $(D - Q$ bonds) in PDMS-SiO_2 and PDMS-$SiO_2 - CaO$ systems, confirming that PDMS is chemically bonded to SiO_2 inorganic network, both modifying the organic structure of the HA-based hydrogels, designed in the present work. Other authors [250, 251] assigned the chemical shifts D_B and D_C either to cyclic PDMS molecules in four-member rings or to D units located in different positions inside the PDMS chain, being in a less constrained environment and near to cross-linking points, like D_2 at a $D_2 - D - Q$ structure.

From the above described, it is observed that a higher hyaluronic acid (HA) concentration within the system decreases the chemical crosslinking of D units with SiO_2 structures; which can be due to the great volume of the biopolymer HA chains and their electrostatic forces, hindering $D - Q$ hybrid bonds, but triggering the formation of Q_4 and Q_3

silicon domains and D_3 and D_2 PDMS domains. These observations may suggest that the HA-based hybrid hydrogels have zones rich in silicon (SiO_2), rich in silica PDMS ($(CH_3)_2 \cdot SiO_2$) and rich in HA. However, it is also probable that high molecular polymeric HA chains coated the surface of silica nanoparticles during room temperature drying process, inhibiting the PDMS domains to crosslink with the SiO_2 structure, therefore promoting an increase of Q_4 structures [250].

However, when decreasing HA concentration (33HA<50HA<67HA), by increasing water into the hybrid *sol-gel* systems, PDMS modification leads to the formation of highly hybrid $D - Q$ crosslinked polymeric structures, as observed in the chemical shift D_A between -15.5 ppm and -17.4 ppm; whereas a low water content, monodentate and bidentate species are formed [248].

^{29}Si MAS NMR spectra of HA-based hybrid hydrogels dried at room temperature present chemical shifts related to monodendate M, D, T and Q structural units trapped within the densified PDMS-modified SiO_2 structure. When drying the hybrid hydrogels through freeze-drying process, the monodendate structural units are expelled from the crosslinked structure through supercritical conditions and polycondensation reactions are interrupted, causing the disappearance of resonance peaks assigned to monodendate units and a decrease in intensity of resonance peaks due to chemical shifts assigned to highly crosslinked Q_3 and Q_4 structural units. However, when drying HA-based hybrid hydrogels at 60 °C, resonance peaks attributed to Q_3 and Q_4 structural units show really low intensities, suggesting that temperature helps the polycondensation of monodendate M, D, T structural units, enhancing the formation of hybrid $D - Q$ bonds.

Finally, ^{29}Si MAS NMR spectra of freeze-dried hybrid hydrogels show a decrease in intensity of the chemical shift related to Q_4 structural units in comparison to hybrid hydrogels dried at room temperature. This can be attributed to an increase of Q_3 structural units resulted from the very high surface area in the hybrid hydrogel caused by the type of drying process and the large number of surface hydroxyl groups present. These hydroxyl groups ($-OH$) were unable to polycondense into a highly crosslinked SiO_2 structure (more Q_4 structural units) as the hybrid hydrogels were getting freeze [242].

From these observations it can be concluded several things: 1) high molecular polymeric HA chains may coat the PDMS-modified SiO_2 structure; 2) high molecular

polymeric HA chains may coat silica (SiO_2) nanoparticles inhibiting the incorporation of PDMS into the structure; 3) chemically unmodified polymeric HA chains (unhybridized HA chains) and low molecular polymeric HA chains may prefer to be located between silica (SiO_2) and PDMS domains, affecting the number and nature of crosslinking between those domains; 4) drying process also affects the crosslinking in HA-based hybrid hydrogels, enhancing or inhibiting polycondensation reactions; 5) freeze-drying process increases Q_3 structural units within the network because of the formation of a very high surface area and the increase in the number of surface hydroxyl groups present in the hybrid hydrogel; 6) temperature (60 °C) helps the polycondensation of monodendate M, D, T structural units, enhancing the formation of hybrid $D - Q$ bonds. To better understand the M, D, T structural units, **Figure 40** displays a schematic representation of them [246].
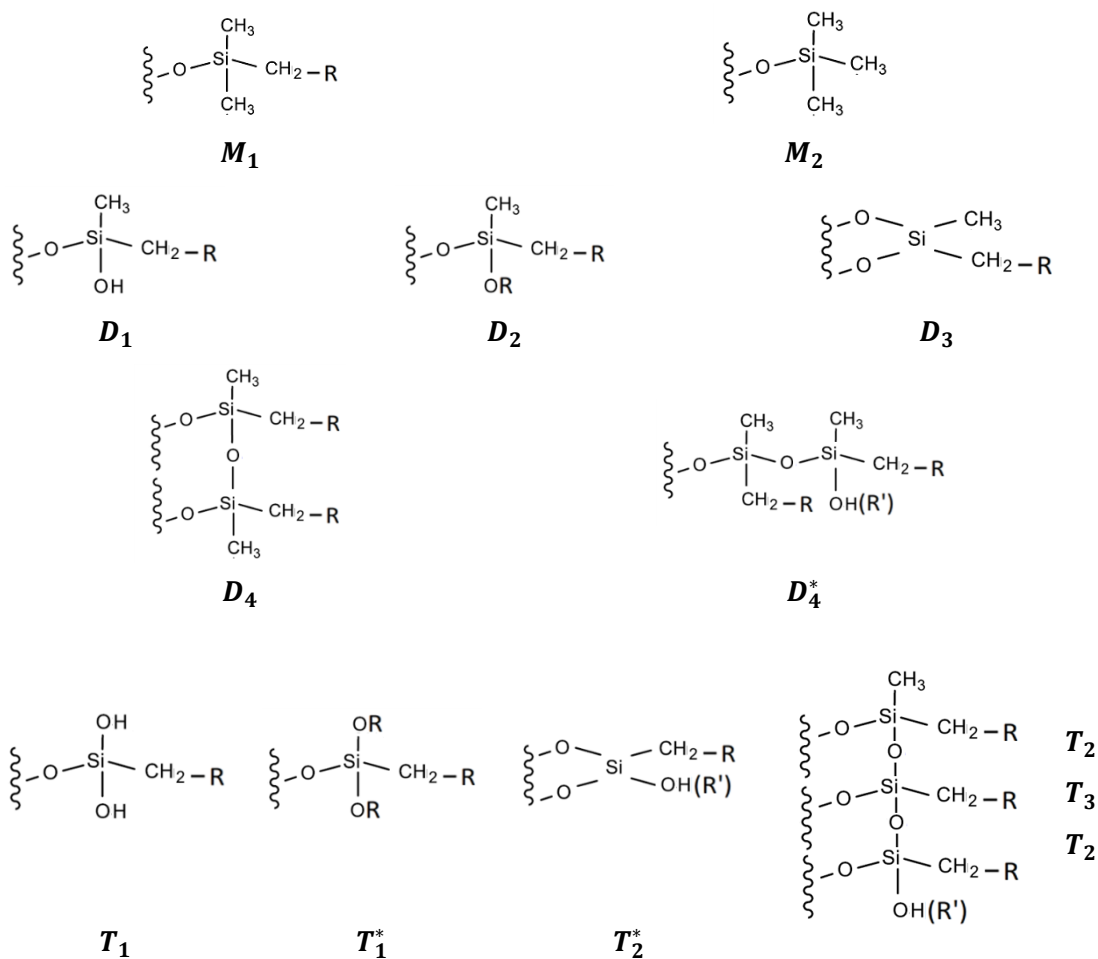
Figure 40. Structural units in hybrid APTES-PDMS-modified SiO_2 structures.

3.5.4 MORPHOLOGICAL CHARACTERIZATION OF HA – BASED HYBRID HYDROGELS BY SCANNING ELECTRON MICROSCOPY (SEM)

The designed HA-hybrid hydrogels have micrometric and nanometric organic-inorganic interpenetrating networks. **Figure 41** shows SEM images, at different magnifications, of 50HA-based hybrid hydrogels morphology. These materials exhibit some surface irregularities that can be attributed to silica precipitation nodes [233] and different pore shapes and sizes, showing pore diameters between $5 \leq \phi \leq 30$ µm.

Since porous materials possess interesting applications, controlling their pore size, distribution and morphology plays an important role in their mechanical, biological and degradative properties. Therefore, synthesis conditions, aging and drying process have strong influence on hybrid hydrogel textural properties. Particle size is closely related to reagent addition rate and the type of solvent used in the *sol-gel* process. Porous structure is closely related to aging and drying conditions, resulting in the appearance of different kinds of pores, including micro and mesopores [233].

From SEM images, it is observed that drying process affects directly on the hybrid hydrogels morphology. Room temperature drying process produces dense morphologies. The 50HA-6RT hybrid hydrogel shows a flat homogeneous morphology with round pores of $10 \leq \phi \leq 15$ µm. This can be due to a slow but constant drying rate, which helps the hybrid structure to shrink slowly and densify by reducing number and size of pores. This type of drying process can make the hybrid hydrogel to shrink until its structure collapse due to capillary tension [233].

On the other hand, freeze-drying produces highly porous morphologies and materials with larger surface areas. 50HA-6FD hybrid hydrogels shows morphologies with abundant small irregular pores, in comparison with hydrogels dried at room temperature. These materials present mean pore diameters of $\phi <10$ µm. Moreover, it can be observed that freeze-dried hydrogels have small pores within the bigger ones. These irregularities in pore shape and size are due to the formation of water crystals when freezing the hybrid hydrogels at -20 °C. However, since ethanol (byproduct of hydrolysis reactions) freezes at -110°C, it remains in liquid state within the hydrogel structure when water is freeze, leading to the formation of semi round porous when ethanol is expelled (in gas form) through hypercritic conditions from the hybrid matrix.

60 °C drying process produces morphologies with big pores. Liquids (ethanol and water) entrapped within the surface layers are evaporated rapidly, producing pores with $20 \leq \phi \leq 30$ µm in 50HA-6T hybrid hydrogels. Liquids trapped within inner matrix layers delay to reach evaporation temperature, decreasing their evaporation rate and producing pores with smaller diameters, between $5 \leq \phi \leq 15$ µm.

50HA 6 pH	Freeze-dried HA-based hybrid hydrogels	Room temperature-dried HA-based hybrid hydrogels	60º C dried HA-based hybrid hydrogels
250x			
500x			
1000x			
2500x			
8000x			
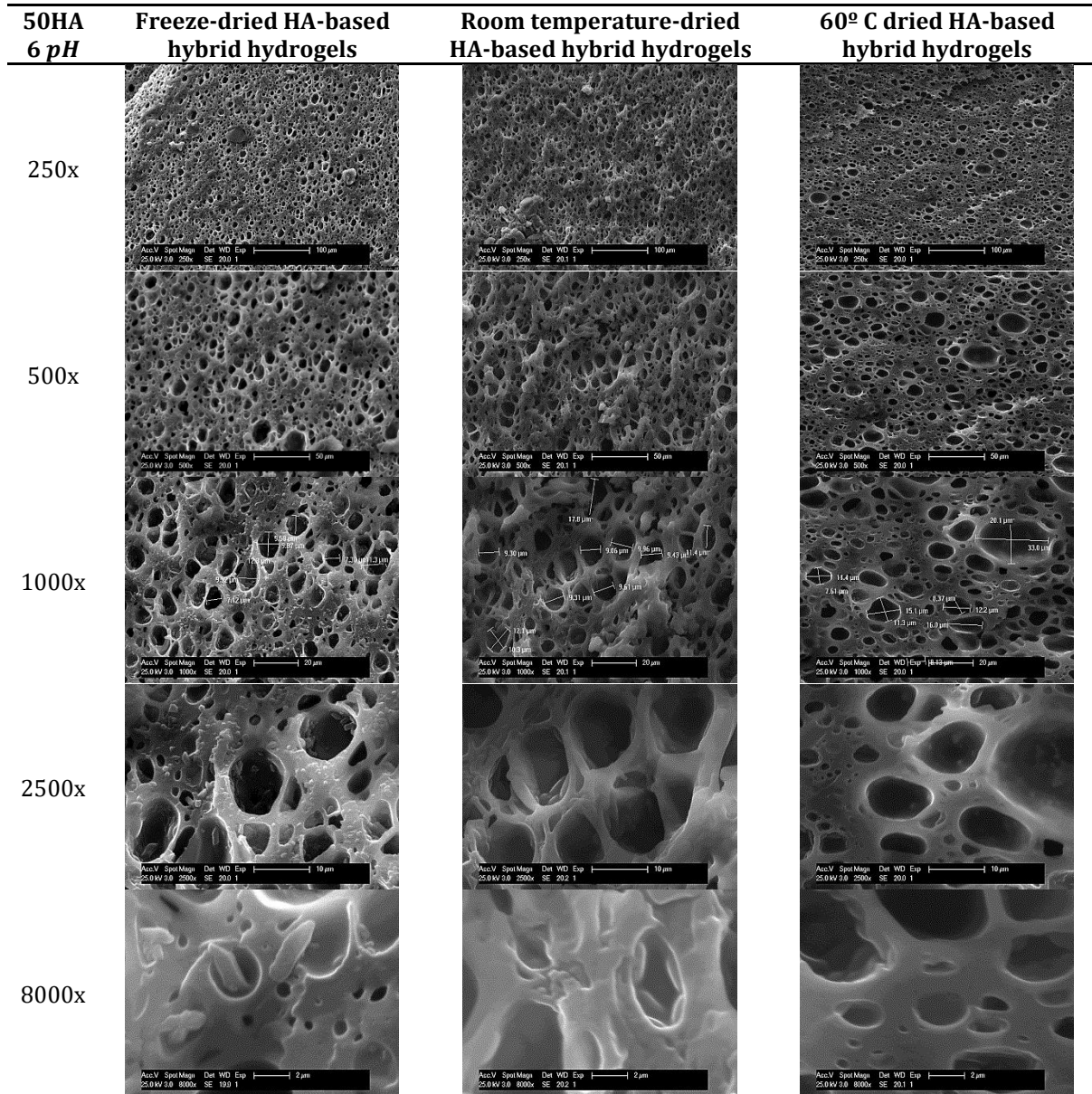
Figure 41. Morphology, pore shape and size in 50HA-based hybrid hydrogels synthesized at 6 pH.

3.5.5 MORPHOLOGICAL CHARACTERIZATION OF A PCL SCAFFOLD FILLED WITH HA – BASED HYBRID HYDROGEL BY ENVIRONMENTAL SCANNING ELECTRON MICROSCOPY (ESEM)

Manufacturing porous 3D scaffolds resembling the chemical composition and architecture of the extracellular matrix (ECM) of cartilage is the main challenge tissue engineers are facing. The HA-based hybrid hydrogels are three-dimensional hydrophilic polymer-inorganic networks crosslinked by covalent bonds forming a water-insoluble hydrogel [14]. These HA-based hydrogels will be tested as matrices to build up scaffolds providing highly desirable 3D environments for cell growth. As shown in **Figure 41**, conventional drying process (freeze-dried and oven dried techniques) can provide a precisely control of pore size, interconnectivity and pore geometry in hydrogels as long as drying conditions are controlled throughout the whole drying process. However, 3D printing can produce 3D scaffolds with an organized interconnected pore structure (**Figure 42**), which may ensure good functionality and good mechanical strength, holding a good promise for the regeneration of cartilaginous tissue. In **Figure 42** it can be superficially observed that the 50HA-6W hybrid hydrogel fills completely the 3D printed artificial square-pore PCL scaffold.

To better observe how the 50HA-6W hybrid hydrogel interpenetrates the 3D printed artificial square-pore PCL scaffold, **Figure 43** shows the ESEM images of the slices of each of the elements needed to manufacture a 3D artificial scaffolds that could resemble the chemical composition and architecture of cartilage tissue.

Optical Microscopy 25X
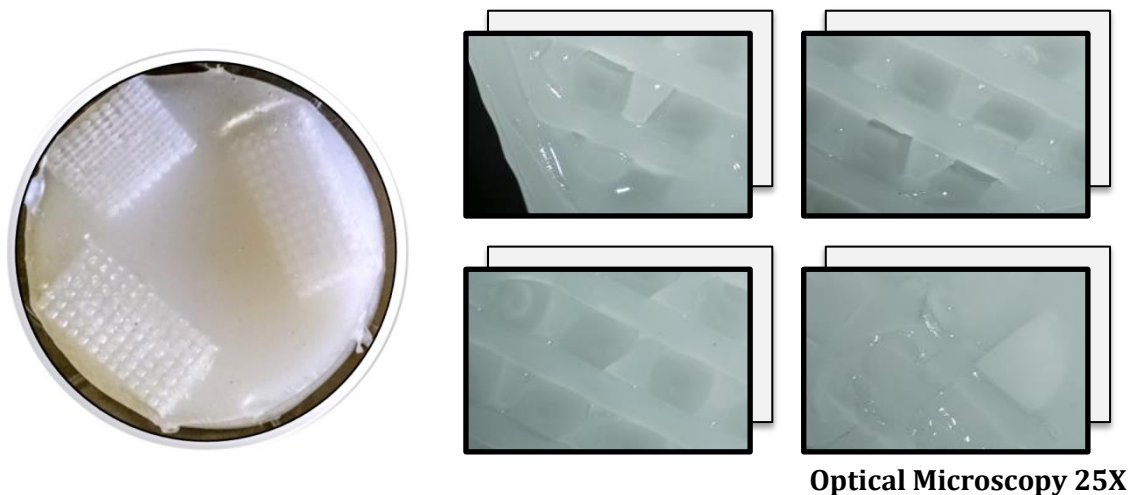
Figure 42. Physical appearance of the 50HA-6W hybrid hydrogel being used as filler matrix of a PCL 3D scaffold, trying to resemble chemical composition and architecture of cartilage tissue.

In **Figure 43** it is observed that PCL scaffold **(A)** has an organized interconnected square-pore structure. The HA-based hybrid hydrogel **(B)** shows a compact morphology right after aging time. Their pores are filled with water from synthesis and syneresis process. The hybrid hydrogel **(C, D)** shows good interpenetration into the PCL scaffold; however, some defects (pores), caused by the entrapped air within the hydrogel during infiltration method, prior to gelation, are observed in the hydrogel 3D matrix. Since PCL demonstrates a hydrophobic behavior, the hydrogel is not completely adhered to it.
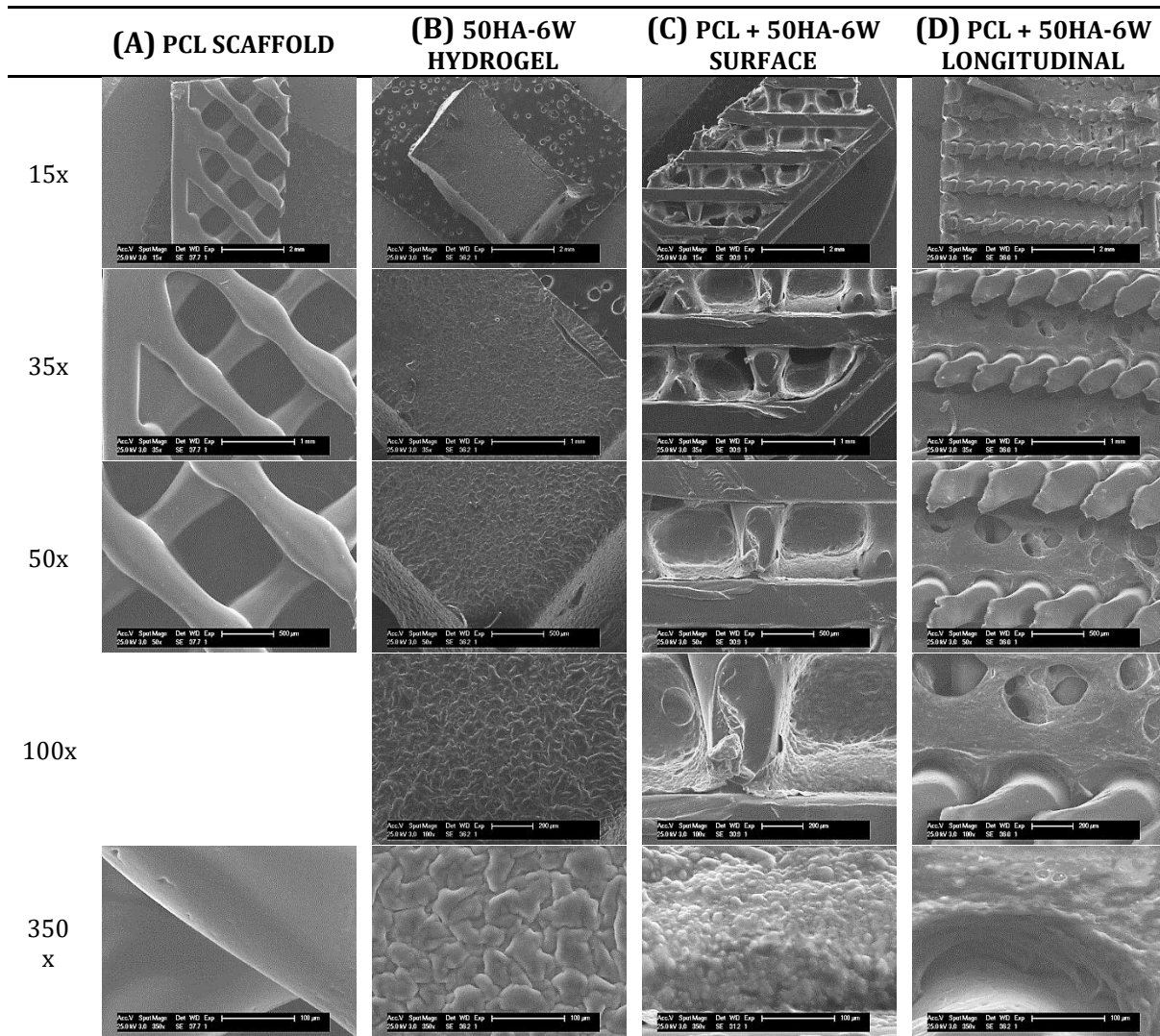
Figure 43. Elements needed to manufacture 3D scaffolds resembling the chemical composition and architecture of cartilage tissue. **(A)** ESEM image of a PCL scaffold. **(B)** ESEM image of the hydrated HA-based hybrid hydrogel after aging time. **(C)** ESEM image of the surface of PCL filled with the 50HA-6W hybrid hydrogel. **(D)** ESEM image of a longitudinal slice of the PCL filled with the 50HA-6W hybrid hydrogel.

3.5.6 THERMAL CHARACTERIZATION OF HA-BASED HYBRID HYDROGELS BY THERMOGRAVIMETRIC ANALYSIS (TGA)

HA-based hybrid hydrogels were thermally characterized to identify temperatures at which thermal decomposition occurs. Polymer fraction (hyaluronic acid and PDMS silicone) in HA-based hybrid hydrogels was also studied by thermal decomposition under air atmosphere. Thermogravimetric analysis (weight loss curves and derivative weight loss curves) of HA-based hybrid hydrogels is shown in **Figure 44**.

Figure 44-A shows TGA curves comparing the three studied compositions of HA-based hybrid hydrogel dried through a specific drying process (freeze-drying, room temperature drying or 60 °C drying). **Figure 44-B** shows TGA curves comparing the three different drying processes affecting one HA-based hybrid hydrogel composition (67HA, 50HA or 33HA).
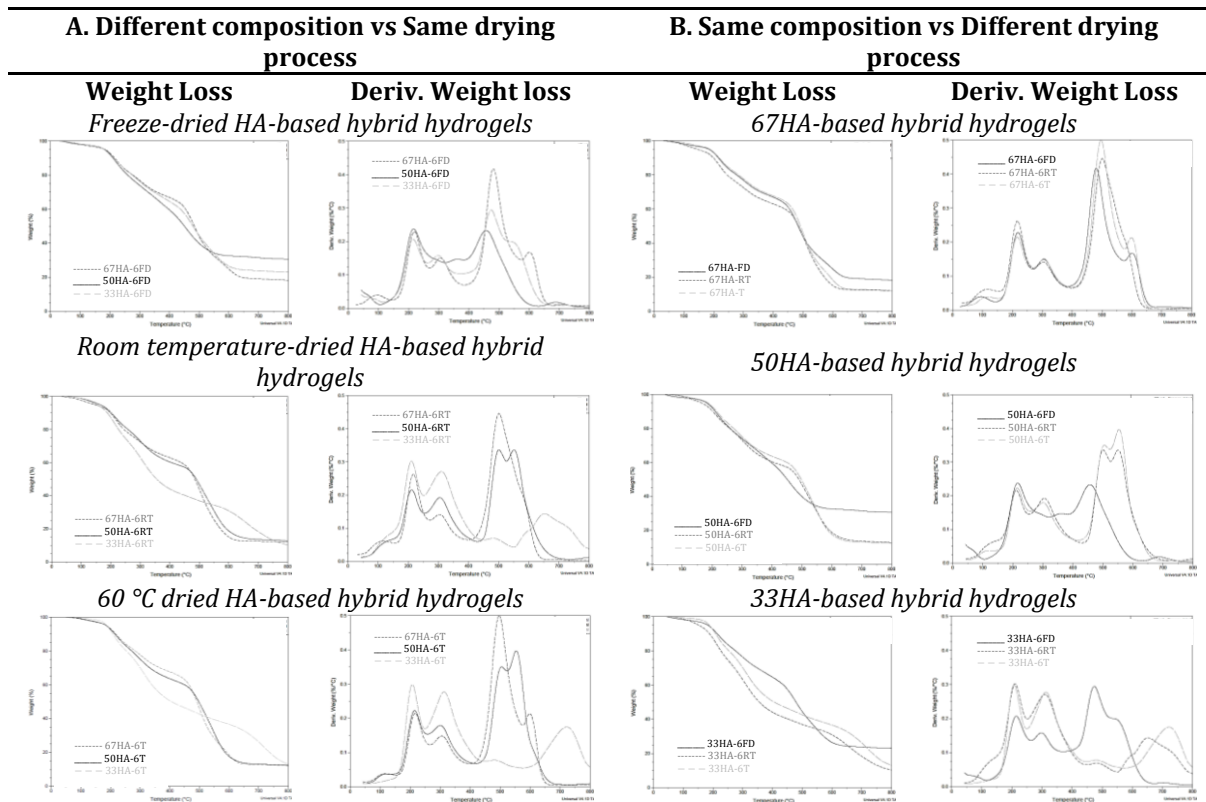
Figure 44. Thermogravimetric analysis (TGA) and derivative TGA curves of HA-based hybrid hydrogels synthesized at 6 *pH*.

TGA analysis in HA-based hybrid hydrogels has several stages of weight loss. The first thermal stage occurs between 40 °C and 150 °C, being attributed to moisture loss (adsorbed water) and residual water and ethanol loss by evaporation, both are byproducts of hydrolysis-polycondensation reactions [252, 253]. Room temperature-dried HA-based hybrids are the hydrogels with larger amount of water and ethanol entrapped within the structure, thus experiencing greater weight losses of ~5.5% at ~116 °C in comparison to freeze-dried hybrid hydrogels (weight losses of ~2.55% at ~82 °C) and 60 °C-dried hybrid hydrogels (weight losses of ~2.55% at ~111 °C).

The second thermal stage occurs between 200-380 °C. The main decomposition of pure hyaluronic acid, attributed to the partial break of its molecular structure, takes place at a temperature range between 200 °C and 300 °C (T_{onset} at 214 °C) [254]. The designed HA-based hybrid hydrogels have an average weight loss of ~21% at ~215 °C. Moreover, HA residues are further degraded at ~312 °C, presenting weight losses between 30% and 60% in the designed hydrogels. 33HA-based hybrids dried at both, room temperature and 60 °C, reached almost a 60% of weight loss. This second stage, attributed to HA thermal degradation, involves the disintegration of intermolecular bonds and the partial breaking of high molecular HA polymeric chains into lower molecular HA polymeric chains. It is observed that derivative thermo-stability in hydrogels is clearly influenced by the hybrid hydrogels composition and drying process, as shown in **Table 5**.

Table 5. Maximum temperature decomposition peak (°C) and weight losses (%) in each thermal stage from thermogravimetric analysis of HA-based hybrid hydrogels.

Samples	T_{max} (ºC)				Δm (%)			
Thermal Stages	**I** (25-150 °C)	**II** (200-360 °C)	**III** (400-600 °C)	**IV** (600-800 °C)	**I** (25-150 °C)	**II** (200-360 °C)	**III** (400-600 °C)	**IV** (Final Weight °C)
67HA-6FD	94.45	218.74	307.16	481.42	603.15	3.41	18.98	32.16	71.27	81.79
50HA-6FD	72.67	217.46	357.13	457.07	687.72	2.05	28.87	38.97	67.73	69.33
33HA-6FD	79.08	214.90	299.47	475.01 549.33	---	2.16	18.30	36.05	60.02 75.87	76.97
67HA-6RT	108.55	216.18	304.59	500.64	---	5.87	23.53	37.16	87.33	87.94
50HA-6RT	117.52	211.05	305.88	499.36 550.61	---	24.81	19.43	41.46	61.80 86.24	87.24
33HA-6RT	121.36	211.05	311.00	486.55	650.56	5.59	25.28	59.27	65.79	89.69
67HA-6T	113.67	216.18	307.16	496.80	601.00	3.35	17.93	32.22	76.61	81.79
50HA-6T	109.83	213.62	302.03	504.48 554.46	---	2.71	17.74	37.95	58.8 86.95	87.65
33HA-6T	108.55	208.49	313.56	487.83	721.03	1.59	19.24	52.89	62.01	86.94

The earliest thermal degradation for the second stage was found for the hybrids with less HA concentration (33HA) as follows: 33HA-6T hydrogel dried at 60 °C (T_{onset} at 208.49 °C, mas loss 19.24%), then 33HA-6RT dried at room temperature (T_{onset} at 211.05 °C, mas loss 25.28%) and finally by freeze-dried 33HA-6FD

(T_{onset} at 214.90 °C, mas loss 18.30%). According to this information, drying the 33HA hybrid hydrogels at 60 °C might have cause a pre-degradation of HA, producing less thermostable materials. On the other hand, 50HA-6FD hybrid hydrogel was the most thermostable hydrogel during the second stage (HA degradation), having T_{onset} at 217.46 °C and 357.13 °C with weight losses of 28.87% and 38.97%, respectively. This could be caused by a better efficiency in HA chemical modification (HA-APTES grafting) and to the possible hydrogen bonding interaction between molecules due to the presence of amino ($-NH_2$) and hydroxyl ($-OH$) groups in APTES, TEOS and PDMS as well as ($-OH$), ($COOH$), ($C = O$) in hyaluronic acid [254].

The increase of temperature at which HA thermal degradation occurs in the designed HA-based hybrid hydrogels ($T = 214\,°C - 219\,°C$) may suggest that chemically modified HA chains (HA-APTES molecules) are thermally more stable than unhibridized HA chains. The incorporation of APTES may have provided thermal stability to HA polymeric chains, since the incorporated aminopropyl groups are closely packed into the internal surface of HA-hybrid hydrogels, working as bridging points between HA polymeric chains and the PDMS-modified SiO_2 structure, resulting in a PDMS-modified inorganic SiO_2 structure coated by high molecular HA polymeric chains [242], as shown in **Figure 45**. On the other hand, the HA-based hybrid hydrogels dried at room temperature and at 60 °C present lower temperatures ($T < 214\,°C$) at which HA thermal degradation occurs. This can be due to low molecular polymeric HA chains and chemically unmodified polymeric HA chains preferring to be located between silica (SiO_2) and PDMS domains, affecting the number and nature of crosslinking between those domains, facilitating HA thermal degradation to start.
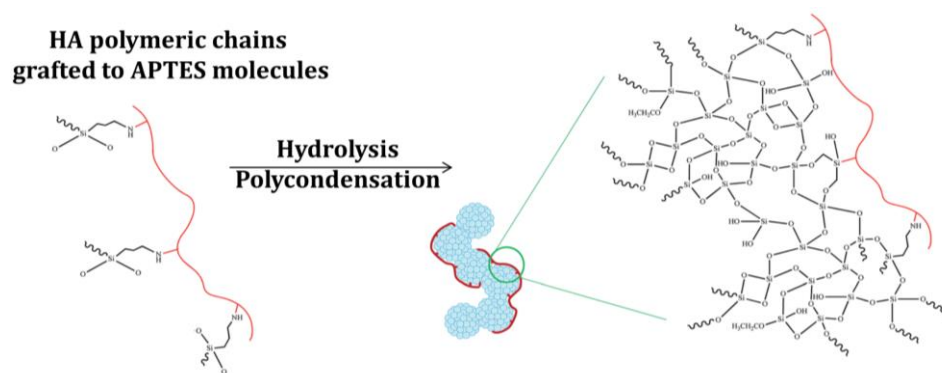
Figure 45. PDMS-modified SiO_2 structure being surrounded by HA chains grafted to APTES, working as a connecting agent to form HA-based hybrid hydrogels.

The third thermal stage, attributed to PDMS chain thermal degradation, takes place between 400°C and 600 °C. During thermal PDMS degradation, two simultaneous and competitive degradation mechanisms are produced: 1) *molecular mechanism* occurring through cyclic oligomers formation due to the redistribution of siloxane bonds, with the participation of d orbitals of silicon (Si) atoms; and 2) *radical mechanism* consisting on the direct oxidation of methyl groups *via* hydroperoxide formation, decomposing silicone (PDMS) into CO_2, H_2O and H_2, causing the densification of the material [233]. According to Almeida *et al* [250], weight loss at $\sim$375 $°C$ is attributed to PDMS decomposition, forming cyclic oligomers (mainly hexamethylcyclotrisiloxane) through $Si - O$ bond scission, resulting in a chain folded cyclic conformation which is energetically more favorable. The second weight loss that arises above $\sim$400 $°C$ is related to the final decomposition of the cyclic oligomers.

According to above data, HA-based hybrid hydrogels show better thermal stability since the initial PDMS degradation appears at higher temperature, between 400°C and 600 °C. The first derivative peak at $\sim$487 $°C$ corresponds to methyl oxidation, from $Si - CH_3$ bonds, which is assumed to be initiated by O_2, by means of hemolytic cleavage mechanism to form silanol ($Si - OH$) groups, which would condense into siloxane bridges at higher temperatures. Additionally, this first peak may have also arisen due to the oxidation of aminopropyl groups from APTES molecules, being ungrafted during thermal degradation of HA. According to some authors [250], when hybrid materials are heated above 300 °C, some D units are oxidized to T units and then to further Q units. The second derivative peak at $\sim$550 $°C$ is related to the final decomposition of the cyclic PDMS oligomers. During these two degradation steps, the major degradation products are a mixture of oligomers with CO_2 and water. According to Peña-Alonso *et al.* [251], the chemical incorporation of APTES into a PDMS-modified SiO_2 structure produces an increase in the temperature at which both derivative peaks of PDMS thermal degradation appear, boosting thermal stability in HA-based hybrid hydrogels. Moreover, the increasing temperature at which derivative peaks appear may indicate that most methyl and aminopropyl groups, from PDMS and APTES, are located over the whole hydrogel volume, being difficult to remove, suggesting an homogeneous incorporation of PDMS and APTES into the materials network. [233, 251].

Only a determined percentage of the organic component (PDMS) can react with the inorganic fractions (APTES-TEOS) to produce the hybrid material; thus, unreacted PDMS chains of different molecular weight are entrapped into the hydrogels network. However,

some of these chains can be removed from the matrix core through drying process, especially the freeze-drying process.

Chain conformation of PDMS into the hybrid hydrogels directs the kinetic of its thermal decomposition reaction. As oxidative degradation of PDMS begins with the oxygen attacking dimethyl groups ($Si - (CH_3)_2$), the more accessible is the organic group, the activation energy to accomplish depolymerization reaction is lower [233]. Thus, the greater the number and size of pores is in the materials (greater surface area), as in freeze-dried HA-based hybrid hydrogels, the easier is for the oxygen to attack methyl groups ($Si - (CH_3)_2$), decreasing degradation temperature of PDMS thermal decomposition. Consequently, freeze-dried HA-based hybrid hydrogels present PDMS thermal degradation at lower temperatures ($T_{onset} \sim 450 - 482\ °C$) than in the HA-based hybrid hydrogels dried at room temperature ($T_{onset} \sim 486 - 500\ °C$) and HA-based hybrid hydrogels dried at 60 °C ($T_{onset} \sim 487 - 505\ °C$).

A fourth final significant stage of weight loss appears above 600 °C. At this temperature, hybrid materials completely oxidize their organic components (HA, PDMS and aminopropyl groups in APTES), leaving as residues only amorphous silica (SiO_2). When all the organic components are degraded, inorganic polycondensation reactions take place, resulting in the formation of Q_4 structural units, representing a [SiO_4] tetrahedron-network. 67HA-6FD and 67HA-6T hybrid hydrogels oxidize at lower temperatures ($T_{onset} \sim 601 - 604\ °C$, weight loss $\sim 80 - 87\%$) than 50HA-6FD, 33HA-6RT and 33HA-T hybrid hydrogels, oxidizing at higher temperatures ($T_{onset} \sim 650 - 722\ °C$, weight loss $\sim 70\% - 90\%$). Thus, drying and oxidative conditions play an important role in thermo-oxidative resistance, changing thermal history of hybrid hydrogels [253].

From the previous analysis, several conclusions are arisen: 1) since freeze-dried hybrid hydrogels have a greater surface area and a larger number of surface hydroxyl ($-OH$) groups, the amount of adsorbed moisture increases on the materials surface. Consequently, when starting TG analysis, the surface adsorbed water is easier to evaporate, decreasing temperature in the first thermal stage; 2) APTES grafted to high molecular polymeric HA hybridized chains gives thermal stability to materials by increasing thermal degradation temperature of HA in freeze-dried hydrogels; 3) since high molecular weight polymeric HA chains coat silica (SiO_2) nanoparticles, PDMS tends to stay outside HA chains triggering a faster degradation of methyl groups in PDMS because oxygen enters easily through pores,

thus facilitating oxidation of D units from PDMS into T units and further Q units, and decreasing reaction temperature of PDMS in thermal degradation of freeze-dried hydrogels; 4) hybrids dried at room temperature and at 60 °C show more densified structures, hindering evaporation of adsorbed moisture and entrapped ethanol, increasing temperature in the first thermal stage; 5) in hybrids dried at room temperature and at 60 °C, HA degrades at lower temperatures since ungrafted HA chains and low molecular weight HA chains are entrapped between SiO_2 and PDMS domains, being easier to degrade; 6) as ungrafted HA degrades, PDMS-modified SiO_2 network is reorganized and siloxane chains are reoriented in a way that the structure is stabilized, causing an increase of the thermal decomposition temperature of PDMS; 7) APTES gives thermal stability to PDMS chains.

3.6 CHARACTERIZATION OF CHONDROITIN SULFATE – BASED PDMS-MODIFIED SiO_2 ORGANIC – INORGANIC HYBRID HYDROGELS

CS-based hybrid hydrogels are characterized to determine their chemical, structural and morphological properties. Chondroitin sulfate (CS) has a biochemical structure similar to that of hyaluronic acid. CS is a sulfated glycosaminoglycan (GAG) composed of a chain of alternating sugars (N-acetylgalactosamine and glucuronic acid). Chondroitin sulfate is found attached to proteins as part of proteoglycans, which work as important constituents of cartilage structure. Chondroitin sulfate provides much of the cartilage resistance to compression.

Hydrogels based on chondroitin sulfate have been studies as part of biopolymer gel-systems based on hyaluronic acid, chitosan and collagen. However, these materials have fragile resistance and degradation properties in comparison to native cartilage tissue. The importance of studying chondroitin sulfate hydrogels crosslinked with a PDMS-modified SiO_2 structure relays on finding the optimal composition and drying process needed to decrease their natural degradative and biological properties.

3.6.1 STRUCTURAL CHARACTERIZATION OF CS – BASED HYBRID HYDROGELS BY FOURIER TRANSFORM INFRARED SPECTRSCOPY (FT-IR)

The infrared spectra of CS-based hybrid hydrogels are shown in **Figure 46**. Important bands attributed to both CS chemical modification (CS-APTES) and further formation of organic-inorganic PDMS-modified SiO_2 structure crosslinking CS chains are observed in the FT-IR spectra: 1) the band at 1740 cm^{-1} can be related to stretching vibration ($\vartheta_{C=O}$) of carboxyl $COOH$ group in chondroitin sulfate [224,225]; 2) the band at 1560 cm^{-1} is assigned to the formation of amide II bonding between the carboxyl COO^- groups in CS and the amine group in APTES [226]: 3) the band located at 1259 cm^{-1} is related to the symmetric deformation of the CH_3 group in the $Si - (CH_3)_2$ bonds from PDMS [227, 228]; 4) the band at 850 cm^{-1} corresponds to the presence of hybrid crosslinked SiO_2 (Q units) – PDMS (D units) structures, that is (TEOS) $Si - O - Si$ (PDMS) bonds; 5) the band at 793 cm^{-1} is assigned to $Si - X$ bonds, where $X = O, C$. $Si - O$ bonds correspond to the silicon tetrahedron $[SiO_4]$ and $Si - C$ bonds correspond to PDMS and APTES molecules [227, 228].

The drying process influenced the final state of the hybrid hydrogels. The FT-IR spectra of 100CS-7RT hydrogel shows a higher intensity of the band at 850 cm^{-1}, suggesting a better integration of PDMS into the SiO_2 inorganic structure crosslinking; thus showing the best formation of crosslinking hybrid network.
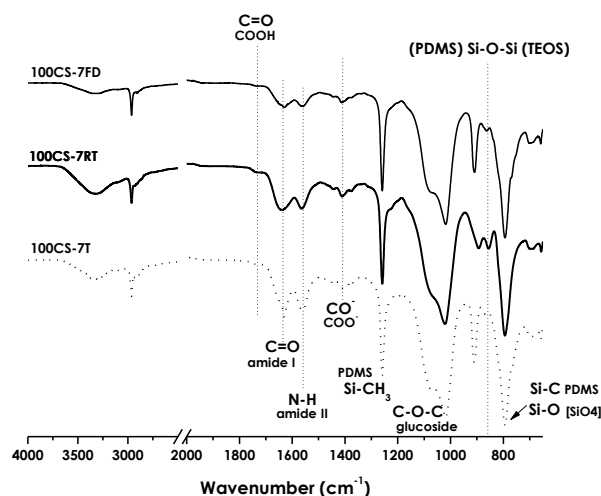
Figure 46. FT-IR spectra of CS-based hybrid hydrogels synthesized at 7 pH.

3.6.2 STRUCTURAL CHARACTERIZATION OF CS – BASED HYBRID HYDROGELS BY RAMAN SPECTROSCOPY

The Raman spectra of the CS-based hybrid hydrogels are shown in **Figure 47**. The identified bands were assigned according to literature data [229, 237], as shown in **Table 4**. Raman spectra of the CS-based hybrid hydrogels show similar bands as the ones described before in the Raman spectra (**Figure 37**) of the hyaluronic acid (HA) hydrogels. Therefore, several Raman bands related to silica-based hybrid materials and polysaccharide-based hydrogels are observed in the Raman spectra of the current studied CS-based hybrid hydrogels. From the Raman spectra, it can be observed that the intensity of the bands depends on the hydrogel pH synthesis and drying process.

In the Raman spectra of the CS-hydrogels there are observed several of the Raman scattering due to bond vibrations related to the polysaccharide, chondroitin sulfate (CS) [236, 237]; the chemical modification of CS with APTES [229, 230]; and the formation of the PDMS-modified SiO_2 structure crosslinking the chondroitin sulfate molecules [230-235]. These bands are summarized as follows: 1) the band at 820 cm^{-1} related to the stretching vibration of $C - O - C$ bonds due to the chondroitin sulfate chain composed of alternating repetitive units of N-acetylgalactosamine and glucuronic aid; 2) the incorporation of APTES to CS chains is proven with the band at 1060 cm^{-1} assigned to the stretching vibration of $C - C$ bonds, being near to the Si atom in the carbon chain from APTES; 3) the formation of crosslinking SiO_2 structure is confirmed by the bands at 1036 cm^{-1} and 495 cm^{-1} assigned to $Si - O - Si$ bonds; and 4) the incorporation of PDMS is observed with the band at 707 cm^{-1}, attributed to $C - Si - C$ symmetric stretching vibration.

CS-based hybrid hydrogels were prepared by controlling two different pH values during synthesis process, affecting efficiency in the chemical modification (amidation reaction) of chondroitin sulfate and further crosslinking *via* hydrolysis-condensation reactions. As a result, it is observed in Raman spectra, that bands due to $C - O - C$ bonds in the chondroitin sulfate chain and to PDMS-modified SiO_2 organic-inorganic hybrid structure differ in intensity.

According to literature, in order to increase efficiency in the chemical modification of polysaccharides when using EDC and NHS and to catalyze *sol-gel* reactions, an acidic environment ($pH = 4.5 - 6.5$) is needed during synthesis process. Nevertheless, a neutral pH

$(7.0 - 7.3\,pH)$ can be used in both types of reactions, even if reaction efficiency may decrease in comparison to systems synthesized under acidic conditions. Using neutral pH during synthesis process may be a good option if the main objective is to seed or inject cells right after gelation of hydrogels.

The pH at which synthesis process occur, affecting directly gelling time of hydrogels, and the type of drying process will modify the CS-based PDMS-modified SiO_2 organic-inorganic hybrid structure when hydrolysis-reactions are taking place. The intensity of the important bands described before referred to the polycondensation of SiO_2 structure and the incorporation of PDMS into it will vary depending predominately on pH and then drying process.

When using a $6\,pH$ polycondensation rate increases, since acidic conditions catalyze *sol-gel* reactions. Thus, the hydrogels prepared at $6\,pH$ show a better SiO_2 network crosslinked to chondroitin sulfate polymer chains as can be seen in bands located at 1036 cm^{-1} and 820 cm^{-1}, being attributed to $O - Si - O$ bonds of SiO_2 structure and $C - O - C$ bonds of CS chains composed of alternating repetitive units, respectively, in comparison to hydrogels prepared at $7\,pH$. Moreover, in both types of hydrogels, the bands attributed to PDMS are observed, indicating that the incorporation of PDMS chains into the organic-inorganic structure occurs; either by the formation of $(PDMS: (CH_3)_2 \cdot SiO_2)\,D - Q\,(TEOS: SiO_2)$ bonds or by the PDMS chains being entrapped within the structure with no chemical bonding.

During *sol* state, prior to gelation, the hydrolysis and condensation reactions occur at a certain rate depending on the pH; however, when gelling transition starts, reaction rate decreases due to the reduction in the mobility of the components. Therefore, an acid pH enhances the hybrid network formation leading into a denser structure with less monodendate and bidendate D, T, Q structural units. Furthermore, when allowing the hybrid hydrogels to age and then dried at a constant but slow rate, the hydrogel network will be reinforced through further polymerization.

Likewise variation in pH causes structural changes; drying process affects polycondensation rate and formation of crosslinked D, T, Q structural units. Variation on micro and nanostructure can be modulated by the type and duration of drying process.

Freeze-dried CS-based hybrid hydrogels
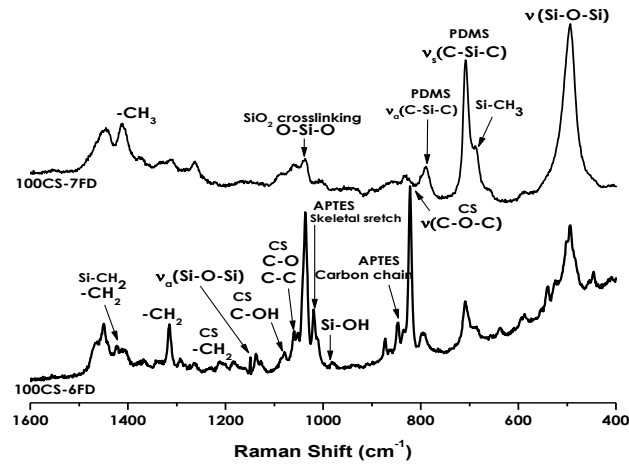
Room temperature CS-based hybrid hydrogels
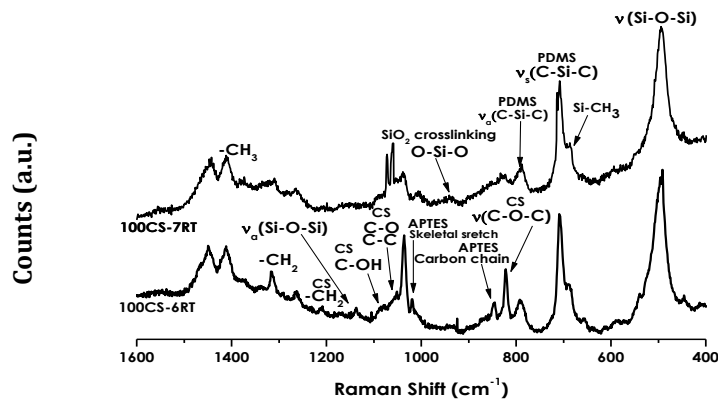
60° C dried CS-based hybrid hydrogels
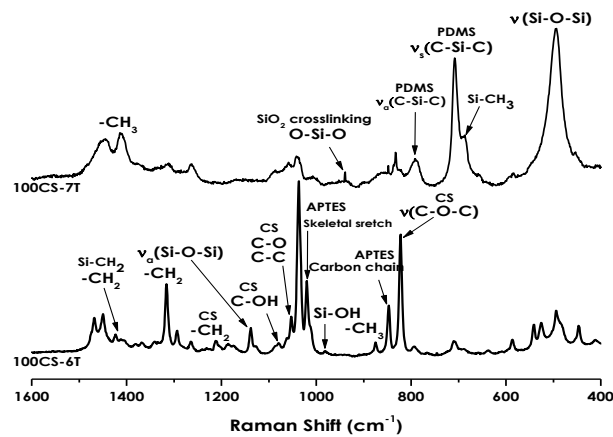
Figure 47. Raman spectra of CS-based hybrid hydrogels synthesized at 6 *pH* and 7 *pH*.

Raman spectral mapping is a method used in this research to generate detailed chemical images based on a CS-based hybrid hydrogel Raman spectrum. A complete spectrum is acquired at each and every pixel of the image and then transformed to generate false color images based on the hydrogel composition and structure: 1) Raman peak intensity yields images of the hydrogel concentration and distribution; 2) Raman peak position yields images of molecular structure and phases, and material stress/strain; 3) Raman peak width yields images of crystallinity and phase.

The Raman mapping images provide chemical distribution and structural information within the studied material: 1) distribution of components and grain or particle size; 2) changes of crystallinity and phase across the sample; 3) size and shape of contaminant particles; 4) interaction/mixing of components at phase boundaries; 4) Distribution of stress or strain across a sample.

After irradiating the CS-based hybrid hydrogel samples for 5 hours with the Raman laser to collect data, it was used sequential sample movement and spectrum acquisition in each sample experiment. Hundreds, thousands or even millions of spectra were obtained from the hydrogel's defined image area and they are used to generate the false color images as observed in **Figure 48**.
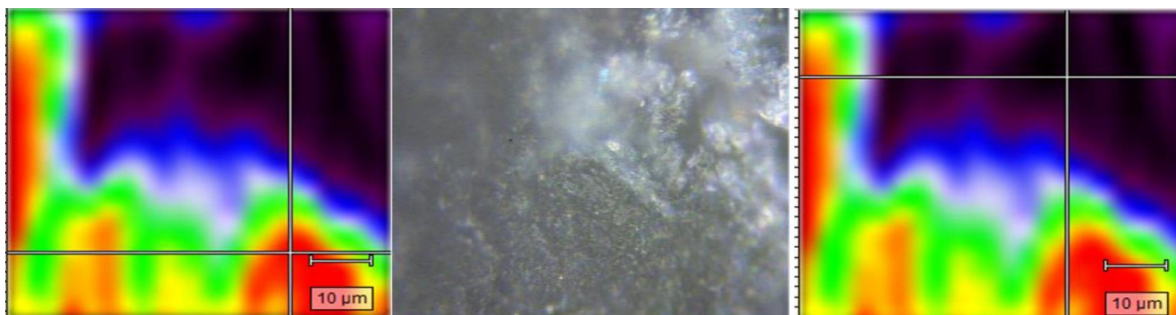
Figure 48. Raman mapping representing $Ratio\ v_{Si-O-Si}/v_{C-O-C}$ and optical microscopic image of a CS-based hybrid hydrogel synthesized at $7\ pH$ and dried at room temperature. Red spots are related to predominant zones of the inorganic component ($Si - O - Si$). Darker spots are related to predominant zones of organic component ($C - O - C$).

In the Raman spectra of CS-based hybrid hydrogels there are two important bands at 495 cm⁻¹ and 820 cm⁻¹ being related to the hybrid inorganic-organic characteristic of the hydrogels. These bands are assigned to the stretching vibration of $Si - O - Si$ and $C - O - C$ bonds, attributed to the formation of crosslinking SiO_2 structure and the chondroitin sulfate chains composed of alternating repetitive units of N-acetylgalactosamine and glucuronic acid, respectively.

The Raman mapping was brought about with all the obtained spectra during the acquisition time of each CS-based hybrid hydrogel, representing the ratio $(v_{Si-O-Si}/v_{C-O-C})$ of both bands, the inorganic and organic band as shown in **Figure 49**. In the Raman mapping it is observed that all the samples (100CS-6FD, 100CS-7FD, 100CS-7RT, 100CS-7T) have organic and inorganic domains; red spots are related to predominant zones of the inorganic component $(Si - O - Si)$ and darker spots are related to predominant zones of organic component $(C - O - C)$. However, it appears that the organic-inorganic distribution can be affected by pH and drying process.

In the color images, several spot patterns can be observed. The spot pattern of the CS-based hybrid hydrogels synthesized at $6\ pH$ (100CS-6FD hydrogel) illustrates an organic matrix, attributed to chondroitin sulfate chains and represented by dark colors, surrounding a homogeneous PDMS-modified SiO_2 organic-inorganic network, mostly represented by green, yellow and red colors. Small organic domains are observed within the PDMS-modified SiO_2 organic-inorganic network. On the other hand, the spot pattern of the CS-based hybrid hydrogels synthesized at $7\ pH$ (100CS-7FD, 100CS-7RT, 100CS-7T hydrogels) illustrates big and round organic (dark colors) and inorganic (red colors) domains interconnected by chains of homogeneous PDMS-modified SiO_2 organic-inorganic network (green and yellow large and thin spots).

Correlating the colors in the Raman mapping with the Raman spectra in each pixel forming the map, four bands stand out in the mapping spectra: 1) 820-830 cm⁻¹ attributed to $v(C - O - C)$ of N-acetylgalactosamine and glucuronic acid rings from chondroitin sulfate; 2) 790 cm⁻¹ attributed to $v_a(C - Si - C)$ and CH_3 rocking from PDMS 3) 710 cm⁻¹ attributed to $v_s(C - Si - C)$ from PDMS; and 4) 495 cm⁻¹ attributed to $v_s(Si - O - Si)$ and $\delta(O - Si - O)$.

The CS-based hydrogels are hybrids crosslinked with an organic-inorganic network, resulting in a material having zones rich in SiO_2, PDMS and/or chondroitin sulfate.

100CS-6FD

O

I

Raman Shift (cm⁻¹)

100CS-7FD

O

I

Raman Shift (cm⁻¹)

100CS-7RT

O

I

Raman Shift (cm⁻¹)

100CS-7T

O

I

Raman Shift (cm⁻¹)
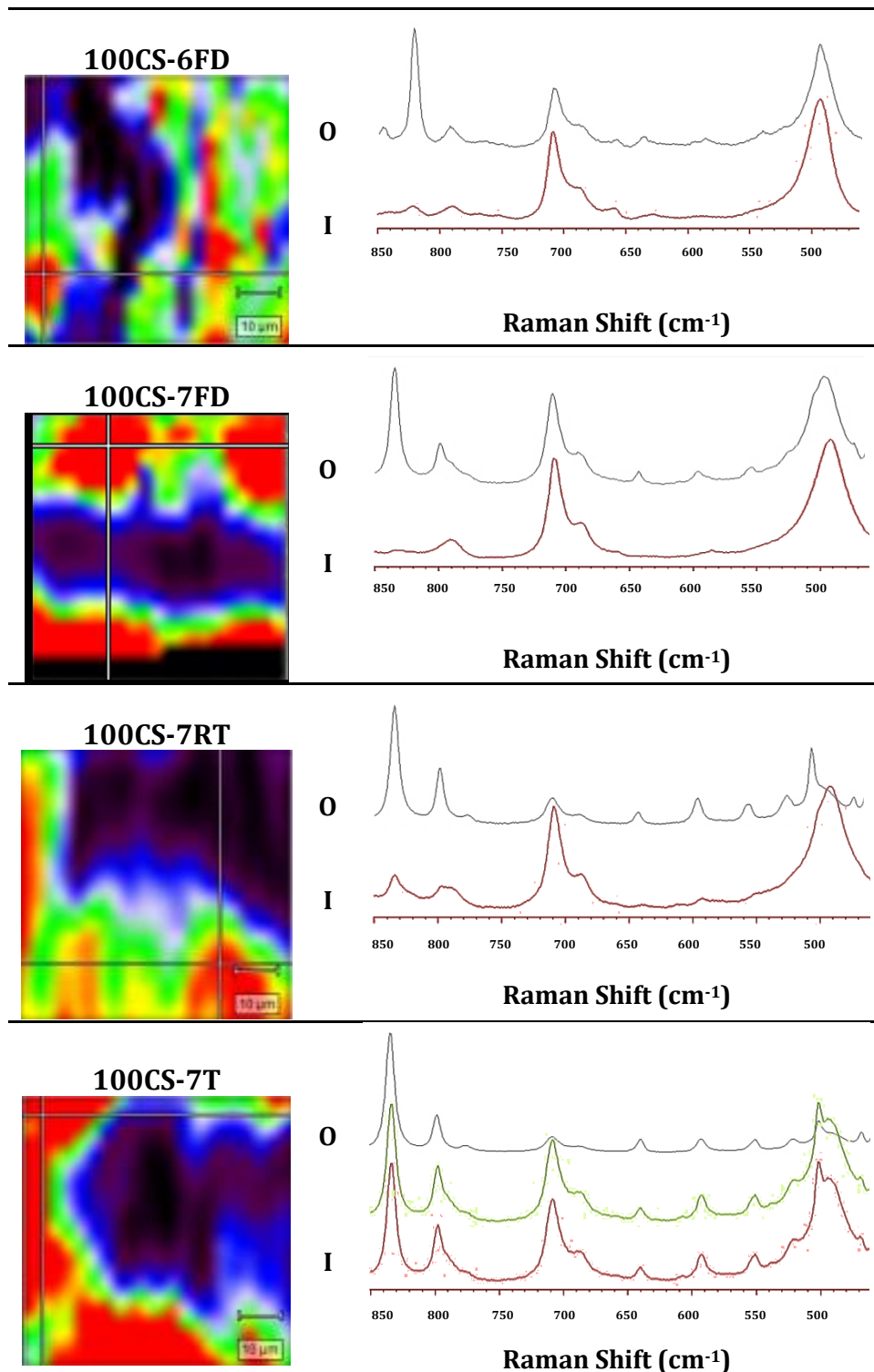
Figure 49. Raman mapping and Raman spectra representing $Ratio$ $\upsilon_{Si-O-Si}/\upsilon_{C-O-C}$ of CS-based hybrid hydrogels. Red spots are related to predominant zones of the inorganic **(I)** component $(Si-O-Si)$. Darker spots are related to predominant zones of organic **(O)** component $(C-O-C)$.

The difference among the materials spectra indicates the hybrid hydrogel structure is built up by several network conformations, being affected by pH at which the hydrogels are synthesized. Light acidic conditions ($6\ pH$) enhances an inorganic crosslinking resulting in a homogeneous inorganic crosslinking structure in contrast to neutral conditions ($7\ pH$), yielding materials with organic and inorganic domains interconnected with hybrid organic-inorganic PDMS-modified SiO_2 chains.

From Raman mapping it can be suggested several structural conformations: 1) chondroitin sulfate chains with no chemical modification; 2) chondroitin sulfate chains chemically modified with APTES (CS-APTES molecules); 3) chondroitin sulfate chains chemically modified and crosslinked with the inorganic SiO_2 structure; 4) chondroitin sulfate chains chemically modified and crosslinked with the hybrid organic-inorganic PDMS-modified SiO_2 structure; 5) organic-inorganic PDMS-modified SiO_2 networks; 6) inorganic SiO_2 structure; and 7) PDMS chains entrapped within the organic and/or inorganic structure.

3.6.3 STRUCTURAL CHARACTERIZATION OF CS – BASED HYBRID HYDROGELS BY ^{13}C AND [29]Si MAGIC ANGLE SPINNING (MAS) – NUCLEAR MAGNETIC RESONANCE SPECTROSCOPY (NMR)

FT-IR and Raman spectroscopies were useful techniques to understand some of the chemical characteristics of the designed CS-based hybrid hydrogels: 1) a possible CS-APTES grafting (chemical modification of CS molecules); 2) a possible chemical crosslinking of CS with a SiO_2 inorganic network; 3) a possible chemical incorporation of PDMS into the SiO_2 network, not only being entrapped within the hybrid hydrogel structure. Nevertheless, Nuclear Magnetic Resonance spectroscopy will confirm if the designed hydrogels can be labeled as organic-inorganic hybrid materials: chondroitin sulfate chemical crosslinked by a PDMS-modified SiO_2 inorganic network.

According to literature data, chondroitin sulfate-based hybrid hydrogels present the same carbon resonances as described for hyaluronic acid-based hybrid hydrogels. 13C MAS NMR spectra of the CS-based hybrid hydrogels, shown in **Figure 50**, can prove the coupling of APTES (primary amine) with CS molecules to yield amide ($C - N$) bonds.
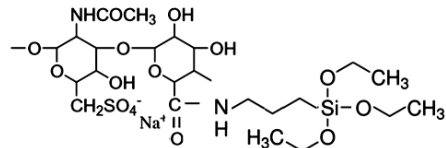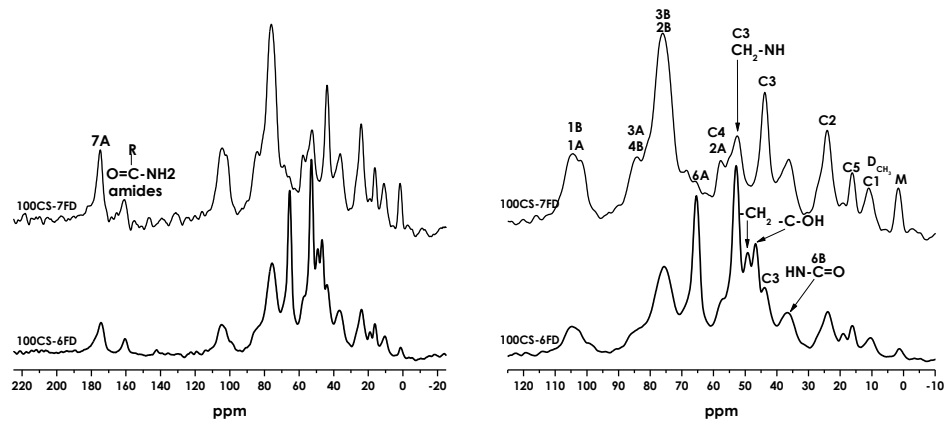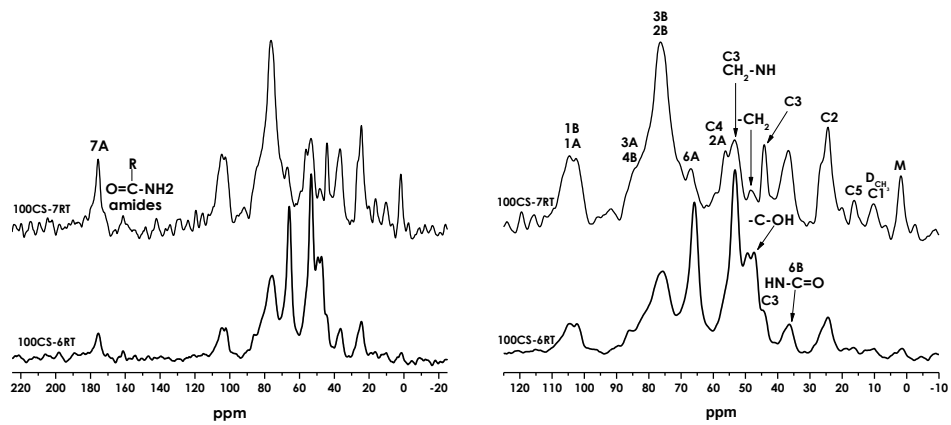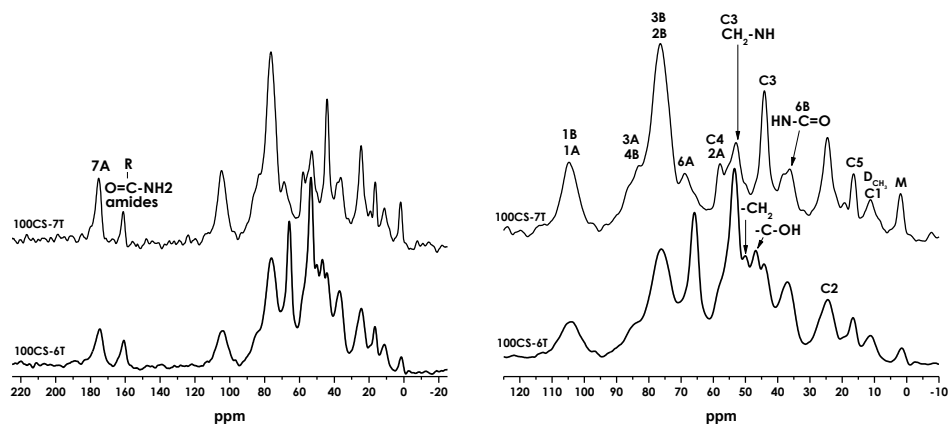
Figure 50. ^{13}C MAS NMR spectra of CS-based hybrid hydrogels synthesized at 6 *pH* and 7 *pH*.

The following resonance peaks confirm the amidation of CS with APTES: 1) resonance at 36 ppm [240, 244] is attributed to the carbon 6B from CS directly attached to the nitrogen atom of APTES molecules, resulting in the formation of an amide bond ($O = C - NH$); 2) resonance at 53 ppm [241] is assigned to carbon C3 ($CH_2 - NH$) bearing the grafting of chondroitin sulfate molecules ($CH_2 - NH - CS$). However, the presence of the peak at 43.5 ppm, assigned to carbon C3 ($CH_2 - NH_2$), indicated that not all of the APTES molecules were attached to chondroitin sulfate; 3) resonance at 160 ppm [244], attributed to amides, may also confirm CS-APTES coupling.

^{13}C MAS NMR spectra of hybrid hydrogels synthesized at $7\,pH$ and dried at 60°C (100CS-7T) present two resonances, one at 36 ppm and the other at 38 ppm, both attributed to (carbon 6B from CS) $-C - NH$ and $-C - NH_2$ bonds, respectively. Resonance at 36 ppm confirms CS-APTES coupling as mentioned before. Resonance at 38 ppm [244] may be attributed to amines produced by the partial degradation of chondroitin sulfate when dried at 60 °C. Moreover, the hydrogels synthesized at $7\,pH$ shows resonances at 60 ppm and 17 ppm due to carbons C4 and C5 in APTES molecules and the resonance at 48 ppm [244] due to $-CH_2$ in TEOS suggest that hydrolysis reactions do not occur in all ethyl groups from APTES and TEOS molecules to form silanol ($Si - OH$) groups. Finally, the chemical incorporation of PDMS into the SiO_2 network can be observed in the resonance peaks arising from the chain end M siloxane units at 1.8 ppm and the D siloxane units at 0.6 ppm [245].

^{13}C MAS NMR spectra of hybrid hydrogels synthesized at $6\,pH$ show better chemical modification of chondroitin sulfate molecules and better efficiency in hydrolysis reactions as observed in the higher intensity of the resonance peaks due to CS-APTES coupling and the lower intensity of the resonance peaks due to ethyl groups in comparison to resonance peaks of ^{13}C MAS NMR spectra of hybrid hydrogels synthesized at $7\,pH$. Finally, resonance peak at 46 ppm attributed to $-C - OH$ attributed to self-condensation between $-COO^-Na^+$ and $-OH$ groups in chondroitin sulfate-based materials show higher intensities [226].

Structural changes caused by hydrolytic-polycondensation reactions in CS-based hybrid hydrogels can be detected by ^{29}Si MAS NMR spectroscopy. The formation of monodendate, bidentate or polymeric Si species in the studied HA hybrid hydrogels can be observed in the ^{29}Si MAS NMR spectra shown in **Figure 51**.
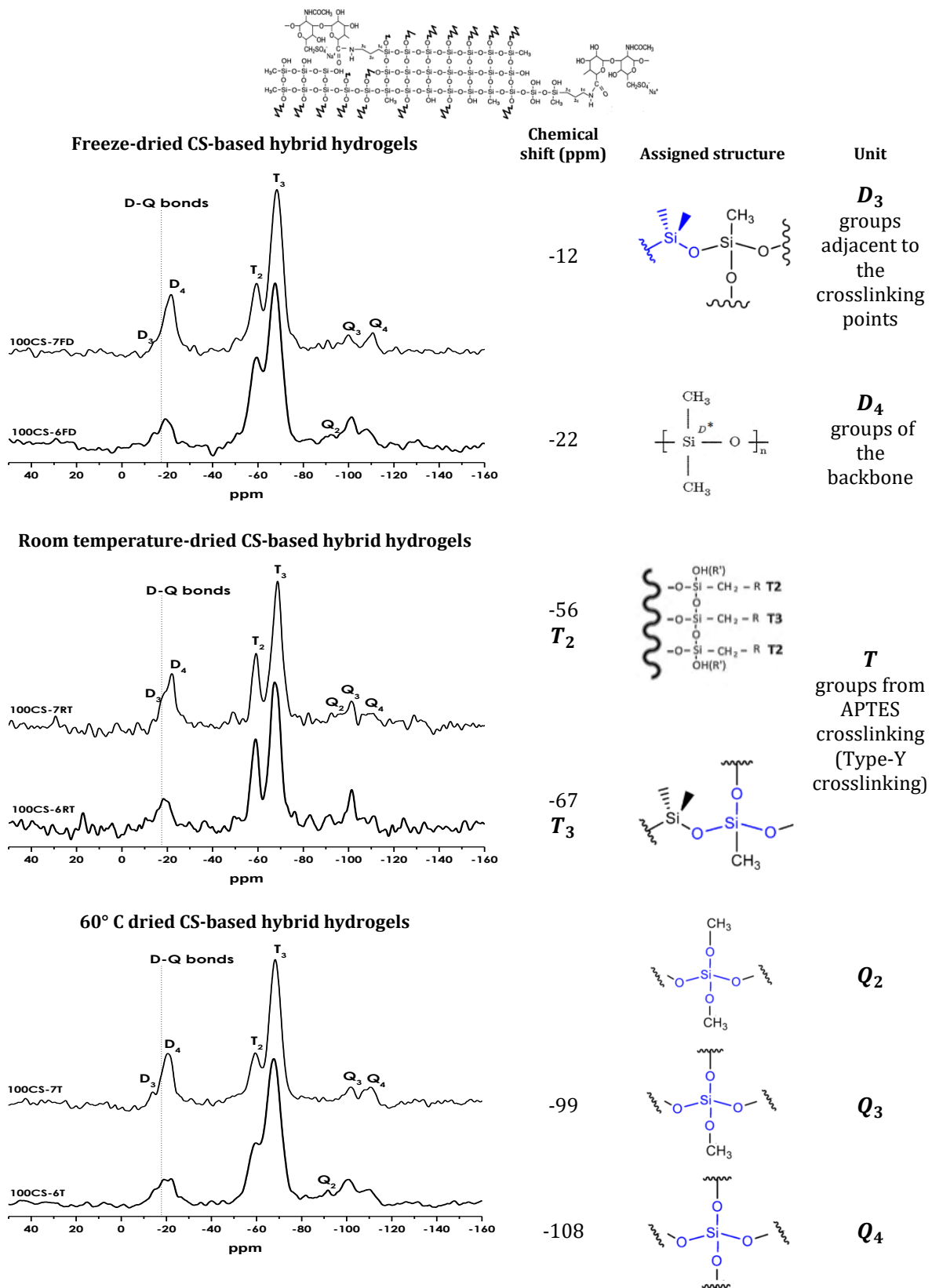
Figure 51. ^{29}Si MAS NMR spectra of CS-based hybrid hydrogels synthesized at 6 pH and 7 pH.

The ^{29}Si MAS NMR spectra of CS-based hybrid hydrogels show several Si resonances, proving the formation of a PDMS-modified SiO_2 organic-inorganic network crosslinking the chondroitin sulfate chains. The hybrid hydrogels spectra show the following signals: 1) $\boldsymbol{T}$ structural units $(CH_2CH_2CH_2NH_2 - SiO_3)$ between -40 ppm and -80 ppm [241-243, 248] corresponding to trifunctional species (APTES) grafted to the $-COO^-Na^+$ group in the chondroitin sulfate chains (CS-APTES) [247] and covalently bonded to organosilanes precursors (TEOS-PDMS) through hydrolysis-polycondensation reactions; 2) $\boldsymbol{Q}$ structural units (SiO_4) between -80 ppm and -120 ppm [248, 249] attributed to silanol $(Si - OH)$ groups associated with vicinal or free silanols and siloxanes; 3) $\boldsymbol{D}$ structural units $((CH_3)_2 \cdot SiO_2)$ between -4 and -23 ppm [246, 248, 249] assigned to difunctional dimethylsiloxane units within silicon chains.

In the ^{29}Si MAS NMR spectra of CS-based hybrid hydrogels synthesized at both, $6\,pH$ and $7\,pH$, the Q_4 structural units represent interlinked SiO_4 tetrahedrons in the interior of the mesopore structure of hybrid hydrogels, while Q_3 and Q_2 structural units, associated to silanol $(Si - OH)$ groups, are located on the hydrogels surface. The chemical shifts referred to T_2 and T_3 indicate the formation of new siloxane linkages $(Si - O - Si)$ of APTES silicon with surface silicon Q_3, Q_2 structural units from TEOS.

The relative sharp intensity of T_3 chemical shift indicates that the incorporated aminopropyl groups are closely packed into the internal surface of CS-hybrid hydrogels, suggesting that surface silanol $(Si - OH)$ groups, associated to Q_2 and Q_3 structural units are attached to aminopropylsilane (APTES) molecules *via* siloxane bonds [243] and that chondroitin sulfate chains surrounds the T_3, T_2 structural units from APTES and Q_3, Q_2 structural units from TEOS. The relative absence of chemical shifts between -46 ppm and -50 ppm due to T_1 suggests that unreacted APTES molecules are not trapped within the aerogels and xerogels PDMS-modified SiO_2 structure [242].

In ^{29}Si MAS NMR spectra of CS-based hybrid hydrogels synthesized at $6\,pH$, several differences in comparison to hybrid hydrogels synthesized at $7\,pH$ are observed: 1) T_2 and Q_3 chemical shifts show signals with sharper intensities; 2) Q_4 chemical shift show a signal with a softer intensity; 3) Q_2 chemical shift appears; 4) D_3, D_4 and $D - Q$ bonds chemical shifts appear with sharper intensities.

In ^{29}Si MAS NMR spectra of hybrid hydrogels synthesized at $6\,pH$, the increase in intensity of T_2 signal implies that different grafting degrees occur for different pH at which hybrid-organosilanes hydrogels were synthesized [241]. The increase in intensity of the chemical shift related to Q_3 structural units can be attributed to an increase of hydroxyl groups ($-OH$) unable to polycondese into a highly crosslinked SiO_2 structure (more Q_4 structural units), thus increasing the number of surface hydroxyl groups.

According to pH of synthesis and drying process in CS-based hybrid hydrogels, the chemical shift D_A between -15.5 ppm and -17.5 ppm attributed to D units crosslinked to oxide-based structures ($D-Q$ bonds) in PDMS-SiO_2 systems, confirming that PDMS is chemically bonded to SiO_2 inorganic network, modifying the organic structure of the CS-based hydrogels [227, 250, 251].

From the above described, it is observed that a neutral ($7\,pH$) of synthesis increases the chemical inorganic crosslinking of D units with SiO_2 structures. This can be due to the conditions at which chondroitin sulfate is chemically more stable. According to J.A. Vázquez *et al.* [255], the conditions to maximize chondroitin sulfate isolation from an animal cartilaginous tissue, *via* enzyme digestion, were established at 52.9°C and 7.31 pH, suggesting that this polysaccharide reacts better under neutral to light alkaline pH environments. Thus, when the chondroitin sulfate is chemically more stable, the great volume of the biopolymer CS unbroken chains and their electrostatic forces make them be close together forming an organic (biopolymer) domain with the amide bond ($C-N$) connecting the inorganic crosslinking structure outside that organic domain. At the same time, the inorganic crosslinking structure will form inorganic domains producing $D-Q$ bonds and triggering the formation of Q_4 and Q_3 silicon domains and D_3 and D_2 PDMS domains.

From the previous analysis, it can be concluded several things: 1) variation in intensity of T_2 signal implies that different grafting degrees occur for different pH at which hybrid-organosilanes hydrogels were synthesized; 2) variation in Q_3 structural units suggests an increase of hydroxyl groups ($-OH$) unable to polycondese into a highly crosslinked SiO_2 structure (more Q_4 structural units); 3) chondroitin sulfate reacts better under neutral $pH = 7$; 4) the biopolymer (chondroitin sulfate) forms organic domains; 5) the inorganic crosslinking structure forms inorganic domains producing $D-Q$ bonds; 6) drying process may not affect polycondensation reactions.

3.6.4 MORPHOLOGICAL CHARACTERIZATION OF CS – BASED HYBRID HYDROGELS BY SCANNING ELECTRON MICROSCOPY (SEM)

The designed CS-hybrid hydrogels have micrometric and nanometric organic-inorganic interpenetrating networks. **Figure 52** and **Figure 53** show SEM images, at different magnifications, of 100CS-based hybrid hydrogels synthesized at $6\,pH$ and 100CS-based hybrid hydrogels synthesized at $7\,pH$, respectively.
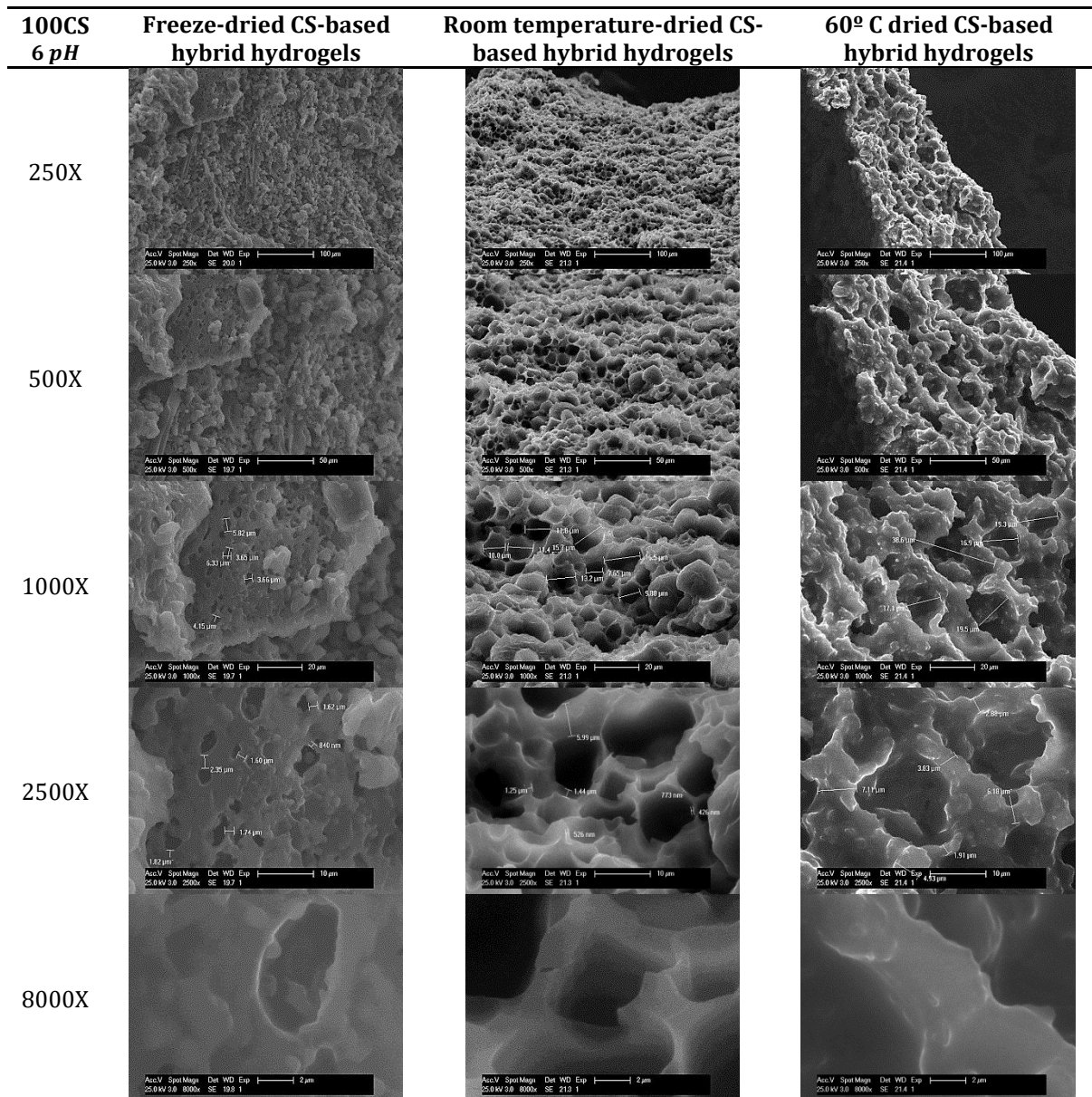
Figure 52. Morphology, pore shape and size in 100CS-based hybrid hydrogels synthesized at $6\,pH$.

Observing SEM images, pH and drying process affect directly on the hybrid hydrogels morphology. Both types of materials (100CS-pH6, 100CS-pH7) exhibit similar morphologies with some surface irregularities that can be attributed to silica precipitation nodes [233] along with different pore shapes and sizes. These differences depend on the type of drying process, showing as a result a mean pore diameter ranging from 10 μm to 30 μm.

Room temperature drying process produces porous homogeneous morphologies. The 100CS-6RT hybrid hydrogel has irregular surfaces and small round pores (mean pore diameter of $10 \leq \phi \leq 15$ μm) interconnected through thin sharp walls. On the other hand, the 100CS-7RT hybrid hydrogel also shows irregular surfaces and small round pores, though being interconnected through thicker walls. These differences can be due to pH and slow but constant drying rate, helping the hybrid structure to shrink slowly as the pores are formed when the water is evaporated.

Freeze-drying process tends to produce highly porous morphologies, developing materials with large surface areas. The 100CS-6RT hybrid hydrogel shows an inhomogeneous morphology coexisting two types, granulated areas with different particle size and porous areas with small pores ($\phi < 5$ μm). The 100CS-7RT hybrid hydrogel shows an inhomogeneous morphology coexisting two types, dense laminated areas and porous areas with small pores ($5 \leq \phi \leq 10$ μm). Moreover, it can be observed that freeze-dried hydrogels have small pores within the bigger ones. Thus, the greater the porous area is and the smaller their pores are, the larger the surface area in the hybrid hydrogels is. As previously described, the irregular pore shape and size is due to the formation of water crystals when the hybrid hydrogels are freeze at -20 °C. Since ethanol (byproduct of hydrolysis reactions) freezes at -110 °C, it remains in liquid state within the hydrogel structure when water freezes, causing the formation of semi round porous when ethanol is expelled (in gas form) through hypercritic conditions from the hybrid matrix.

60 °C drying process produces morphologies with big pores. Liquids (ethanol and water) entrapped within the surface layers are evaporated rapidly, creating those big pores. The 100CS-6RT hybrid hydrogel shows a homogeneous morphology with irregular sharp thick walls connecting irregular big pores ($20 \leq \phi \leq 30$ μm). It seems that the material may have experienced degradation during drying process, which may have been due to a less efficient crosslinking process of chondroitin sulfate as shown in [29]Si MAS spectra, since SiO_2 crosslinking networks give polysaccharide thermal stability. The 100CS-7RT hybrid hydrogel

shows an irregular surface with several layers interconnected through big pores. The liquids (mainly ethanol) entrapped within the surface layers evaporated faster ($T_{boiling}$ of ETOH is 78 °C), causing the breaking of those surface layers and the formation of huge pores ($\phi \geq 30$ μm). Water entrapped within the inner matrix layers delays to reach evaporation temperature, decreasing evaporation rate and producing pores with smaller diameters ($5 \leq \phi \leq 15$ μm).

100CS 7 pH	Freeze-dried CS-based hybrid hydrogels	Room temperature-dried CS-based hybrid hydrogels	60º C dried CS-based hybrid hydrogels
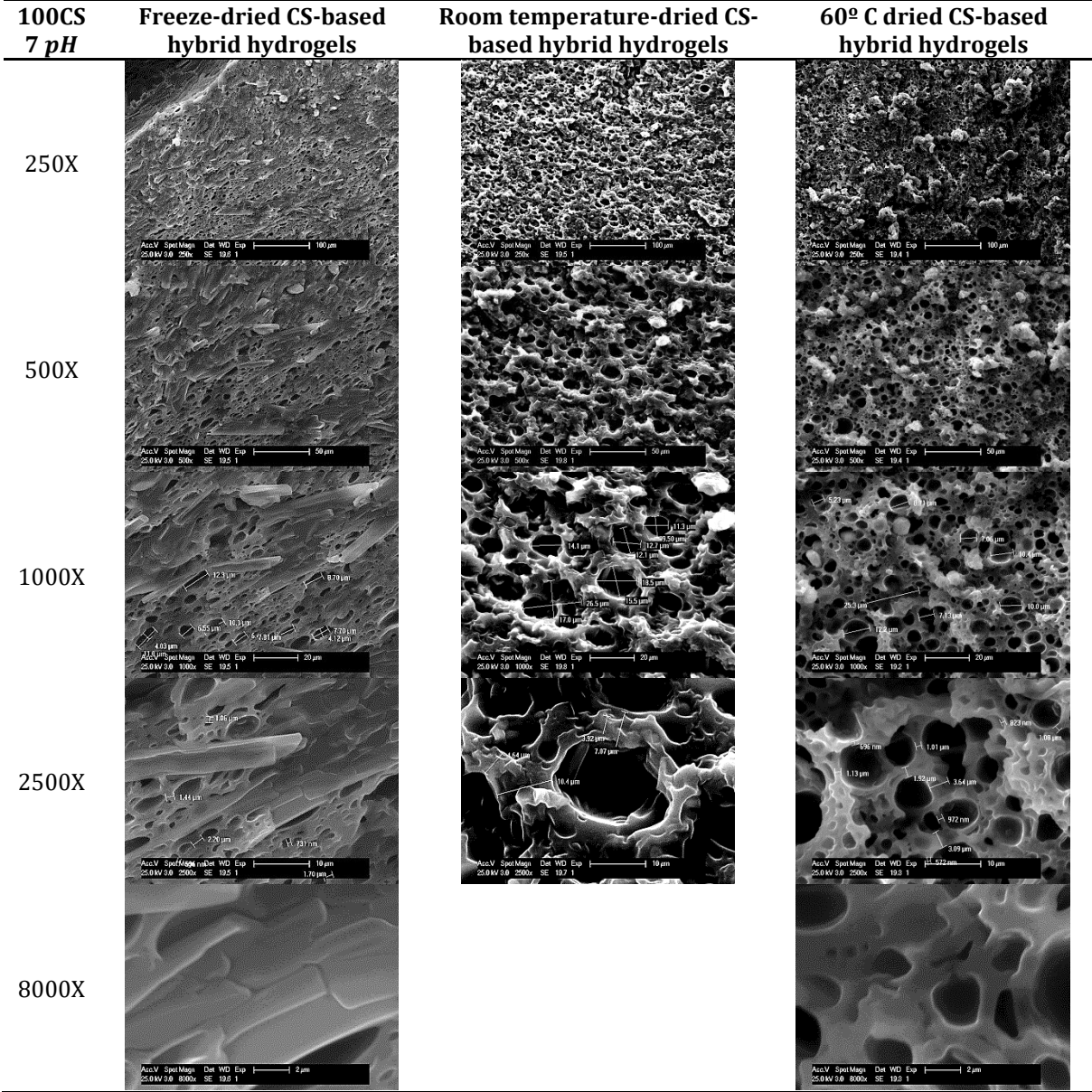
Figure 53. Morphology, pore shape and size in 100CS-based hybrid hydrogels synthesized at 7 pH.

3.6.5 THERMAL CHARACTERIZATION OF CS – BASED HYBRID HYDROGELS BY THERMOGRAVIMETRIC ANALYSIS (TGA)

CS-based hybrid hydrogels were thermally characterized to identify temperatures at which thermal decomposition occurs. Polymer faction (chondroitin sulfate and PDMS silicone) in CS-based hybrid hydrogels was also studied by thermal decomposition under air atmosphere. Thermogravimetric analysis (weight loss curves and derivative weight loss curves) of CS-based hybrid hydrogels is shown in **Figure 54**.

Figure **54-A** shows TGA curves comparing the two studied compositions of CS-based hybrid hydrogels dried through a specific drying process (freeze-drying, room temperature drying or 60 °C drying). **Figure 54-B** shows TGA curves comparing the three different drying processes affecting one CS-based hybrid hydrogel composition (100CS-*pH*6, 100CS-*pH*7).
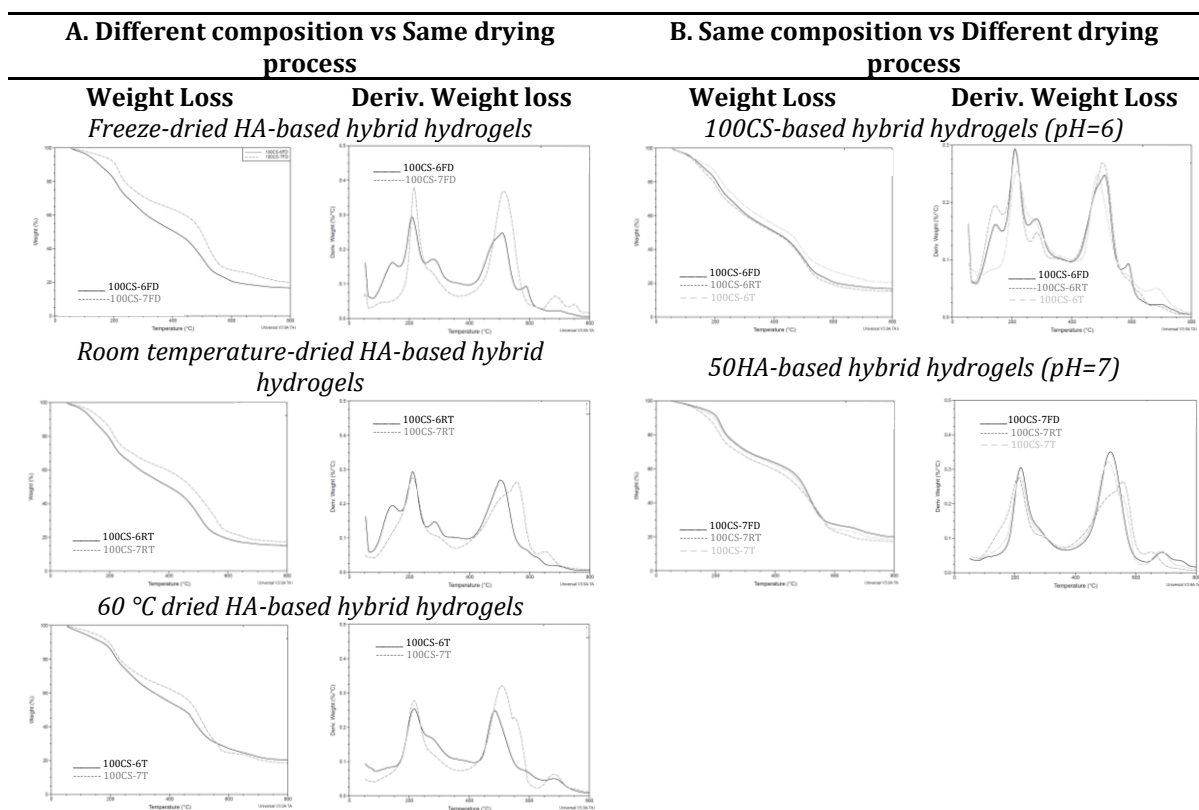
Figure 54. Thermogravimetric analysis (TGA) and derivative TGA curves of CS-based hybrid hydrogels synthesized at 6 *pH* and 7 *pH*.

TGA analysis in CS-based hybrid hydrogels shows several stages of weight loss. The first thermal stage occurs between 40-160 °C, being attributed to moisture loss (adsorbed water) and residual water and ethanol loss by evaporation, both are byproducts of hydrolysis-polycondensation reactions [252, 253]. Since 100CS-pH6 hybrid hydrogels demonstrated to have less efficient crosslinking reactions by showing more silanol ($Si - OH$) groups in Q_3 and T_2 structural units, they tend to easily hydrolyze and adsorb larger amounts of water, thus experiencing greater weight losses in the first thermal stage. Additionally, room temperature dried CS-based hybrids are the hydrogels with larger amounts of water and ethanol entrapped within the structure in comparison to freeze-dried hybrid hydrogels and 60 °C-dried hybrid hydrogels. It is observed that derivative thermo-stability in hydrogels is clearly influenced by pH and drying process, as shown in **Table 6**.

Table 6. Maximum temperature decomposition peak (°C) and weight losses (%) in each thermal stage from thermogravimetric analysis of CS-based hybrid hydrogels.

Samples	T_{max} (ºC)						Δm (%)					
Thermal Stages	I (25-150 °C)	II (200-360 °C)	III (400-600 °C)		IV (600-800 °C)		I (25-150 °C)	II (200-360 °C)	III (400-600 °C)		IV (Final Weight °C)	
100CS-6FD	145.39	210.96	281.76	510.59	590.29	703.28		12.43	30.83	48.89	76.09	81.36	83.35
100CS-7FD	112.07	220.81	289.73	516.40		687.93	747.66	3.91	24.52	34.36	73.90		78.25	80.11
100CS-6RT	144.23	211.62	285.13	504.14	594.51	695.59		15.35	33.99	46.56	79.24	83.08	84.82
100CS-7RT	128.92	210.92	293.24	511.49	557.43	654.24		8.88	29.24	37.12	64.03	78.17	82.69
100CS-6T	124.32	217.75	272.88	485.77	588.38	686.40		8.55	26.58	43.62	70.24	75.01	79.73
100CS-7T	115.13	216.22	291.26	510.27	551.62	684.87	758.38	5.38	24.73	35.12	66.35	75.88	80.51	81.55

The second thermal stage occurs between 200 °C and 380 °C. The main decomposition of pure chondroitin sulfate, attributed to the partial break of its molecular structure, takes place at a temperature range between 200 °C and 300 °C. According to literature [256], degradation of chondroitin sulfate ends at approximately 250 °C and can vary up to 370 °C. In the design CS-hybrid hydrogels, their maximum degradation point in the second thermal stage is reached at $T_{onset} \sim 215\ °C$; having an average weight loss of ~28.5% when reaching ~250 °C. Chondroitin sulfate residues are further degraded at ~286 °C, indicating reduction in its thermal stability by liberating sulfated groups and carboxylic acids. In the CS-hybrid hydrogels, this event occurs between 250 °C and 350 °C, presenting weight losses between 35% and 50%. 100CS-pH6 hydrogels show better thermal stability than 100CS-pH7 hydrogels, by increasing the temperature range at which chondroitin sulfate starts, ends and reaches its maximum point of degradation and by reducing their percentage of weight loss. This could be caused by a better efficiency in CS chemical modification (CS-APTES grafting)

and to the possible hydrogen bonding interaction between molecules due to the presence of amino ($-NH_2$) and hydroxyl ($-OH$) groups in APTES, TEOS and PDMS as well as ($-OH$), ($COOH$), ($C = O$) in chondroitin sulfate [254].

As explain before in HA-based hybrid hydrogels, the increase of temperature at which polysaccharide degradation occurs may suggest that chemically modified CS chains (CS-APTES molecules) are thermally more stable than unhibridized CS chains. The incorporation of APTES may have provided thermal stability to CS polymeric chains, since the incorporated aminopropyl groups are closely packed into the internal surface of CS-hybrid hydrogels, working as bridging points between CS polymeric chains and the PDMS-modified SiO_2 structure, resulting in a PDMS-modified inorganic SiO_2 structure coated by high molecular CS polymeric chains [242].

100CS-pH7 hybrid hydrogels have lower temperature at which CS thermal degradation starts. This can be due to low molecular polymer CS chains and chemically unmodified polymeric CS chains preferring to be located between silica (SiO_2) and PDMS domains, affecting the number and nature of crosslinking between those domains, facilitation CS thermal degradation to start.

The third thermal stage, attributed to PDMS chain thermal degradation, takes place between 400 °C and 600 °C. Two simultaneous PDMS degradation mechanisms occurred: 1) *molecular mechanism* and 2) *radical mechanism* causing the densification of the material [233] when D units are oxidized to T units and then to further Q units [250]. CS-based hybrid hydrogels show good thermal stability since the initial PDMS degradation appears at ~450 °C. The first derivative peak at ~510 °C may correspond to methyl oxidation from $Si-CH_3$ bonds forming silanol ($Si-OH$) groups, which would condense into siloxane bridges at higher temperatures, and to aminopropyl group oxidation from APTES molecules, being ungrafted during thermal degradation of CS. The second derivative peak at ~550 °C for 100CS-pH7 hydrogels and ~590 °C for 100CS-pH6 hydrogels is related to the final decomposition of the cyclic PDMS oligomers. According to Peña-Alonso *et al.* [251], the chemical incorporation of APTES into a PDMS-modified SiO_2 structure produces an increase in the temperature at which PDMS thermal degradation starts, boosting thermal stability in CS-based hybrid hydrogels.

A fourth final significant thermal stage of weight loss appears above 600 °C. At this temperature, hybrid materials completely oxidized their organic components (CS, PDMS and

aminopropyl groups in APTES), leaving as residues only amorphous silica (SiO_2). When all the organic components are degraded, inorganic polycondensation reactions take place, resulting in the formation of Q_4 structural units, representing a $[SiO_4]$ tetrahedron-network. Thus, drying and oxidative conditions play an important role in thermos-oxidative resistance, changing thermal history of hybrid hydrogels.

From the previous analysis, several conclusions are arisen: 1) 100CS-*pH*6 hybrid hydrogels may have a large number of surface hydroxyl ($-OH$) groups, since its crosslinking is not so efficient as 100CS-*pH*7 hybrid hydrogels, making them easily to adsorb moisture. Consequently, when starting TG analysis, 100CS-*pH*6 hydrogels loose a greater amount of weight; 2) APTES, chemically bonded to chondroitin sulfate chains and SiO_2 network, provides thermal stability to both, chondroitin sulfate chains when being hybridized and to PDMS chains when modifying SiO_2 structure; 3) when D units in PDMS starts to oxidize into T units and then into further Q units, the inorganic structure tends to densify by a reorientation of siloxane chains.

3.7 SWELLING AND DEGRADABILITY PROPERTIES OF HYALURONIC ACID – BASED PDMS – MODIFIED SiO_2 ORGANIC – INORGANIC HYBRID HYDROGELS

Once the HA-based PDMS-modified SiO_2 organic-inorganic hybrid hydrogels are characterized and analyzed, their swelling and degradability properties were studied. The chosen polysaccharide hydrogels compositions to test their swelling and degradation properties are 50HA-*pH*6 hydrogels. Swelling and degradation ratios of the hybrid hydrogels were determined by the classical gravimetric method. Wet and dried hybrid *gels* were put into 0.01M PBS: Phosphate Buffer Solution ($pH = 7.4$) at 37 ± 0.5 °C composed of $NaCl$ and KCl salts. PBS worked as saline solution taking place of the blood plasma. The swollen polysaccharide-based hybrid hydrogels were weighed at various times to evaluate swelling equilibrium and degradation rate. To study the effect of pH during synthesys process on the swelling equilibruim and degradtion rate of the polysaccharide-based hybrid hydrogels, HA-*pH*6 and HA-*pH*7 hydrogels were tested. The changes experienced by the hybrid hydrogels during swelling and degradation process are analyzed through pH measurements, weight losses, rheology, ESEM and SEM images.

3.7.1   SWELLING PROPERTIES OF HA – BASED HYBRID HYDROGELS

The swelling properties of the HA-based hybrid hydrogels were studied. **Figure 55** shows 50HA-6RT hybrid hydrogel swelling capability in real time when undergoing an increasing water pressure. The images corresponding to each applied pressure, from 1.1 Torr to 8.4 Torr, are displayed. Dried pores in the hybrid hydrogel are perceived in **Figure 55-A**. As water pressure increased, the pores started to get occluded by droplets of water and to lose their shape when the pore walls completely absorbed those water droplets. It can be settled that water absorption occurred gradually until the entire hydrogel porous were fully hydrated, as shown in **Figure 55-T**.
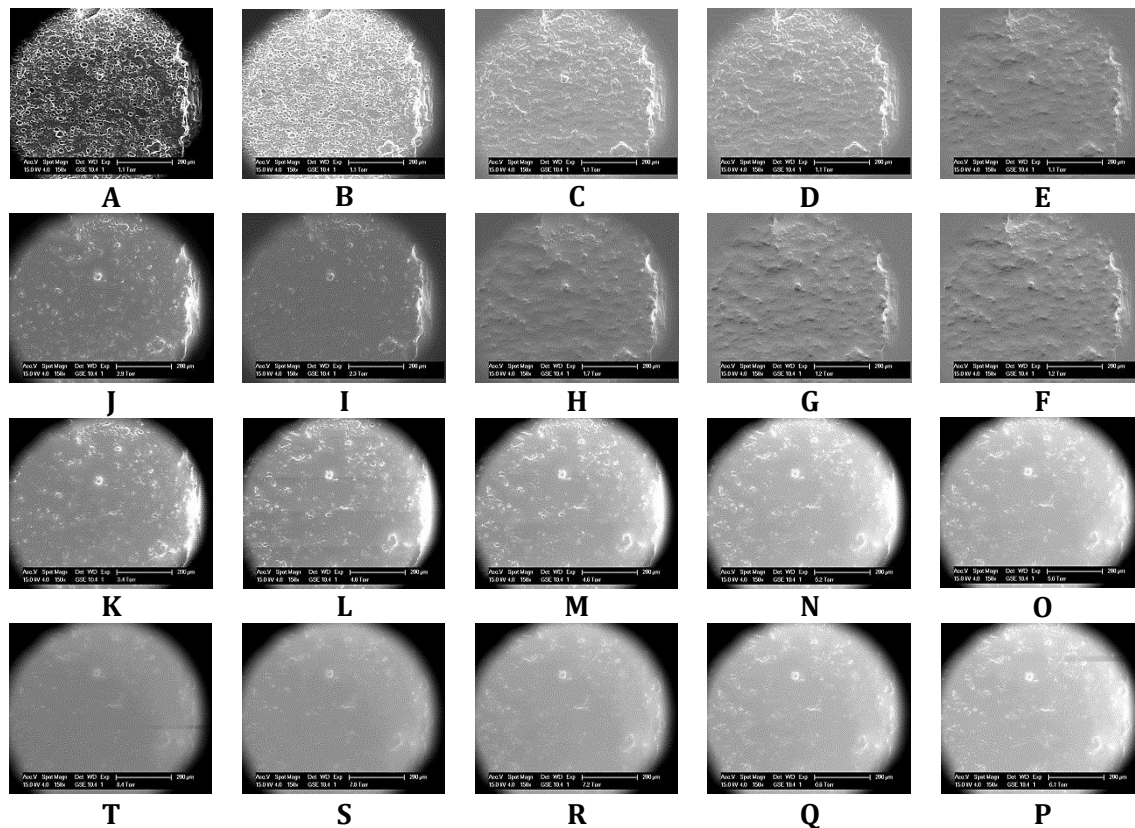
Figure 55. 50HA-based hybrid hydrogel (50HA-6RT) undergoing an increasing water pressure from 1.1-8.4 Torr to evaluate its swelling capability through Environmental Scanning Electron Microscopy.

Soft tissues, such as cartilage and skin, are characterized by having a highly hydrated extracellular matrix, mainly made of water, glycoproteins, proteoglycans and glycosaminoglycans. Due to the hydrated nature of soft tissues, tissue engineering should

pursue the aim to design and fabricate a biomaterial that guarantees both, good hydration and good mechanical resistance, similar to the natural extracellular matrix. These biomaterial characteristics allow cells to perform a regenerative function and to have a suitable time for resorption.

As explained before, the hydration degree of the HA-based hybrid hydrogels was measured at 37 °C using buffer solution (PBS) at $7.4\ pH$. **Figure 56** shows the hydration process of hybrid hydrogels. Before starting the swelling assay, the samples (wet *gels, xerogels* and *aerogels*) were rigid solid networks (**Figure 56-A**). Immediately after being soaked into the buffer solution, *gels* started to hydrate as their polymer chains swelled and became flexible, allowing water molecules diffusion within the organic-inorganic matrix (**Figure 56-B**). As water was being absorbed into the hydrogel matrix, the volume and size of the HA-based hybrid hydrogel gradually increased (**Figure 56-A**). Finally, when chain relaxation reached a minimum energy state, equilibrium between chain relaxation and contraction of the polymeric network was also reached, getting a stable level of hydration (**Figure 56-C**).

A.

| WET *GEL* after aging process **50HA-6W** | *AEROGEL* **50HA-6FD** | *XEROGEL* **50HA-6RT** | *XEROGEL* **50HA-6T** |

B.   **C.**
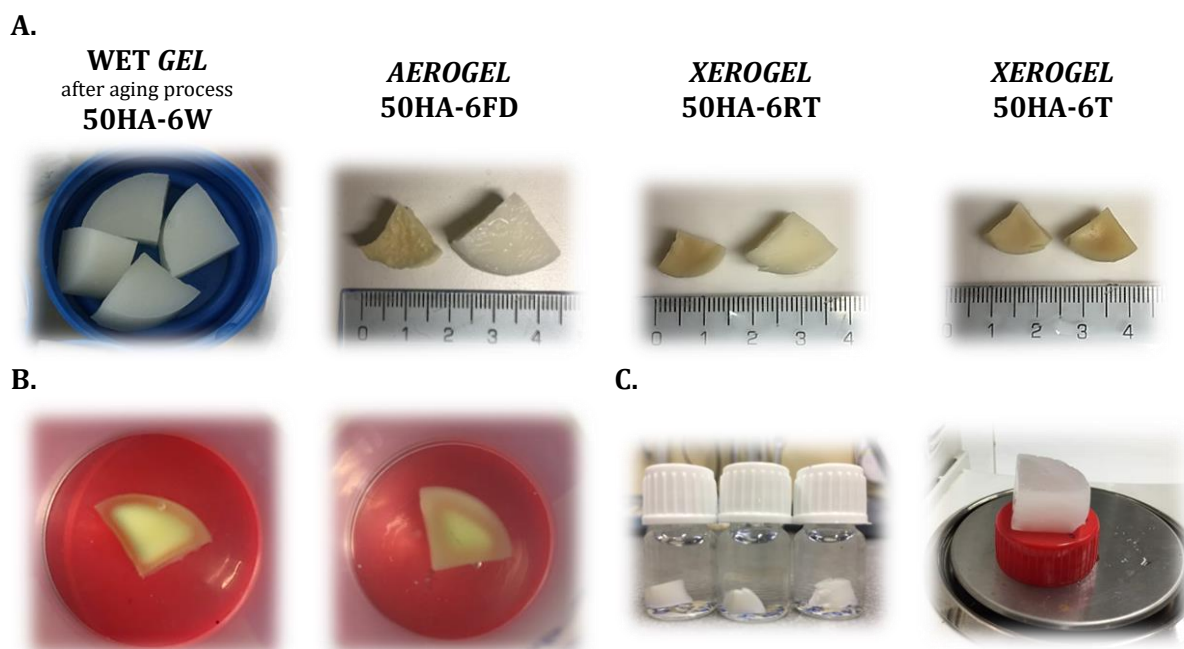
Figure 56. Hydration process of 50HA-$pH6$ hybrid hydrogel immersed into $7.4\ pH$ PBS at 37 °C: **(A)** Dried hybrid hydrogels before and after few minutes of immersion. **(B)** Gradual hydration of 50HA-6RT hydrogels as HA polymer chains begin to swell. **(C)** Maximum hydration of 50HA-6FD hybrid hydrogel reaching a 600% of swelling degree.

As shown in **Figure 56**, both 50HA-*pH*6 and 50HA-*pH*7 hybrid hydrogels underwent uniform volumetric expansion in response to several stimuli of physiological conditions (37 °C and 7.4 *pH*), suggesting that these hybrid hydrogels showed a great added value by combining potential and restrictions of their precursors: 1) silicon PDMS hydrophobicity and elasticity; 2) silica SiO_2 structure providing stiffness to the hydrogel; 3) HA biopolymer providing natural hydrophilic capability and nontoxic characteristics to the hydrogels, necessary to mimic Extracellular Matrix.

Hydration degree and swelling equilibrium of HA-based hybrid hydrogels are affected by three important factors: 1) polysaccharide concentration; 2) synthesis *pH*; and 3) drying process. These variables also affect the crosslinking density and structure of hybrid hydrogels before and after immersion. **Figure 57** shows the swelling degree evolution of 50HA-based hybrid hydrogels synthesized at 6 *pH* or 7 *pH* and dried through different processes.
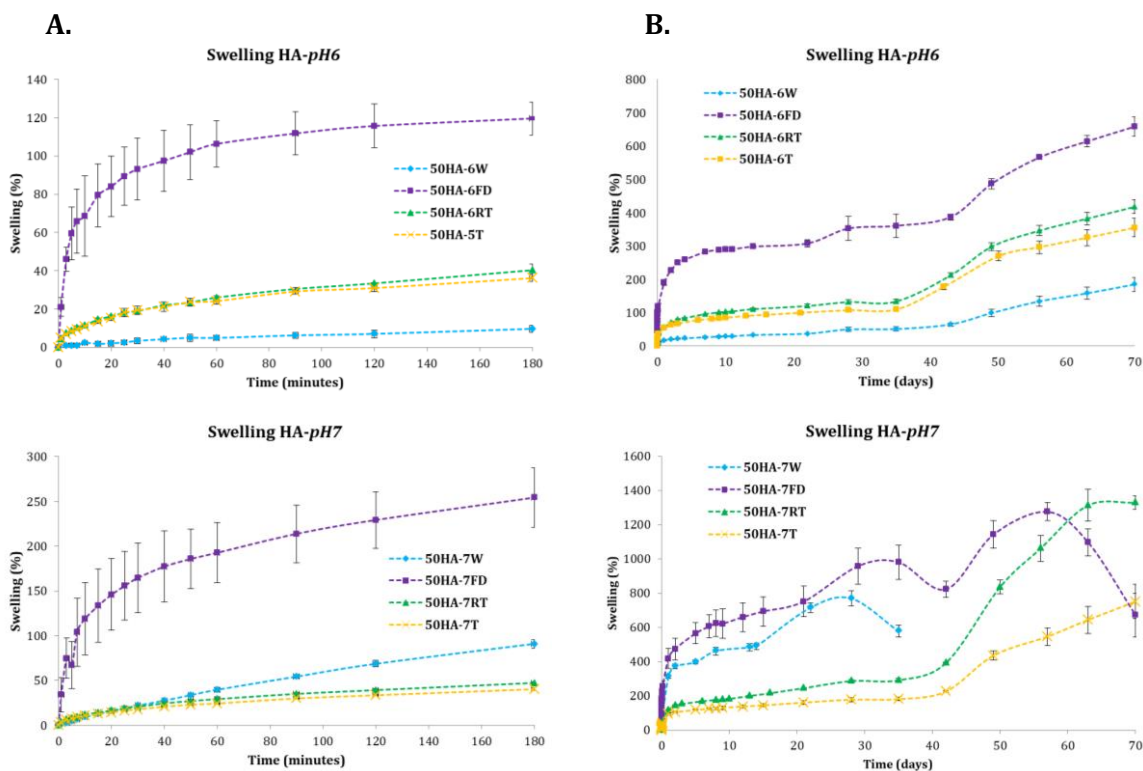
Figure 57. Swelling degree evolution of 50HA-based hybrid hydrogels evaluated for 70 days at physiological conditions. Column **(A)** shows swelling (%) of 50HA-*pH*6 and 50HA-*pH*7 up to 180 minutes. Column **(B)** shows swelling (%) of 50HA-*pH*6 and 50HA-*pH*7 up to 70 days.

It is observed that HA-*pH*7 hybrid hydrogels showed a higher swelling degree (reaching almost double swelling degree) and degradation rate than HA-*pH*6 hybrid hydrogels. In both type of HA hydrogels, freeze-drying samples are the hydrogels showing the highest swelling degree. Room temperature-drying and 60 °C-drying HA-hydrogels reach faster their swelling equilibrium. The 50HA-6W wet hydrogel (hydrogels soaked into PBS immediately after aging process without experiencing a drying process) are the ones experiencing the fastest and constant swelling equilibrium, near 200% at 70 days of immersion. However, the 50HA-7W wet hydrogel is the one with the fastest degradation rate, reaching its maximum swelling degree, near 800%, at 30 days of immersion under physiological conditions, and collapsing its structure immediately after those 30 days.

Figure 58 shows Raman spectra of 50HA-*pH*6 and 50HA-*pH*7 hybrid hydrogels. Several differences can be observed between the spectra of both types of hydrogels. The main difference is that important bands related to HA hybridization (HA-APTES) and SiO_2 crosslinking structure are not visible in the spectra of 50HA-*pH*7 hybrid hydrogel. The absence of these bands suggests that HA crosslinking in 50HA-*pH*7 is not efficient as in 50HA-*pH*6 hybrid hydrogels. The inefficient crosslinking affect directly to the swelling properties of 50HA-*pH*7 hybrid hydrogels.
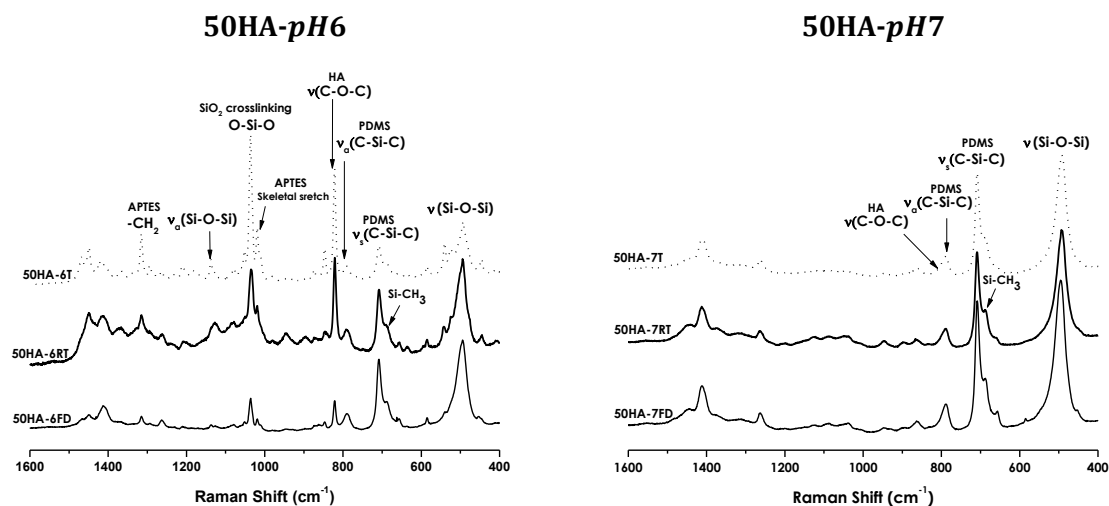
Figure 58. Raman spectra of 50HA-*pH*6 and 50HA-*pH*7 hybrid hydrogels.

Unlike 50HA-*pH*7 hybrid hydrogels, the 50HA-*pH*6 hybrid hydrogels show a stronger and dense inorganic PDMS- modified SiO_2 crosslinking that restrains their swelling degree.

The hydrophilic characteristics of HA-based hydrogels are caused by the presence of hydrophilic molecules ($-OH, -CONH, -CONH_2$ and SO_3H) found in the polymeric components. These molecules give hydrogels different absorption potential [215] and the ability to respond to different stimuli, including temperature, pH and salt [216]. Therefore, the PDMS-modified SiO_2 crosslinking matrix acted as a stiffer structure restricting the swelling degree of 50HA-$pH6$ hybrid hydrogels by restricting their number and type of hydrophilic molecules, making them to have smooth and better control of degradation kinetics. Most of the hydrogels shows a swelling equilibrium at 35 days of immersion.

Moreover, freeze-dried hybrid hydrogels (50HA-6FD and 50HA-7FD) have highly porous morphologies and large surface areas, allowing an easier diffusion of water molecules into the hybrid matrix. However, a stronger inorganic PDMS-modified SiO_2 crosslinking structure in 50HA-6FD hybrid hydrogels restricts water diffusion into them, reaching a swelling equilibrium of 350% at 35 days of immersion in comparison to 50HA-7FD hybrid hydrogels that reached a swelling equilibrium of 1000% at the same 35 days of immersion. After that immersion time, the 50HA-7FD hybrid hydrogel began to lose strength and mass, and finally collapsing at 55 days of immersion

Room temperature- and 60 °C- dried hybrid hydrogels (50HA-6RT, 50HA-7RT, 50HA-6T, and 50HA-7T) have similar swelling behavior. Both drying processes let the structure of the hybrid hydrogels densified and decrease number and size of pores, thus hindering water diffusion. 50HA-6RT and 50HA-6T hydrogels show swelling degree of 410% and 350% at 70 days of immersion, respectively. However, 50HA-7RT and 50HA-7T hydrogels show swelling degree of 1350% and 780% at 70 days of immersion, respectively. The differences in swelling degrees among hydrogels are due to pH synthesis.

Wet hydrogel (50HA-6W) shows the most stable swelling behavior by having a swelling equilibrium of 50% at 35 days of immersion and reaching a maximum swelling degree of 200% at 70 days of immersion. Since HA-6W hydrogel preserved its hydrated nature after aging time, the material did not suffer shrinking neither constriction nor rehydration of its structure when immersed into PBS, as experienced by the other hydrogels (HA-6FD, HA-6RT and HA-6T). This physical stability helped the 50HA-6W hybrid hydrogel to keep its structure without experiencing physical stress and therefore experiencing longer swelling equilibrium times. 50HA-7W hydrogel is the one with the fastest degradation rate.

3.7.2 DEGRADATIVE PROPERTIES OF HA – BASED HYBRID HYDROGELS

Figure 59 shows *pH* variation and weight loss of 50HA-based hybrid hydrogels immersed into PBS at physiological conditions (37±5 °C; 7.4 *pH*) to evaluate degradation kinetics.

When analyzing *pH* variation in PBS over the 42 days of *in vitro* degradation tests in 50HA-*pH*6 hybrid hydrogels, it can be observed that during the first 7 days *pH* decreased in the three samples, being 50HA-6RT *pH* the one decreasing the most (6.9 *pH*), since unreacted reagents, non-crosslinked HA chains and ethanol remains trapped within the hydrogel matrix may have been expelled into the solution. During the 21 days of immersion, *pH* values decreased to their lowest levels (6.6 − 6.8 *pH*), but after those 21 days of immersion, *pH* values increased, reaching neutral values (7 − 7.2 *pH*) at the end of the assay. In general, *pH* values throughout the assay can be considered within the rage of $6.5 \leq pH \leq 7.4$ which is needed for cell proliferation; thus, suggesting that 50HA-*pH*6 hydrogels are chemically stable.
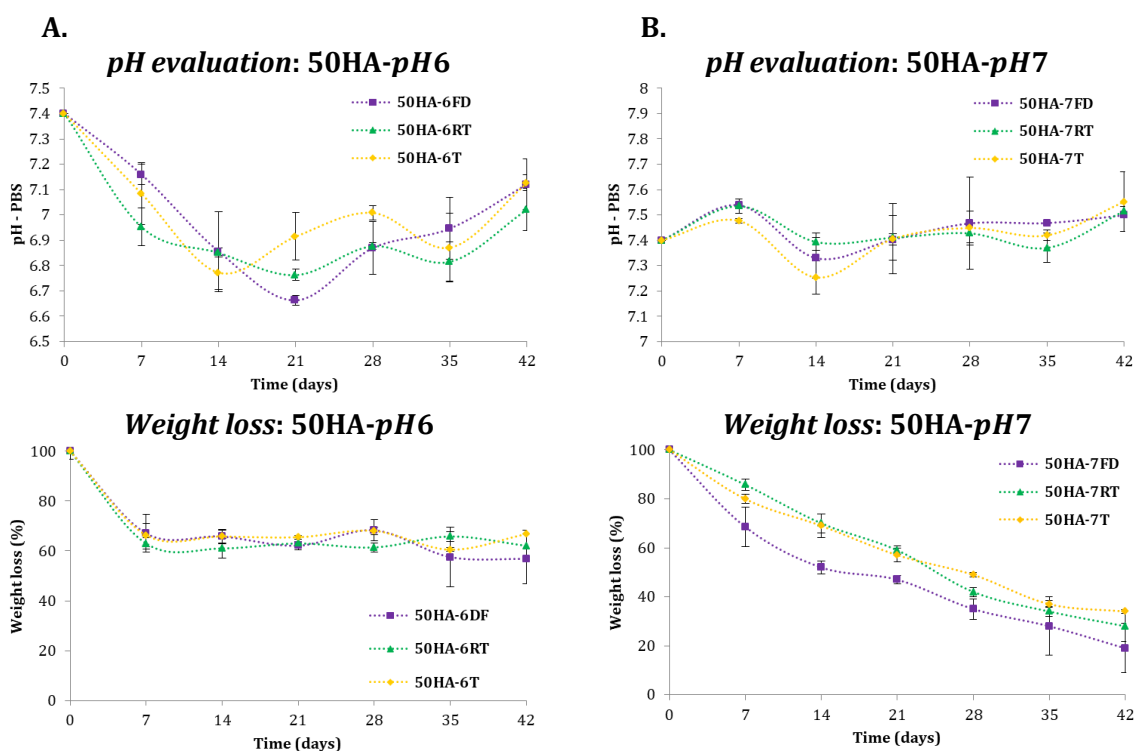
Figure 59. *pH* variation and weight loss of 50HA-based hybrid hydrogels evaluated during 42 days into PBS immersion at physiological conditions. Column **(A)** shows *pH* variation and weight loss (%) of 50HA-*pH*6 hydrogel. Column **(B)** shows *pH* variation and weight loss (%) of 50HA- *pH*7 hydrogel.

When analyzing pH variation in PBS over the 42 days of *in vitro* degradation tests in 50HA-pH7 hybrid hydrogels, it can be observed that during the first 7 days pH slightly increased ($7.6 - 7.5\ pH$) in the three samples. At 14 days of immersion, pH values decreased to their lowest levels ($7.2 - 7.3\ pH$), but after those 14 days of immersion, pH values were kept constant till the end of the assay, showing values near the initial one in the buffer solution ($7.4\ pH$). In general, it can be considered that pH did not vary throughout the assay; thus fulfilling the condition of having values within the rage of $6.5 \leq pH \leq 7.4$ needed for cell proliferation.

Analyzing weight losses of 50HA-pH6 hybrid hydrogels while being immersed into PBS during 42 days will help to establish their degradation kinetics. It can be observed that during the first 7 days of immersion the hydrogels lose between 32% and 37% of their total weight. As time went on, the hybrids kept their weigh losses up to 40% at the end of the assay. Correlating these values with pH variation in 50HA-pH6 hybrid hydrogels, it can be confirmed that during the first 7 days of immersion pH in the buffer solution decreased and hydrogels lose ~30% of their weight due to the release of unreacted reagents, non-crosslinked HA chains, low molecular weight HA chains and ethanol remains, all of them being entrapped within their matrix. After this release, the hydrogels proved to have chemical equilibrium under physiological conditions by showing no further weight loss; thus confirming a good covalent inorganic HA crosslinking.

Analyzing weight losses of 50HA-pH7 hybrid hydrogels while being immersed into PBS during 42 days will help to establish their degradation kinetics. It can be observed that throughout the 42 days of immersion the hydrogels experienced weight losses, reaching maximum weight losses between 70% and 80%. Freeze-dried hydrogel (50HA-7FD) was the material experiencing the most weight loss, which is due to the high porosity produced during drying process and the inefficient inorganic crosslinking caused by the $pH = 7$ of synthesis. Although pH in the soaking PBS did not fluctuate, presenting values near the starting one ($7.4\ pH$), hydrogels did experience strong weight losses, suggesting that degradation products do not produce acidic or basic mediums.

Degradation experienced by the organic part (HA and PDMS) of the hybrid hydrogels is determined by various factors such as polymerization, unreacted monomers, molecular weight, morphology, types of bonding and porosity. Degradation of the inorganic part (SiO_2

crosslinking network) of the hybrid hydrogels is determined by a mechanism of surface degradation *via* silanol $(Si - OH)$ groups, dependent on pH of the surrounding medium.

In vitro degradation assays have shown that highly porous materials begin to degrade faster than those with little porosity since the first ones exhibit a larger contact area in which the buffer solution can act and thus facilitating hydrolytic degradation. Hydrolysis starts in cleavage sites where water molecules are consumed to affect the separation of a larger molecule into several component parts. HA-based hybrid hydrogels are attacked in several of their cleavage sites: 1) hydrolysis of the amide bonding (HA-APTES grafting) resulting in compounds with amine $(-NH_2)$ and carboxylic acid $(COOH)$ groups; 2) the hydrolysis of the inorganic-organic PDMS-modified SiO_2 network forming compounds with silanol $(Si - OH)$ groups; 3) hydrolysis of hyaluronic acid polymeric chains by breaking them into D-glucuronic acid and N-acetyl-D-glucosamine compounds and very low-molecular-weight hyaluronan chains.

The hydrolysis of amides occurs when the nucleophile (water or hydroxyl ion) attacks the carbon of the carbonyl group of the amide molecule. Since PBS has a slightly basic pH, in aqueous base, hydroxyl ions are better nucleophiles than polar molecules such as water. In contrast, in acidic solutions, the carbonyl group becomes protonated, leading to a much easier nucleophilic attack. In both type of hydrolyses, the products are compounds with carboxylic acid groups.

50HA-6pH hybrid hydrogels proved to have better crosslinked structures resulting from $pH = 6$ of synthesis. These medium conditions during synthesis lead to the production of more interconnected silica (SiO_2) – silicon $(PDMS)$ network, hindering the penetration of the buffer solution into the materials.

Figure 60 shows SEM images of the HA-6pH hybrid hydrogels after being immersed into PBS for 14 days. The materials were kept with moisture. It can be observed the degree of degradation hydrogels suffered within their pores over the 14 days of immersion.

Morphology of the HA-6W hybrid hydrogel did not change significantly after the immersion period. It can be observed that the material maintained its swollen structure. Since HA-6W hydrogel preserved its hydrated nature after aging time, the material did not suffer shrinking neither constriction nor rehydration of its structure when immersed into PBS, as

experienced by the other hydrogels (HA-6FD, HA-6RT and HA-6T); helping it to maintain its physical stability within the crosslinked network, thus reducing physical stress which can lead to faster hydrolytic degradation.

Regarding dried hydrogels (HA-6FD, HA-6RT and HA-6T), their morphologies show little degradation signs, their pore walls present few fractures and some dissolved areas; but their bulk structures continue to be well-formed, interconnected and showing good pore sizes, necessary for cells to proliferate and spread around the material. Freeze-dried hybrid hydrogels (HA-6FD) have higher surface areas due to a great number of pores but with smaller sizes, this characteristic continues after the 14 days of immersion into PBS. Room temperature-dried hybrid hydrogels (HA-6RT) and 60 °C-dried hybrid hydrogels (HA-6T) have bigger pores than starting ones, which is attributed to moisture.
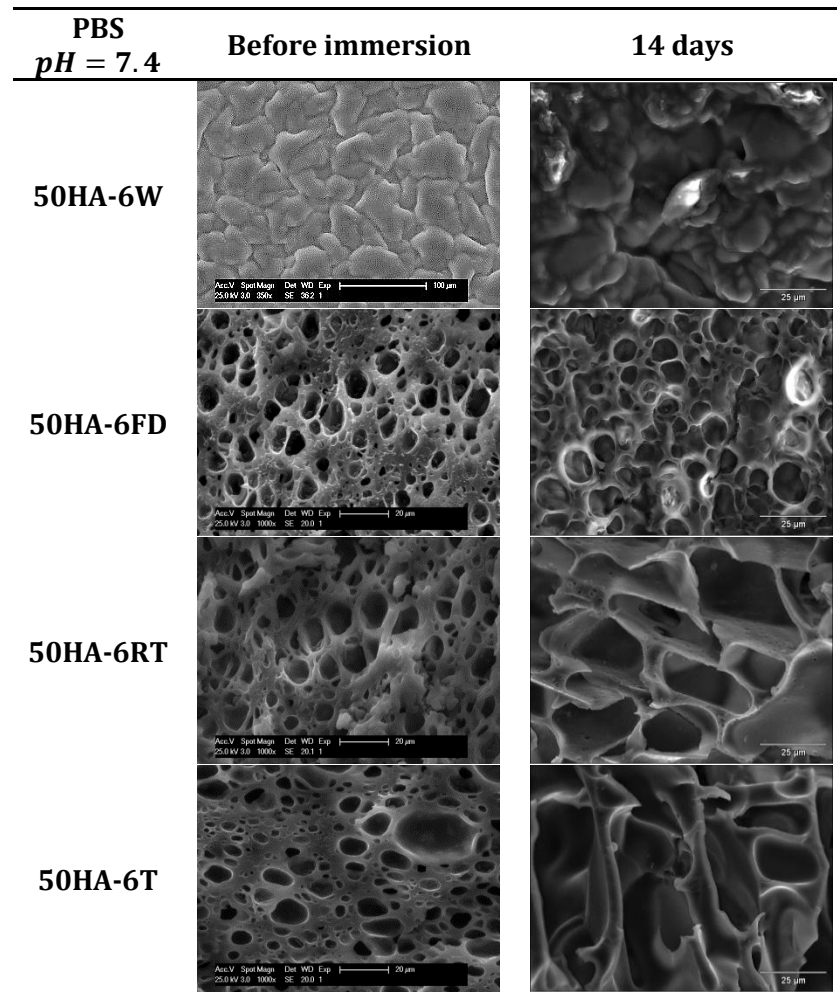
Figure 60. Morphology of the 50HA-pH6 hybrid hydrogels when being immersed into PBS for 14 days. The hydrogels were kept with moisture when taking SEM images.

To further evaluate degradation degree in HA-6pH hybrid hydrogels when being immersed into PBS, the materials were dried at 37 °C for 24 hours after each period of immersion time and then SEM images of them were taken. **Figure 61** shows 50HA-6FD hybrid hydrogels, **Figure 62** shows 50HA-RT hybrid hydrogels and **Figure 63** shows 50HA-6T hybrid hydrogels after 7, 21 and 35 days of immersion into PBS at physiological conditions.
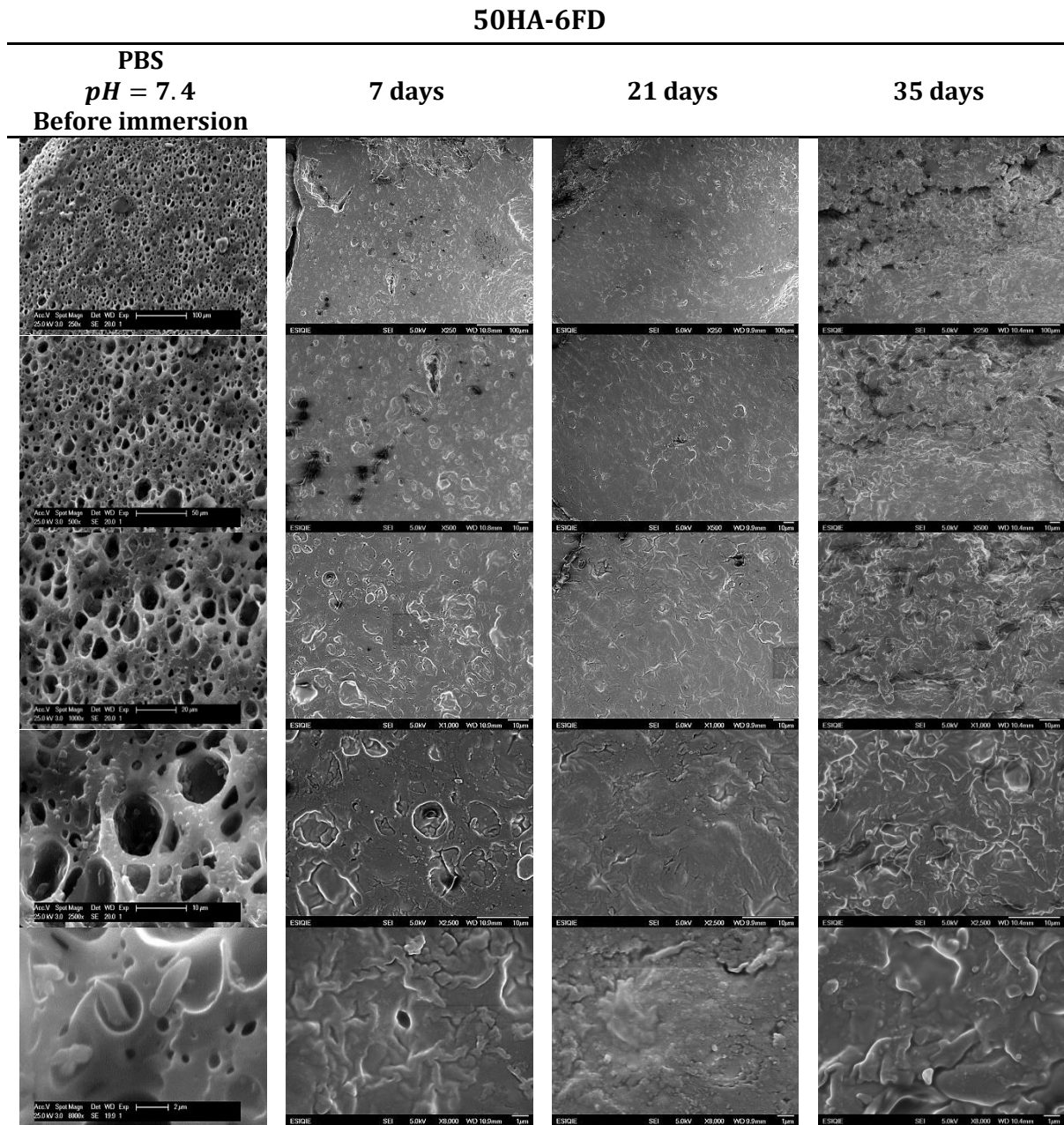
Figure 61. Morphology of 50HA-6FD hybrid hydrogel at different immersion times into PBS. The hydrogels were dried at 37 ° when taking SEM images.

50HA-6RT

PBS $pH = 7.4$ Before immersion	7 days	21 days	35 days
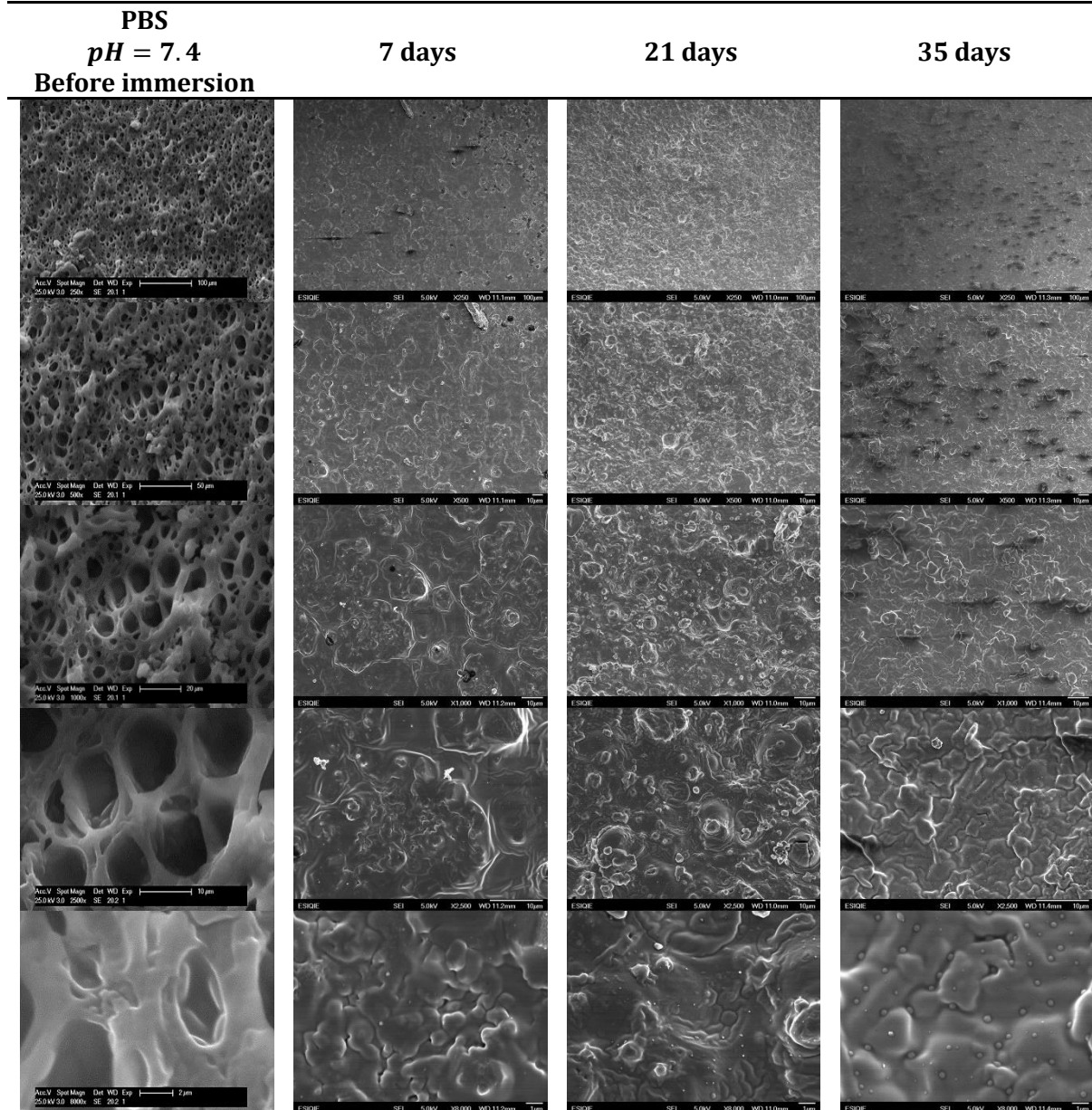
Figure 62. Morphology of 50HA-6RT hybrid hydrogel at different immersion times into PBS. The hydrogels were dried at 37 °C when taking SEM images.

It can be observed that the three types of HA-*pH*6 porous hybrid hydrogels shrunk and constrained when being dried; however, the presence of the porous can still be appreciated, since the contour and indentation of the porous located at the surfaces are visible. Although the materials did not experience a high degree of degradation, it can be

observed that at 35 days of immersion, the indentations and grooves are more profound, being caused by the materials degradation. Moreover, crystalline formations can be observed from day 21 to day 35 of immersion into PBS, which are attributed to precipitation of $NaCl$ and KCl salts from PBS as shown in **Figure 64**.

50HA-6T

PBS $pH = 7.4$ Before immersion	7 days	21 days	35 days
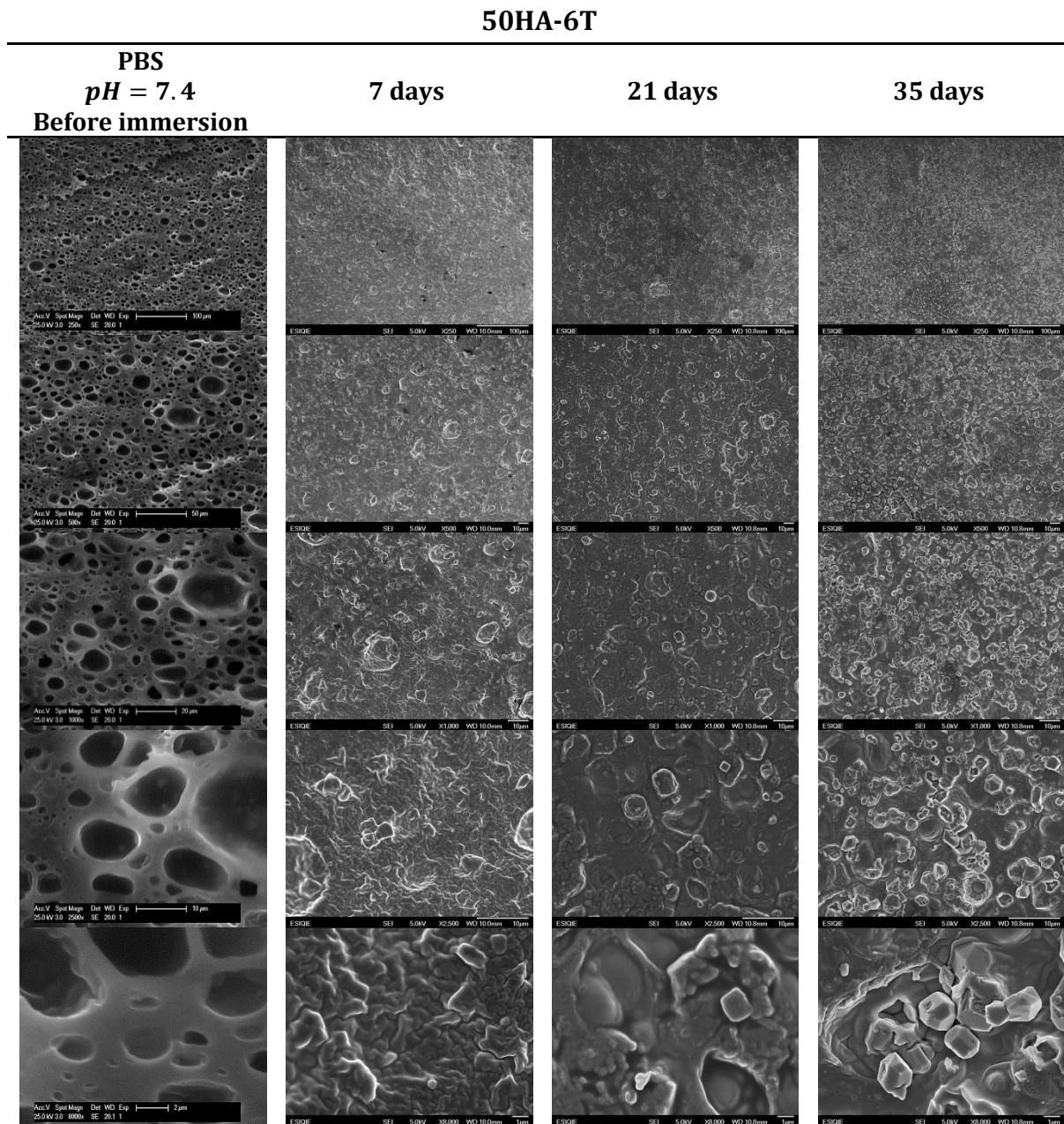
Figure 63. Morphology of 50HA-6T hybrid hydrogel at different immersion times into PBS. The hydrogels were dried at 37 °C when taking SEM images.

Elemental mappings of 50HA-$pH6$ hybrid hydrogels, immersed for 35 days into PBS at physiological conditions, are shown **Figure 64**. In both hydrogels (50HA-RT and 50HA-6T), the Carbon (C) and Silicon (Si) along with Oxygen (O) elements appear to be homogeneously distributed along the sample; however, Silicon has a stronger presence in the entire sample, suggesting that the organic components (HA chains) degrade faster than the organic-inorganic PDMS-modified SiO_2 structure within the HA-based hybrid hydrogels. This behavior is better seen in the HA-based hydrogels dried at 60 °C (50HA-6T) since hyaluronic acid chains may have suffer a bit of thermal degradation.
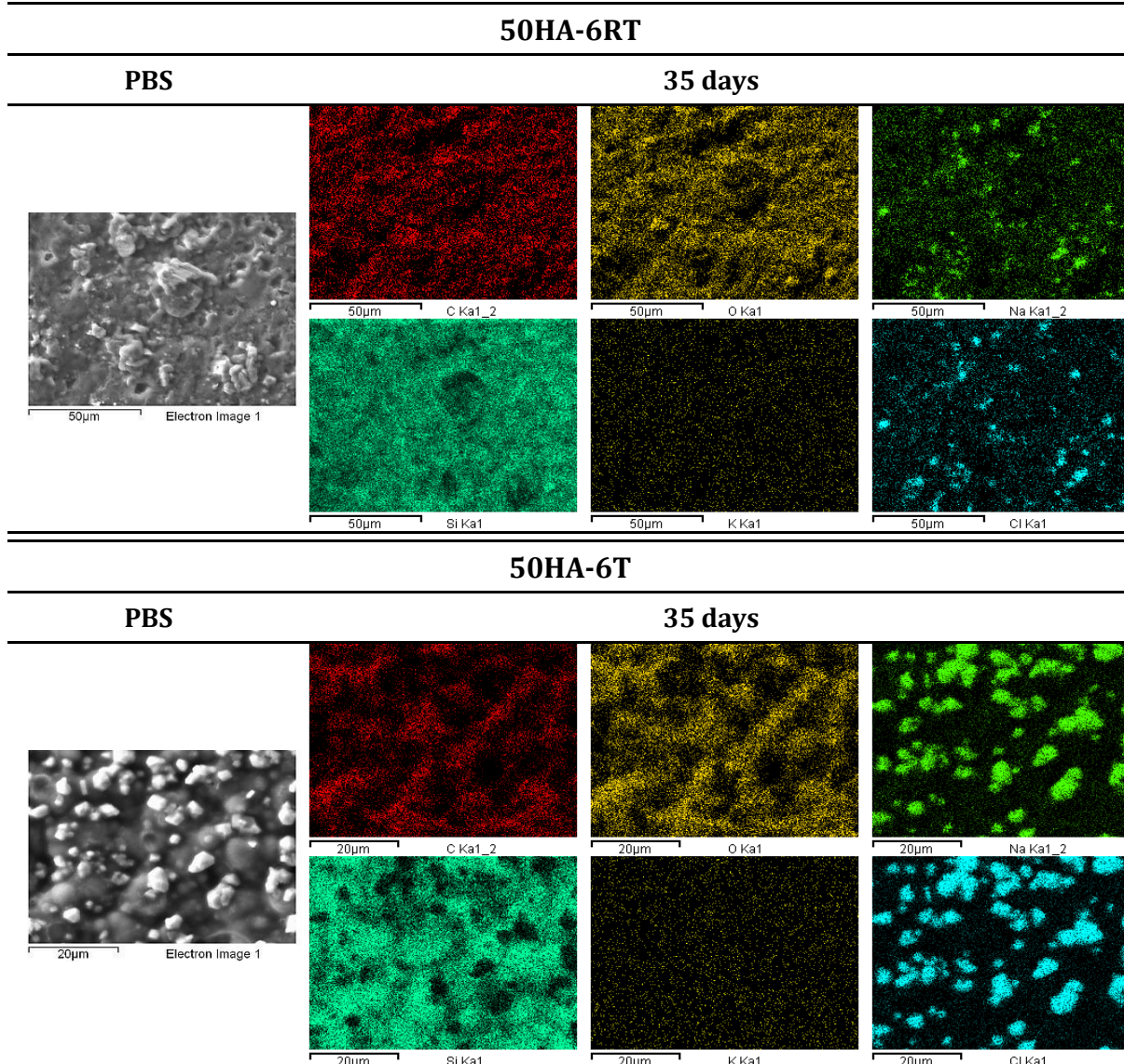
Figure 64. Elemental mapping on the surface of 50HA-$pH6$ hybrid hydrogel immersed for 35 days into PBS. The hydrogels were dried at 37 °C before mapping.

3.7.3   RHEOLOGICAL PROPERTIES OF HA – BASED HYBRID HYDROGELS

The rheological properties of 50HA-$pH6$ hybrid hydrogels during degradation assays were evaluated by monitoring the storage modulus (G') and loss modulus (G") as a function of frequency through rheometry by dynamic oscillatory measurements with 25 mm diameter parallel plate geometry as shown in **Figure 65,** revealing the effect of PDMS-modified SiO_2 crosslinking structure on the viscoelasticity of HA-based hybrid hydrogels.

The materials were carefully placed into the lower plate after which the upper plate was lowered to a 2.5 mm gap. After that, dynamical oscillatory frequency sweeps for HA-based hybrid hydrogels were performed at 37 °C (physiological temperature) with constant strain (0.1866%) and the frequency was set from 0.1 to 10 Hz.

50HA-6W
3 mm thickness

50HA-6W
ϕ =25 mm

50HA-6W

Rheometer

50HA-6W
1st day of immersion

50HA-6W
Day 28th of immersion
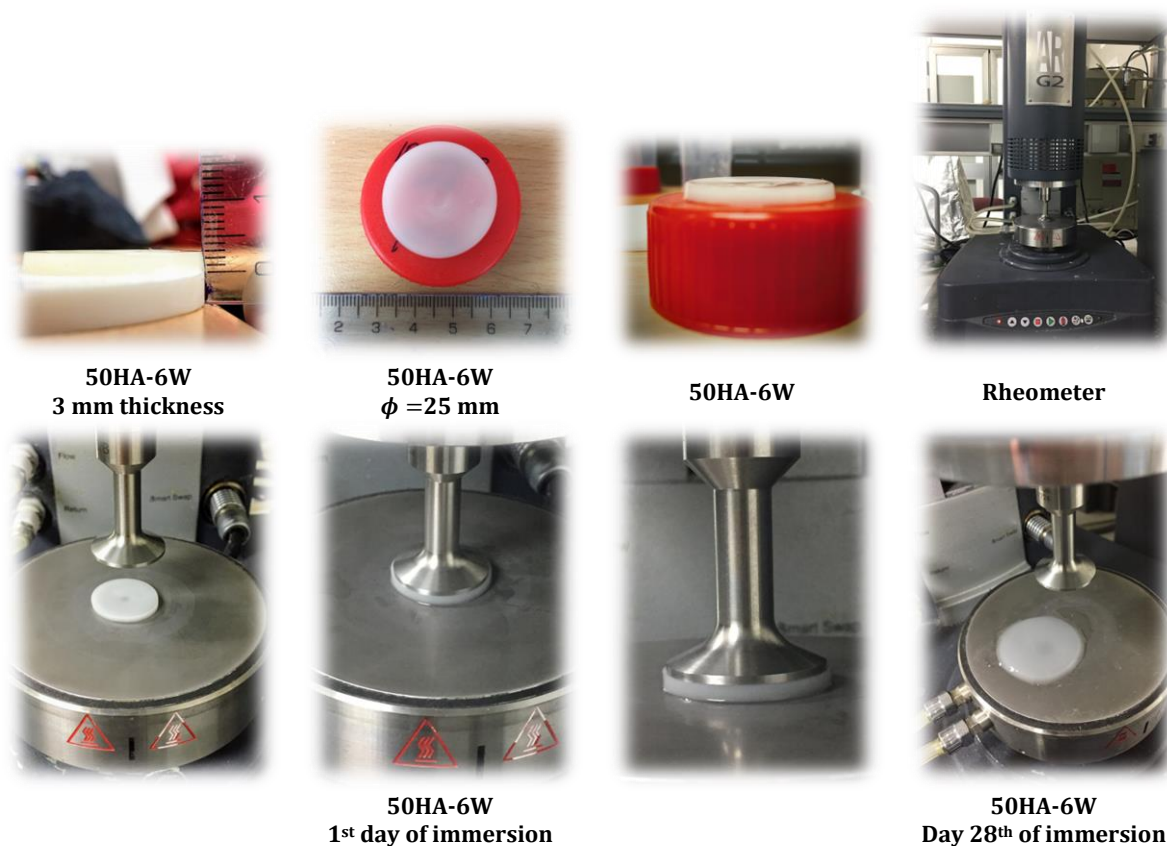
Figure 65. Rheological assays in 50HA-$pH6$ hybrid hydrogels under physiological conditions.

Storage modulus (G') and loss modulus (G'') of different 50HA-$pH6$ hybrid hydrogels exhibited similar linear rheological behaviors, (**Figure 66**) regardless of the drying process they experienced. G' and G" values remained almost constant as frequency increased.

A **B**

50HA-6W

50HA-6FD

50HA-6RT

50HA-6T
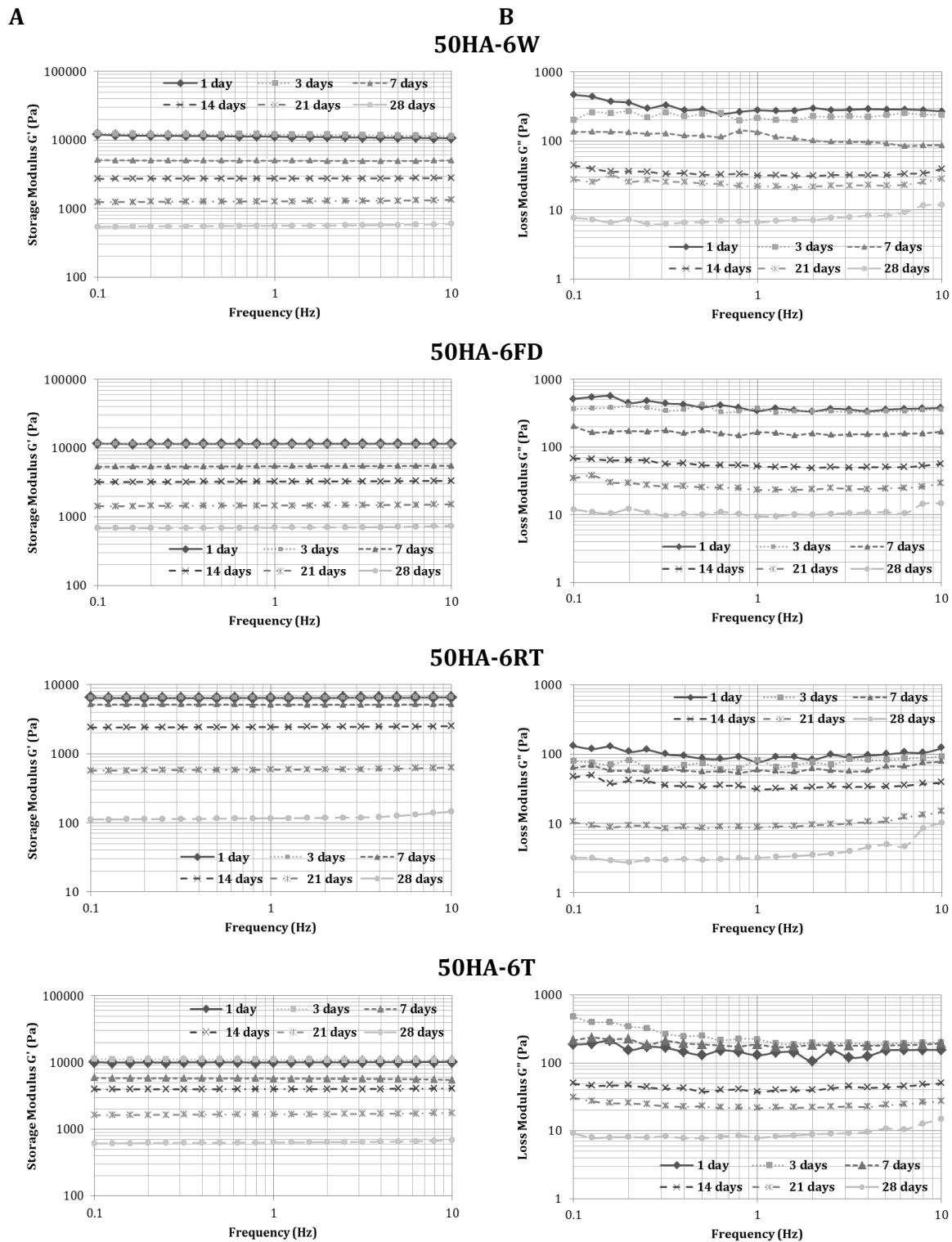
Figure 66. Dynamic oscillatory frequency sweep curves for 50HA-*pH*6 hybrid hydrogels. **(A)** Storage modulus and **(B)** loss modulus at 37 °C as a function of frequency (Hz) for 50HA-*pH*6 hybrid hydrogels.

This linear rheological behavior implied that the HA-based hybrids have similar microstructure, bearing dynamic deformations. It was observed that storage modulus (G') was far higher than loss modulus (G") in the range of the whole frequency sweep, which means that great proportion of energy was stored in the deformation of the hydrogel itself. The highly elastic nature of these 50HA-*pH*6 hydrogels was thus indicated.

In **Figure 66** it is observed that when increasing degradation time, both storage modulus (G') and loss modulus (G") values decreased. In the first day of immersion, 50HA-*pH*6 hydrogels showed G' values above 10,000 Pa and in the 28th day of immersion, 50HA-*pH*6 hydrogels showed G' values near ~800 Pa. However, 50HA-6RT hydrogel showed smaller storage modulus (G') and loss modulus (G") values than the other 50HA-*pH*6 hybrid hydrogels as immersion time passed; thus, losing its physicochemical, structural and rheological stability which would lead to a faster degradation rate.

Studying rheological and mechanical properties in hydrogels used as substrate or scaffolds intended to replace cartilage tissue is really important since local matrix stiffness on cells has important implication for cell locomotion, growth, differentiation, disease, regeneration and proliferation. Normal tissue cells probe elasticity as they anchor and pull on their surroundings. A tissue cell not only applies forces, but also responds through cytoskeleton organization to resistance that a cell senses from normal tissue matrix, synthetic substrate or an adjacent cell. Therefore, designing scaffolds with similar elasticity to cartilage tissue would be preferable for regeneration.

Yang *et al.* [133] studied the viscoelastic properties of several tissues such as epidermis, dermis, articular cartilage and tooth germ. In this study, the dynamic oscillatory frequency sweep curves (G' and G") of those tissues exhibited nonlinear rheological behaviors at a constant strain of 1%. Cartilage tissue showed a storage modulus (G') of 10,000 Pa at 1 Hz. The studied 50HA-*pH*6 hybrid hydrogels showed storage modulus (G') near 10,000 Pa during the first days of immersion. Thus, suggesting that these hybrid hydrogels can replace cartilage tissue meanwhile cells begin to proliferate and then begin to regenerate it.

3.8 SWELLING AND DEGRADABILITY PROPERTIES OF CHONDROITIN SULFATE – BASED PDMS – MODIFIED SiO_2 ORGANIC – INORGANIC HYBRID HYDROGELS

Once the CS-based PDMS-modified SiO_2 organic-inorganic hybrid hydrogels are characterized and analyzed, their swelling and degradability properties were studied. Since the other types of drying process favors early degradation process, the chosen polysaccharide hydrogels compositions to test their swelling and degradation properties are the 100CS-6RT and 100CS-7RT hybrid hydrogels. Swelling and degradation ratios of the hybrid hydrogels were determined by the classical gravimetric method. Dried hybrid *gels* were put into 0.01M PBS: Phosphate Buffer Solution ($pH = 7.4$) at 37 ± 0.5 °C composed of $NaCl$ and KCl salts. PBS worked as saline solution taking the place of blood plasma. The swollen polysaccharide-based hybrid hydrogels were weighed at various times to evaluate swelling equilibrium and degradation rate. The changes experienced by the hybrid hydrogels during swelling and degradation process are analyzed through hydration tests and ESEM images.

3.8.1 SWELLING PROPERTIES OF CS – BASED HYBRID HYDROGELS

The swelling properties of the CS-based hybrid hydrogels were studied. **Figure 67** shows 100HA-7RT hybrid hydrogel swelling capability in real time when undergoing an increasing water pressure. The images corresponding to each applied pressure, from 0.6 Torr to 6.6 Torr, are displayed. Dried pores in the hybrid hydrogel are observed in **Figure 67-A**. As water pressure increased, the pores started to get occluded by droplets of water and to lose their shape when the pore walls completely absorbed those water droplets. It can be settled that water absorption occurred gradually until the entire hydrogel porous were fully hydrated, as shown in **Figure 67-O**.

Due to the hydrated nature of soft tissues, tissue engineering should pursue the aim to design and fabricate a biomaterial that guarantees both, good hydration and good mechanical resistance, similar to the natural extracellular matrix. These biomaterial characteristics allow cells to perform a regenerative function and to have a suitable time for resorption.
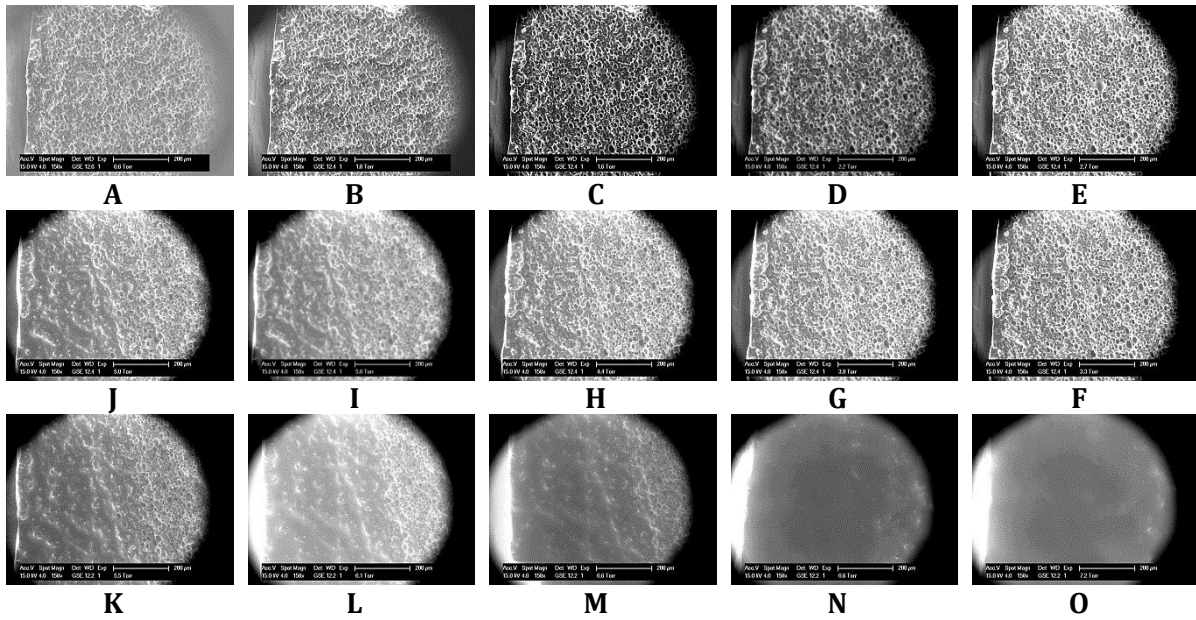
Figure 67. 50HA-based hybrid hydrogel (50HA-6RT) undergoing an increasing water pressure from 1.1-8.4 Torr to evaluate its swelling capability through Environmental Scanning Electron Microscopy.

As explained before, the hydration degree of the HA-based hybrid hydrogels was measured at 37 °C using buffer solution (PBS) 7.4 pH. **Figure 68** shows the 100CS-7RT hybrid hydrogel after being immersed into PBS for 45 days.
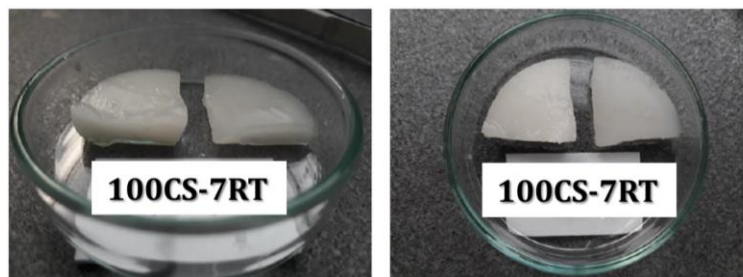
Figure 68. Maximum hydration degree of the 100CS-7RT hybrid hydrogel, reaching 160% of swelling degree when being immersed into PBS under physiological conditions for 45 days.

Before starting the swelling assay, the samples (*xerogels*) were rigid solid networks. Immediately after being soaked into the buffer solution, *gels* started to hydrate as their

polymer chains swelled and became flexible, allowing water molecules diffusion within the organic-inorganic matrix. As water was being absorbed into the hydrogel matrix, the volume and size of the CS-based hybrid hydrogel gradually increased. Finally, when chain relaxation reached a minimum energy state, equilibrium between chain relaxation and contraction of the polymeric network was also reached, getting a stable level of hydration. The swollen hydrogel showed a white spongy odorless texture.

As shown in **Figure 68**, 100 CS-6RT and 100CS-7RT hybrid hydrogels underwent uniform volumetric expansion in response to several stimuli of physiological conditions (37 °C and 7.4 pH), suggesting that these hybrid hydrogels showed a great added value by combining potential and restrictions of their precursors: 1) silicon PDMS hydrophobicity and elasticity; 2) silica SiO_2 structure providing stiffness to the hydrogel; 3) CS biopolymer providing natural hydrophilic capability and nontoxic characteristics to the hydrogels, necessary to mimic Extracellular Matrix.

Hydration degree and swelling equilibrium of CS-based hybrid hydrogels are affected by three important factors: 1) polysaccharide concentration; 2) synthesis pH; and 3) drying process. These variables also affect the crosslinking density and structure of hybrid hydrogels before and after immersion. **Figure 69** shows the swelling degree evolution of 100CS-based hybrid hydrogels synthesized at 6 pH or 7 pH and dried at room temperature conditions.
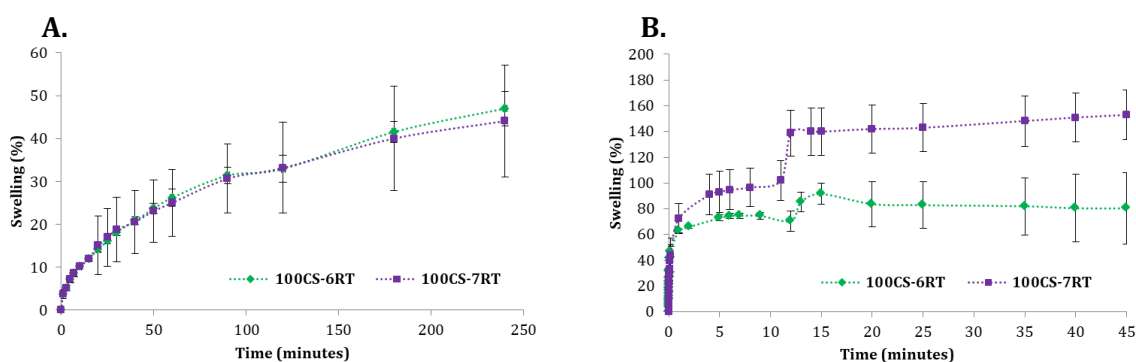
Figure 69. Swelling degree evolution of 100CS-based hybrid hydrogels evaluated for 45 days under physiological conditions. Column **(A)** shows swelling (%) of 100CS-6RT and 100CS-7RT up to 240 minutes. Column **(B)** shows swelling (%) of 100CS-6RT and 100CS-7RT up to 45 days.

It is observed that 100CS-7RT hybrid hydrogels showed a higher swelling degree (reaching almost double swelling degree) and degradation rate than 100CS-6RT hybrid hydrogels. Both hybrid hydrogels showed similar swelling behaviors by reaching their swelling equilibrium at the same time.

The difference among the materials indicates the hybrid hydrogel structure and swelling capability are affected by pH at which the hydrogels were synthesized. As could be seen in Raman mapping, light acidic conditions ($6 \, pH$) enhances an inorganic crosslinking resulting in a homogeneous inorganic crosslinking structure, which better restrain swelling degree; in contrast to neutral conditions ($7 \, pH$), yielding materials with organic and inorganic domains interconnected with hybrid organic-inorganic PDMS-modified SiO_2 chains, boosting a faster and higher degradation degree.

3.9 BIOLOGICAL PROPERTIES OF HYALURONIC ACID – BASED PDMS – MODIFIED SiO_2 ORGANIC – INORGANIC HYBRID HYDROGELS

The MTT cytotoxicity study was performed using fibroblast and mother cells cultured at 37 °C in a humid atmosphere with 95% air and 5% CO_2 (standard conditions). Three replica of each selected sample were used to perform the MTT assay. The materials were sterilized with an ethanol 70% – water 30% solution. The degree of cytotoxicity of the materials was determined by the release of "toxic" substances while being immersed into SBF and their effect on the cells while being in contact with them.

The eluents, SBF in which the materials were immersed, were collected after 1, 4, 7 and 14 days. Then, fibroblast and mother cells were cultivated for 24 hours into those eluents. Finally the MTT assay was carried out. The percentage of cell viability of each sample was compared with a control (100% of cell viability). **Figure 70** shows the result of cell viability for the HA-based hybrid hydrogels.

On average, all the studied samples have cell viability above 80%, indicating a very low toxicity. A material is considered to be not cytotoxic when its viability is above 75% and non-biocompatible when its viability is below 70% in respect to the control media. All the tested materials show less cell viability in the first day of immersion. Over the next days, cell viability increased and remained near 100%.

A.

67HA-*pH*7 hybrid hydrogels

B.

50HA-FD hybrid hydrogels

C.

50HA-6RT and 50HA-7FD hybrid hydrogels
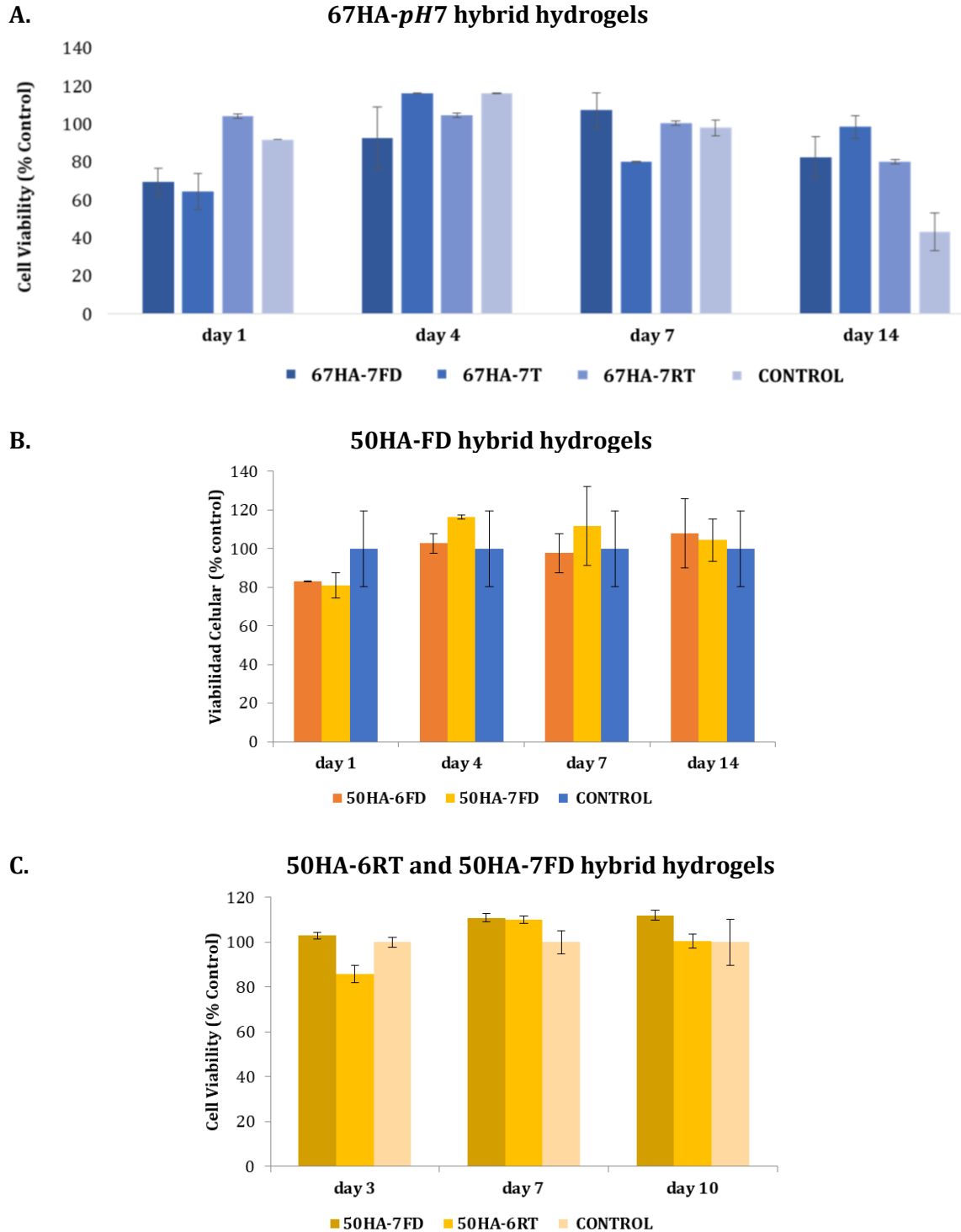
Figure 70. MTT assay evaluating cytotoxicity of HA-based hybrid hydrogels during 14 days under physiological conditions. **(A)** 67HA-*pH*7 hybrid hydrogels tested with fibroblast cells. **(B)** 50HA-FD hybrid hydrogels tested with fibroblast cells. **(C)** 50HA-6RT and 50HA-7FD hybrid hydrogels tested with mother cells obtained from dental pulp.

In general, HA-based hybrid hydrogels with a lower HA concentration (50HA), synthesized at $pH = 7$ and undergoing room temperature and freeze-drying processes show better cell viability. Room temperature drying process allows the HA-based hybrid hydrogel to better crosslink the PDMS-modified SiO_2 network, avoiding early degradation. Freeze-drying process produces materials with high surface area and toxic byproducts are eliminated; thus reducing cytotoxicity. HA-based hybrid hydrogels synthesized at $pH = 7$ helps the materials to reduce the release of acidic media, increasing cell viability. 50HA-based hybrid hydrogels show better cell viability than 67HA-based hybrid hydrogels.

Figure 71 shows the Alamar Blue® assay evaluating fibroblast cell proliferation. It can be observed that cell behavior is similar to cell behavior in the MTT assay. 67HA-$pH7$ shows less cell proliferation than 50HA-based hybrid hydrogels. It can be concluded that less HA concentration boosts good cell viability and cell proliferation.
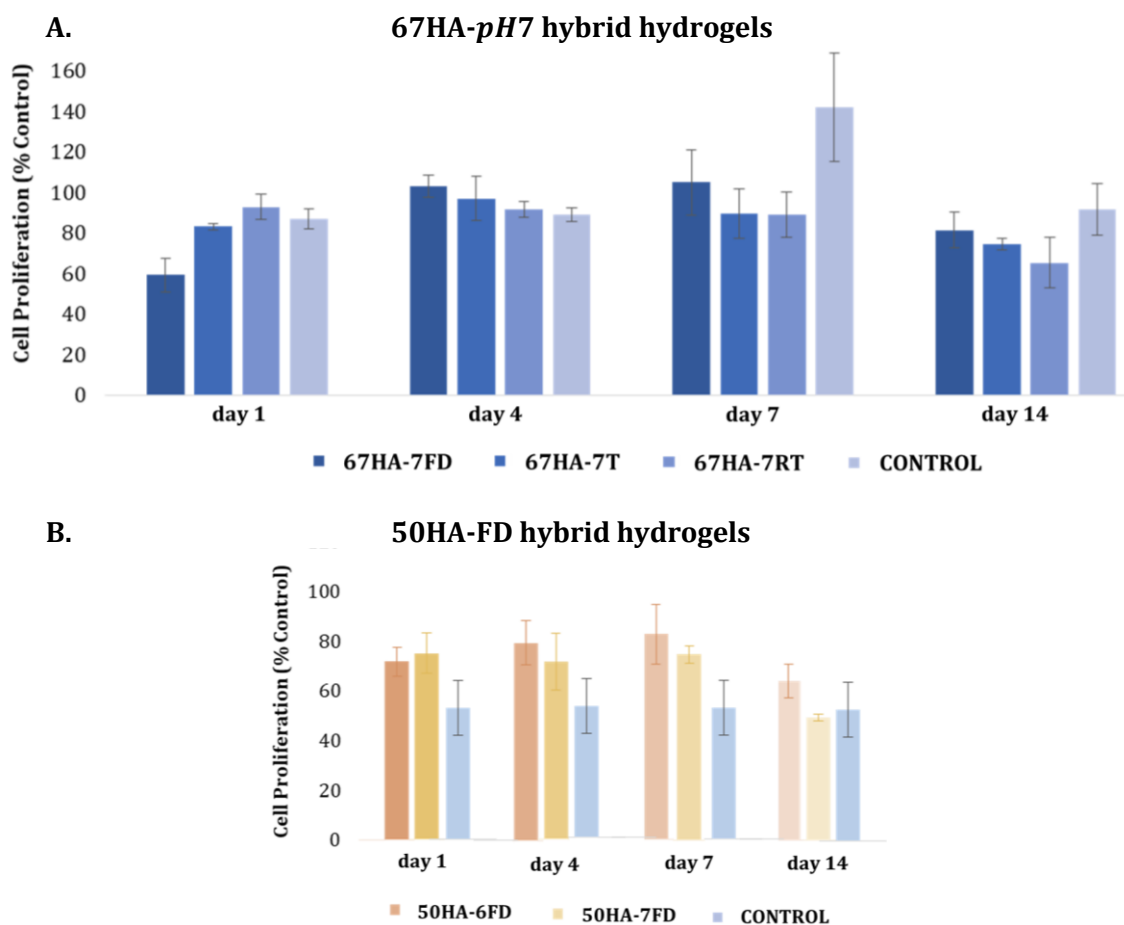
Figure 71. Alamar Blue® assay evaluating cell proliferation of 50HA-based hybrid hydrogels during 14 days under physiological conditions.

3.10 BIOLOGICAL PROPERTIES OF CHONDROITIN SULFATE – BASED PDMS – MODIFIED SiO_2 ORGANIC – INORGANIC HYBRID HYDROGELS

The MTT cytotoxicity study was performed using fibroblast cells cultured at 37 °C in a humid atmosphere with 95% air and 5% CO_2 (standard conditions). Three replica of each selected sample were used to perform the MTT assay. The materials were sterilized with an ethanol 70% – water 30% solution. The degree of cytotoxicity of the materials was determined by the release of "toxic" substances while being immersed into SBF and their effect on the cells while being in contact with them.

According to the limits set by international norms (*cell viability* $\geq 75\%$; *non cytotoxic* and *cell viability* $\leq 70\%$; *non biocompatible*), the 100CS-7RT hybrid hydrogel has cell viability above 80%, indicating a very low toxicity. However, 100CS-7T and 100CS-7FD hybrid hydrogels have cell viability around 70%, suggesting that those hydrogels are non-biocompatible. **Figure 72** shows the result of cell viability for the CS-based hybrid hydrogels.
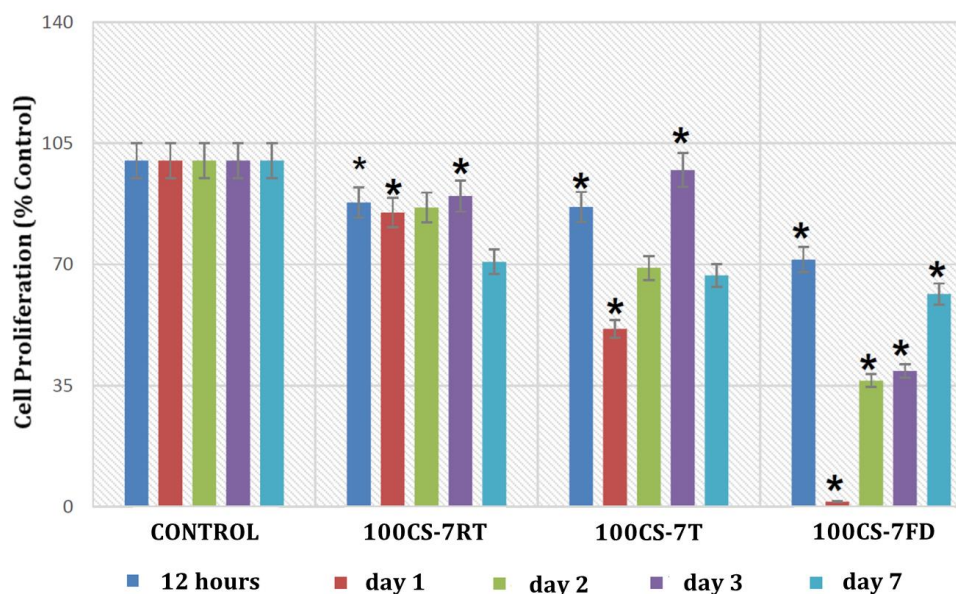
Figure 72. MTT assay to evaluate cytotoxicity of 100CS-based hybrid hydrogels using fibroblast cells evaluated for 7 days under physiological conditions. Significant differences obtained in ANOVA versus negative control (∗ *respresent* $p < 0.05$).

125

The percentage of cell viability can also be correlated with the cell phenotype being cultured. **Figure 73** shows the appearance of fibroblasts cultured with the eluents of the CS-based hybrid hydrogesl at several periods of time.
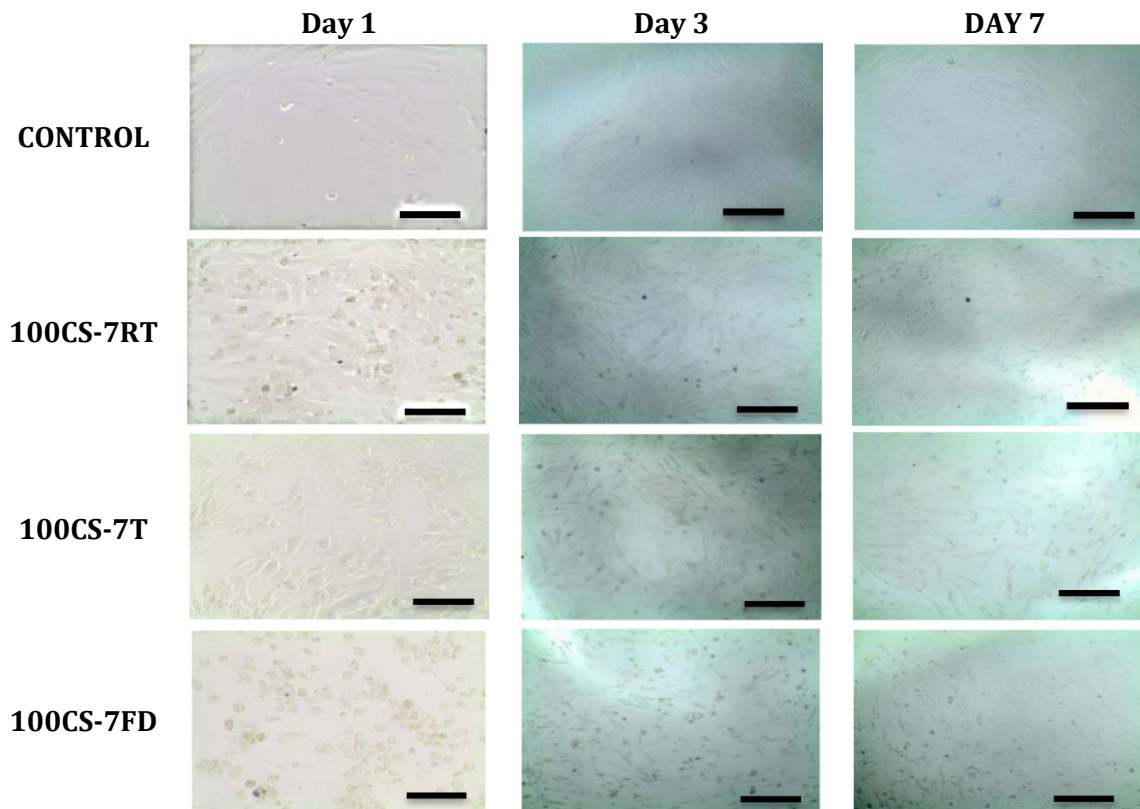
Figure 73. Micrographs taken from the culture of fibroblast cells under physiological conditions with the eluents of the 100CS-pH7 hybrid hydrogels dried through three different processes at determined times, which correspond to the MTT assay. Scale is 15 µm.

The micrographs displayed in **Figure 73** show that culture cells of 100CS-7RT and 100CS-7T hybrid hydrogels eluents at 24 hours have typical cell phenotype growth. Cells cultured in eluents from 100CS-7L at 24 hours are round, with nucleus in which the chromatin condensed and dense clusters are formed. At 72 hours, the three cell culutres have similar characteristics, although 100CS-7RT and 100CS-7T hybrid hydrogels eluents keep a greater cell population. After 7 days, the three culture samples have homogenized their cell characterisitics; however, in 100CS-7RT and 100CS-7T hybrid hydrogels eluents the fibroblasts are more distended and with a healthier appearance.

CONCLUSION

Biological 3D hybrid hydrogels, capable of mimicking the natural cartilage extracellular matrix, using polysaccharides as hyaluronic acid (HA) and chondroitin sulfate (CS) modified by 3-aminopropyl triethoxysilane (APTES) and crosslinked by a PDMS-modified SiO_2 organic-inorganic structure in order to decrease their natural hydrophilicity were successfully developed. Polysaccharide-based PMDS-modified SiO_2 organic-inorganic hybrid hydrogels were evaluated to study their physical, chemical, rheological and biological properties to establish if they would work as biomaterials for cartilage substitution and regeneration.

The polysaccharide chains were chemically modified and hybridized *via* amidation of the carboxylic groups with inorganic modifier (APTES) molecules. The polysaccharide chains were crosslinked by a three dimensional PDMS-modified SiO_2 organic-inorganic matrix *via sol-gel* method. The inorganic crosslinking (SiO_2) network provided restriction to swelling degree in hybrid hydrogels. The organic-inorganic silicone (PDMS) decreased the natural hydrophilicity of polysaccharides; thus slowing down degradation rates of the developed hybrid hydrogels.

Synthesis conditions such as starting polysaccharide concentration solution, pH and temperature determined gelling (*sol-gel* transition) times and efficiency in the polysaccharide chemical modification and further hydrolysis-condensation reactions to build up the PMDS-modified SiO_2 organic-inorganic matrix. Furthermore, drying process affects swelling and degradative properties of polysaccharide-based PMDS-modified SiO_2 organic-inorganic hybrid hydrogels.

Polysaccharide-based PMDS-modified SiO_2 organic-inorganic hybrid hydrogels, especially 50HA-6FD, 50HA-7FD, 50HA-6RT and 100CS-7RT hydrogel samples, proved to have good biological properties by having cell viability and cell proliferation above 80% when being tested with fibroblast cells.

Polysaccharide-based PMDS-modified SiO_2 organic-inorganic hybrid hydrogels have potential application as biomaterials for regeneration and substitution of cartilage tissue. However, further biological *in vitro* and *in vivo* studies are needed.

REFERENCES

1.   D. Puppi, F.C., A.M. Piras, E. Chellini, *Polymeric materials for bone and cartilage repair.* Progress in Polymer Science, 2010. **35**: p. 403 - 440.
2.   S. Fickert, T.S., M. Niks, and C. Weiss · S. Thier, *Feasibility of arthroscopic 3-dimensional, purely autologous chondrocyte transplantation for chondral defects of the hip: a case series.* Arch Orthop Trauma Surg, 2014. **134**: p. 971–978.
3.   C. Baynata, C.A., J.P. Vincent, P. Schiele, P. Buisson, F. Dubrana, F.X. Gunepin, *Actifit® synthetic meniscal substitute: Experience with 18 patients in Brest, France.* Orthopaedics & Traumatology: Surgery & Research, 2014. **100S**: p. S385–S389.
4.   P. Verdonk, A.D., K. F. Almqvist, R. Verdonk, and J. Victor, *Treatment of osteochondral lesions in the knee using a cell-free scaffold.* Bone Joint J, 2015. **97-B**: p. 318–23.
5.   Scopp, J.M.C.a.J.M., *Treatment of articular cartilage defects of the knee with microfracture and enhanced microfacture techniques.* Sports Med Arthrosc., 2016. **24**(2): p. 63-68.
6.   Erggelet, C., *Enhanced Marrow StimulationTechniques for Cartilage Repair.* Operative Techniques in Orthopaedics, 2014. **24**(1): p. 2-13.
7.   J. Gille, P.B., P. Volpi, L. de Girolamo, E. Reiss, W. Zoch,and S. Anders, *Outcome of Autologous Matrix Induced Chondrogenesis (AMIC) in cartilage knee surgery: data of the AMIC Registry.* Arch Orthop Trauma Surg, 2013. **133**: p. 87–93.
8.   T. Turajane, T.T., S. Honsawek, U. Chaveewanakorn, J. Aojanepong, and K. I. Papadopoulos, *Assessment of chondrogenic differentiation potential of autologous activated peripheral blood stem cells on human early osteoarthritic cancellous tibial bone scaffold.* Musculoskelet Surg, 2014. **98**: p. 35–43.
9.   A.K. Gaharwar, P.J.S., G. Shmidt, *Chapter 24: Nanocomposite polymer biomaterials for tissue repair of bone and cartilague: a material science perspective*, in *Nanomaterials Handbook*. 2011, Taylor and Francis Group, LLC: USA. p. 1 - 20.
10. C. Chung, J.A.B., *Engineering cartilage tissue.* Advanced Drug Delivery Reviews, 2008. **60**: p. 243 - 262.
11. Gregory Chang, D.X., Orrin Sherman, Eric Strauss, Laith Jazrawi, Michael P. Recht, Ravinder R. Regatte, *High resolution morphologic imaging and T2 mapping of cartilage at 7 Tesla: comparison of cartilage repair patients and healthy controls* Magn Reson Mater Phy, 2013. **26**: p. 539–548.
12. C. Mathieu, A.C., V. Lascau-Coman, G.E. Rivard, and C.D. Hoemann, *Stereological analysis of subchondral angiogenesis induced by chitosan and coagulation factors in microdrilled articular cartilage defects.* Osteoarthritis and Cartilage, 2013. **21**: p. 849-859.
13. Alberto Siclari, G.M., Chiara Gentili, Christian Kaps, Ranieri Cancedda, and Eugenio Boux, *Cartilage repair in the knee with subchondral drilling augmented with a platelet-rich plasma-immersed polymer-based implant.* Knee Surg Sports Traumatol Arthrosc, 2014. **22**: p. 1225–1234.
14. D. A. Sánchez-Téllez, L.T.-J., L. M. Rodríguez-Lorenzo, *Hydrogels for cartilage Regeneration, from polysaccharides to hybrids.* Polymers, 2017. **9**(12): p. 671.
15. Mario Alberto Accardi, S.D.M., Anthony Callanan, Sangwon Chung, Philippa M. Cann, Molly M. Stevens, and Daniele Dini, *Effects of Fiber Orientation on the Frictional Properties and Damage of Regenerative Articular Cartilage Surfaces.* Tissue Engineering: Part A, 2013. **19**: p. 2300-2310.
16. Myriam Lebourg, J.R.R., Tiago Sousa, Joao Mano, and José Luis Gómez Ribelles, *Different hyaluronic acid morphology modulates primary articular chondrocyte behavior in hyaluronic acid-coated polycaprolactone scaffolds.* J Biomed Mater Res Part A 2013. **101 A**: p. 518–527.
17. E.J. Levorson, O.H., P.M. Mountziaris, F.K. Kasper, and A.G. Mikos, *Cell-Derived Polymer/Extracellular Matrix Composite Scaffolds for Cartilage Regeneration, Part 2: Construct*

Devitalization and Determination of Chondroinductive Capacity. Tissue Eng Part C Methods, 2014. **20**(4).

18. Tanya J. Levingstone, A.M., Glenn R. Dickson, Fergal J. O'Brien, and John P. Gleeson, *A biomimetic multi-layered collagen-based scaffold for osteochondral repair.* Acta Biomaterialia, 2014. **10**: p. 1996–2004.

19. Amanda J. Sutherland, E.C.B., S. Connor Dennis, Gabriel L. Converse, Richard A. Hopkins, Cory J. Berkland, Michael S. Detamore, *Decellularized Cartilage May Be a Chondroinductive Material for Osteochondral Tissue Engineering.* PLoS ONE, 2015. **10**(5): p. e0121966.

20. María Sancho-Tello, F.F., Pablo Gastaldi, Amparo Ruiz-Saurí, José J. Martín de Llano, Edurne Novella-Maestre, Carmen M. Antolinos-Turpín, José A. Gómez-Tejedor, José L. Gómez Ribelles, Carmen Carda, *Time evolution of in vivo articular cartilage repair induced by bone marrow stimulation and scaffold implantation in rabbits.* Int J Artif Organs, 2015. **38**(4): p. 210-223.

21. JianhuaWang, Q.Y., Niangmei Cheng, Xiaojun Tao, Zhihua Zhang, Xiaomin Sun, Qiqing Zhang, *Collagen/silk fibroin composite scaffold incorporated with PLGA microsphere for cartilage repair.* Materials Science and Engineering C, 2016. **61**: p. 705–711.

22. Zhenxing Shao, X.Z., 1 Yanbin Pi, Ling Yin, La Li, Haifeng Chen, Chunyan Zhou, Yingfang Ao, *Surface modification on polycaprolactone electrospun mesh and human decalcified bone scaffold with synovium-derived mesenchymal stem cells-affinity peptide for tissue engineering.* J Biomed Mater Res Part A, 2015. **103A**: p. 318–329.

23. Y. Zhang, C.-L.T., W.-J. Chen, Q. Zhang, and S.-L. Wang, *Dynamic compression combined with exogenous SOX-9 promotes chondrogenesis of adipose-derived mesenchymal stem cells in PLGA scaffold.* European Review for Medical and Pharmacological Sciences, 2015. **19**: p. 2671-2678.

24. M. Lehmann, F.M., K. Mannigel, K. Kaltschmidt, U. Sack, U. Anderer, *Three-dimensional scaffold-free fusion culture: the way to enhanced chondrogenesis of in vitro propagated human articular chondrocytes.* European Journal of Histochemistry, 2013. **57**: p. e31.

25. Heenam Kwon, L.S., Dana M. Cairns, Roshni S. Rainbow, Rucsanda C. Preda, David L. Kaplan, and Li Zeng, *The influence of scaffold material on chondrocytes under inflammatory conditions.* Acta Biomaterialia, 2013. **9**.

26. David Pretzel, S.L., Hannes Ahrem, Michaela Endres, Christian Kaps, Dieter Klemm, and Raimund W Kinne, *A novel in vitro bovine cartilage punch model for assessing the regeneration of focal cartilage defects with biocompatible bacterial nanocellulose.* Arthritis Research & Therapy, 2013. **15**: p. R59.

27. Pratthana Chomchalao, S.P., Manote Sutheerawattananonda, and Waree Tiyaboonchai, *Fibroin and fibroin blended three-dimensional scaffolds for rat chondrocyte culture.* BioMedical Engineering OnLine, 2013. **12**: p. 28.

28. Sang-Uk Lee, J.-Y.L., Sun Young Joo, Yong Suk Lee, and Changhoon Jeong, *Transplantation of a Scaffold-Free Cartilage Tissue Analogue for the Treatment of Physeal Cartilage Injury of the Proximal Tibia in Rabbits.* Yonsei Med J, 2016. **57**(2): p. 441-448.

29. Niamh A. O'Sullivan, S.K., Mitun P. Ranka, Katherine L. Zaleski, Michael J. Yaremchuk, Lawrence J. Bonassar, and Mark A. Randolph, *Adhesion and integration of tissue engineered cartilage to porous polyethylene for composite ear reconstruction.* J Biomed Mater Res Part B, 2015. **103B**: p. 983–991.

30. Iris Schleicher, K.S.L., Ursula Sommer, Ines Schappat, Alexander P. Martin, Gabor Szalay, and Reinhard Schnettler, *Allogenous bone with collagen for repair of deep osteochondral defects.* journal of surgical research, 2013. **185**: p. 667-675.

31. N.-J. Chang, C.-F.L., C.-C. Lin, W.-L. Chen, C.-F. Li, Y.-T. Lin, M.-L. Yeh, *Transplantation of autologous endothelial progenitor cells in porous PLGA scaffolds create a microenvironment for the regeneration of hyaline cartilage in rabbits.* Osteoarthritis and Cartilage, 2013. **21**: p. 1613-1622.

32. Shaili Sharma, A.L., Kuiwon Choi, Kwangmeyung Kim, Inchan Youn, Stephen B. Trippel, Alyssa Panitch, *Biomimetic Aggrecan Reduces Cartilage Extracellular Matrix From Degradation and Lowers Catabolic Activity in Ex Vivo and In Vivo Models.* Macromolecular Bioscience, 2013. **13**: p. 1228–1237.

33.   Chunming Ding, Z.Q., Wenbo Jiang, Haowei Li, Jianhe Wei, Guangdong Zhou, Kerong Dai, *Regeneration of a goat femoral head using a tissue-specific, biphasic scaffold fabricated with CAD/CAM technology.* Biomaterials, 2013. **34**: p. 6706-6716.

34.   Erik I. Waldorff, B.J.R., Terri A. Zachos, Bruce S. Miller, Jonathan McHugh, Steven A. Goldstein, *Preclinical Evaluation of a Novel Implant for Treatment of a Full-Thickness Distal Femoral Focal Cartilage Defect.* The Journal of Arthroplasty, 2013. **28**: p. 1421–1429.

35.   Sandra Camarero-Espinosa, B.R.-R., Christoph Weder, E. Johan Foster, *Directed cell growth in multi-zonal scaffolds for cartilage tissue engineering.* Biomaterials, 2016. **74**: p. 42-52.

36.   Aaron J. Krych, F.W., Kenneth W. Ng, Stephen Doty, Russell F. Warren, Suzanne A. Maher, *Matrix generation within a macroporous non-degradable implant for osteochondral defects is not enhanced with partial enzymatic digestion of the surrounding tissue: evaluation in an in vivo rabbit model.* J Mater Sci: Mater Med, 2013. **24**: p. 2429–2437.

37.   Flanigan, V.H.I.a.D.C., *New and Emerging Techniques in Cartilage Repair: Other Scaffold-Based Cartilage TreatmentOptions.* Oper Tech Sports Med, 2013. **21**: p. 125-137.

38.   Y.S. Kim, D.-Y.P., Y.H. Cho, J.W. Chang, J.W. Choi, J. K. Park, B.H. Min, Y. S. Shin and C.H. Kim, *Cultured chondrocyte and porcine cartilagederived substance (PCS) construct as a possible dorsal augmentation material in rhinoplasty: A preliminary animal study.* Journal of Plastic, Reconstructive & Aesthetic Surgery, 2015. **68**: p. 659-666.

39.   G. Filardo, E.K., F. Perdisa, B. Di Matteo, A. Di Martino, F. Iacono, S. Zaffagnini, F. Balboni, V. Vaccari, M. Marcacci, *Osteochondral scaffold reconstruction for complex knee lesions: a comparative evaluation.* The Knee, 2013. **20**: p. 570-576.

40.   Elizaveta Kon, G.F., Alessandro Di Martino, Maurizio Busacca, Antonio Moio, Francesco Perdisa, and Maurilio Marcacci, *Clinical Results and MRI Evolution of a Nano-Composite Multilayered Biomaterial for Osteochondral Regeneration at 5 Years.* The American Journal of Sports Medicine, 2014. **42**(1).

41.   Elizaveta Kon, G.F., Francesco Perdisa, Alessandro Di Martino, Maurizio Busacca, Federica Balboni, Andea Sessa, Maurillo Marcacci, *A one-step treatment for chondral and osteochondral knee defecs: clinical resutls of a biomimetic scaffold implantation at 2 years of follow-up.* J Mater Sci: Mater Med, 2014. **25**(10): p. 2437-2444.

42.   M. Caminal, X.M., D. Codina, R. M. Rabanal, A. Morist, J. Barrachina, F. Garcia, A. Pla, and J. Vives, *Transitory improvement of articular cartilage characteristics after implantation of polylactide:polyglycolic acid (PLGA) scaffolds seeded with autologous mesenchymal stromal cells in a sheep model of critical-sized chondral defect.* Biotechnol Lett, 2014. **36**: p. 2143–2153.

43.   Marco Delcogliano, F.d.C., Edoardo Scaravella, Giovanni Ziveri, Carlo Felice De Biase, Domenico Marotta, Pietro Marenghi, and Antonio Delcogliano, *Use of innovative biomimetic scaffold in the treatment for large osteochondral lesions of the knee.* Knee Surg Sports Traumatol Arthrosc, 2014. **22**: p. 1260–1269.

44.   Frank McCormick, B.C., Benedict Nwachukwu, Joshua D.Harris, H. Davis Adkisson, and Jack Farr, *Treatment of Focal Cartilage Defects With a Juvenile Allogeneic 3-Dimensional Articular Cartilage Graft.* Operative Techniques in Sports Medicine, 2013. **21**: p. 95-99.

45.   H. Chiang, C.-J.L., C.-H. Hsieh, C.-Y. Shen, Y.-Y. Huang, C.-C. Jiang, *Clinical feasibility of a novel biphasic osteochondral compositefor matrix-associated autologous chondrocyte implantation.* Osteoarthritis and Cartilage, 2013. **21**: p. 589-598.

46.   Elizaveta Kon, G.F., Giulia Venieri, Francesco Perdisa, and Maurilio Marcacci *Tibial plateau lesions. Surface reconstruction with a biomimeticnosteochondral scaffold: Results at 2 years of follow-up.* Injury, Int. J. Care Injured, 2014. **45S**: p. S121–S125.

47.   Geoffrey D. Abrams, N.A.M., Lisa A.Fortier, Brandon L.Roller, and Brian J. Cole, *BioCartilage: Background and OperativeTechnique.* Operative Techniques in Sports Medicine, 2013. **21**: p. 116-124.

48.   Blanka Sharma, S.F., Matthew Gibson, Shimon Unterman, Daniel A. Herzka, Brett Cascio, Jeannine Coburn, Alexander Y. Hui, Norman Marcus, Garry E. Gold, and Jennifer H. Elisseeff, *Human Cartilage Repair with a Photoreactive Adhesive-Hydrogel Composite.* Sci. Transl. Med., 2013. **5**: p. 167 ra6.

49. Verena M. A. Quarch, E.E., Joachim Lotz, and Karl-Heinz Frosch, *Fate of large donor site defects in osteochondral transfer procedures in the knee joint with and without TruFit Plugs.* Arch Orthop Trauma Surg, 2014. **134**: p. 657–666.

50. Lajos Bartha, D.H., Jeroen Pieper, Fabiénne Péters, Jens Riesle, Andras Vajda, Pal Kaposi Novak, Laszlo Rudolf Hangody, Gabor Vasarhelyi, Laszlo Bodó, Clemens van Blitterswijk, Joost de Wijn, Annamaria Kenyeres, Laszlo Modis, Eszter Balo, and Laszlo Hangody, *A clinical feasibility study to evaluate the safety and efficacy of PEOT/PBT implants for human donor site filling during mosaicplasty.* Eur J Orthop Surg Traumatol, 2013. **23**: p. 81-91.

51. G. Porcellini, G.M., F. Campi, A. Pellegrini, C.S. Bodanki and P. Paladini, *Arthroscopic treatment of early glenohumeral arthritis.* J Orthopaed Traumatol, 2013. **14**: p. 23-29.

52. A. Krase, R.A., E. Steck, C. Hurschler and W. Richter, *BMP activation and Wnt-signalling affect biochemestry and functional biomechanical properties of cartilage tissue engineering constructs.* Osteoarthritis Cartilage, 2014. **22**(2): p. 284-292.

53. J.A. Panadero, L.V., J.L. Gomez Ribelles, S. Lanceros-Mendez and V. Sencadas, *In vitro mechanical fatigue behavior of poly-e-caprolactone macroporous scaffolds for cartilage tissue engineering: Influence of pore filling by a poly(vinyl alcohol) gel.* Journal of Biomedical Materials Research Part B: Applied Biomaterials, 2014. **103**(5): p. 1037-1043.

54. M. Motavalli, G.A.W., J. E. Dennis and J. M. Mansour, *Investigating a continuous shear strain function for depth-dependent properties of native and tissue engineering cartilage using pixel-size data.* Journal of Mechanical Behavior of Biomedical Materials, 2013. **28**: p. 62-70.

55. J. A. A. Hendriks, L.M., J. Riesle, J. R. de Wijn, and C. A. van Blitterswijk, *The effect of scaffold-cell entrapment capacity and physico-chemical properties on cartilage regeneration.* Biomaterials, 2013. **34**(17): p. 4259-4265.

56. A. J. Griebel, M.K., T. Novak, C. C. van Donkelaar and C. P. Neu, *Direct noninvasive measurement and numerical modeling of depth-dependent strains in layered agarose constructs.* Journal of Biomechanics, 2014. **47**(9): p. 2149-2156.

57. H. Ahn, K.J.K., S. Y. Park, J. E. Huh, H. J. Kim and W-R. Yu, *3D braid scaffolds for regeneration of articular cartilage.* Journal of the Mechanica Behavior of Biomedical Materials, 2014. **34**: p. 37-46.

58. R. F. MacBarb, A.L.C., J. C. Hu and K. A. Athanasiou, *Engineering functional anisotropy in fibrocartilage neotissues.* Biomaterials, 2013. **34**(38): p. 9980-9989.

59. A. Moradi, S.P., F. Ataollahi, A. A. Khalil, T. Kamarul and B. Pingguan-Murphy, *A comparison study of different physical treatments on cartilage matrix derived porous scaffolds for tissue engineering applications.* Science and Technology of Advanced Materials, 2014. **15**(6): p. 065001.

60. G. Peng, S.M.M., K. A. Athanasiou and A. H. Reddi, *Surface Zone Articular Chondrocytes Modulate the Bulk and Surface Mechanical Properties of the Tissue-Engineered Cartilage.* Tissue Engineering: Part A, 2014. **20**(23-24): p. 3332-3341.

61. P. Causin, R.S.a.M.V., *A multiscale approach in the computational modeling of the biophysical environment in artificial cartilage tissue regeneration.* Biomechanics and Modeling in Mechanobiology, 2013. **12**(4): p. 763-780.

62. H. Da, S.-J.J., G-L. Meng, J-H- Cheng, W. Zhou, Z. Xiong, Y-J- Mu and J. Liu, *The Impact of Compact Layer in Biphasic Scaffold on Osteochondral Tissue Engineering.* PLoS One, 2013. **8**(1): p. e54838.

63. K. Shimomura, Y.M., W. Ando, R. Nansai, H. Fujie, D. A. Hart, A. Gobbi, K. Kita, S. Horibe, K. Shino, H. Yoshikawa and N. Nakamura, *Osteochondral Repair Using a Scaffold-Free Tissue-Engineered Construct Derived from Synovial Mesenchymal Stem Cells and a Hydroxyapatite-Based Artificial Bone.* Tissue Engineering: Part A, 2014. **20**(17-18): p. 2291-2304.

64. Y. Dabiri, L.P.L., *Influences of the depth-dependent material inhomogeneity of articular cartilage on the fluid pressurization in the human knee.* Medical Engineering & Physics, 2013. **35**(11): p. 1591-1598.

65. D. M. Pierce, T.R.a.G.A.H., *Modeling sample/patient-specific structural and diffusional responses of cartilage using DT-MRI.* International Journal for Numerical Methods in Biomedical Engineering, 203. **29**(8): p. 807-821.

66. D.P. Chang, F.G., G. D. Jay and S. Zauscher, *Interaction of lubricin with type II collagen surfaces: Adsorption, friction, and normal forces.* Journal of Biomechanics, 2014. **47**(3): p. 659-666.

67. G. W. Greene, A.O., M. Osterber, H. Zhu and R. Horn, *A cartilage-inspired lubrication system.* Soft Matter, 2014. **10**: p. 374-382.

68. K. C. Laurenti, L.C.D.A.H., A. R.odrigues dos Santos Jr, J. M. D. de Almeida Rollo, R. B. de Menezes Reiff, A. M. Minarelli Gaspar, B. de Moraes Purquerio, and C. A. Fortulan. , *Cartilage reconstruction using self-anchoring implant with functional gradient.* Materials Research, 2014. **17**(3): p. 638-649.

69. S. Utzschneider, V.L., M. Dedic, A. C. Paulus, C. Shröder, O. Gottschalk, *Biological activity and migration of wear particles in the knee joint: an in vivo comparison of six different polyethylene materials.* Journal of Materials Science: Materials in Medicine, 2014. **25**(6): p. 1599-1612.

70. S. Nürnberger, C.M., I. Ponomarev, D. Barnewitz, C. Resinger, W. Klepal, C. Albrecht, and S. Marlovits, *Equine articular chondrocytes on MACT scaffolds for cartilage defect treatment.* Anatomia Histologia Embryologia, 2013. **42**(5): p. 332-343.

71. A. Vahdati, D.R.W., *Implant size and mechanical properties influence the failure of the adhesive bond between cartilage implants and native tissue in a finite element analysis.* Journal of BIomechanics, 2013. **46**(9): p. 1554-1560.

72. S. E. Bulman, C.M.C., J. M. Murphy, N. Medcalf, A. E. Ryan, and F. Barry, *Pullulan: a new cytoadhesive for cell-mediated cartilage repair.* Stem Cell Research & Therapy, 2015. **6**(1): p. 34.

73. L. Vikingsson, J.A.G.-T., G. Gallego Ferrer, and J. L. Gómez Ribelles, *An experimental fatigue study of a porous scaffold for the regeneration of articular cartilage.* Journal of BIomechanics, 2015. **48**(7): p. 1310-1317.

74. Hongsen Chiang, C.-C.J., *Repair of articular cartilage defects: review and perspectives.* J Formos Med Assoc 2009. **108**(2): p. 87-101.

75. B. L. Seal, T.C.O., A. Panitch, *Polymeric biomaterials for tissue and organ regeneration.* Materials Science and Engineering R, 2001. **34**: p. 147-230.

76. Prathamesh M. Kharkar, K.L.K., and April M. Kloxin, *Designing degradable hydrogels for orthogonal control of cell microenvironments.* Chem. Soc. Rev., 2013. **42**: p. 7335-7372.

77. K. Deligkaris, T.S.T., W. Olthuis, A. van den Berg, *Hydrogel-based devices for biomedical applications.* Sensors and Actuators B: Chemical, 2010. **147**(2): p. 765-774.

78. I. L. Kima, R.L.M., J. A. Burdicka, *Hydrogel design for cartilage tissue engineering: A case study with hyaluronic acid.* Biomaterials, 2011. **32**(34): p. 8771-8782.

79. Martins, E.A.N.M., Y.M.; Baccarin, R.Y.A.; Cogliati, B.; Silva, L.S.L.C. , *Evaluation of chitosan-GP hydrogel biocompatibility in osteochondral defects: An experimental approach.* BMC Veterinary Research, 2014. **10**(197).

80. Kazusa, H.N., T.; Shibuya, H.; Ohkawa, S.; Kamei, G.; Adachi, N.; Deie M.; Nakajima, N.; Hyon, S.H.; Ochi, M., *Strong adhesiveness of a new biodegradable hydrogel glue, LYDEX, for use on articular cartilage.* J. Appl. Biomater. Funct. Mater. , 2013. **11**(3): p. 180-186.

81. Mesallati, T.B., C.T.; Kelly, D.J. , *Engineering articular cartilage-like grafts by self-assembly of infrapatellar fat pad-derived stem cells.* Biotechnol. Bioeng. , 2014. **111**: p. 1686–1698.

82. Bhat, S.L., L.; Kumar, A., *In vitro neo-cartilage formation on a three-dimensional composite polymeric cryogel matrix.* Macromol. Biosci. , 2013. **13**: p. 827-837.

83. Foss, C.M., E.; Migliaresi, C.; Motta, A. , *Silk fibroin/hyaluronic acid 3D matrices for cartilage tissue engineering.* Biomacromolecules, 2013. **14**: p. 38-47.

84. Boere, K.W.V., J.; Seyednejad, H.; Rahimian, S.; Gawlitta, D.; van Steenbergen, M.J.; Dhert, W.J.; Hennink, W.E.; Vermonden, T.; Malda, J., *Covalent attachment of a three-dimensionally printed thermoplast to a gelatin hydrogel for mechanically enhanced cartilage constructs.* Acta Biomaterialia, 2014. **10**: p. 2602–2611.

85. Parmar, P.A.C., L.W.; St-Pierre, J.P.; Horejs, C.M.; Peng, Y.Y.; Werkmeister, J.A.; Ramshaw, J.A.; Stevens, M.M.; Paresh, A.; Parmar, L.W.C.; et al., *Collagen-mimetic peptide-modifiable hydrogels for articular cartilage regeneration.* Biomaterials, 2015. **54**: p. 213-225.

86. Omobono, M.A.Z., X.; Furlong, M.A.; Kwon, C.H.; Gill, T.J.; Randolph, M.A.; Redmond, R.W. , *Enhancing the stiffness of collagen hydrogels for delivery of encapsulated chondrocytes to articular lesions for cartilage regeneration.* J. Biomed. Mater. Res. Part A 2015. **103A**: p. 1332-1338.

87. Liao, I.C.M., F.T.; Estes, B.T.; Zhao, X.; Guilak, F., *Composite three-dimensional woven scaffolds with interpenetrating network hydrogels to create functional synthetic articular cartilage.* Adv. Funct. Mater. , 2013. **23**: p. 5833–5839.

88. Antonioli, E.L., A.O.; Ferretti, M.; Cohen, M.; Marciano, F.R.; Corat, E.J.; Trava-Airoldi, V.J., *An evaluation of chondrocyte morphology and gene expression on superhydrophilic vertically-aligned multi-walled carbon nanotube films.* Mater. Sci. Eng. C 2013. **33**: p. 641–647.

89. Liu, M.I., Y.; Ebina, Y.; Sasaki, T.; Hikima, T.; Takata, M.; Aida, T. , *An anisotropic hydrogel with electrostatic repulsion between cofacially aligned nanosheets.* Nature, 2015. **517**: p. 68-72.

90. Leone, G.B., A.B.; Lamponi, S.; Magnani, A., *States of water, surface and rheological characterisation of a new biohydrogel as articular cartilage substitute.* Polym. Adv. Technol. , 2013. **24**: p. 824–833.

91. Drira, Z.Y., V.K. , *Nanomechanical measurements of polyethyleneglycol hydrogels using atomic force microscopy.* J. Mech. Behav. Biomed. Mater. , 2013. **18**: p. 20–28.

92. Ronken, S.W., D.; Daniels, A.U.; Kurokawa, T.; Gong, J.P.; Arnold, M.P. , *Double-network acrylamide hydrogel compositions adapted to achieve cartilage-like dynamic stiffness.* Biomech. Model. Mechanobiol. , 2013. **12**: p. 243–248.

93. Snyder, T.N.M., K.; Intrator, M.; Dregalla, R.C.; Park, D. , *A fibrin/hyaluronic acid hydrogel for the delivery of mesenchymal stem cells and potential for articular cartilage repair.* J. Biol. Eng. , 2014. **8**: p. 10.

94. Ahearne, M.L., Y.; Kelly, D.J., *Combining freshly isolated chondroprogenitor cells from the infrapatellar fat pad with a growth factor delivery hydrogel as a putative single stage therapy for articular cartilage repair.* Tissue Eng. Part A 2014. **20**: p. 930–939.

95. Mesallati, T.B., C.T.; Kelly, D.J. , *A comparison of self-assembly and hydrogel encapsulation as a means to engineer functional cartilaginous grafts using culture expanded chondrocytes.* Tissue Eng. Part C 2014. **20**: p. 52–63.

96. Ramesh, S.R., K.; Vaikkath, D.; Nair, P.D.; Madhuri, V. , *Enhanced encapsulation of chondrocytes within a chitosan/ hyaluronic acid hydrogel: A new technique.* Biotechnol. Lett. , 2014. **36**: p. 1107–1111.

97. Ha, C.W.P., Y.B.; Chung, J.Y.; Park, Y.G. , *Cartilage repair using composites of human umbilical cord blood-derived mesenchymal stem cells and hyaluronic acid hydrogel in a minipig model.* Stem Cells Transl. Med., 2015. **4**: p. 1-8.

98. Zeng, L.C., X.; Zhang, Q.; Yu, F.; Li, Y.; Yao, Y., *Redifferentiation of dedifferentiated chondrocytes in a novel three-dimensional microcavity hydrogel.* J. Biomed. Mater. Res. Part A 2015. **103A**: p. 193–1702.

99. Murakami, T.S., N.; Yamaguchi, T.; Yarimitsu, S.; Nakashima, K.; Sawae, Y.; Suzuki, A. , *Evaluation of a superior lubrication mechanism with biphasic hydrogels for artificial cartilage.* Tribol. Int., 2015. **89**: p. 19–26.

100. Chen, K.Z., D.; Cui, X.; Wang, Q. , *Research on swing friction lubrication mechanisms and the fluid load support characteristics of PVA–HA composite hydrogel.* Tribol. Int. , 2015. **90**: p. 412–419.

101. Baykal, D.U., R.J.; Mansmann, K.; Marcolongo, M.; Kurtz, S.M. , *Evaluation of friction properties of hydrogels based on a biphasic cartilage model.* J. Mech. Behave. Biomed. Mater. , 2013. **28**: p. 263–273.

102. Guo, Y.G., J.; Bai, D.; Wang, H.; Zheng, X.; Guo, W.; Tian, W. , *Hemiarthroplasty of the shoulder joint using a custom-designed high-density nano-hydroxyapatite/polyamide prosthesiswith a polyvinyl alcohol hydrogel humeral head surface in rabbits.* Artif. Organs 2014. **38**: p. 580–586.

103. Chiang, C.-W.C., W-C.; Liu, H-W.; Chen, C-H. , *Application of synovial fluid mesenchymal stem cells: Platelet-rich plasma hydrogel for focal cartilage defect.* J. Exp. Clin. Med. , 2014. **6**: p. 118–124.

104. Sridhar, B.V.B., J.L.; Silver, J.S.; Leight, J.L.; Randolph, M.A.; Anseth, K.S. , *Development of a cellularly degradable PEG hydrogel to promote articular cartilage extracellular matrix deposition.* Adv. Healthc. Mater. , 2015. **4**: p. 702–713.

105. Smeriglio, P.L., J.H.; Dhulipala, L.; Behn, A.W.; Goodman, S.B.; Smith, R.L.; Maloney, W.J.; Yang, F.; Bhutani, N. , *Comparative potential of juvenile and adult human articular chondrocytes for cartilage tissue formation in three-dimensional biomimetic hydrogels.* Tissue Eng. Part A, 2015. **21**: p. 147–155.

106. Zhao, F.H., W.; Yan, Y.; Zhang, H.; Zhang, G.; Tian, D.; Gao, H. , *The application of polysaccharide biocomposites to repair cartilage defects* Int. J. Polym. Sci. , 2014. **2014**: p. 654597.

107. Zeng, L.Y., Y.; Wang, D.A.; Chen, X., *Effect of microcavitary alginate hydrogel with different pore sizes on chondrocyte culture for cartilage tissue engineering.* Mater. Sci. Eng. C 2014. **34**: p. 168–175.

108. Rackwitz, L.D., F.; Janjanin, S.; Nöth, U.; Tuan, R.S. , *Functional cartilage repair capacity of de-differentiated, chondrocyteand mesenchymal stem cell-laden hydrogels in vitro. .* Osteoarthr. Cartil., 2014. **22**: p. 1148–1157.

109. Ponnurangam, S.O.C., G.D.; Chernyshova, I.V.; Wood, K.; Hung, C.T.; Somasundaran, P. , *Beneficial effects of cerium oxide nanoparticles in development of chondrocyte-seeded hydrogel constructs and cellular response to interleukin insults.* Tissue Eng. Part A 2014. **20**: p. 2908–2019.

110. Dashtdar, H.M., M.R.; Abbas, A.A.; Suhaeb, A.M.; Selvaratnam, L.; Tay, L.X.; Kamarul, T. , *PVA-chitosan composite hydrogel versus alginate beads as a potential mesenchymal stem cell carrier for the treatment of focal cartilage defects* Knee Surg. Sports Traumatol. Arthrosc. , 2015. **23**: p. 1368–1377.

111. Choi, B.K., S.; Fan, J.; Kowalski, T.; Petrigliano, F.; Evseenko, D.; Lee, M. , *Covalently conjugated transforming growth factor-β1 in modular chitosan hydrogels for the effective treatment of articular cartilage defects.* Biomater. Sci. , 2015. **3**: p. 742.

112. Tan, H.M., K.G., *Injectable, biodegradable hydrogels for tissue engineering applications.* Materials 2010. **3**: p. 1746-1767.

113. Seol, D.M., M.J.; Ramakrishnan, P.S.; Kurriger, G.L.; Choe, H.; Jang, K.; Martin, J.A.; Lim, T.H. , *Biocompatibility and preclinical feasibility tests of a temperature-sensitive hydrogel for the purpose of surgical wound pain control and cartilage repair* J. Biomed. Mater. Res. Part B 2013. **101B**: p. 1508–1515.

114. Petit, A.S., M.; Müller, B.; Meyboom, R.; van Midwoud, P.; Bruin, P.; Redout, E.M.; Versluijs-Helder, M.; van der Lest, C.H.; Buwalda, S.J.; et al. , *Release behavior and intra-articular biocompatibility of celecoxib-loaded acetyl-capped PCLA-PEG-PCLA thermogels* Biomaterials 2014. **35** p. 7919–7928.

115. Muzzarelli, R.A.A.G., F.; Busilacchi, A.; Sollazzo, V.; Gigante, A. , *Chitosan, hyaluronan and chondroitin sulfate in tissue engineering for cartilage regeneration: A review. .* Carbohydr. Polym. , 2012. **89** p. 723–739.

116. Tamaddon, M.W., R.S.; Brand, D.D.; Czernuszka, J.T. , *Characterisation of freeze-dried type ii collagen and chondroitin sulfate scaffolds.* J. Mater. Sci. Mater. Med., 2013 **24** p. 1153–1165.

117. Park, H.L., K, Y. , *Cartilage regeneration using biodegradable oxidized alginate/hyaluronate hydrogels* J. Biomed. Mater. Res. Part A 2014 **102A** p. 4519–4525.

118. Walker, K.J.M., S.V. , *Anisotropic temperature sensitive chitosan-based injectable hydrogels mimicking cartilage matrix* J. Biomed. Mater. Res. Part B 2015 **103B** p. 1149–1160.

119. Sheehy, E.J.M., T.; Vinardell, T.; Kelly, D.J. , *Engineering cartilage or endochondral bone: A comparison of different naturally derived hydrogels* Acta Biomater. , 2015. **13**: p. 245–253.

120. Kaderli, S.V., E.; Watrelot-Virieux, D.; Roger, T.; Gurny, R.; Scapozza, L.; Möller, M.; Boulocher, C.; Jordan, O. , *Efficacy study of two novel hyaluronic acid-based formulations for viscosupplementation therapy in an early osteoarthrosic rabbit model* Eur. J. Pharm. Biopharm. , 2015. **96**: p. 388–395.

121. Ren, C.D.G., S.; Kurisawa, M.; Ying, J.Y. , *Cartilage synthesis in hyaluronic acid–tyramine constructs.* J. Mater. Chem. B 2015 **3**: p. 1942.

122. Kim, J.L., B.; Kim, S.; Choi, B.; Evseenko, D.; Lee, M. , *TGF-β1 conjugated chitosan collagen hydrogels induce chondrogenic differentiation of human synovium-derived stem cells* J. Biol. Eng. , 2015. **9**: p. 1.

123. Jovanović, Z.R., A.; Kačarević-Popović, Z.; Stojkovska, J.; Perić-Grujić, A.; Ristić, M.; Matić, I.Z.; Juranić, Z.D.; Obradovic, B.; Mišković-Stanković, V. , *Bioreactor validation and biocompatibility of Ag/poly(n-vinyl-2-pyrrolidone) hydrogel nanocomposites* Colloids Surf. B Biointerfaces 2013 **105** p. 230-235.

124. Dua, R.C., J.; Ramaswamy, S. , *Augmentation of engineered cartilage to bone integration using hydroxyapatite* J. Biomed. Mater. Res. Part B, 2014. **102 B** p. 922-932.

125. Pan, Y.S., Q.; Pan, C.; Wang, J. , *Compressive mechanical characteristics of multi-layered gradient hydroxyapatite reinforced poly (vinyl alcohol) gel biomaterial* J. Mater. Sci. Technol. , 2013 **29**: p. 551–556.

126. Yodmuang, S.M., S.L.; Nover, A.B.; Mandal, B.B.; Agarwal, M.; Kelly, T.A.; Chao, P.H.; Hung, C.; Kaplan, D.L.; Vunjak-Novakovic, G. , *Silk microfiber-reinforced silk hydrogel composites for functional cartilage tissue repair* Acta Biomater. , 2015. **11** p. 27-36.

127. Parkes, M.M., C.; Dini, D.; Cann, P. , *Tribology-optimised silk protein hydrogels for articular cartilage repair* Tribol. Int. , 2015 **89** p. 9–18.

128. Su, R.S.K., Y.; Liu, J.C. , *Resilin: Protein-based elastomeric biomaterials* Acta Biomater. , 2014. **10** p. 1601–1611.

129. Kuo, C.Y.C., C.H.; Hsiao, C.Y.; Chen, J.P. , *Incorporation of chitosan in biomimetic gelatin/chondroitin-6-sulfate/hyaluronan cryogel for cartilage tissue engineering* Carbohydr. Polym. , 2015 **117** p. 722–730.

130. Zhao, L.G., H. J; Lim, Y.M.; Nho, Y.C.; Kim, S.Y. , *Hyaluronic acid/chondroitin sulfate-based hydrogel prepared by gamma irradiation technique* Carbohydr. Polym. , 2014 **102** p. 598–605.

131. Ni, Y.T., Z.; Cao, W.; Lin, H.; Fan, Y.; Guo, L.; Zhang, X. , *Tough and elastic hydrogel of hyaluronic acid and chondroitin sulfate as potential cell scaffold materials* Int. J. Biol. Macromol. , 2015 **74** p. 367–375.

132. Park, H.C., B.; Hu, J.; Lee, M. , *Injectable chitosan hyaluronic acid hydrogels for cartilage tissue engineering* Acta Biomater. , 2013 **9** p. 4779–4789.

133. Yang, R.T., L.; Cen, L.; Zhang, Z. , *An injectable scaffold based on crosslinked hyaluronic acid gel for tissue regeneration* RSC Adv. , 2016 **6**: p. 16838.

134. Fiorica, C.P., F.S.; Pitarresi, G.; Gulino, A.; Agnello, S.; Giammona, G. , *Injectable in situ forming hydrogels based on natural and synthetic polymers for potential application in cartilage repair. .* RSC Adv. , 2015 **5** p. 19715.

135. Matsuzaki, T.M., T.; Tabata, Y.; Saito, T.; Matsumoto, T.; Nagai, K.; Kuroda, R.; Kurosaka, M. , *Intra-articular administration of gelatin hydrogels incorporating rapamycinemicelles reduces the development of experimental osteoarthritis in a murine model* Biomaterials 2014 **35** p. 9904–9911.

136. Nims, R.J.C., A.D.; Albro, M.B.; Hung, C.T.; Ateshian, G.A. , *Synthesis rates and binding kinetics of matrix products in engineered cartilage constructs using chondrocyte-seeded agarose gels* J. Biomech. , 2014. **47** p. 2165–2172.

137. Sun, J.T., H. , *Alginate-based biomaterials for regenerative medicine applications.* Materials 2013 **6** p. 1285–1309.

138. Shi, Y., ; Xiong, D.S.; Peng, Y.; Wang, N. , *Effects of polymerization degree on recovery behavior of PVA/PVP hydrogels as potential articular cartilage prosthesis after fatigue test* eXPRESS Polym. Lett. , 2016 **10** p. 125–138.

139. Bichara, D.A.B.-S., H.; Ling, D.; Malchau, E.; Bragdon, C.R.; Muratoglu, O.K. , *Osteochondral defect repair using a polyvinyl alcohol-polyacrylic acid (PVA-PAAc) hydrogel* Biomed. Mater. , 2014. **9**: p. 045012.

140. Yang, H.Y.v.E., R.J.; Timmer, K.; Craenmehr, E.G.M.; Huang, J.H.; Öner, F.C.; Dhert, W.J.A.; Kragten, A.H.M.; Willems, N.; Grinwis, G.C.M.; et al. , *A novel injectable thermoresponsive and cytocompatible gel of poly(N-isopropylacrylamide) with layered double hydroxides facilitates siRNA delivery into chondrocytes in 3D culture* Acta Biomater. , 2015. **23** p. 214–228.

141. Yang, S.S.C., W.H.; Song, B.R.; Jin, H.; Lee, S.J.; Lee, S.H.; Lee, J.; Kim, Y.J.; Park, S.R.; Park, S-H.; et al. , *Fabrication of an osteochondral graft with using a solid freeform fabrication system* Tissue Eng. Regen. Med. , 2015 **12** p. 239 - 248.

142. Kim, J.E.K., S.H.; Jung, Y. , *In situ chondrogenic differentiation of bone marrow stromal cells in bioactive self-assembled peptide gels* J. Biosci. Bioeng. , 2015. **120**: p. 91–98.

143. Park, Y.B.S., M.; Lee, C.H.; Kim, J.A.; Ha, C.W. , *Cartilage repair by human umbilical cord blood-derived mesenchymal stem cells with different hydrogels in a rat model.* J. Orthop. Res. , 2015. **33**(11): p. 1580–1586.

144. Mao, H.K., N.; Chen, G. , *Cellular uptake of single-walled carbon nanotubes in 3D extracellular matrix-mimetic composite collagen hydrogels.* J. Nanosci. Nanotechnol. , 2014. **14**: p. 2487-2492.

145. Aberle, T.F., K.; Rist, E.; Benz, K.; Schlosshauer, B. , *Cell-type specific four-component hydrogel.* PLoS ONE 2014. **9**: p. e86740.

146. Chung, J.Y.S., M.; Ha, C.W.; Kim, J.A.; Lee, C.H.; Park, Y.B. , *Comparison of articular cartilage repair with different hydrogel-human umbilical cord blood-derived mesenchymal stem cell composites in a rat model.* Stem Cell Res. Ther. , 2014. **5**(2): p. 39.

147. Salamon, A.v.V., S.; van Nieuwenhove, I.; Baudisch, F.; Graulus, G.-J.; Benecke, V.; Alberti, K.; Neumann, H.-G.; Rychly, J.; Martins, J.C.; et al. , *Gelatin-based hydrogels promote chondrogenic differentiation of human adipose tissue-derived mesenchymal stem cells in vitro.* Materials 2014 **7**: p. 1342–1359.

148. Fisher, M.B.H., E.A.; Söegaard, N.B.; Dodge, G.R.; Steinberg, D.R.; Mauck, R.L. , *Maximizing cartilage formation and integration via a trajectory-based tissue engineering approach.* Biomaterials 2014. **35**: p. 2140–2148.

149. Song, K.L., L.; Li, W.; Zhu, Y.; Jiao, Z.; Lim, M.; Fang, M.; Shi, F.; Wang, L.; Liu, T. , *Three-dimensional dynamic fabrication of engineered cartilage based on chitosan/gelatin hybrid hydrogel scaffold in a spinner flaskwith a special designed steel frame.* Mater. Sci. Eng. C 2015. **55**: p. 384–392.

150. Mhanna, R.K., A.; Palazzolo, G.; Vallmajo-Martin, Q.; Becher, J.; Möller, S.; Schnabelrauch, M.; Zenobi-Wong, M. , *Chondrocyte culture in three dimensional alginate sulfate hydrogels promotes proliferation while maintaining expression of chondrogenic markers.* Tissue Eng. A 2014 **20**: p. 1454–1464.

151. Kesti, M.M., M.; Becher, J.; Schnabelrauch, M.; D'Este, M.; Eglin, D.; Zenobi-Wong, M. , *A versatile bioink for three-dimensional printing of cellular scaffolds based on thermally and photo-triggered tandem gelation.* Acta Biomater. , 2015. **11**: p. 162–172.

152. Ishikawa, M.Y., K.; Urano, K.; Tanaka, Y.; Hatanaka, T.; Nii, A. , *Biocompatibility of cross-linked hyaluronate (Gel-200) for the treatment of knee osteoarthritis* Osteoarthr. Cartil. , 2014. **22**: p. 1902–1909.

153. Mazaki, T.S., Y.; Yamane, K.; Yoshida, A.; Nakamura, M.; Yoshida, Y.; Zhou, D.; Kitajima, T.; Tanaka, M.; Ito, Y.; et al. , *A novel, visible light-induced, rapidly cross-linkable gelatin scaffold for osteochondral tissue engineering.* Sci. Rep. , 2014. **4**: p. 4457.

154. Zhao, M.C., Z.; Liu, K.; Wan, Y.Q.; Li, X.D.; Luo, X.W.; Bai, Y.G.; Yang, Z.L.; Feng, G. , *Repair of articular cartilage defects in rabbits through tissue-engineered cartilage constructed with chitosan hydrogel and chondrocytes.* J. Zhejiang Univ.-Sci. B (Biomed. Biotechnol.), 2015. **16**: p. 914–923.

155. Kyomoto, M.M., T.; Yamane, S.; Hashimoto, M.; Takatori, Y.; Ishihara, K. , *Effect of UV-irradiation intensity on graft polymerization of 2-methacryloyloxyethyl phosphorylcholine on orthopedic bearing substrate.* Mater. Res. Part A 2014 **102A**: p. 3012–3023.

156. Sardinha, V.M.L., L.L.; Belangero, W.D.; Zavaglia, C.A.; Bavaresco, V.P.; Gomes, J.R. , *Tribological characterization of polyvinyl alcohol hydrogel as substitute of articular cartilage* Wear 2013. **301**: p. 218–225.

157. Shi, Y.X., D. , *Microstructure and friction properties of PVA/PVP hydrogels for articular cartilage repair as function of polymerization degree and polymer concentration.* Wear 2013 **35**: p. 280–285.

158. Chen, T.H., M.J.; Brown, E.B.; Zuscik, M.J.; Awad, H.A. , *Engineering superficial zone features in tissue engineered cartilage.* Biotechnol. Bioeng. , 2013. **110**: p. 1476–1486.

159. Blum, M.M.O., T.C. , *Low friction hydrogel for articular cartilage repair: Evaluation of mechanical and tribological properties in comparison with natural cartilage tissue.* Mater. Sci. Eng. C 2013. **33**: p. 4377–4383.

160. Fan, C.L., L.; Zhang, C.; Liu, L. , *A tough double network hydrogel for cartilage tissue engineering.* J. Mater. Chem. B 2013. **1**: p. 4251.

161. Blum, M.M.O., T.C. , *Investigation of friction and surface degradation of innovative boundary lubricant functionalized hydrogel material for use as artificial articular cartilage.* Wear 2013. **301**: p. 201–209.

162. Giavaresi, G.B., E.; Melandri, D.; Giardino, R.; Tschon, M.; Torricelli, P.; Cenacchi, G.; Rotini, R.; Castagna, A.; Veronesi, F.; et al. , *Response of human chondrocytes and mesenchymal stromal cells to a decellularized human dermis* BMC Musculoskelet. Disord. , 2013. **14**: p. 12.

163. Stocco, E.B., S.; Dalzoppo, D.; Lora, S.; Sartore, L.; Folin, M.; Parnigotto, P.P.; Grandi, C. , *Tailored PVA/ECM scaffolds for cartilage regeneration.* Biomed. Res. Int. , 2014. **2014**: p. 762189.

164. Baek, J.H.K., K.; Yang, S.S.; Park, S.H.; Song, B.R.; Yun, H.W.; Jeong, S.I.; Kim, Y.J.; Min, B.H.; Kim, M.S. , *Preparation of extracellular matrix developed using porcine articular cartilage and in vitro feasibility study of porcine articular cartilage as an anti-adhesive film.* Materials 2016. **9**: p. 49.

165. Chen, X.Z., F.; He, X.; Xu, Y.; Yang, Z.; Chen, L.; Zhou, S.; Yang, Y.; Zhou, Z.; Sheng, W.; et al. , *Chondrogenic differentiation of umbilical cord-derived mesenchymal stem cells in type i collagen-hydrogel for cartilage engineering.* Inj. Int. J. Care Inj. , 2013 **44**: p. 540–549.

166. Wu, L.G., S.; Shah, S.; Kyupelyan, L.; Petrigliano, F.A.; McAllister, D.R.; Adams, J.S.; Karperien, M.; Tuan, T.L.; Benya, P.D.; et al. , *Extracellular matrix domain formation as an indicator of chondrocyte dedifferentiation and hypertrophy.* Tissue Eng. Part C 2014. **20**: p. 160–168.

167. Lam, J.L., S.; Lee, E.J.; Trachtenberg, J.E.; Meretoja, V.V.; Dahlin, R.L.; van den Beucken, J.J.; Tabata, Y.; Wong, M.E.; Jansen, J.A.; et al., *Osteochondral defect repair using bilayered hydrogels encapsulating both chondrogenically and osteogenically pre-differentiated mesenchymal stem cells in a rabbit model* Osteoarthr. Cartil. , 2014. **22**: p. 1291–1300.

168. Lu, H.-T.S., M.-T.; Lin, Y.-F.; Lan, J.; Chin, Y.-P.; Hsieh, M.-S.; Cheng, C.-W.; Chen, C.-H. , *Injectable hyaluronic-acid-doxycycline hydrogel therapy in experimental rabbit osteoarthritis.* Vet. Res. , 2013. **9**: p. 68.

169. Matsiko, A.G., J.P.; O'Brien, F.J. , *Scaffold mean pore size influences mesenchymal stem cell chondrogenic differentiation and matrix deposition* Tissue Eng. Part A. , 2015. **21** p. 486–497.

170. Hui, J.H.R., X.; Afizah, M.H.; Chian, K.S.; Mikos, A.G. , *Oligo[poly(ethylene glycol)fumarate] hydrogel enhances osteochondral repair in porcine femoral condyle defects* Clin. Orthop. Relat. Res. , 2013 **471**: p. 1174–1185.

171. Kwon, H., Rainbow, R.S.; Sun, L.; Hui, C.K.; Cairns, D.M.; Preda, R.C.; Kaplan, D.L.; Zeng, L. , *Scaffold structure and fabrication method affect proinflammatory milieu in three-dimensional-cultured chondrocytes* J. Biomed. Mater. Res. Part A 2015. **103A**: p. 534–544.

172. J.A.M. Steele, S.D.M., A. Callanan, H. Autefage, M.A. Accardi, D. Dini, M.M. Stevens, *Combinatorial scaffold morphologies for zonal articular cartilage engineering.* Acta Biomaterialia, 2014. **10**: p. 2065-2075.

173. Lee, W.D.H., M.B.; Pilliar, R.M.; Stanford, W.L.; Kandel, R.A. , *Engineering of hyaline cartilage with a calcified zone using bone marrow stromal cells* Osteoarthr. Cartil., 2015. **23**: p. 1307–1315.

174. Kaderli, S.B., C.; Pillet, E.; Watrelot-Virieux, D.; Rougemont, A.L.; Roger, T.; Viguier, E.; Gurny, R.; Scapozza, L.; Jordan, O. , *A novel biocompatible hyaluronic acid–chitosan hybrid hydrogel for osteoarthrosis therapy* Int. J. Pharm. , 2015. **483**: p. 158–168.

175. Medved, F.G., P.; Lotter, O.; Albrecht, D.; Amr, A.; Schaller, H.E. , *Severe posttraumatic radiocarpal cartilage damage: First report of autologous chondrocyte implantation* Arch. Orthop. Trauma Surg. , 2013. **133**: p. 1469–1475.

176. Niemietz, T.Z., G.; Hagmann, S.; Diederichs, S.; Gotterbarm, T.; Richter, W. , *Xenogeneic transplantation of articular chondrocytes into full-thickness articular cartilage defects in minipigs: Fate of cells and the role of macrophages.* Cell Tissue Res. , 2014 **358**: p. 749–761.

177. Adachi, N.O., M.; Deie, M.; Nakamae, A.; Kamei, G.; Uchio, Y.; Iwasa, J. , *Implantation of tissue-engineered cartilage-like tissue for the treatment for full-thickness cartilage defects of the knee.* Knee Surg. Sports Traumatol. Arthrosc. , 2014. **22**: p. 1241–1248.

178. Buwalda, S.J.B., K.W.; Dijkstra, P.J.; Feijen, J.; Vermonden, T.; Hennink, W.E. , *Hydrogels in a historical perspective: From simple networks to smart materials* J. Control. Release 2014. **190**: p. 254–273.

179. Vikingsson, L.G.F., G.; Gómez-Tejedor, J.A.; Gómez Ribelles, J.L. , *An "in vitro" experimental model to predict the mechanical behavior of macroporous scaffolds implanted in articular cartilage* J. Mech. Behave. Biomed. Mater. , 2014 **32**: p. 125–131.

180. Yusong, P.Q., S.; Chengling, P.; Jing, W. , *Prediction of mechanical properties of multilayer gradient hydroxyapatite reinforced poly(vinyl alcohol) gel biomaterial* J. Biomed. Mater. Res. Part B 2013 **101B**: p. 729–735.

181. Pan, Y.X., D. , *Stress-relaxation models of nano-HA/PVA gel biocomposites* Mech. Time-Depend. Mater. , 2013. **17**: p. 195–204.

182. Du, G.G., G.; Hou, R.; Cheng, Y.; Chen, T.; Fu J. , *Tough and fatigue resistant biomimetic hydrogels of interlaced self-assembled conjugated polymer belts with a polyelectrolyte network* Chem. Mater. , 2014, . **26**: p. 3522–3529.

183. Cao, Y.X., D.; Niu, Y.; Mei, Y.; Yin, Z.; Gui, J. , *Compressive properties and creep resistance of a novel, porous, semidegradable poly(vinyl alcohol)/poly(lactic-co-glycolic acid) scaffold for articular cartilage repair* J. Appl. Polym. Sci. , 2014 **131**: p. 40311.

184. Gonzalez, J.S.A., V.A. , *Mechanical properties of polyvinyl alcohol/hydroxyapatite cryogel as potential artificial cartilage. .* J. Mech. Behav. Biomed. Mater. , 2014. **34**: p. 47–56.

185. Chen, K.Z.D.D., Z.; Wang, S.; Ge, S. , *Research on the interstitial fluid load support characteristics and start-up friction mechanisms of PVA-HA-silk composite hydrogel. .* J. Bionic Eng., 2014. **11**: p. 378–388.

186. Mansour, J.M.G., D.W.; Chung, C.Y.; Heebner, J.; Althans, J.; Abdalian, S.; Schluchter, M.D.; Liu, Y.; Welter, J.F. , *Towards the feasibility of using ultrasound to determine mechanical properties of tissues in a bioreactor. .* Ann. Biomed. Eng. , 2014. **40**: p. 2190–2202.

187. Yun, A.L., S-H.; Kim, J. , *A phase-field model for articular cartilage regeneration in degradable scaffolds. .* Bull. Math. Biol. , 2013. **75**: p. 2389–2409.

188. Sandker, M.J.P., A.; Redout, E.M.; Siebelt, M.; Müller, B.; Bruin, P.; Meyboom, R.; Vermonden, T.; Hennink, W.E.; Weinans, H. , *In situ forming acyl-capped PCLA-PEG-PCLA triblock copolymer based hydrogels. .* Biomaterials 2013. **34**: p. 8002–8011.

189. Fukui, T.K., N.; Kurokawa, T.; Yokota, M.; Kondo, E.; Gong, J.P.; Yasuda, K. , *Intra-articular administration of hyaluronic acid increases the volume of the hyaline cartilage regenerated in a large osteochondral defect by implantation of a double-network gel. .* J. Mater. Sci. Mater. Med. , 2014 **25**: p. 1173–1182.

190. Haaparanta, A.M.J., E.; Cengiz, I.F.; Ellä, V.; Kokkonen, H.T.; Kiviranta, I.; Kellomäki, M. , *Preparation and characterization of collagen/PLA, chitosan/PLA, and collagen/chitosan/PLA hybrid scaffolds for cartilage tissue engineering. .* J. Mater. Sci. Mater. Med. , 2014. **25**: p. 1129–1136.

191. Lin, H.C., A.W.; Alexander, P.G.; Beck, A.M.; Tuan, R.S. , *Cartilage tissue engineering application of injectable gelatin hydrogel with in situ visible-light-activated gelation capability in both air and aqueous solution. .* Tissue Eng. Part A 2014. **2014**: p. 2402–2411.

192. Li, X.L., Y.; Zuo, Y.; Qu, D.; Liu, Y.; Chen, T.; Jiang, N.; Li, H.; Li. J. , *Osteogenesis and chondrogenesis of biomimetic integrated porous PVA/gel/V-n-HA/pa6 scaffolds and bmscs construct in repair of articular osteochondral defect. .* J. Biomed. Mater. Res. Part A 2015 **103A** p. 3226–3236.

193. Ayerst, B.I.D., A.J.; Nurcombe, V.; Cool, S.M.; Merry, C.L. , *New strategies for cartilage regeneration exploiting selected glycosaminoglycans to enhance cell fate determination* Biochem. Soc. Trans., 2014 **42**: p. 703–709.

194. Hoch, E.T., G.E.; Borchers, K. , *Biopolymer-based hydrogels for cartilage tissue engineering. .* Bioinspir. Biomim. Nanobiomater. , 2016. **5**: p. 51–66.

195. Tuan, R.S.C., A.F.; Klatt, B.A. , *Cartilage regeneration. .* J. Am. Acad Orthop. Surg., 2013. **21**: p. 303–311.

196. Sivashanmugam, A.K., R.A.; Priya, M.V.; Nair, S.V.; Jayakumar, R. , *An overview of injectable polymeric hydrogels for tissue engineering. .* Eur. Polym. J. , 2015. **72**: p. 543–565.

197. Hu, X.L., D.; Zhou, F.; Gao, C. , *Biological hydrogel synthesized from hyaluronic acid, gelatin and chondroitin sulfate by click chemistry. .* Acta Biomater. , 2011. **7**: p. 1618–1626.

198. Yang, J.-A.Y., J.; Hwang, B.W.; Hoffman, A.S.; Hahn, S.K. , *In situ-forming injectable hydrogels for regenerative medicine. .* Prog. Polym. Sci. , 2014. **39**: p. 1973–1986.

199. Mirahmadi, F.T.-S., M.; Shokrgozar, M.A.; Bonakdar, S. , *Enhanced mechanical properties of thermosensitive chitosan hydrogel by silk fibers for cartilage tissue engineering. .* Mater. Sci. Eng. C 2013. **33**: p. 4786–4794.

200. Moreira Teixeira, L.S.P., J.; Luyten, F.P. , *Skeletal tissue regeneration: Where can hydrogels play a role? .* Int. Orthop. , 2014. **38**: p. 1861–1876.

201. Camci-Unal, G.C., D.; Annabi, N.; Demarchi, D.; Khademhosseini, A. , *Synthesis and characterization of hybrid hyaluronic acid-gelatin hydrogels. .* Biomacromolecules 2013. **14**: p. 1085–1092.

202. Pot, M.W.F., K.A.; Adawy, A.; van Enckevort, W.J.; van Moerkerk, H.T.; Vlieg, E.; Daamen, W.F.; van Kuppevelt, T.H. , *Versatile wedge-based system for the construction of unidirectional collagen scaffolds by directional freezing: Practical and theoretical considerations. .* Appl. Mater. Interfaces 2015. **7**: p. 8495–8505.

203. Mao, H.K., N.; Chen, G. , *Cell response to single-walled carbon nanotubes in hybrid porous collagen sponges. .* Colloids Surf. B Biointerfaces 2015. **126**: p. 63–69.

204. Daly, A.C.C., S.E.; Rencsok, E.M.; Kelly, D.J. , *A comparison of different bioinks for 3D bioprinting of fibrocartilage and hyaline cartilage. .* Biofabrication 2016. **8**: p. 045002.

205. Seol, Y.J.P., J.Y.; Jeong, W.; Kim, T.H.; Kim, S.Y.; Cho, D.W. , *Development of hybrid scaffolds using ceramic and hydrogel for articular cartilage tissue regeneration. .* J. Biomed. Mater. Res. Part A 2015. **103A**: p. 1404–1413.

206. Xu, T.B., K.W.; Albanna, M.Z.; Dice, D.; Zhao, W.; Yoo, J.J.; Atala, A. , *Hybrid printing of mechanically and biologically improved constructs for cartilage tissue engineering applications. .* Biofabrication 2013. **5**: p. 015001.

207. Vázquez-Portalatín, N.K., C.E.; Panitch, A.; Liu, J.C. , *Characterization of collagen type I and II blended hydrogels for articular cartilage tissue engineering. .* Biomacromolecules 2016. **17**: p. 3145–3152.

208. Mintz, B.R.C., J.A. Jr. , *Hybrid hyaluronic acid hydrogel/poly(ε-caprolactone) scaffold provides mechanically favorable platform for cartilage tissue engineering studies. .* J. Biomed. Mater. Res. Part A 2014. **102A**: p. 2918–2926.

209. Sun, W.X., B.; Li, Y.; Qin, M.; Wu, J., Lu, K.; Wu, J., Cao, Y., Jiang, Q.; Wang, W. , *Polymer-supramolecular polymer double-network hydrogel. .* Adv. Funct. Mater. , 2016. **26**: p. 9044–9052.

210. Formica, F.A.Ö., E.; Hess, S.C.; Stark, W.J.; Maniura-Weber, K.; Rottmar, M.; Zenobi-Wong, M. , *A bioinspired ultraporous nanofiber-hydrogel mimic of the cartilage extracellular matrix. .* Adv. Funct. Mater. , 2016 **5**: p. 3129–3138.

211. Kang Mi-Lan, J.S.-Y., and Im Gun-Il, *Hyaluronic acid hydrogel functionalized with self-assembled micelles of amphiphilic PEGylated kartogenin for the treatment of osteoarthritis.* Tissue Engineering: Part A, 2017. **23**(13-14): p. 630-639.

212. Huang, H.Z., X.; Hu, X.; Dai, L.; Zhu, J.; Man, Z.; Chen, H.; Zhou, C.; Ao, Y. , *Directing chondrogenic differentiation of mesenchymal stem cells with a solid-supported chitosan thermogel for cartilage tissue engineering* Biomed. Mater. , 2014. **9**: p. 035008.

213. Buchtová, N.R., G.; Boyer, C.; Guicheux, J.; Rambaud, F.; Vallé, K.; Belleville, P.; Sanchez, C.; Chauvet, O.; Weiss, P.; et al. , *Nanocomposite hydrogels for cartilage tissue engineering: Mesoporous silica nanofibers interlinked with siloxane derived polysaccharide.* J. Mater. Sci. Mater. Med. , 2013. **24**: p. 1875–1884.

214. Wang, T.L., J.H.; Yang, F. , *Effects of hydrogel stiffness and extracellular compositions on modulating regeneration by mixed populations of stem cells and chondrocytes in vivo* Tissue Eng. Part A 2016. **22**: p. 1348–1356.

215. Desireé Alesa Gyles, L.D.C., José Otávio Carréra Silva Jr., Roseane Maria Ribeiro-Costa, *A review of the designs and prominent biomedical advances of natural and synthetic hydrogel formulations.* European Polymer Journal, 2017. **88**: p. 373-392.

216. S-J Jeon, A.W.H., and R.C. Hayward, *Shape-Morphing Materials from Stimuli-Responsive Hydrogel Hybrids.* Accounts of Chemical Research, 2017. **50**: p. 161-169.

217. June E. Jeon, C.d.V., Christina Theodoropoulos, Travis J. Klein and Dietmar W. Hutmacher, *Multiphasic construct studied in an ectopic osteochondral defect model.* J. R. Soc. Interface, 2014. **11**: p. 20140184.

218. A. Childs, U.D.H., N.J. Castro, H. Fenniri, and L.G. Zhang, *Novel biologically-inspired rosette nanotube PLLA scaffolds for improving human mesenchymal stem cell chondrogenic differentiation.* Biomedical Materials, 2013. **8**(6): p. 065003.

219. J. Maciulaitis, M.D., S. Rekstyle, M. Bratchikov, A. Darinskas, A. Simbelyte, G. Daunoras, A. Laurinaviciene, A. Laurinavicius, R. Gudas, M. Malinauskas, and R. Maciulaitis, *Preclinical study*

of SZ20180 material 3D microstructured scaffolds for cartilage tissue engineering made by femtosecond direct laser writing lithography. Biofabrication, 2015. **7**: p. 015015.

220. Sascha Heinemann, T.C.a.M.F.D., *Bio-inspired silica-collagen materials: applications and perspectives in the medical field.* Biomater. Sci., 2013. **1**: p. 688-702.

221. J. Kuo, D.A.S., G.D. Prestwich, *Chemical modification of hyaluronic acid by carbodiimides.* Bioconjugate Chem, 1991. **2**(4): p. 232-241.

222. G. Chen, J.G., J. Nie, and G. Ma, *Preparation, characterization, and application of PEO/HA core shell nanofibers based on electric field induced phase separation during electrospinning.* Polymer, 2016. **83**: p. 12-19.

223. R. Peña-Alonso, F.R., J. Rubio, J.L. Oteo, *Study of the hydrolysis and condensation of 3-Aminopropyltriethoxysilane by FT-IR spectroscopy.* Journal of Materials Science, 2007. **42**(2): p. 595-603.

224. N. Eslahi, A.S., M. Mehrojoo, M.A. Shokrgozar, S. Bonakdar, *Hybrid cross-linked hydrogels based on fibrous protein/block copolymers and layered silicate nanoparticles tunable thermosensitivity, biodegradability and mechanical durability.* RSC Adv., 2016. **6**: p. 62944-62957.

225. K. Haxaire, Y.M., M. Milas, and M. Rinaudo, *Hydration of polysaccharide hyaluronan observed by IR spectrometry. I. Preliminary experiments and band assignments.* Biopolymers-Biospectroscopy Section, 2003. **72**(1): p. 10-20.

226. X. Hu, D.L., F. Zhou, and C. Gao, *Biological hydrogel synthesized from hyaluronic acid, gelatin and chondroitin sulfate by click chemestry.* Acta Biomaterialia, 2011. **7**(4): p. 1618-1626.

227. D.A. Sánchez-Téllez, L.T.-J., L.M. Rodríguez-Lorenzo, *Optimization of the CaO and P2O5 contents on PDMS-SiO2-CaO-P2O5 hybrids intended for bone regeneration.* Journal of Materials Science, 2015. **50**(18): p. 5993-6006.

228. L. Téllez, J.R., F. Rubio, E. Morales, J. L. Oteo, *FT-IR study of the hydrolysis and polymerization of tetraethyl orthosilicate and polydimethyl siloxane in the presence of tetrabutyl orthotitanate.* Spectroscopy Letters, 2004. **37**(1): p. 11-31.

229. Y. Sun, M.Y., M. Kunimoto, M. Nakamura, T. Homma, *Depth profiling of APTES self-assembled monolayers using surface-enhanced confocal Raman microspectroscopy.* Spectrochimica Acta Part A: Molecular and Biomolecular Spectroscopy, 2017. **184**: p. 1-6.

230. Y. Sun, M.Y., M. Kunimoto, M. Nakamura,T. Homma, *Estimated phase transition and melting temperature of APTESself-assembled monolayer using surface-enhanced anti-stokes andstokes Raman scattering.* Applied Surface Science, 2016. **363**: p. 572–577.

231. Y. Qi, L.C., S. Jiang, J. Yu, B. Yu, C. Xiao and L. Qian, *Investigation of silicon wear against non-porous and micro-porous SiO2 spheres in water and in humid air.* RSC Adv., 2016. **6**.

232. D. Cai, A.N., Rüdiger Kuckuk, H. Michael Heise, *Raman, mid-infrared, near-infrared and ultraviolet–visible spectroscopy of PDMS silicone rubber for characterization of polymer optical waveguide materials.* Journal of Molecular Structure, 2010. **976**: p. 274–281.

233. A. Tamayo, J.R., *Structure modification by solvent addition into TEOS/PDMS hybrid materials.* Journal of Non-Crystalline Solids, 2010. **356**: p. 1742–1748.

234. D.A. Sánchez-Téllez, L.T.-J., L.M. Rodríguez-Lorenzo, M.A. Mazo, J. Rubio, A. Tamayo, *Surface effects on the degradation mechanism of bioactive PDMS-SiO2-CaO-P2O5 hybrid materials intended for bone regeneration.* Ceramics International, 2017. **43**: p. 476–483.

235. L. Jayes, A.P.H., C. Séné, S. F. Parker, U. A. Jayasooriya, *Vibrational spectroscopic analysis of silicones: A Fourier Transform-Raman and Inelastic Neutron Scattering Investigation.* Anal. Chem., 2003. **75**: p. 742-746.

236. J. A. Alkrad, Y.M., D. Stroehl, S. Wartewig, R. Neubert, *Characterization of enzymatically digested hyaluronic acid using NMR, Raman, IR, and UV-Vis spectroscopies.* Journal of Pharmaceutical and Biomedical Analysis, 2003. **31**: p. 545-550.

237. A. Kotzianová, J.R., M. Pokorný, J. Hrbáč, V. Velebný, *Raman spectroscopy analysis of biodegradable electrospun nanofibers prepared from polymer blends.* Monatsh Chem, 2016. **147**: p. 919–923.

238. V. Crescenzia, A.F., D. Capitani, L. Mannina, D. Renier, D. Bellini, *Hyaluronan networking via Ugi's condensation using lysine as cross-linker diamine.* Carbohydrate Polymers, 2003. **53**: p. 311-316.

239. V. Crescenzi, A.F., A. L. Segre, D. Capitani, L. Mannina, D. Renier, D. Bellini, *NMR structural study of hydrogels based on partially deacetylated hyaluronan.* Macromol. Biosci., 2002. **2**: p. 272–279.

240. Benjamin A. Ashu-Arrah, J.D.G., *Supercritical carbon dioxide versus toluene as reaction media in silica functionalisation: Synthesis and characterisation of bonded aminopropyl silica intermediate.* Journal of Chromatography A, 2017. **1501**: p. 18-25.

241. A. F. Peixoto, A.C.F., C. Pereira, J. Pires, C. Freire, *Physicochemical characterization of organosilylated halloysite clay nanotubes.* Microporous and Mesoporous Materials, 2016. **219**: p. 145-154.

242. Y. Duan, S.C.J., B. Lama, M. P. Espe, *Self-crosslinkable poly(urethane urea)-reinforced silica aerogels.* RSC Adv., 2015. **5**: p. 71551.

243. Z. Luan, J.A.F., J. B. Wooten, D. E. Miser, *Preparation and characterization of (3-aminopropyl)triethoxysilane-modified mesoporous SBA-15 silica molecular sieves.* Microporous and Mesoporous Materials, 2005. **83**: p. 150-158.

244. F. Ullah, F.J., M. B. H. Othman, A. Khan, R. Gul, Z. Ahmad, H. Md. Akil, *Synthesis and functionalization of chitosan built hydrogel with induced hydrophilicity for extended release of sparingly soluble drugs.* Journal of Biomaterials Science, Polymer Edition, 2018. **29**(4): p. 376-396.

245. D. J. T. Hill, C.M.L.P., A. K. Whittaker, *NMR study of the gamma radiolysis of poly(dimethyl siloxane) vacuum at 303 K.* Polymer, 2002. **43**: p. 1051-1059.

246. M. Meléndez-Zamudio, A.V., J. A. González-Calderón, R. Meléndrez, M. Meléndez-Lira, J. Cervantes, *Study of a polydimethylsiloxane (PDMS) elastomer generated by γ irradiation: Correlation between properties (thermal and mechanical) and structure (crosslink density value).* J Inorg Organomet Polym, 2017. **27**: p. 622–632.

247. W. Zhao, Y.S., X. Gao, Q. Qian, X. Chen, R. Wittenbrink, D. Wang, *Confined crystallization behaviors in polyethylene/silica nanocomposites: Synergetic effects of interfacial interactions and filler network.* Journal of Polymer Science, Part B: Polymer Physics, 2017. **55**: p. 498–505.

248. Klaus Albert, B.P., Ernst Bayer, and Roland Schnabel, *Characterization of chemically modified glass surfaces by 13C and 29 Si CP/MAS NMR Spectroscopy.* Journal of Colloid and Interfaces Science 1991. **142**(1): p. 35-40.

249. J. C. Almeida, A.W., P. S. Gomes, L. C. Alves, M. H. Vaz Fernandes, I. M. Miranda Salvado, M. H. R. Fernandes, *A biocompatible hybrid material with simultaneous calcium and strontium release capability for bone tissue repair.* Materials Science and Engineering C, 2016. **62**: p. 429–438.

250. J.C. Almeida, A.G.B.C., J.J.H. Lancastre, I.M. Miranda Salvado, F.M.A. Margaça, M.H.V. Fernandes, L.M. Ferreira, M.H. Casimiro, *Structural characterization of PDMS-TEOS-CaO-TiO2 hybrid materials obtained by solegel.* Materials Chemistry and Physics, 2014. **143**: p. 557-563.

251. R. Peña-Alonso, F.R., J. Rubio, *The role of γ-Aminopropyltriethoxysilane (γ-APS) on thermal stability of TEOS-PDMS ormosils.* Journal of Sol-Gel Science and Technology, 2005. **36**: p. 77-85.

252. K. Lewandowska, A.S., S. Grabska, M. Michalska, *Characterisation of chitosan/hyaluronic acid blend films modified by collagen.* Progress on Chemistry and Application of Chitin and its Derivatives, 2017. **22**: p. 125-134.

253. G. Huerta-Angeles, M.B., J. Kulhánek, V. Pavlík, D.Smejkalová, H. Vágnerová, V. Velebný, *Linolenic acid grafted hyaluronan: Process development, structuralcharacterization, biological assessing, and stability studies.* Carbohydrate Polymers, 2016. **152**: p. 815–824.

254. K. Lewandowska, A.S., S. Grabska, B. Kaczmarek, *Surface and thermal properties of collagen/hyaluronic acid blendscontaining chitosan.* International Journal of Biological Macromolecules, 2016. **92**: p. 371–376.

255. J. A. Vázquez, J.F., R. Novoa-Carvallal, R. L. Reis, L. T. Antelo, R. I. Pérez-Martín, J, Valcarcel, *Isolation and Chemical Characterization of Chondroitin Sulfate from Cartilage By-Products of Blackmouth Catshark (Galeus melastomus).* Mar. Drug, 2018. **16**: p. 344-358.

256. A.P. Vasconcelos Oliveira, V.d.A.F., J. Martins de Oliveira, A.L. Coelhoa, L. de Araújo P. Vieira, F.A. Rocha da Silva, F.A.A. Figueredo Sobrinho, E. Batista Duarte, B.W. de Souzaa, M, de sá Moreira de Souza Filho, *Characteristics of Chondroitin Sulfate Extracted of Tilapia (Oreochromis niloticus) Processing.* Procedia Engineering 2017. **200**: p. 193-199.

Sociedad Mexicana
de Materiales A.C.

The Organizing Committee
Acknowledges the Participation of

Daniela Anahi Sanchez Tellez

in the

XXIV International Materials Research Congress

Cancún, México. August 2015

J. Gerardo Cabañas Moreno
Sociedad Mexicana de Materiales
PRESIDENT

XXIV
INTERNATIONAL
MATERIALS RESEARCH
CONGRESS 2015
CANCÚN MÉXICO

INTERNATIONAL MATERIALS RESEARCH CONGRESS

M R S
MATERIALS RESEARCH SOCIETY®
Advancing materials. Improving the quality of life.

MINISTERIO
DE ECONOMÍA
Y COMPETITIVIDAD

CSIC
CONSEJO SUPERIOR DE INVESTIGACIONES CIENTÍFICAS

VICEPRESIDENCIA DE INVESTIGACIÓN CIENTÍFICA Y TÉCNICA

Vicepresidencia Adjunta de Internacionalización

Madrid, 25 de Abril de 2016

Luis Mª Rodríguez Lorenzo

Instituto de Ciencia y Tecnología de Polímeros

Estimado Dr. Rodríguez

Por Resolución de la Presidencia del CSIC, de 28 de marzo, se ha concedido el proyecto "Geles biológicos híbridos sintetizados a partir del ácido hialurónico y sulfato de condroitina con potencial aplicación en el reemplazo y regeneración de cartílago" que solicitó con número de referencia MHE-200011 en el programa EMHE-CSIC 2015.

De acuerdo a lo establecido en la Resolución, los términos administrativos y económicos en los que se concede el proyecto son los siguientes:

FECHA DE INICIO DEL PROYECTO: 01 Marzo 2016

FECHA FIN DEL PROYECTO: 31 Diciembre 2018

PARTICIPANTES EN EL PROYECTO:

Nombre	Apellido 1º	Apellido 2º	Función
LUIS Mª	RODRÍGUEZ	LORENZO	RESPONSABLE ESPAÑOL
LUCÍA	TELLEZ	JURADO	RESPONSABLE EXTRANJERO
DANIELA ANAHÍ	SÁNCHEZ	TELLEZ	INVESTIGADOR EXTRANJERO

Las condiciones económicas y administrativas son las que constan en la propuesta que ha presentado y la cantidad concedida:

Año 1: 8.425 €	Año 2: 8.300 €	Año 2: 8.425 €	Total: 25.150 €

SEP
SECRETARÍA DE
EDUCACIÓN PÚBLICA

Escuela Superior de Ingeniería
Química e Industrias
Extractivas

RECONOCIMIENTO

SIMPO
QUIMIA'2016

Extiende el presente

a:

Daniela Anahí Sánchez Téllez, Lucía Téllez Jurado,
Luis María Rodríguez Lorenzo

Por haber obtenido el **Primer Lugar** en el concurso de carteles, en la categoría: Difusión de la
Investigación, con el trabajo: "Geles biológicos sintetizados a partir del ácido hialurónico y sulfato de
condroitina con potencial aplicación en el remplazo y regeneración de cartílago"

XI SIMPOSIO INTERNACIONAL DE INGENIERÍA QUÍMICA DE LA ESIQIE DEL IPN (SIMPOQUIMIA):
"EDUCACIÓN Y TECNOLOGÍAS DEL FUTURO: PROCESOS SUSTENTABLES, REFORMA ENERGÉTICA Y ENERGÍAS ALTERNAS"

"La Técnica al Servicio de la Patria"

Ciudad de México
27 de Mayo de 2016

Ing. Víctor Manuel Feregrino Hernández
Subdirector Académico

M. en E. Dante Real Miranda
Director

www.esiqie.ipn.mx

80 AÑOS IPN

1 00 AÑOS ESIME

XXV INTERNATIONAL MATERIALS RESEARCH CONGRESS

14-19 August 2016 / Cancún, México

The Organizing Committee

Acknowledges the Participation of

Daniela Anahi Sanchez Tellez

in the

XXV International Materials Research Congress

Dr. José Gerardo Cabañas Moreno

PRESIDENT OF SMM

Sociedad Mexicana
de Materiales A.C.

MATERIALS RESEARCH SOCIETY®
Advancing materials. Improving the quality of life.

universidad deLeón

XXXIX CONGRESO DE LA SOCIEDAD IBÉRICA DE BIOMECÁNICA Y BIOMATERIALES (SIBB)

La Excma. Sra. Dª Mª Dolores Alonso-Cortés Fradejas, Vicerrectora de Relaciones Institucionales y con la Sociedad de la Universidad de León y D. Juan García López, Presidente del Comité Organizador del Congreso

CERTIFICAN

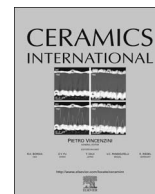Que   D.A. SÁNCHEZ-TÉLLEZ, L. TÉLLEZ-JURADO, J.RUBIO, A. TAMAYO, L.M. RODRÍGUEZ-LORENZO.

han presentado la **COMUNICACIÓN** titulada "THE POTENTIAL OF HYBRIDS FOR BONE REGENERATION, BIOACTIVITY BIODEGRADATION AND CYTOTOXICITY" en el XXXIX Congreso de la Sociedad Ibérica de Biomecánica y Biomateriales (SIBB) celebrado en León, los días 21, 22 y 23 de octubre de 2016, organizado por la Universidad de León, en colaboración con la Sociedad Ibérica de Biomecánica y Biomateriales, Centro de Alto Rendimiento Deportivo de León (CAR León), Consejo Superior de Deportes, Instituto de Estudios de Ciencias de la Salud de Castilla y León, European Society for Biomaterials, Departamento de Educación Física y Deportiva y Facultad de Ciencias de la Actividad Física y del Deporte de la Universidad de León.

Y para que conste a los efectos oportunos, firman el presente documento en León, a veintitrés de octubre de dos mil dieciséis.

Mª Dolores Alonso-Cortés Fradejas

Juan García López

CrossMark

Surface effects on the degradation mechanism of bioactive PDMS-SiO$_2$-CaO-P$_2$O$_5$ hybrid materials intended for bone regeneration

D.A. Sánchez-Téllez[a,*], L. Téllez-Jurado[a], L.M. Rodríguez-Lorenzo[b,c], M.A. Mazo[d], J. Rubio[d], A. Tamayo[d,*]

[a] Instituto Politécnico Nacional-ESIQIE, Depto. de Ing. en Metalurgia y Materiales, UPALM-Zacatenco, 07738 Mexico City, Mexico
[b] Biomaterials Group, ICTP-CSIC, Juan de la Cierva, 3, 28006 Madrid, Spain
[c] Networking Biomedical Research Centre in Bioengineering, Biomaterials and Nanomedicine, CIBER-BBN, Spain
[d] Ceramics and Glass Institute, CSIC, Kelsen 5, 28049 Madrid, Spain

ARTICLE INFO

ABSTRACT

The purpose of this work is to study the dissolution mechanism of SiO$_2$-based bioactive hybrid materials containing both CaO and P$_2$O$_5$ in their structures and to determine the influence of apatite crystallization over the surface features of the hybrids during degradation. Hybrid materials were synthesized using *sol–gel* method. Tetraethoxysilane (TEOS), hydroxyl terminated polydimethylsiloxane (PDMS), Ca(NO$_3$)$_2$·4H$_2$O, and triethyl phosphate (TEP) were used as reactants. The degradation and bioactivity of the hybrid materials were tested by soaking the specimens into simulated body fluid (SBF). Raman spectroscopy, tensiometry and N$_2$ adsorption/desorption curves were used to measure the changes during the degradation experiments. Several mathematical approaches have been taken to analyze the results. The growth of an apatite layer on the surface of SiO$_2$-modified PDMS-P$_2$O$_5$-CaO hybrid materials occurs together with degradation of the silica-based matrix. The dissolution kinetics depends upon the composition of the material. It varies from a surface-driven mechanism in the case of low-P$_2$O$_5$ samples to a degradation path which fits into a Weibull type kinetic model, typical of matrix dissolution processes in materials enriched in P$_2$O$_5$. During degradation, the surface parameters, fractal constant and anisotropy of the pores were determined. The slight increase of the fractal constant in low-containing P$_2$O$_5$ materials suggests the formation of a homogeneous silica-like layer in the first stage of degradation, which also works as anchoring nucleus for subsequent apatite formation. In all the cases, the degradation leads to ink-bottle shaped pores, increasing their volume as degradation occurs, but keeping their neck shape.

1. Introduction

The healing of critical size bone defects or low-quality bone fractures, as osteoporotic bones, requires longer times of healing than desired. And the longer healing times may result in several clinical complications. To prevent unforeseen difficulties, promising approaches, focused on the development of fixation devices that induce a simultaneous quick bone regeneration and material degradation while assuring enough mechanical properties to sustain the formation of the new functional tissue, are being studied [1–3].

Bioactive ceramics and bioactive glasses have attractive properties for bone repair and regeneration, such as osteointegration ability, and reasonable resorbability. They are capable of creating chemical bonds with the surrounding living tissue [4] thanks to the similarity of their chemical composition with that of natural bone. Nevertheless, organic-

inorganic hybrid materials can be more attractive than ceramics and glasses since they are capable of overcoming some of the weaknesses of these materials, such as fragility or low mechanical resistance in bending. These hybrid materials are made of a combination of silica-based glasses with organic compounds chemically incorporated into the molecular structure of the vitreous silica [5]. The organic-inorganic hybrid materials can be synthesized through several approaches, being the *sol–gel* method the most widely used. This method is preferred due to its ability to tune the composition and texture of the biomaterials to fulfill the requirements of the final use.

One of the required properties for hybrid materials designed for bone regeneration is bioactivity, which is speculated to be the responsible for bone bonding [6]. Bioactivity is referred as the ability of the material to promote growth of a biologically active thin apatite layer on its surface [5,7,8]. This apatite-like layer, formed when the

---

* Corresponding authors.
  E-mail addresses: danielatellez06@gmail.com (D.A. Sánchez-Téllez), aitanath@icv.csic.es (A. Tamayo).

European Society for Biomaterials

Organized by:
Hellenic Society for Biomaterials

September 4-8, 2017 ATHENS/GREECE
Megaron Athens International Conference Centre

Translational activities for exploiting research on Biomaterials

C E R T I F I C A T E

Awarded to

Daniela Anahí Sánchez Téllez

for attending the

28th Annual Conference of the European Society for Biomaterials (ESB 2017)

which was held from the 4th to the 8th of September 2017

at the Megaron Athens International Conference Center (MAICC) in Athens, Greece

Prof. Maria Chatzinikolaidou
ESB 2017 Chair

Prof Matteo Santin
ESB President

ESB 2017

12:00–13:00 📖 Hall: **Kokkali Hall**

Session OP-24 | Biomaterials for Cartilage

Chairs: **Véronique Migonney** | LBPS/CSPBAT UMR7244 Université Paris13, France
David Eglin | AO Foundation, Switzerland
YSF Chair: **Francesca Veronesi** | Rizzoli Orthopedic Institute, Italy

12:00 OP-097 3-D Printed Silica-Gelatin Hybrid Scaffolds for Cartilage Tissue Engineering - Effect of Material Geometry on Cartilaginous Matrix Formation
Siwei Li, Maria Nelson, Molly Stevens, Julian Jones | Imperial College London, United Kingdom

12:15 OP-098 Si-HPMC/Si-Chitosan Hybrid Hydrogel for Cartilage Regenerative Medicine: From In Vitro to In Vivo Assessments in Nude Mice and Canine Model of Osteochondral Defects
Cécile Boyer, Julie Lesoeur, Sophie Sourice, Claire Vinatier, Gildas Réthoré, Pierre Barreau, Marion Fusellier, Olivier Geffroy, Pierre Weiss, Olivier Gauthier, Jérôme Guicheux | University of Nantes, France

12:30 OP-099 Novel Collagen-Doped Fibrous Biomaterials for Articular Cartilage Repair
Michael Gasik, Anne-Marie Haaparanta, Virpi Muhonen, Alexandra Zühlke, Ines Hiropoulos, Kaisa Laine, Yevgen Bilotsky, Minna Kellomäki, Ilkka Kiviranta | Aalto University Foundation, Finland

12:45 OP-100 Design and Characterisation of a Drug Delivery System: 3D Ice-Templated Scaffolds with Controlled Architecture Loaded with Model Drug FITC-Albumin for Cartilage Tissue Regeneration
Constantin E. Tanase, Omar Qutachi, Kevin M. Shakesheff, Serena M. Best, Ruth E. Cameron | University of Cambridge, United Kingdom

---

12:00–13:00 📖 Hall: **MC3 Hall**

Session OP-25 | Hybrid Biomaterials

Chairs: **Diego Mantovani** | Laval University, Canada
Maria Letizia Focarete | University of Bologna, Italy
YSF Chair: **Daniela Anahí Sánchez Téllez** | ESIQIE-IPN; ICTP-CSIC, Spain

12:00 OP-101 PEG-PHPMA Block Copolymers Bearing Pendant Benzylthioether Groups - Synthesis, Self-Assembly in Water and Micellar Core-Crosslinking via Platinum Coordination Chemistry
Sytze Buwalda, Benjamin Nottelet, Jean Coudane | CNRS-University of Montpellier-ENSCM, France

12:15 OP-102 Hyaluronan Hydrogel/calcium Phosphates Composites for Medical Application
Marina Sokolova, Dagnija Loca, Janis Locs | Riga Technical University, Latvia

Hydrogels for Cartilage Regeneration, from Polysaccharides to Hybrids

Daniela Anahí Sánchez-Téllez [1,2,*] [ID]**, Lucía Téllez-Jurado [1] and
Luís María Rodríguez-Lorenzo [2,3]** [ID]

[1]   Instituto Politécnico Nacional-ESIQIE, Depto. Ing. en Metalurgia y Materiales, UPALM-Zacatenco,
     Mexico City 07738, Mexico; ltellezj@ipn.mx
[2]   Networking Biomedical Research Centre in Bioengineering, Biomaterials and Nanomedicine,
     Centro de Investigación Biomédica en Red—Bioingeniería, Biomateriales y Nanomedicina (CIBER-BBN),
     Av. Monforte de Lemos 3-5, Pabellón 11, Planta 0, 28029 Madrid, Spain; luis.rodriguez-lorenzo@ictp.csic.es
[3]   Department Polymeric Nanomaterials and Biomaterials, ICTP-CSIC, Juan de la Cierva 3,
     28006 Madrid, Spain
*   Correspondence: danielatellez06@gmail.com; Tel.: +34-695-198-353 or +521-55-29-54-32-91

Abstract: The aims of this paper are: (1) to review the current state of the art in the field of cartilage substitution and regeneration; (2) to examine the patented biomaterials being used in preclinical and clinical stages; (3) to explore the potential of polymeric hydrogels for these applications and the reasons that hinder their clinical success. The studies about hydrogels used as potential biomaterials selected for this review are divided into the two major trends in tissue engineering: (1) the use of cell-free biomaterials; and (2) the use of cell seeded biomaterials. Preparation techniques and resulting hydrogel properties are also reviewed. More recent proposals, based on the combination of different polymers and the hybridization process to improve the properties of these materials, are also reviewed. The combination of elements such as scaffolds (cellular solids), matrices (hydrogel-based), growth factors and mechanical stimuli is needed to optimize properties of the required materials in order to facilitate tissue formation, cartilage regeneration and final clinical application. Polymer combinations and hybrids are the most promising materials for this application. Hybrid scaffolds may maximize cell growth and local tissue integration by forming cartilage-like tissue with biomimetic features.

Keywords: cartilage regeneration; polymeric hydrogels; polysaccharides; hybrid hydrogels; hybrid scaffolds

---

1. Introduction: Current Clinical Approaches and the Need for New Developments

The aim of this paper is to review the current state of the art of materials for cartilage substitution and regeneration. Section 1 describes the current state of the art in clinical treatments. Polymeric hydrogels used in cartilage regeneration and the reasons hindering their clinical success are reviewed in Section 2. The preparation techniques using polysaccharides and the resulting hydrogel properties are described in Section 3. Finally, future trends are explored in Section 4.

Several reviews about hydrogels for cartilage regeneration have been published for the last 10 years, focusing on preparation and characterization, natural and synthetic polymer precursors, gelation kinetics, cell and drug delivery, growth factors, mechanical properties and biocompatibility. Nevertheless, most of those reviews do not propose new alternatives to improve hydrogels properties which can fulfill the real clinical needs in terms of tissue regeneration, mechanical properties and degradation kinetics. Therefore, this paper reviews relevant literature published during 2013–2017, related to the application, fabrication, characterization, in vitro and in vivo assays of biomaterials

Universidad
Carlos III de Madrid

Universidad
Carlos III de Madrid

Trabajo Fin de Máster

"Síntesis y caracterización de un hidrogel híbrido a partir de sulfato de condroitina con potencial aplicación en el reemplazo y regeneración de cartílago"

Víctor Raúl Huamán Cárdenas

Tutor/es

Diego Velasco Bayón

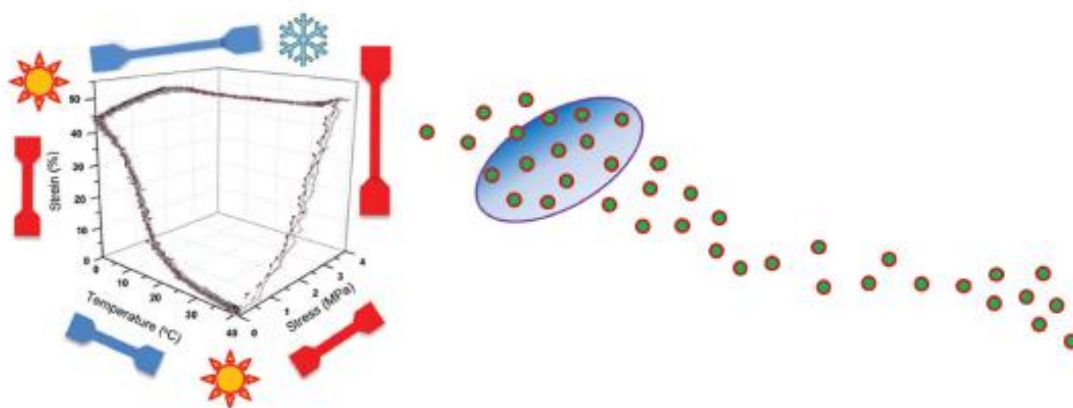Luis María Rodríguez Lorenzo

Daniela Anahí Sánchez Téllez

Madrid, 18 de junio del 2018

Palabras clave: Hidrogel, sulfato de condroitina, geles híbridos.

How Smart are the Polymers?

Laura Peponi, PhD,
Jean Marie Raquez, PhD
Editors

Chapter 14

IS YOUR POLYMER SMART ENOUGH? BETTER MAKE A HYBRID!

Daniela Anahí Sánchez-Téllez[1,2,*], *Lucía Téllez-Jurado, PhD*[1]
and Luís María Rodríguez-Lorenzo, PhD[2,3]

[1]Department of Engineering in Metalurgy and Materials,
Instituto Politécnico Nacional-ESIQIE,
Mexico City, Mexico
[2]Networking Biomedical Research Centre in Bioengineering,
Biomaterials and Nanomedicine, CIBER-BBN, Spain
[3]Institute of Polymer Science and Technology-
Spanish Research Council (CSIC), Madrid, Spain

ABSTRACT

The main advantages of inorganic–organic hybrids are the combination of frequent dissimilar properties of organic and inorganic components in one material and the opportunity to develop an almost unlimited set of new materials with a large spectrum of known and yet unknown properties, because of the many possible combinations. Usually, in composite materials, polymer networks serve as organic matrices and inorganic components (Si, Ti, Sn, Al-based compounds, etc.) serve as fillers dispersed into the polymer network. These composites can be considered within Class I hybrids. In this class, weak bonds between components can be found such as Van der Waals forces or hydrogen bonds. Moreover there is Class II hybrids where components are linked by strong chemical bonds such as ionic or ionic-covalent bonds. Two types of reactions can be used to synthesize Class II hybrids: the simultaneous polymerization and the sequential polymerization of organic and inorganic monomers. Different structures can be obtained by altering the polymerization procedure: inorganic phase nanodomains

* Corresponding Author Email: danielatellez06@gmail.com.